

DISS. ETH NO. 22523

# **Synthesis of Monomers for Topochemical Approaches Towards Poly[n]catenanes and 2D Polymers**

A thesis submitted to attain the degree of

DOCTOR OF SCIENCES of ETH ZURICH

(Dr. sc. ETH Zurich)

presented by

**Simon Timothy Cerqua**

Dipl.-Chem., University of Mainz

born on August 1st, 1984

citizen of Germany and the USA

accepted on the recommendation of

Prof. Dr. A. Dieter Schlüter, examiner

Prof. Dr. Nicholas D. Spencer, co-examiner

Dr. Bernd Schweizer, co-examiner

2015



"If we never did anything we shouldn't do, we'd never feel good about doing the things we should." Francis Underwood (Kevin Spacey)

Dedicated to

Armando Ernest Cerqua

Irena Marjanna (Erika) Cerqua (née Schmelter)

Josef Kutzmutz

Maria Kutzmutz (née Neubauer)



## Contents

<b>A. List of Abbreviations</b>	<b>VII</b>
<b>B. Abstract</b>	<b>IX</b>
<b>C. Zusammenfassung</b>	<b>XI</b>
<b>1. Introduction and Motivation</b>	<b>1</b>
<b>2. Theoretical Background</b>	<b>8</b>
2.1. Solid-state Photoreactions . . . . .	8
2.2. Polycatenanes . . . . .	15
2.3. Terpyridine-based Complexes for Catenation . . . . .	19
2.4. 2D Polymers . . . . .	26
<b>3. Goal</b>	<b>30</b>
<b>4. Results and Discussion</b>	<b>32</b>
4.1. Part A: Synthesis of a 2,2':6',2''-Terpyridine Ligand <b>7</b> . . . . .	32
4.2. Part A: Complexation and Decomplexation Studies . . . . .	42
4.3. Part A: Crystals and Irradiation . . . . .	61
4.4. Part B: Synthesis of a Monomer <b>6</b> for 2D Polymerization . . . . .	98
<b>5. Summary and Outlook</b>	<b>118</b>
5.1. Summary . . . . .	118
5.2. Outlook . . . . .	119
<b>6. Experimental</b>	<b>122</b>
6.1. Materials and Methods . . . . .	122
6.2. Synthesis Part A . . . . .	125
6.3. Synthesis Part B . . . . .	143
<b>7. Appendix</b>	<b>153</b>
7.1. Crystallographic data . . . . .	153
<b>8. References</b>	<b>161</b>
<b>9. Acknowledgments</b>	<b>174</b>
<b>10. Curriculum Vitae</b>	<b>176</b>
<b>11. Publications</b>	<b>178</b>
11.1. Poster Presentations . . . . .	178



### A. List of Abbreviations

$\delta$	= Chemical shift (in ppm)
$\lambda$	= Wavelength (in nm)
abs.	= Absolute
AFM	= Atomic force microscopy
Ant	= Anthracene
aq.	= Aqueous
Ar	= Aromatic compound
BuLi	= Butyllithium
calcd	= Calculated
conc.	= Concentrated
COSY	= Correlated spectroscopy
DCM	= Dichloromethane / methylene chloride
DDQ	= 2,3-Dichloro-5,6-dicyano-1,4-benzoquinone
DIPEA	= <i>N,N</i> -Diisopropylethylamine
DMF	= <i>N,N</i> -Dimethylformamide
DMSO	= Dimethyl sulfoxide
ESI	= Electrospray ionization
Et <sub>2</sub> O	= Diethylether
EtOAc	= Ethyl acetate
EtOH	= Ethanol
eq.	= Equivalent
HMBC	= Heteronuclear Multiple-bond Correlation
HSQC	= Heteronuclear Single Quantum Coherence
HOAc	= Acetic acid
3-HPA	= 3-Hydroxypicolinic acid
HRMS	= High Resolution Mass Spectrometry
<i>J</i>	= Spin-spin coupling constant (in Hz)
LED	= Light-emitting diode
M	= Mol/L
MALDI-TOF	= Matrix-assisted laser desorption / ionization - time of flight
MeNH <sub>2</sub>	= Methylamine

## A. List of Abbreviations

---

MeOH	= Methanol
MLCT	= Metal-to-ligand charge-transfer
MS	= Mass spectrometry
MW	= Microwave
m/z	= Mass-to-charge ratio
NH <sub>4</sub> OAc	= Ammonium acetate
NMP	= <i>N</i> -Methyl-2-pyrrolidone
NMR	= Nuclear magnetic resonance
ODCB	= <i>o</i> -Dichlorobenzene
OM	= Optical microscopy
ppm	= Parts per million
PrOH	= Propyl alcohol
Py	= Pyridine compound
POM	= Polarized optical microscope
R <sub>f</sub>	= Retardation factor
rGPC	= Recycling Gel Permeation Chromatography
RU	= Repeating unit
rt	= Room temperature
SEM	= Scanning electron microscope
scsc	= Single-crystal-to-single-crystal
TBAF	= Tetrabutylammonium fluoride
TCE	= 1,1,2,2-Tetrachloroethane
TEA	= Triethylamine
Tf <sub>2</sub> O	= Trifluoromethanesulfonic anhydride
TFA	= Trifluoroacetic acid
THF	= Tetrahydrofuran
TIPS	= Triisopropylsilyl
TLC	= Thin layer chromatography
TMS	= Trimethylsilyl
Tpy/terpyridine	= 2,2':6',2''-Terpyridine
Triflate	= Trifluoromethanesulfonate
UV/Vis	= Ultraviolet / Visible
XRD	= X-ray diffraction



### B. Abstract

Poly[n]catenanes refer to interlocked macrocyclic molecules, which are connected both topologically and through covalent bonds (Figure 0.1). Current scientific research in the field assumes that these polymers will have novel properties in terms of their rheology, as well as their dynamic, mechanic, and thermal behavior based on their independent motion caused by almost free rotation and the additional mobility of the linked rings. To this day, there has been no report of a successful synthesis of this class of polymers.

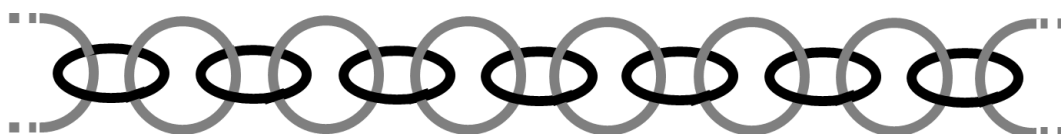


Figure 0.1: Cartoon of a poly[n]catenane chain.

Two-dimensional polymers (2DPs) are one monomer unit thick, covalently bonded, and free-standing sheets (Figure 0.2) with a defined internal order. Such polymers have been observed in nature e.g., as graphenes. Two-dimensional polymers have been prepared recently through solid-state photopolymerization of rationally synthesized organic monomer crystals. Using crystals for solid-state photopolymerization has the advantage of drawing on the crystals' high order and results in a single product. Such 2DPs with structurally designed precision could be useful for, among other things, ultrafiltration, membrane support, and catalysis.

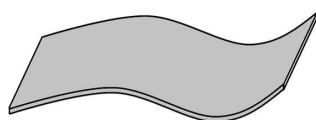


Figure 0.2: Cartoon of a sheet representing a 2D polymer.

This thesis includes two approaches based on topochemical polymerizations. The first part engages in tracing potential paths towards the synthesis of a poly[n]catenane. It includes the iterative organic synthesis of a U-shaped premonomer ligand that carries one terpyridine unit and two anthracene moieties. This premonomer ligand is then interlocked with another through metal complexation, thereby furnishing a duplex. The thesis also includes a documentation of the complexation process of the premonomer ligand and zinc salts. After successful bis-complexation and crystallization, the duplex-shaped compound serves as a monomer. The monomer's backbone is designed to be rigid in order to control its conformation, and to make it suitable for the subsequent pre-organization in which the anthracene moieties are stacked

## B. Abstract

---

to form one-dimensional arrays across the monomers. Irradiating these pre-organized arrays with light, the anthracene units undergo a [4+4]-cycloaddition—fixing them covalently. The irradiated crystals are then dissolved and demetallated. Although the above described concepts present a clear progress in the synthesis of a poly[n]catenane, a breakthrough in proving and isolating a poly[n]catenane, including the typical polymer characterizations, requires additional effort.

The second part of this thesis documents the synthesis of a monomer to achieve 2D polymers, as well as first attempts at polymerization in two-dimensions with such a monomer on the air/water interface. The monomer resembles a symmetric three-bladed rotor, which consists of stacked triazines connected by three anthracene blades through amine linkers. A single-crystal of this monomer should arrange in a  $C_{3h}$  symmetric conformation to allow a solid-state photopolymerization laterally in two dimensions of neighboring monomers by the face-to-face stacked anthracene blades.

Ultimately, the synthesis of the amine-bearing monomer was successful and the photoirradiation of the monomer on the air/water interface indicated a polymerization.

### C. Zusammenfassung

Poly[n]catenane sind verschlungene, makrozyklische Moleküle, welche durch topologische und kovalente Bindungen verbunden sind (Abbildung 0.3). Aktuelle Studien gehen davon aus, dass diese Polymere neuartige Eigenschaften besitzen: So wird von einer neuen Rheologie, sowie veränderten dynamischen, mechanischen und thermischen Eigenschaften ausgegangen. Diese Eigenschaften basieren auf der unabhängigen Bewegung, der nahezu freien Rotation und der zusätzlichen Wendigkeit der verbundenen Ringe dieser Polymere. Bis zum heutigen Tage gibt es jedoch noch keine erfolgreich dokumentierte Synthese eben dieser Polymerklasse.

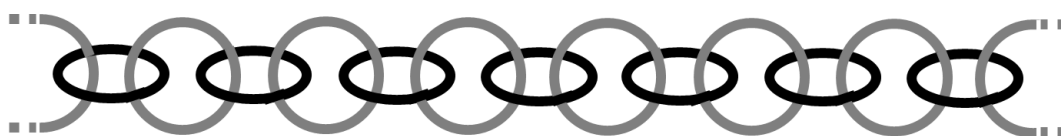


Figure 0.3: Schematische Darstellung einer Poly[n]catenankette.

Zweidimensionale Polymere (2DPs) sind eine Monomereinheit dick und durch kovalente Bindungen verbunden. Sie bestehen aus freistehende Schichten (Abbildung 0.4) mit einer definierten internen Ordnung. In der Natur kommen diese Polymere z.B. als Graphene vor. Erst kürzlich wurden zweidimensionale Polymere durch eine Festkörperphotopolymerisation von rational synthetisierten, organischen Monomerkristallen hergestellt. Bei einer Festkörperphotopolymerisation von Kristallen wird die hohe Ordnung der Kristalle genutzt um ein einzelnes Produkt zu erhalten. Diese 2DPs sind strukturell präzise konstruiert und könnten daher Anwendung in den Bereichen Ultrafiltration, Membranunterstützung, Katalyse u. ä. finden.

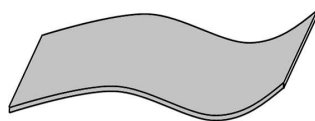


Figure 0.4: Schematische Darstellung einer Schicht, dass ein 2D Polymer repräsentiert.

Diese Arbeit umfasst zwei Ansätze, die beide auf topochemischen Polymerisationen basieren. Der erste Teil verfolgt die Ermittlung potentieller Wege zur Synthese eines Poly[n]catenans. Er beinhaltet die stufenweise, organische Synthese eines U-förmigen Prämonomerligands, welches eine Terpyridin-Einheit und zwei Anthrazen-Einheiten umfasst. Dieser Prämonomerligand wird anschliessend mit einem weiteren durch eine Metallkomplexierung zu einem Duplex verriegelt. Die Arbeit beinhaltet auch die Komplexierungsprozesse des Prämonomerligands mit Zinksalzen. Nach erfolgreicher Biskomplexierung und Kristallisierung dient die zum Duplex geformte Verbin-

## C. Zusammenfassung

---

derung als Monomer. Das Rückgrat des Monomers wurde rigide konstruiert, um die Konformation des Monomers zu kontrollieren und es für die anschliessende Präorganisation brauchbar zu machen. Bei der Präorganisation schichten sich die Anthrazen-Einheiten um so eindimensionale Stränge entlang der Monomere zu bilden. Durch die Lichtbestrahlung dieser präorganisierten Anordnungen gehen die Anthrazen-Einheiten eine [4+4]-Cycloaddition ein und werden kovalent fixiert. Die bestrahlten Kristalle werden anschliessend gelöst und demetalliert. Obwohl das zuvor beschriebene Konzept einen klaren Fortschritt in der Poly[n]catenansynthese darstellt, erfordert der bahnbrechende Beweis und die Isolierung eines Poly[n]catenans, mit dessen klassischen Polymercharakterisierungen, einen zusätzlichen Aufwand.

Der zweite Teil dieser Arbeit befasst sich mit der Synthese eines Monomers zur Herstellung eines 2D Polymers. Darüber hinaus wird mit diesem Monomer die ersten Polymerisationen in zwei Dimensionen auf der Wasser/Luft Grenzfläche erprobt. Das Monomer ähnelt einem symmetrischen dreiblättrigem Rotor und besteht aus übereinander geschichtete Triazinen, die mit drei Anthrazen-Blätter durch eine Aminverbindung verbunden sind. Ein Einzelkristall von solch einem Monomer sollte eine  $C_{3h}$  Symmetrie aufweisen, welche eine zweidimensionale laterale Festkörperphotopolymerisation mit benachbarten Monomere durch die einander gegenübergeschichteten Anthrazenen-Blätter erlaubt.

Letztendlich war die Synthese des aminhaltigen Monomers erfolgreich und die Photobestrahlung des Monomers an der Wasser/Luft Grenzfläche deutete auf eine Polymerisation hin.

### 1. Introduction and Motivation

The research of Hermann Staudinger in the 1920s marks the beginning of the synthesis of synthetic high molecular weight compounds, nowadays known as polymers.<sup>[1]</sup> The synthesis of polymers is achieved by connecting a large number of small molecules (monomers) to form a macromolecule.<sup>[2]</sup> Roughly one hundred years later, polymers, or plastics, are found in a wide range of materials, clearly impacting almost all aspects of human life. Packaging (food foils, Styropor<sup>®</sup>), building and construction (adhesives and sealing), automotive (tires, car seats), medical & health (prostheses, pill capsules), electronic devices (organic light-emitting diodes, device covers), agriculture (greenhouses, mulching films), and sport materials, are just a few areas in which plastics are crucial.<sup>[3]</sup> The world production of plastics in 2013 was nearly 300 million tons and has increased by ca. 3 % annually during the last decade.<sup>[3]</sup>

Keeping in mind how crucial plastics have become in a great variety of fields, it seems prudent to polymer chemistry to investigate improved synthesis procedures, to discover alternate polymer structures, and to develop new production processes, as well as to replace current and inferior materials with newly designed polymers.<sup>[4]</sup> The introduction of supramolecular polymers, polyrotaxanes, dendronized polymers, poly[n]catenanes, two-dimensional polymers (2DPs), and others over the last decade exemplify such a progress in polymer research. Still, the research of these complex polymer structures is in its infancy, thereby offering a variety of uncharted paths towards the synthesis and application of polymers.<sup>[5]</sup> This thesis presents an attempt to map out exactly one of these possible paths to synthesize new varieties of polymers such as polycatenanes<sup>[6–13]</sup> and 2DPs<sup>[14,15]</sup>.

Catenanes are interlocked macrocyclic molecules that are connected exclusively topologically (Fig. 1.1b). The transition to polycatenanes is achieved by enlarging the ring components.<sup>[9]</sup> If the macrocyclic rings are only connected linearly, then these are also referred to as poly[n]-catenanes. Synthetically the largest poly[n]catenane did not exceed more than seven repeating units (RUs),<sup>[16]</sup> and is therefore rather considered as an oligocatenane. The topological connection of poly[n]catenanes are clearly different to that of conventional polymers, which are usually linearly connected by covalent bonds (Fig. 1.1a). Research projects unique properties of these polymers in terms of rheology, as well as dynamic, mechanic, and thermal behavior.<sup>[12]</sup>

2D polymers represent a class of polymers which consist of laterally propagated repeating units, forming sheet-like structures (Fig. 1.1c). Junji Sakamoto and coworkers have defined these polymers as free-standing, one monomer unit thick, covalently bonded networks, having a long-

## 1. Introduction and Motivation

---

range order.<sup>[14]</sup> Such sheets with a structural designed precision (long-range order) could be useful for ultrafiltration, membrane support, catalysis, and others.<sup>[17]</sup> In nature, such 2D sheets are found in graphene, which can be obtained through the exfoliation of graphite e.g., through scotch tape peeling.<sup>[18,19]</sup> The first synthetic 2DP was thus obtained through rational organic synthesis in 2012 by Patrick Kissel *et al.*<sup>[20]</sup> A monomer was synthesized with three reaction sites, allowing for a lateral polymerization, which formed sheet-like layered structures in single-crystal upon irradiation. In this regard, the research of polycatenanes, in particular linear polycatenanes, is still somewhat lagging behind.

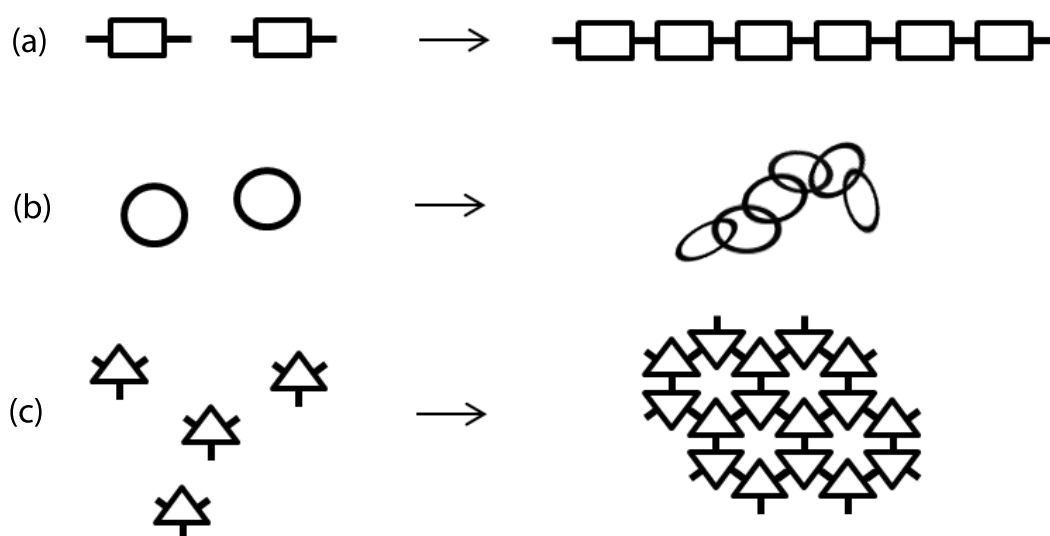


Figure 1.1: a) 1D polymerization, b) 1D poly[n]catenation, and c) 2D polymerization.

The difficulty in producing such remarkable and intricate polymer classes lies in avoiding unwanted and uncontrollable side reactions such as networking/cross-linking. Any attempt to synthesize poly[n]catenanes and 2DPs needs to take into consideration that such a synthesis is, in contrast to polystyrene or polymethylmethacrylate, significantly more complex. A great number of possible side reactions, which can lead to irregular, three dimensional network formation, need to be avoided altogether. To control such a reaction, current literature in the field made use of topochemical solid-state reaction within crystals. In a single-crystal, molecules are highly ordered and occupy a fixed position. In the 1960s, Gerhard Schmidt and Mendel Cohen observed and documented solid-state photoreactions of organic compounds, and thereby laid the foundation for what is today called crystal engineering.<sup>[21–23]</sup> Even 50 years later, the number of published articles concerning photoreactions in solid-state is small. This is probably due to the difficulty of controlling the internal crystal structure of molecules, which would allow

## 1. Introduction and Motivation

---

photoreactions in solid-state to take place. The difficulty is primarily caused by the impact of thermodynamic and kinetic effects on crystallization processes, which are both highly variable and therefore hard to predict.<sup>[24]</sup>

It needs to be noted, however, that topochemical reactions of crystals for the synthesis of poly[n]catenanes have yet not been extensively studied, while there has been reported success of this method in the synthesis of 2DPs.<sup>[20,25–28]</sup> The process of crystallization is, in any case, crucial for crystal engineering. Moreover, for an organic chemist crystallization is usually a purification step and thus a way to isolate the product. Attempts to control the internal structure within a crystal are not undertaken very often. Unraveling the molecular mechanisms that occur during crystallization of organic compounds remains a major scientific challenge.<sup>[29]</sup> Since chemistry alone cannot predict the crystal structure, interdisciplinary efforts including scientists from a variety of fields (chemists, crystallographers, spectroscopists, and theoreticians)<sup>[30,31]</sup> are necessary to understand the nature of crystal packing. Nevertheless, factors like functional groups, actual geometry of the molecule, sterics, and intermolecular interactions (solvent, counterion, host–guest molecules, and others) influence the crystallization process as well.<sup>[31,32]</sup> In consideration of these factors, organic molecules can therefore be, in a sense, designed for crystallization with uncertainty.<sup>[31,32]</sup>

The present work covers two topics with the common denominator of solid-state photoreactions. The first topic features the synthesis of a monomer to potentially synthesize poly[n]catenanes, while the second topic describes the synthesis of a monomer towards 2DPs.

### **Towards Poly[n]catenanes**

Many synthetic approaches to poly[n]catenanes were carried out, but all failed and led to ill-defined structures instead. Accomplishing a catenane requires two steps: the synthesis of all components required for threading and the process of threading itself. In addition, problems of low selectivity and inefficiency of cyclization are generally known in solution chemistry, while the polymerization to poly[n]catenanes requires repetition of threading and cyclization steps. This is the reason why such a polymerization is difficult to realize.<sup>[12,33]</sup> This work will focus on a novel strategy for polycatenation that takes advantage of a topochemical polymerization. In topochemical polymerizations, the monomers need to be pre-organized into an appropriate relative order.<sup>[22,34]</sup> This pre-organization presets a definite reaction process course unequivocally<sup>[35]</sup> and leads to a selective and quantitative polymerization. As of now, such a one-step process has not yet been established for the synthesis of poly[n]catenanes.

## 1. Introduction and Motivation

The use of a topochemical approach for poly[n]catenanes draws on Kissel's<sup>[25]</sup> research of the selective, quantitative topochemical cyclization of his U-shaped model compound **1** (Fig. 1.2a). Kissel's result are strengthened by XRD and NMR spectroscopy measurements. The process is based on a single-crystal-to-single-crystal (scsc) transformation<sup>1</sup>. In this model compound **1**, anthracene was used as connection site, due to its ability to undergo a [4+4]-cycloaddition upon irradiation above 300 nm with anthracene stacking face-to-face within the van-der-Waals distance (ca. 3.4 Å) to form the macrocyclic product **2**. This model compound and its dimerization in the crystal initiated the idea to extend such cyclization reaction to form poly[n]catenanes by designing a duplex U-shaped molecule **3** (Fig. 1.2b). The terphenylene unit from **1** is replaced by a terpyridine bridge, which is known to form octahedral or slightly distorted octahedral complexes upon metal ion addition.<sup>[36,37]</sup>

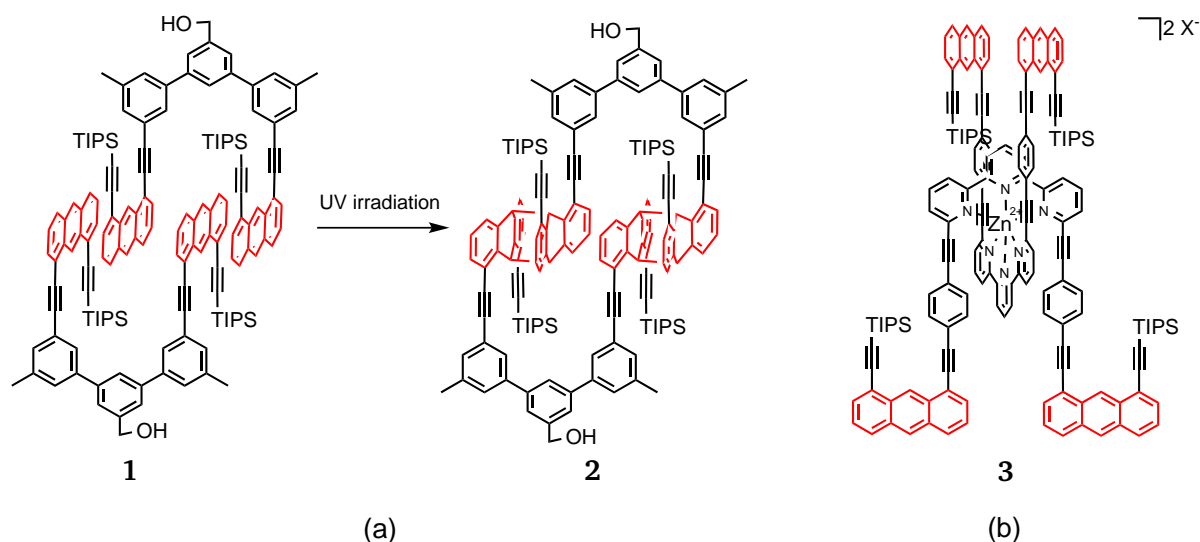


Figure 1.2: a) Kissel's topochemical macrocyclization and b) a potential monomer **3** for the synthesis of poly[n]catenanes.

Based on the mechanically connected macrocycles in a poly[n]catenane (no covalent bonds connecting the rings), properties of these polymers are speculated to be different than conventional polymers in terms of their independent motion by nearly free rotation, and the mobility of the linked rings (Fig. 1.3).<sup>[38]</sup>

Although the synthesis of a poly[2]catenane—which is structurally similar to poly[n]catenane—has been achieved, the properties of such a type of polymer remain unknown. This is due to the lack of documented large scale synthesis of the monomers and, in consequence, of polymers.

<sup>1</sup>The crystal shape retained during irradiation and was subsequently measured by XRD.



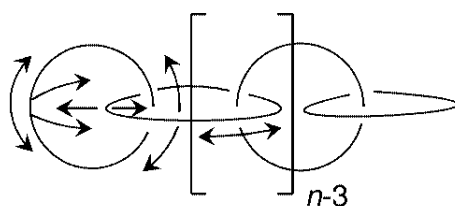


Figure 1.3: Rotation and mobility of the linked rings in a poly[n]catenane. Adapted from (Godt)<sup>[38]</sup> with permission from John Wiley and Sons.

### Towards 2D Polymers

As far back as several decades ago, there have been approaches to synthesize 2DPs through, for example, cross-coupling, self-assembly, parallel growth of  $n$ -stranded polymers in solution, or by confining monomers in two-dimensions and cross-linking them thereafter. A variety of approaches and suggestions for the synthesis of 2DPs are summarized in a review by Sakamoto *et al.*<sup>[14]</sup> In Dieter Schlüter's group, two methods for the synthesis of 2DPs have been tested: 1. through polymerization of monomers on the air/water interface and 2. through exfoliation of single-crystals with 2D stacked polymer sheets. The first method is based on the use of Langmuir monolayers, where monomers are spread onto the air/water interface, then compressed with barrier blocks to arrange in a 2D manner and polymerized by either photoirradiation (anthracene-based monomers)<sup>[25,39,40]</sup> or metal-complexation (terpyridine-based monomers)<sup>[41–43]</sup>. This approach is clearly advantageous in directly producing monolayers, and in offering the possibility of achieving square-centimeter sized sheets, which are only limited by the size of the Langmuir trough.<sup>[43]</sup> The second approach makes use of a single-crystal. Here the confinement of monomers leading to 2DPs is, as mentioned earlier, crucial. The size of resulting 2D polymer sheets is limited by the size of the crystal. In cases where the crystal retains its structural integrity after polymerization, a subsequent XRD measurement will give clear proof of a 2DP formation.

Three monomer sketches (M3, M4 and M6) are given to illustrate possible lateral polymerization (Fig. 1.4).

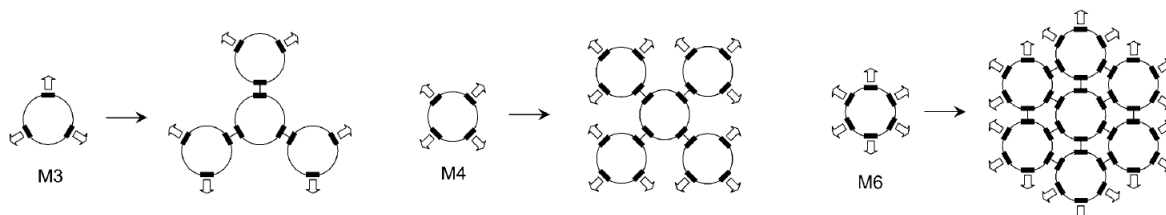


Figure 1.4: Three monomers M3, M4, and M6 with packing ideal for growth in two dimensions. Adapted from (Sakamoto *et al.*)<sup>[14]</sup> with permission from John Wiley and Sons.

## 1. Introduction and Motivation

An organic synthesis of a 2DP by photochemical single-crystal transformation has been achieved recently.<sup>[20,26]</sup> However, the structure of this first 2DP could not be proven by single-crystal XRD, due to essential structural changes that lead to disruption of the crystals during irradiation. The missing important proof in finally establishing this new class of polymers could now be provided with two independent monomers, the triazine-based double-decker monomer **4** by Max Kory *et al.* (Fig. 1.5a) and the triptycene-based monomer **5** by Kissel *et al.* (Fig. 1.5b).<sup>[27,44]</sup>

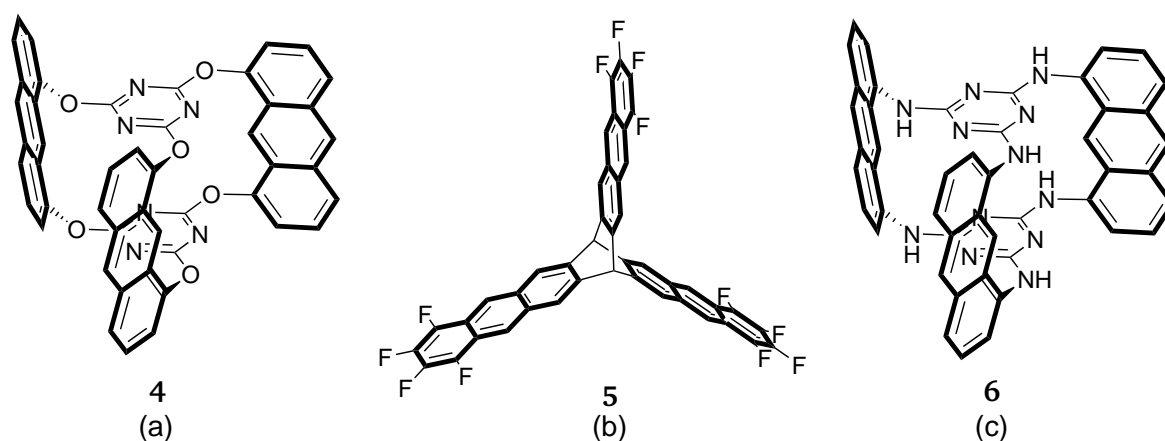


Figure 1.5: a) Kory's triazine-based monomer **4**, b) Kissel's triptycene-based monomer **5**, and c) an amine-bearing triazine-based monomer **6** for 2DP.

Both monomers (**4** & **5**) possess three anthracene units, which undergo photo-induced [4+4]-cycloaddition with adjacent monomers and laterally grow like M3 as depicted in Figure 1.4. The polymerized and depolymerized forms of the crystalline monomers were analyzed by single-crystal XRD (Fig. 1.6 and Fig. 1.7).<sup>[27,28]</sup>

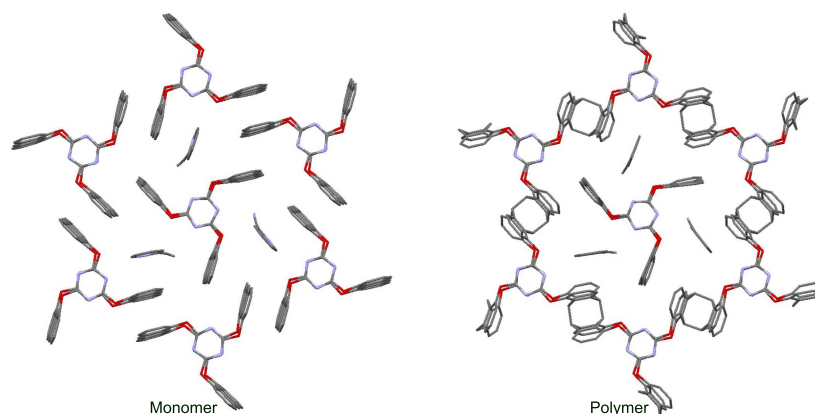


Figure 1.6: Kory's scsc transformation from 2D monomer to 2D polymer.<sup>[28]</sup>

## 1. Introduction and Motivation

---

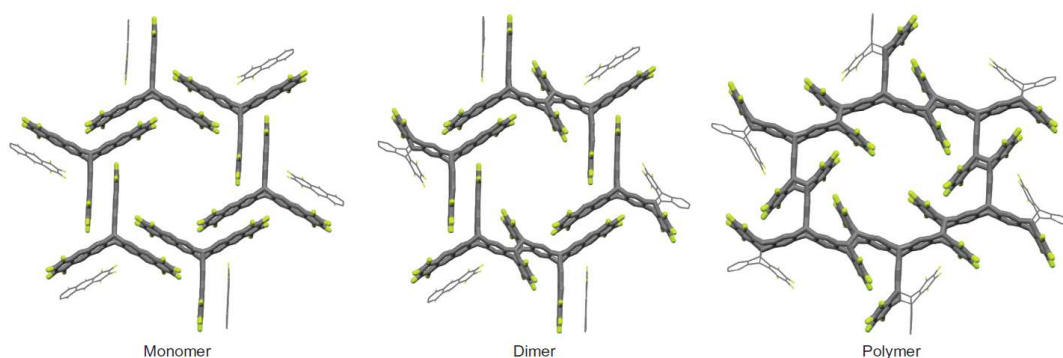


Figure 1.7: Kissel's scsc transformation from 2D monomer to 2D dimer and to 2D polymer (left to right). Reprinted from (Kissel *et al.*)<sup>[27]</sup> with permission from the Nature Publishing Group.

Free-standing monolayered sheets are obtained from such 2DP crystals through exfoliation. However, the exfoliation can be tedious and complex. Hence, it is of interest to have monomers and the respective 2DPs that simplify the process of exfoliation. The successful synthesis of the monomer by Kory *et al.* and its solid-state photopolymerization provided the motivation to aim at a similar amine-bearing monomer **6** (Fig. 1.5c), for which a particularly easy to perform exfoliation and possible functionalization is foreseen. This is expected to be caused by the presence of amine groups, which e.g., can easily be protonated.

The theoretical background of both topics will be clarified in the next chapter, followed by an overview of solid-state photoreactions, polycatenanes, terpyridine-based complexes for catenation, and 2D polymers.

## 2. Theoretical Background

### 2.1. Solid-state Photoreactions

#### General

With the development of X-ray structure analysis<sup>[45,46]</sup> the internal structure of crystals could be determined, and with spectroscopic techniques the progress of topochemical reactions were characterized.<sup>[22,47]</sup> Although synthesizing organic molecules already poses a challenge, taking a step further by attempting to crystallize such compounds is necessary. The XRD analysis of crystals and the improvement of computational simulations help to predict the crystal structure upon crystallization.<sup>[48]</sup> This process presents the foundation for crystal engineering.<sup>[22,32,48,49]</sup> The work of Schmidt and Cohen is seminal in this field. In the series of publications "Topochemistry Part. I to X",<sup>[21-23]</sup> Schmidt and coworkers set forth the "topochemical" factors for "reactions in solid-state with a minimum amount of atomic or molecular movement".<sup>[21-23]</sup> The work clarifies that the reacting bonds have to be parallel to each other at a distance of 3.5 Å - 4.2 Å.<sup>[22,50]</sup> The photoinduced dimerization of *trans*-cinnamic acid and also other [2+2]-photocycloadditions in solid-state belong to the well studied reactions in topochemistry.<sup>[21-23,32,51,52]</sup> The products of such reactions were in general almost inaccessible by other methods such as photoirradiation in solution.<sup>[52]</sup> This underlines the potential power of crystal engineering combined with topochemistry. An example of *o*-ethoxy-*trans*-cinnamic acid, which crystallizes in three different crystal structures namely  $\alpha$ -,  $\beta$ - and  $\gamma$ -polymorph by using different solvents for crystallization, and its photoreactions are shown to demonstrate the rules appointed by Schmidt (Fig. 2.1).<sup>[21-23]</sup>

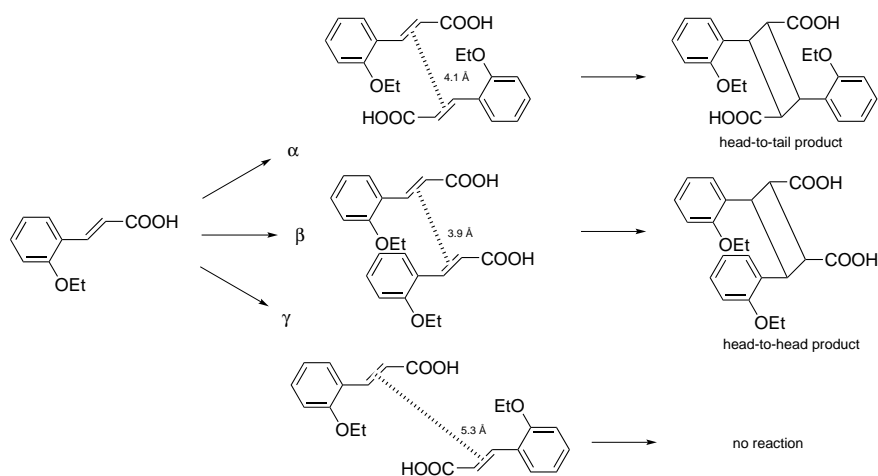


Figure 2.1: The photoreactions of  $\alpha$ -,  $\beta$ -, and  $\gamma$ -polymorph of *o*-ethoxy-*trans*-cinnamic acid.

## 2. Theoretical Background

Upon irradiation of each polymorph of *o*-ethoxy-*trans*-cinnamic acid, the  $\alpha$ - and  $\beta$ -polymorph undergo [2+2]-dimerization, while the  $\gamma$ -polymorph did not react.<sup>[50,51,53]</sup> The distances of the inter-olefinic bonds of  $\alpha$ - and  $\beta$ -polymorph were approximately 4 Å, which, according to Schmidt's research, allow for a photodimerization. The  $\alpha$ -polymorph was aligned in an *anti*-parallel orientation and dimerized head-to-tail, while the  $\beta$ -polymorph was aligned in a *syn*-parallel orientation giving a head-to-head photoproduct. The  $\gamma$ -polymorph did not undergo a dimerization due to the fact that the olefinic bonds were too far apart. In sum, the crystal structure of such photoreactive compound determines the stereoselective product, while in solution a mixture of all possible stereoisomers would be obtained.<sup>[53,54]</sup>

Schmidt's results are more or less in accordance with many other crystal structures found in the Cambridge Structural Database (CSD) that could undergo [2+2] photodimerization in solid-state.<sup>[55]</sup> Still, there are a number of reactions in which the distances were greater than 4.8 Å or where the double bonds were non-parallel.<sup>[56,57]</sup> In addition, a few crystal structures have shown a distance of double bonds that were within suitable range, but no reaction was observed.<sup>[56,57]</sup> These exceptions to the rule need to be taken into considerations as well.

The XRD measurement of a single-crystal captures the average space and time of the structure. This restricts statements of dynamic aspects, chemical impurities, or defect sites, which apply for crystals.<sup>[58]</sup> Considering these restrictions could help to explain the unusual chemical reactivity of molecules within the crystal not expected by topochemical reactions.<sup>[58]</sup> It is safe to assume that Schmidt's rules lack precision in discarding these unexpected photoproducts as defect site reactions, topochemically forbidden, or anomalous.<sup>[26,59]</sup>

9-Cyanoanthracene is a classic example of an anomalous solid-state photoreaction. Instead of the head-to-head product the head-to-tail product was obtained (Fig. 2.2).<sup>[58,60–65]</sup> Other specific anthracene related solid-state photodimerizations are discussed later.

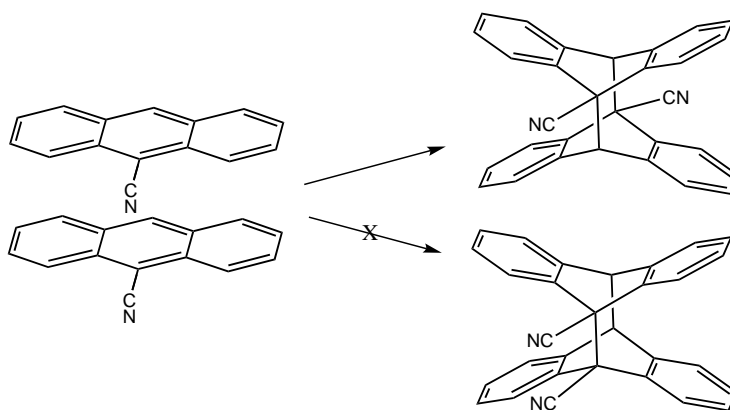


Figure 2.2: The anomalous solid-state photodimerization of 9-cyanoanthracene.

## 2. Theoretical Background

Many photoirradiated crystals suffer disruptions, because the overall stress in the crystal for the transition of starting material to product is partially too large (Fig. 2.3).<sup>[66,67]</sup> This makes drawing a conclusion from the irradiation process quiet difficult and necessitates a recrystallization of the photoproduct. However the recrystallization may give a different crystal structure expected from the pre-irradiated starting material.<sup>[58]</sup> A smooth transfer from starting material to product including the usually nearly unchanged shape of the irradiated crystal is known as single-crystal-to-single-crystal (scsc) transformation or as topotactic reaction (Fig. 2.3).<sup>[66,67]</sup> The XRD measurement of such crystal allows the direct analysis of the photoproduct, and recrystallization of the photoproduct is seldom necessary.

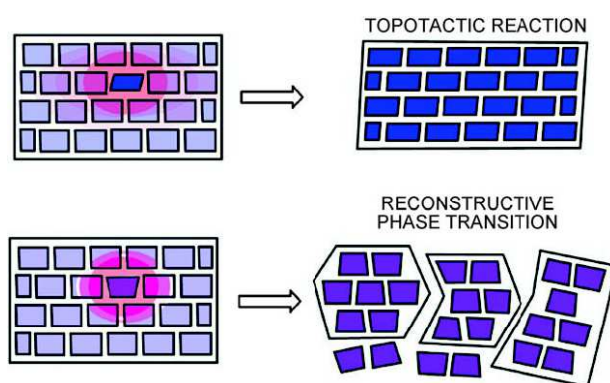


Figure 2.3: Single-crystal-to-single-crystal reaction (top) and a solid-to-solid reconstructive phase transition (bottom). Reprinted from (Garcia-Garibay)<sup>[66]</sup> with permission from John Wiley and Sons.

Due to its restrictive criteria, scsc transformations are quite rare. To achieve this, the process requires minor molecular changes of the atomic position in crystal leading to only a minor change in cell parameters to retain the crystal shape.<sup>[68]</sup>

Gerd Kaupp is therefore a strong advocate for the revision of the strict rules proposed by Schmidt.<sup>[26,59,69,70]</sup> Kaupp states that the molecular movement is crucial to the crystal structure and that genuine topotactic reactions only apply if no geometric change in the lattice, no chemical induced local pressure, and no molecular migrations are observed.<sup>[70]</sup> These observations were supported by his experiments with atomic force microscopy (AFM), scanning near-field optical microscopy (SNOM), grazing incidence X-ray diffraction (GID), and optical microscopy (OM). It has to be stated, however, that the topic of topotactic reactions is discussed controversially.<sup>[26,59,69,70]</sup>

The work of Gerhard Wegner (diacetylenes) and Masaki Hasegawa (diolefines) expanded the approaches of solid-state photoreactions to photopolymerizations (Fig. 2.4).<sup>[35,71–73]</sup> Polymerizations are usually performed in solution (or in bulk), where the monomers remain mobile and

## 2. Theoretical Background

disordered. In ordered systems, such as in a crystal, monomers have a defined position and orientation, and form polymers upon irradiation or heating.

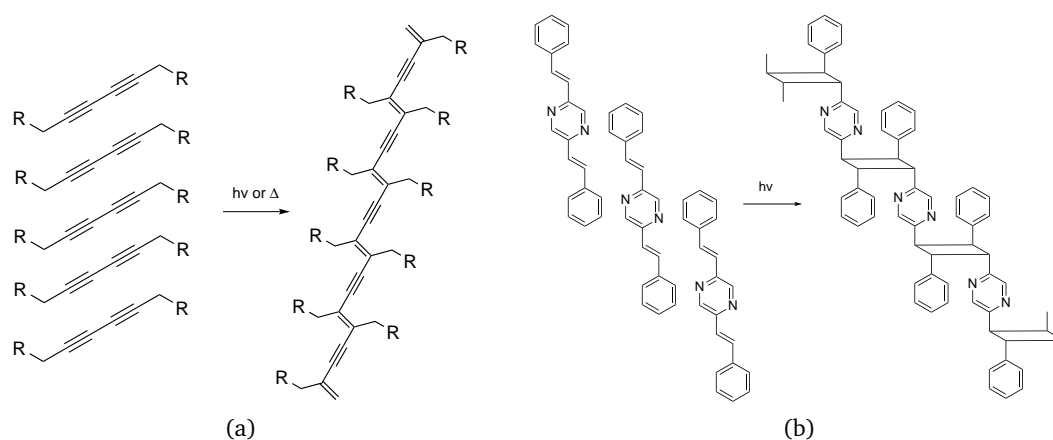


Figure 2.4: Solid-state photopolymerization of a) diacetylenes and b) 2,5-distyrylpyrazines. [54]

The mechanism of the solid-state photopolymerization is described by heterogeneous and homogeneous reactions. It was introduced and intensively explored by Wegner mainly with the poly(1,4-addition) of diacetylenes (Fig. 2.5). [35,54,71,74].

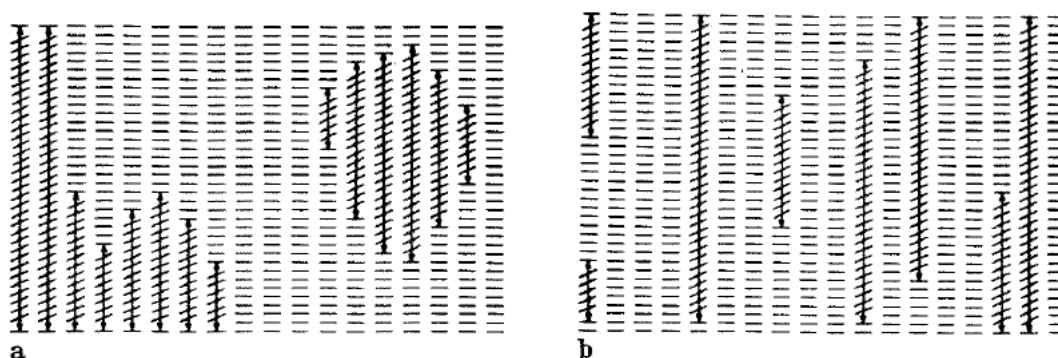


Figure 2.5: Heterogeneous (left) and homogeneous (right) reaction. Adapted from (Wegner) [74] with permission from the American Chemical Society.

A heterogeneous reaction takes place at distinct nucleation sites, which depend on defect sites and surface. Therefore the reaction is found heterogeneously in the crystal and generally destroys the crystal itself. [35,58] While homogeneous reactions are randomly spread within the crystal allowing the crystal shape to maintain. XRD analysis afterwards is then applicable and no additional recrystallization is needed. Keeping in mind that the absorption of light upon irradiation of a crystal is always greater at surface than on the inside, a pure homogeneous reaction cannot be achieved. [35,58] Nevertheless, to promote the homogeneous reaction, the chosen wavelength for irradiation is important. [75,76] Irradiation in the absorption tail of the crystal,

## 2. Theoretical Background

where the molar extinction coefficient is small, should give a higher probability to maintain the structure of the crystal.<sup>[35,58,77,78]</sup> Then the scsc transformation can be monitored by single-crystal XRD measurements.<sup>[58]</sup>

In principle this polymerization gives access to nearly defect-free polymer single crystals, which cannot be achieved with pre-built polymers from classical polymerization methods.<sup>[34,47]</sup> Wegner's classification (Fig. 2.5) in contrast to Garcia-Garibay's illustration in Figure 2.3 considers the difference of growing chains within the crystal and not only reactions involving dimerizations or intramolecular reactions of molecules at local sites within the crystal.

### Anthracene Dimerization

Anthracene was discovered in the process of coal tar distillation. When Carl Fritzsche exposed a saturated solution of anthracene to sunlight, a colorless crystalline compound precipitated, which, upon heating, transformed back to anthracene.<sup>[79-81]</sup> This reaction is illustrated in Figure 2.6.

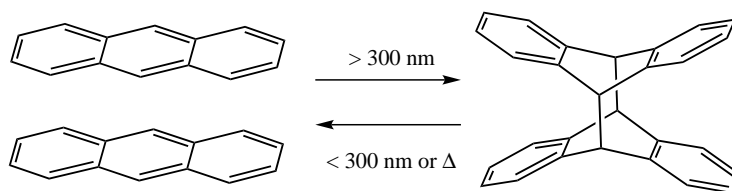


Figure 2.6: Photodimerization and backreaction of anthracene.

The illustration presents the anthracene dimerization via [4+4]-cycloaddition by irradiation with light above 300 nm (in absence of oxygen, as anthracene is sensitive to oxidation)<sup>[79,81-88]</sup> and the corresponding cycloreversion induced by UV light below 300 nm or heat.<sup>[79,89]</sup> The photoreaction of anthracene derivatives in solution may lead to a mixture of head-to-tail and head-to-head products (the ratio depends among others on the steric hindrance of the substituents; usually head-to-tail is dominant) involving the reaction of the central ring.<sup>[81,86,90]</sup> In a crystal structure the anthracenes are prearranged and ideally stack face-to-face in a distance around 4 Å (as discussed earlier). Upon reaction with light the stereoselective photoproduct of the dimer (9,9',10,10'-tetrahydrodianthracene derivative) is formed (see exception Fig. 2.2).<sup>[91]</sup> Anthracenes reacting at other sites than the central ring are rare and will further be omitted.<sup>[79,92-94]</sup>

Many aromatic rings (including anthracenes) reported in literature stack via  $\pi$ - $\pi$ -interactions in different orientations. The parallel face-to-face (often displaced), T-shaped edge-to-face, end-to-



## 2. Theoretical Background

face (Fig. 2.7), or completely offset  $\pi$ -interaction are common.<sup>[55,95–98]</sup> The general amount of anthracene compounds registered in CSD that fulfill Schmidt's rules and stack face-to-face are limited to ca. 130 (out of ca. 600k in 2011).<sup>[99]</sup>

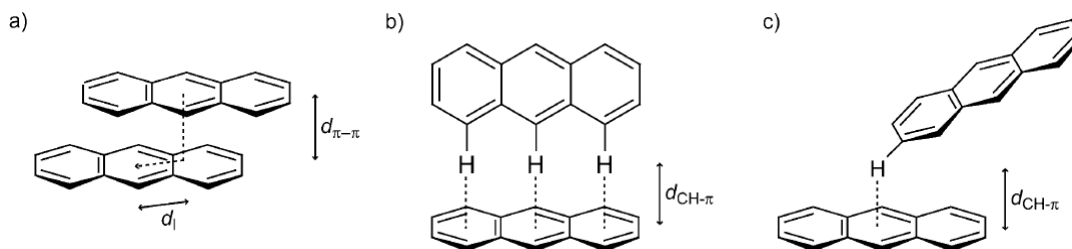


Figure 2.7: The  $\pi$ - $\pi$ -stacking of anthracenes: a) parallel displaced face-to-face, b) T-shaped edge-to-face, and c) end-to-face interactions. Reprinted from (Hinoue *et al.*)<sup>[98]</sup> with permission from John Wiley and Sons.

In order to control the crystal packing of anthracenes, the aim is to make use of interactions that enforce the face-to-face stacking arrangement, which allows for a pre-organization for solid-state photodimerization to take place. Sokolov and coworkers made use of a template that aligned the anthracenes via hydrogen bonding face-to-face (Fig. 2.8).<sup>[100]</sup>

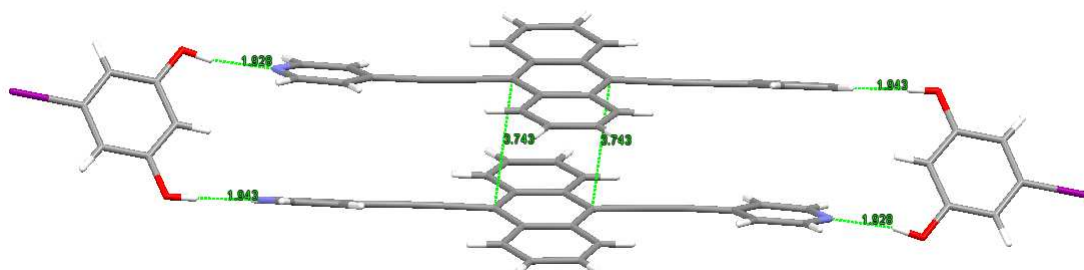


Figure 2.8: XRD crystal structure of an anthracene derivative, which stacks face-to-face induced by hydrogen bonding of a co-crystallizing molecule.<sup>[100]</sup>

End-fluorinated aromatic compounds tend to stack co-facial in an antiparallel way.<sup>[27,101,102]</sup> The use of anthracene 1,5-disulfonic acids (and salt derivatives, that cause ionic interactions as well) prevent the edge-to-face contact through the bulkiness of the sulfonates and increase the face-to-face stacking arrangement.<sup>[98]</sup> The crystal packing is also influenced by other factors in order to fill voids. For example, counterions (e.g., in salts or complexes) or solvents are often integrated in the crystal structure. The position and size of substituents in an aromatic compound have also a great influence to the crystal packing.

In order to prevent crystal cracking upon irradiation, the use of 1,8-disubstituted anthracenes was considered. It should allow to minimize the local structure changes caused by the photoreaction in terms of the distance relationship between adjacent anthracenes to maintain the

## 2. Theoretical Background

overall crystal lattice.<sup>[14]</sup> This is a measure taken for circumventing shrinkage or expansion which can be detrimental to topochemical reactions in general. The distance change before and after irradiation is projected in Figure. 2.9.<sup>[14]</sup>

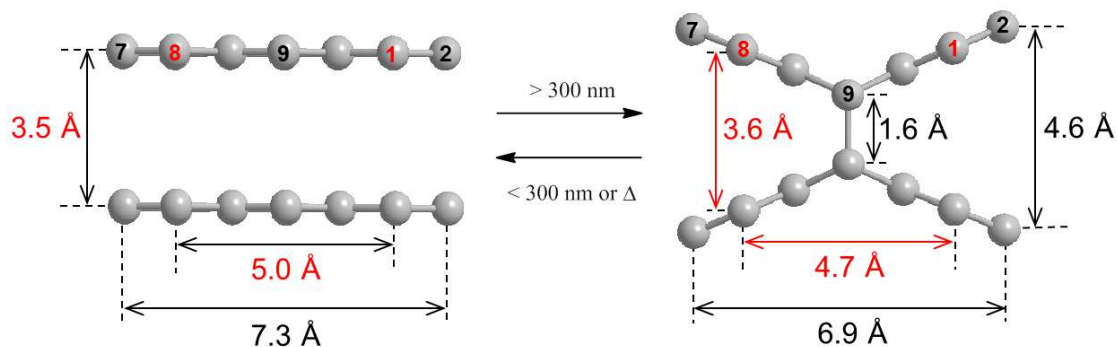


Figure 2.9: Distance measurements of the 1,8-disubstituted anthracene dimerization (side view).<sup>[14]</sup>

The distance between 1,4:1'4' and 5,8:5'8' remains almost the same (0.1 Å variance), the 9,10:9',10' position suffers from shrinkage (1.9 Å variance) and 2,3:2',3' and 6,7:6',7' from expansion (1.1 Å variance).<sup>[103]</sup> If the substituents are utilized at 1,4:1',4' or 5,8:5',8' position and properly chosen (considering bulkiness or other repulsive factors)<sup>[99]</sup>, the crystal should retain during irradiation and it is more likely to succeed the dimerization process.<sup>[103]</sup>

The reaction process itself is not only characterized by XRD measurements, but also by other established analytical tools. For example, with <sup>1</sup>H-NMR spectroscopy the 9,10-anthracene proton signals are upfield shifted upon dimerization to form the anthracene bridgehead signals (9,9',10,10'-tetrahydroanthracene). Many anthracene derivatives have a strong fluorescence spectrum, which is diminished upon dimerization.<sup>[81]</sup> With the help of IR spectroscopy measurements the difference between the change of the out-of-plane C-H (9,10) bend from the anthracene to the corresponding dimer should be sighted.<sup>[26,104]</sup>

Overall, the anthracene dimerization is a straightforward process, which has readily been explored. The controlled crystallization will remain as an open field for research. Since the amount of compounds for topochemical reactions in the CSD is still limited, it is a great platform to improve investigations in this field of science. With the use of anthracene in solid-state reactions the potential for novel compounds and applications are investigated.

## 2. Theoretical Background

### 2.2. Polycatenanes<sup>II</sup>

Catenanes<sup>III</sup> are obtained by interlocking macrocyclic molecules topologically with one another. Depending on the number [n] of rings, it may be generally called [n]catenane.<sup>[105,106]</sup> The first synthesis of a catenane was reported in 1960 by Edel Wasserman.<sup>[107]</sup> This catenane was formed by accident as result of a statistical reaction. One cycle was synthesized on purpose and another cycle formed by chance while being threaded in the first cycle, forming small amounts of [2]catenane. The other approach described by Gottfried Schill and Arthur Lüttringhaus is the direct synthesis by steric control.<sup>[108,109]</sup> In this approach a macrocycle is first synthesized and two alkyne chains were attached to the macrocycle. The end groups of the alkyne chains are able to react in an intramolecular fashion and upon reaction the chain junction of the alkyne chains at the first macrocycle is broken to form a [2]catenane. With these first synthetic encounters of interlocked molecules, a new concept was developed: molecules are not only connected by chemical bonds, but also recognize the existence of topological/mechanical bonds.<sup>[110]</sup> The first mass spectrum supported the existence of such bondings later as well<sup>[111]</sup> and shortly thereafter the first catenane structures in nature were reported in 1967 by Jerome Vinogra *et al.*<sup>[112,113]</sup> This natural evidence and probably the extravagance of such intriguing structures further stimulated the scientific research of catenanes. The first powerful strategy for catenane synthesis involving a metal ion as template (metallo-catenane = catenate) was developed by Christiane Dietrich-Buchecker and Jean-Pierre Sauvage (Fig. 2.10).<sup>[114–116]</sup>

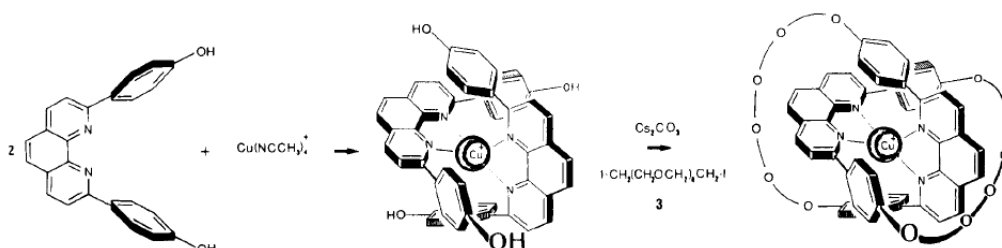


Figure 2.10: Catenate by metal ion templation. Reprinted from (Dietrich-Buchecker *et al.*)<sup>[115]</sup> with permission from Elsevier.

From there on, catenanes were mainly synthesized by this templation method. After removal of the metal ion, the interlocked rings are, except for their mechanical connection, in regards of their motion unrestricted to each other. Due to the fact that they are still able to bind with metal ions as ligands, they are also referred to as catenand.<sup>[115,117,118]</sup> Metal ions are an effective method for templation,<sup>[114,119]</sup> but there are other templation methods available

<sup>II</sup>Parts of this text have been taken from the diploma thesis.<sup>[103]</sup>

<sup>III</sup>Catenane is derived from the Latin word *catena*, which means "chain".

## 2. Theoretical Background

that make use of donor-acceptor effects<sup>[120,121]</sup>, hydrophobic interactions<sup>[116]</sup>, hydrogen bondings<sup>[122–124]</sup>, and assisted halogen bondings<sup>[125]</sup>.

The key step for the catenane synthesis is the cyclization. The Ruggli-Ziegler dilution principle<sup>[126,127]</sup> makes use of high dilution conditions, to promote intramolecular rather than intermolecular reactions. Reactions such as condensation reaction, electrocyclic reaction, cycloaddition, metal catalyzed cross-coupling, olefin metathesis (such as ring-closing metathesis)<sup>[128]</sup>, or others are effective for cyclization. A minor disadvantage for high dilution reactions is the limitation in upscaling due to the great amount of solvent involved.

Higher catenanes such as [3]-, [4]-, [5]catenane (olympiadane), and oligocatenanes were synthesized by iterative reaction steps.<sup>[16,129–131]</sup> With the iterative reactions one can hardly succeed in arriving to even higher degrees of interlocked systems in respect of polycatenanes. Polycatenanes are categorized in a variety of classes (e.g., linear, cyclic, branched etc.)<sup>[6–13]</sup> and shown in Figure 2.11.

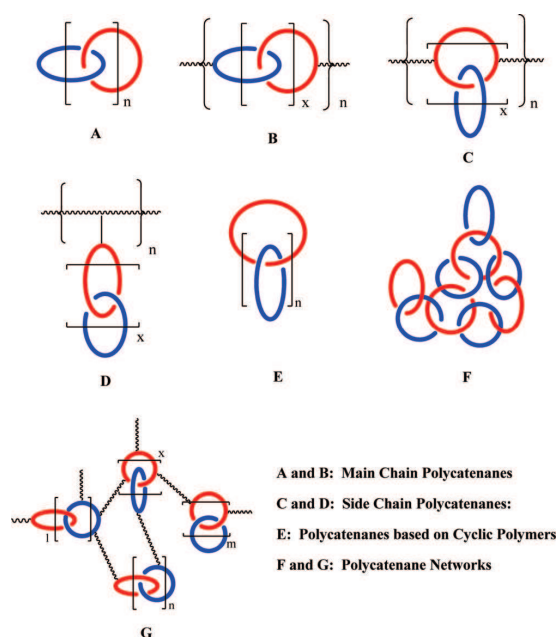


Figure 2.11: Classes of polycatenanes. Reprinted from (Niu *et al.*)<sup>[12]</sup> with permission from the American Chemical Society.

The only "true" polycatenane is the linear polycatenane (poly[n]catenane) shown in the figure as type A. Type B (poly[2]catenane) has been readily synthesized and is an alternating combination of regular covalent bonded molecules and mechanically interlocked macrocycles, and in terms of synthetic approaches the closest accessible polycatenane similar to the linear polycatenanes. Figure 2.12 comprises four possible routes towards poly[n]catenanes. In sum all of them failed and non of these approaches fulfilled its goal.

## 2. Theoretical Background

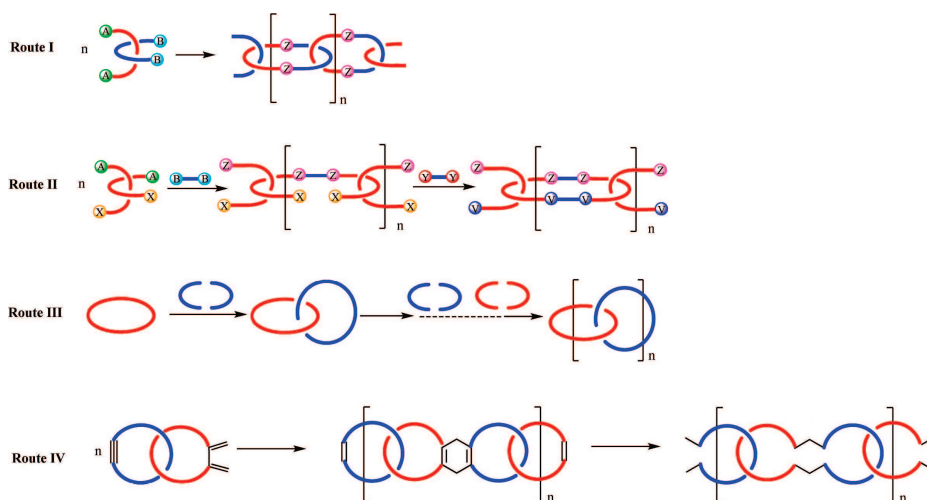


Figure 2.12: Strategies towards poly[n]catenanes. Adapted from (Niu *et al.*)<sup>[12]</sup> with permission from the American Chemical Society.

The failure to produce the expected results can be summarized as follows: Route I and its modification Route II are both template approaches which should in principle allow the reaction as an  $A_2B_2$ -type monomer (e.g., via acetylene homocoupling as of Glaser coupling)<sup>[132]</sup> towards a polycatenane.<sup>[6,12,133,134]</sup> However, the reactive sites will not prefer the intramolecular over intermolecular reaction unless forced by prearrangement, in a way leading to poly[n]catenanes. The outcome of such reaction is the ill-defined polymeric network caused by cross-linking and branching (Fig. 2.13). Route III, the iterative synthesis, leads to oligomers, but cannot be extended to the synthesis of polymers because of the inefficiency of the cyclization.<sup>[11,129,130,135]</sup> Route IV is so far the most promising approach by using a precursor which should, upon a post-polymerization treatment, convert from the "bridged" polycatenane (poly[2]catenane) to a poly[n]catenane.<sup>[11,33]</sup> While the Diels–Alder chemistry for the polymerization was successful, there has been no evidence or reported success of the bridge cleaving to furnish the expected poly[n]catenane. Even though similar concepts of Route IV (via electrocyclic reactions and ring fusing) were proposed, the poly[n]catenane is yet to be discovered.<sup>[38]</sup>

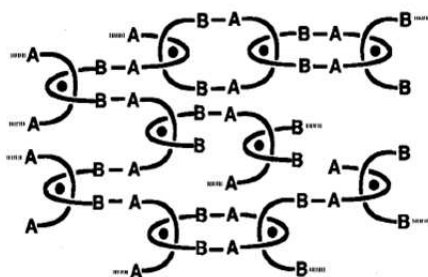


Figure 2.13: Ill-defined structure. Adapted from (Geerts)<sup>[8]</sup> with permission from John Wiley and Sons.

## 2. Theoretical Background

With a rise in interest in metal-organic frameworks (MOFs)<sup>[136]</sup>, many interpenetrating structures have been found and often were associated with polycatenanes. While the differentiation of these MOF type polycatenanes and the previous described polycatenanes is not part of this introduction, the reader is referred to the literature.<sup>[137-139]</sup> Nevertheless some 1D poly[n]catenane MOFs have been shown<sup>[140,141]</sup> and a recent example<sup>[142]</sup> shows the switching capability between a single macrocycle to a polycatenane or directly to a polycage (Fig. 2.14). But due to the inability of isolating the single polycatenane strands and the required incorporation of their metal connection, these can not be considered as poly[n]catenanes and will be omitted in this work.

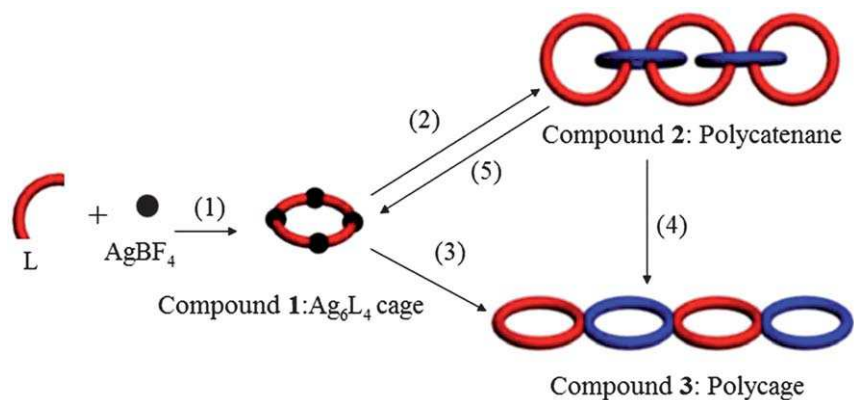


Figure 2.14: Synthesis of the macrocycle (1), its polycatenation (2), linkage to a polycage (3), reaction from a polycatenane to a polycage (4), and the backreaction from a polycatenane to the macrocycle (5). Reprinted from (Chen *et al.*)<sup>[142]</sup> with permission from the Royal Society of Chemistry.

### 2.3. Terpyridine-based Complexes for Catenation<sup>IV</sup>

In the 1930s, Gilbert Morgan and Francis Burstall reported the discovery of 2,2':6',2''-terpyridine (tpy, Fig. 2.15) and its complexation with iron salts forming a deep purple highly crystalline compound.<sup>[36,143,144]</sup> This was the beginning of terpyridine chemistry. In the last twenty years terpyridine compounds gained a great interest along with the demanding use in polymer chemistry for tuning optical and electrochemical properties, metal-mediated self-assembly, and others.<sup>[36,37,145–147]</sup> The relatively uncomplicated complexation with metal cations or protons<sup>[148–152]</sup> made tpy an interesting compound for chemical research. Figure 2.15 illustrates<sup>V</sup> the *trans-trans* conformation of tpy in solution, which presents a free uncoordinated ligand, while after metal cation ( $M^+$ ) addition, terpyridine is usually in a *cis-cis* conformation, forming octahedral or distorted octahedral bis-complexes.<sup>[36,153]</sup> This complexation is based on the chelate effect,<sup>[36,154,155]</sup> due to the three nitrogen atoms in tpy (tridentate ligand) binding with a metal ion, and the  $\pi$ -backbonding from the metal ion to the pyridines. Many examples of terpyridine derivatives and complexations to mono- and/or bis-complexes are shown in literature and a small perspective will be shown in this brief introduction.<sup>[36,37]</sup>

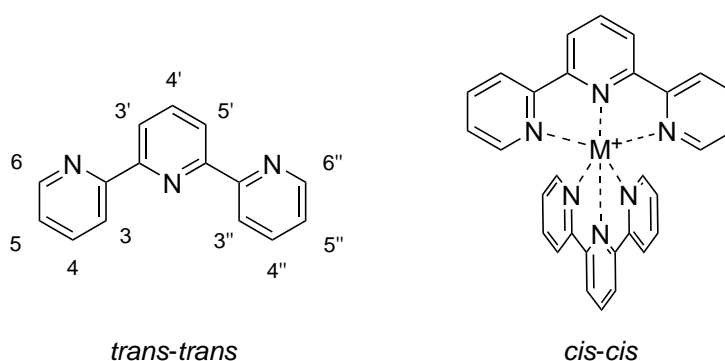


Figure 2.15: Atomic numbering of 2,2':6',2''-terpyridine and two possible conformations.<sup>[156]</sup>

The development of tpy chemistry lasted some time due to the many reaction steps involved in comparison with the comparable earlier discovered 2,2''-bipyridine (bidentate ligand), which has similar properties.<sup>[157,158]</sup> A benefit in using bis(terpyridine)-complexes, in contrast to bipyridine or phenanthroline complexes, is the capability of forming only two metal complexes (mono- or bis-complex) and these can only exist in one stereoisomeric form, while the bidentate ligands could form meridional and facial isomers as well.<sup>[148,156,159]</sup> Terpyridine derivatives are synthesized either by ring-assembly or by cross-coupling (Fig. 2.16).<sup>[36,37,160]</sup>

<sup>IV</sup>Parts of this text have been taken from the diploma thesis.<sup>[103]</sup>

<sup>V</sup>For practical reasons the structures of tpy derivatives shown in many figures in this work are drawn regardless of their actual conformation.

## 2. Theoretical Background

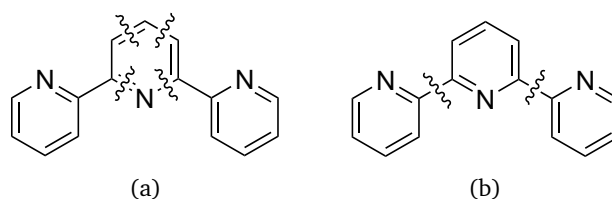


Figure 2.16: Methods of tpy synthesis via a) ring-assembly or b) cross-coupling.<sup>[37]</sup>

The ring-assembly is based on a Kröhnke condensation or a Kröhnke-type mechanism,<sup>[161,162]</sup> while the Pd(0)- or Pd(II)-catalyzed cross-coupling<sup>[163]</sup> is mainly performed by Suzuki<sup>[164,165]</sup>, Negishi<sup>[166,167]</sup>, or Stille<sup>[168,169]</sup> reaction. 4'-Substituted-terpyridines (4'-chloro-tpy<sup>[170,171]</sup> and 4'-hydroxy-tpy<sup>[170]</sup>) are commercially available and allow functionalization at the 4'-position leading to a very broad set of practical compounds e.g., for the use as metallo-supramolecules and polymers.<sup>[145,159,172–174]</sup>

Terpyridines were also introduced as ligands for the metal ion templation of a catenate by Jean-Pierre Sauvage and Michael Ward in 1991 (Fig. 2.17).<sup>[175]</sup> The 5,5''-disubstituted terpyridine was coordinated with Ru(II) and the ring was cyclized with a polyoxyethylene linker. Unfortunately, due to the stability of the complex, the demetallation of the Ru(II) catenate to achieve the catenane was unsuccessful<sup>VI</sup>. Even today ruthenium terpyridine complexes suffer demetallation due to the strong complex stability.

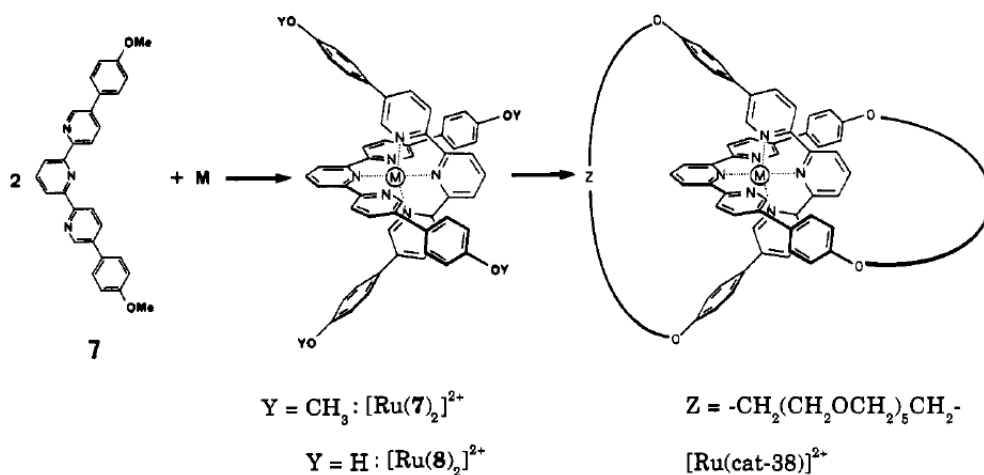


Figure 2.17: The catenation of a terpyridine derivative. Reprinted from (Sauvage and Ward)<sup>[175]</sup> with permission from the American Chemical Society.

Sauvage and Ward first considered using 6,6''-disubstituted tpy instead of the less readily available 5,5''-disubstituted tpy for the catenane approach, but due to the lability, weaker bonding,

<sup>VI</sup>Logically the use of some other metal cations forming more labile complexes e.g., Fe(II) were considered, but the reaction conditions to synthesize the complex were too harsh.



## 2. Theoretical Background

and steric hindrance caused by the spacer's<sup>VII</sup> "pinching" in the complexation (Fig. 2.18), the use of 6,6''-disubstituted tpy for this purpose was discontinued.<sup>[175–178]</sup>

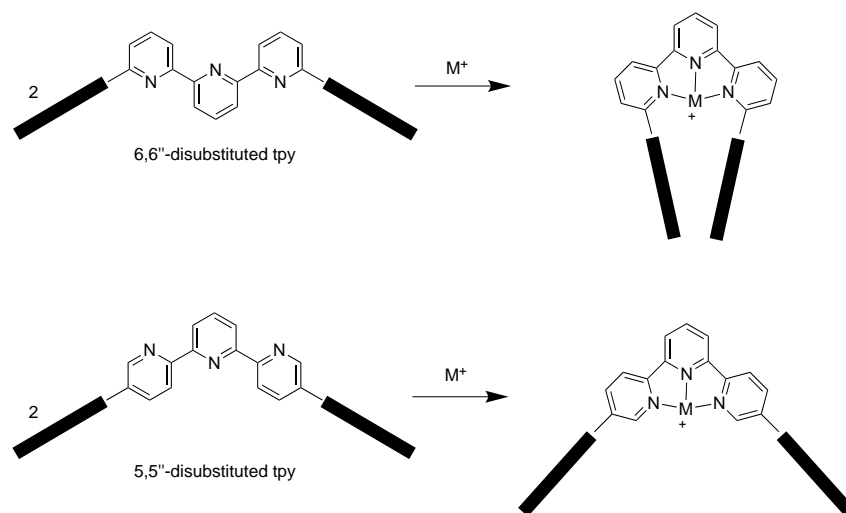


Figure 2.18: The complexation of a 6,6''-disubstituted tpy (top) and a 5,5''-disubstituted tpy (bottom).<sup>[175]</sup>

However, other researchers were interested in  $\pi$ - $\pi$ -stacking effects of 6,6''-disubstituted tpy complexes to understand the face-to-face interactions between the phenylene and pyridine rings. This gave notice of remaining  $\pi$ - $\pi$ -stackings in solution that allows control of the substituents orientation in the molecule (Fig. 2.19).<sup>[179]</sup> The self-recognition by  $\pi$ - $\pi$ -interactions of terpyridines was also observed earlier for various metal cation bis-complexes in solution and solid-state.<sup>[180]</sup> Nevertheless the synthesis, functionalization, and complexation of the 6,6''-disubstituted terpyridines are still insufficiently investigated. Combining these aforementioned investigations of 6,6''-disubstituted terpyridines evokes an exploration making use of the  $\pi$ - $\pi$ -stacking interactions for the poly[n]catenane approach presented in this thesis.

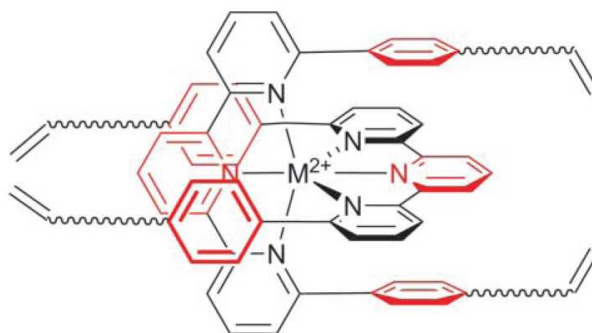


Figure 2.19: The  $\pi$ - $\pi$ -stacking of a 6,6''-disubstituted tpy complex. Reprinted from (Brauchli *et al.*)<sup>[179]</sup> with permission from the Royal Society of Chemistry.

<sup>VII</sup>Indicated as black boxes in the Figure. 2.18.

## 2. Theoretical Background

Monitoring the tpy complexation is easy by comparing the metal free tpy and the tpy complex with solution  $^1\text{H-NMR}$  spectroscopy. The demetallated "free" ligand changes its conformation from *trans-trans* to *cis-cis* by coordination of the pyridines with a metal cation. This causes a chemical shift of the proton signals (illustrated in Fig. 2.20) through the influence of the protons with the ring plane of the central pyridine by the neighboring ligand. With UV/Vis spectroscopy measurements, successful complexation is indicated through a bathochromic shift from the ligand absorption to the complex. In addition some metals cause a MLCT band, which gives absorption in the visible region causing colorful compounds.<sup>[37]</sup>

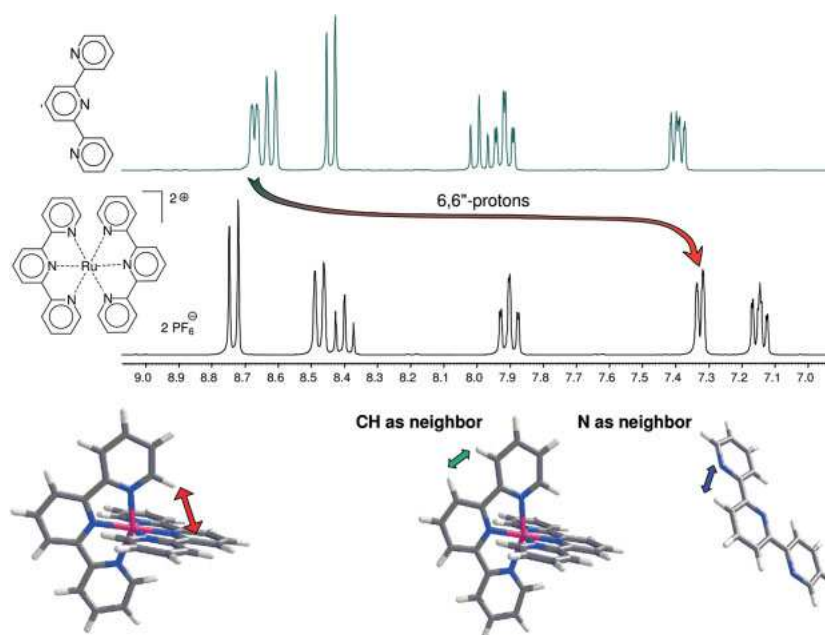


Figure 2.20:  $^1\text{H-NMR}$  spectra of a tpy and its Ru(II) bis-complex. Reprinted from (Schubert *et al.*)<sup>[36]</sup> with permission from John Wiley and Sons.

The following paragraphs illustrate the self-assembly and directional orientation of terpyridines by some examples.

Terpyridine units in supramolecular structures help self-assembly through the directional orientation by its metal complexation. The term of "Playing LEGO<sup>®</sup>" seems applicable,<sup>[181]</sup> as the on paper planed structures become more or less reality by assembling together the appropriate structures later in the flask. Literally this is playing with molecules to form (and often luckily) some extravagant structures. The additional  $\pi$ - $\pi$ -interactions of the substituents with terpyridines eventually led to grid like structures<sup>[182,183]</sup> (Fig. 2.21a) and duplex cleft complexes<sup>[184]</sup> (Fig. 2.21b).

## 2. Theoretical Background

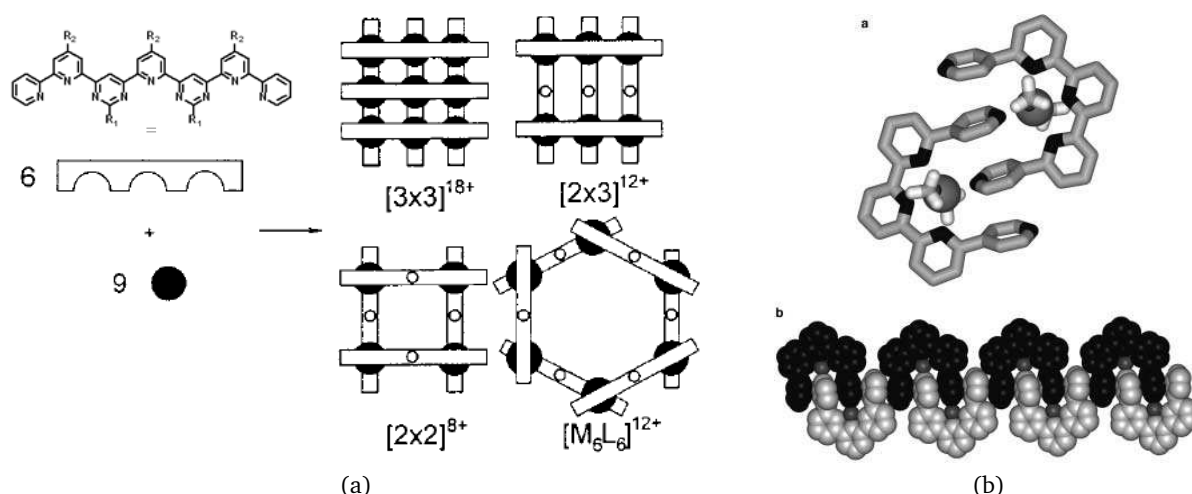


Figure 2.21: a) Terpyridine LEGO<sup>®</sup> like structures and possible combinations. Reprinted from (Breuning *et al.*)<sup>[183]</sup> with permission from John Wiley and Sons. b) XRD crystal structures of the duplex cleft (top) and its spacefilling packing (bottom). Reprinted from (Barboiu *et al.*)<sup>[184]</sup> with permission from John Wiley and Sons.

Ibrahim Eryazici and coworkers were able to form a dinuclear metallomacrocycle by complexation of four terpyridine units. This metallomacrocycle was crystallized and proven with XRD analysis (Fig. 2.22).<sup>[185]</sup> This self-assembled structure was synthesized in 89 % yield by simply adding equimolar amount of iron salt followed by a counterion exchange with  $\text{NH}_4\text{PF}_6$ . The same scientific group was able to document another series of self-assembled molecules forming not only dimer, but also trimer and tetramers, simply by variation of concentration and temperature.<sup>[186]</sup> Self-assembled structures in form of squares<sup>[187,188]</sup> and cages<sup>[189]</sup> of terpyridine derivatives were reported as well (Fig. 2.23).

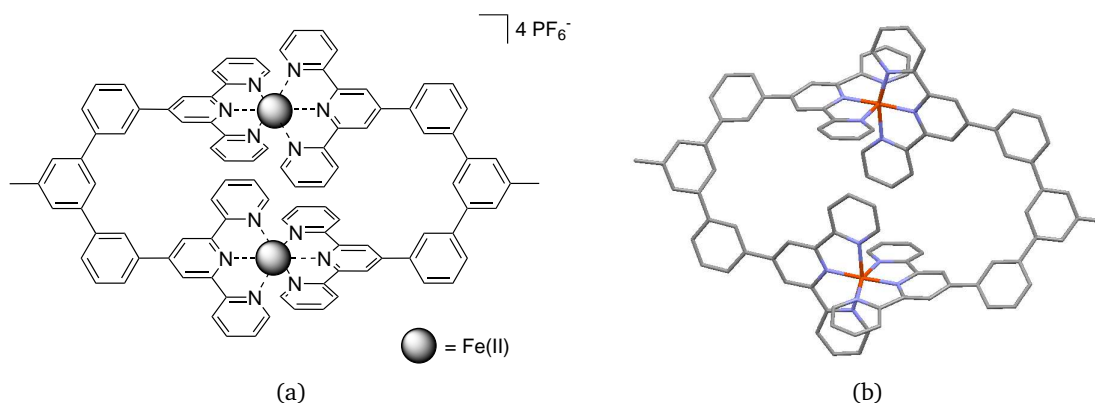


Figure 2.22: a) Scheme and b) XRD crystal structure of an interlocked dinuclear terpyridine metallomacrocycle.<sup>[185]</sup>

## 2. Theoretical Background

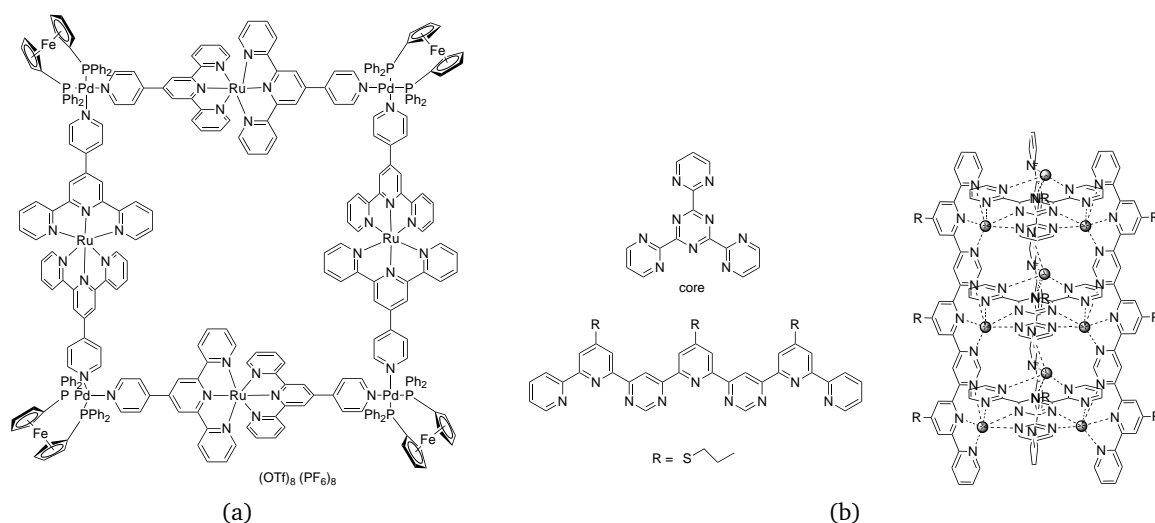


Figure 2.23: a) A square complex<sup>[188]</sup> and b) a cylindrical cage complex<sup>[189]</sup> by self-assembly.

The list of such remarkable structures is never-ending. A reasonable approach is the incorporation of terpyridine units for block-copolymer synthesis. Two independent polymer chains that each possess a terpyridine end group, are combined through metal cation addition only.<sup>[190]</sup> A monomer or a polymer chain that contains two terpyridine units in the molecule, could be used for polymerization by metal cation coordination of both tpy units (Fig. 2.24). This is known as coordination polymers, metallo-supramolecular polymers, and sometimes linked to polyelectrolytes.<sup>[191,192]</sup>

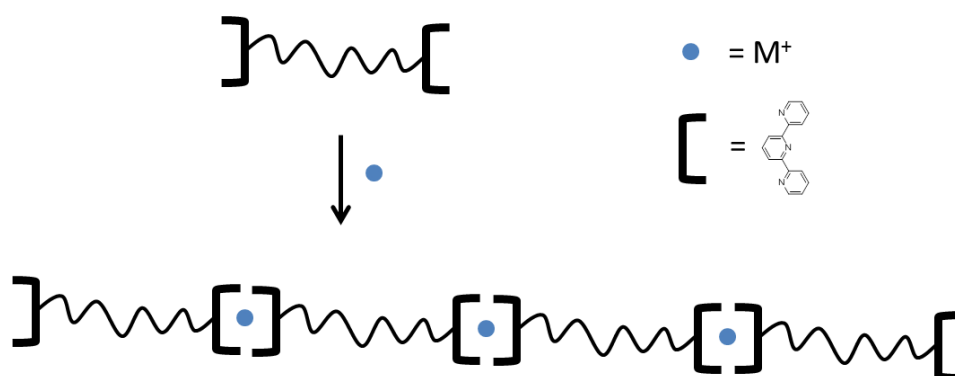


Figure 2.24: Cartoon of a metallo-supramolecular polymerization with terpyridine as connecting unit.<sup>[191]</sup>

The field of coordination polymers has been expanded with the combination of supramolecules and polymers over the last few decades.<sup>[173,181]</sup> The complex stability for such coordination polymers is crucial and dependent on the chosen metal ion. Properties can be influenced by simply changing or exchanging the metal ion in the polymer.<sup>[193]</sup> The reversibility of labile complexes is triggered by UV irradiation, temperature change, redox chemistry, variation of pH, or

## 2. Theoretical Background

by addition of competitive ligands.<sup>[191,194–198]</sup> With these often simple applied methods, novel responsive materials were created.<sup>[37,173,199]</sup>

The example of a metallo-supramolecule, shown in Figure 2.25a, makes use terpyridine complexation and also hydrogen bonding. This polymer could be altered by changing some of the reaction conditions aforementioned. A more general overview of possible metallo-supramolecular polymers is illustrated in Figure 2.25b.<sup>[197,200]</sup> Although these are subtle methods to achieve a variety of metallo-supramolecules, the characterization in contrast to "conventional" polymers is difficult due to the stability of these coordination polymers that are effected by partial or full decomplexation, unwanted charges, and/or paramagnetism. Usual characterization methods such as NMR spectroscopy, GPC, MALDI-TOF analysis, light scattering, viscosity measurements, and others could be useless or a struggle for such polymers.<sup>[36,37,148]</sup>

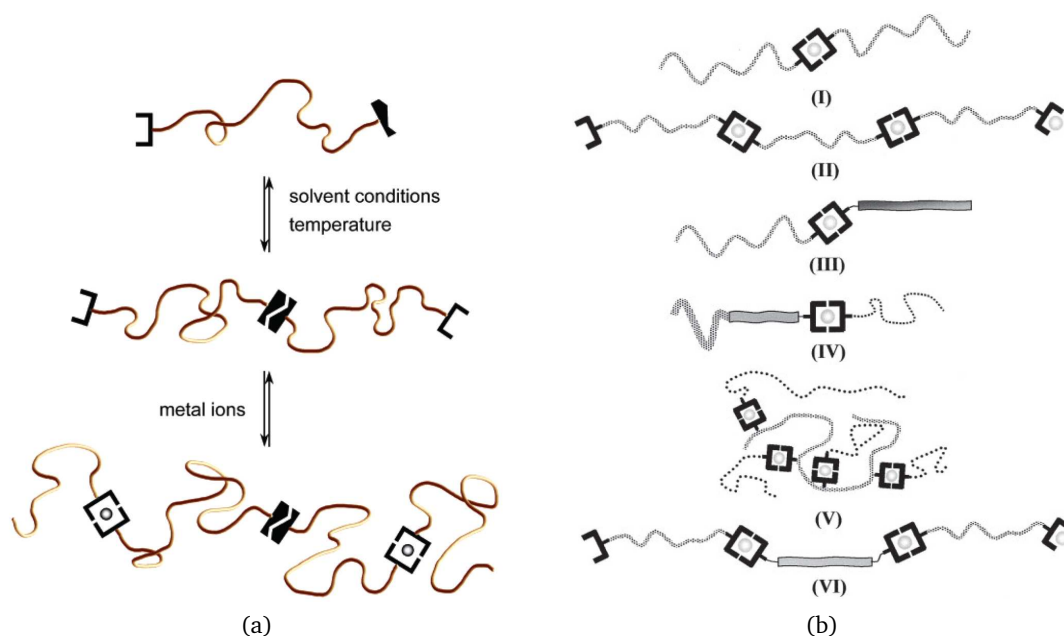


Figure 2.25: a) Cartoon of a polymer synthesized by non covalent bonds, both hydrogen and terpyridine complexation. Reprinted from (Hofmeier *et al.*)<sup>[197]</sup> with permission from the American Chemical Society. b) Cartoon of potential metallo-supramolecular polymers. Reprinted from (Lohmeijer and Schubert)<sup>[181]</sup> with permission from John Wiley and Sons.

### 2.4. 2D Polymers

Classic monomers that undergo polymerization usually propagate in one-dimension and form a polymer chain (Fig. 2.26a). Growth in two-dimensions leads to a sheet-like two-dimensional polymer (2DP). This implies a monomer with at least three reactions sites to form such a sheet (Fig. 2.26b).

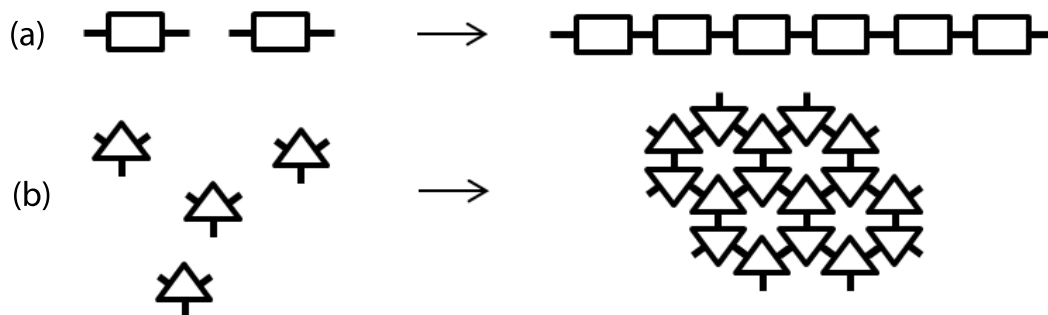


Figure 2.26: a) 1D polymerization and b) 2D polymerization.

The definition of a polymer is based on Staudinger's profound work on macromolecules. Extending this definition for polymers in two-dimensions causes confusion when researching literature. Many two-dimensional materials were referred to as 2DPs and many objects that formed in two-dimensions such as cross-linked 1D polymers, have been defined as such.<sup>[201]</sup> The reader is referred to a few articles and reviews as elaboration on the context.<sup>[14,15,202,203]</sup> A general definition of a 2DP was missing, until Schlüter's group introduced its definition in 2009:

"...one monomer unit thick, covalently bonded molecular sheet with a long-range ordered (periodic) internal structure..."<sup>[14]</sup>

Other definitions are less limiting, such as from Benjamin King's group, which considers "a monolayer of RUs connected by robust bonds",<sup>[26]</sup> while the order could also be represented as different patterns of *tilings*.<sup>[26]</sup> An example of square tiling is given in Figure 2.27, in which the RUs are the vertices connected by edges that cover the plane.<sup>[26,204]</sup>

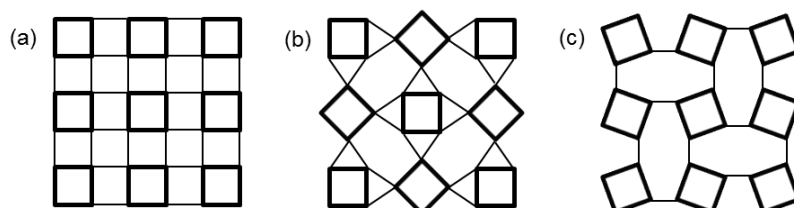


Figure 2.27: a) Connected squares, b) rotation of individual squares, and c) rotation of all squares with different connectivity.<sup>[204]</sup>

## 2. Theoretical Background

In contrast, John Colson and William Dichtel included "all types of covalently linked networks of monomers that have a periodic bonding in two-dimensions such as in layered crystals, multilayers or monolayer films on surfaces or free-standing sheets".<sup>[4,15]</sup> In general, linear polymer chains have been identified as individual chains, regardless of whether they are in bulk or in solution,<sup>[4]</sup> in contrast to synthetic 2D polymers, which only have recently been achieved and identified as individual sheets.<sup>[20,26–28]</sup> The distinction of individuality is an important feature/characteristic and should be taken into consideration for the 2DP definition.<sup>[4]</sup> It should be noted that the definition of a 2DP is still in debate. In spite of that, to understand the basic features of a 2DP, (free-standing) single sheets need to be isolated in order to then explore their potential properties of sheets in these very thin dimensions. It is safe to argue that subsequent investigations of multiple stacked sheets may show other interesting characteristics/features. Historically, the first approaches towards 2DP entities, by an interfacial polymerization on the air/water interface, were reported by Gee *et al.* in the 1930s.<sup>[205–208]</sup> The interfacial approach produced a two-dimensional cross-linked material as an ultrathin film. However, the internal order of this thin film was not proven.<sup>[39,43,209]</sup>

In general, a major difference between thin films of 1D and 2D polymers is that the latter can structurally be described in terms of their repeating units and govern mechanical stability through covalent bonds between the RUs. Thin films of linear polymers lack this internal order and their stability derives from cross-linking and entanglement (Fig. 2.28).<sup>[4]</sup>

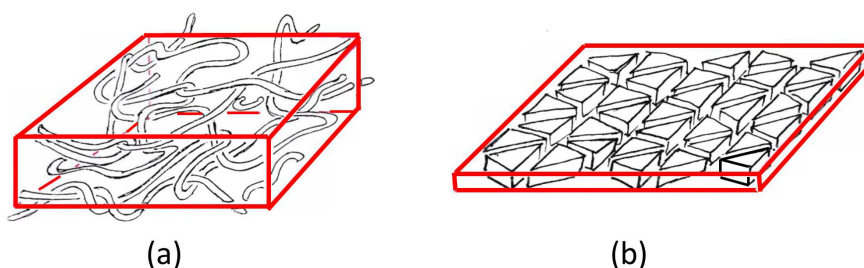


Figure 2.28: a) A cross-linked and entangled polymer film and b) a 2D polymer layer.<sup>[4]</sup>

In nature, 2DPs occur in graphite as layered graphene,<sup>[18]</sup> as well as in inorganic layered crystals such as  $(\text{BN})_x$ <sup>[210,211]</sup>, and  $\text{MoS}_2$ <sup>[210,212]</sup>. The materials are therefore either provided by nature or synthesized under harsh conditions allowing no functionalization of the sheets. Functionalizing either one or both sides of a sheet would be of great interest to many organic and polymer chemists.<sup>[14]</sup> Therefore, the chosen conditions to synthesize a 2DP should be mild in order to control the sheet formation and potential functionality.<sup>[201]</sup> Many metal-organic frameworks (MOFs), covalent organic frameworks (COFs), and inorganic nanosheets have been reported

## 2. Theoretical Background

in forming two-dimensional sheets,<sup>[213–216]</sup> some of them as monolayers.<sup>[217–224]</sup> Most COFs and MOFs are prepared by simultaneous reaction and crystallization, which means that bonds form while the crystal grows.<sup>[27,28]</sup> Occurring defects can only be healed if the formed bonds are reversible. In addition, COFs are often held by interlayer van-der-Waals interactions, which templates the COF formation.<sup>[216,225]</sup> These interactions make exfoliation of such layered structures difficult.<sup>[20]</sup> Synthesis of 2DPs were also addressed by other methods, such as on a solid surface, air/liquid interface, or in layered crystals.<sup>[14,20,27,226]</sup> On a solid surface only nanometer sized sheets were obtained and problems with transferability occurred. The air/liquid interface approaches attempted lateral polymerization up to square-centimeters sized sheets on the Langmuir trough by either complexation or photoreaction. However, the internal structure of the resulting sheets are still unproven.<sup>[39–43]</sup> In 2012, the first rational organic synthesis of a 2DP was reported via photopolymerization in single-crystal and exfoliation of the layered 2DP sheets by Kissel *et al.*,<sup>[20,25,227]</sup> followed by another similar attempt by Radha Bhola *et al.*<sup>[26]</sup>. Both single-crystal approaches were lacking in the proof of a single-crystal XRD of the 2DP due to disruption of the crystals during photoirradiation.

Recently, this missing piece in proving a two-dimensional polymerization by single-crystal XRD was achieved by two independent attempts (Fig. 2.29 & 2.30).<sup>[27,28]</sup>

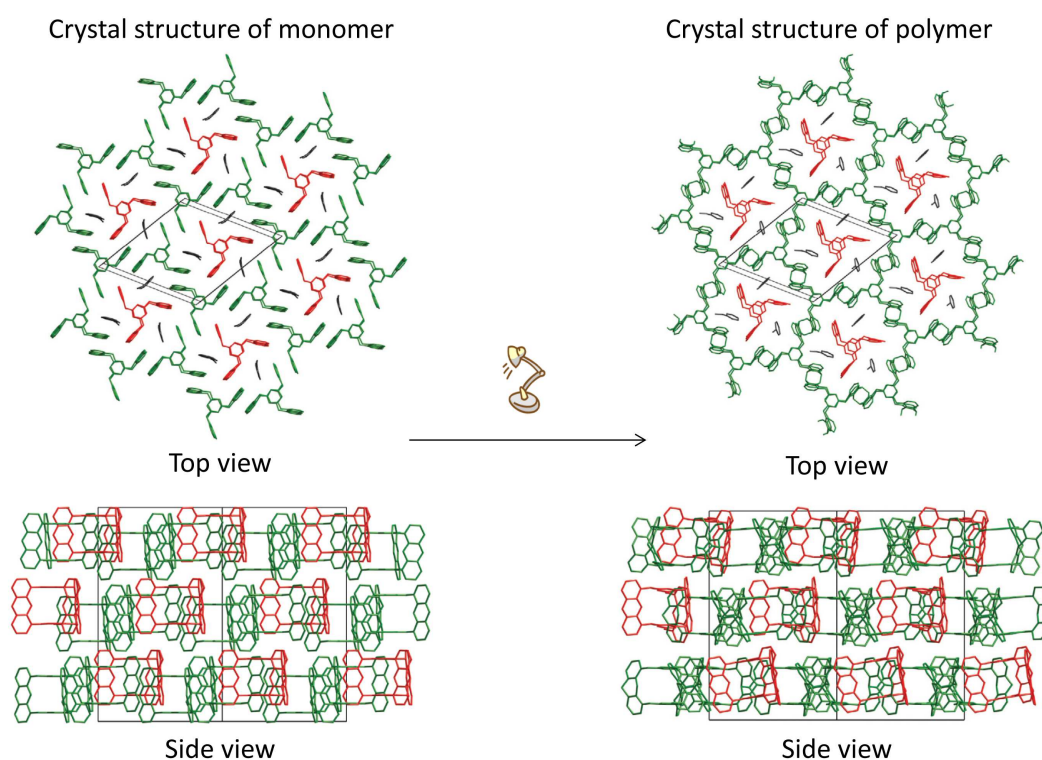


Figure 2.29: Spsc transformation from 2D monomer to 2D polymer by Kory *et al.* Adapted from (Kory *et al.*)<sup>[28]</sup> with permission from the Nature Publishing Group.



## 2. Theoretical Background

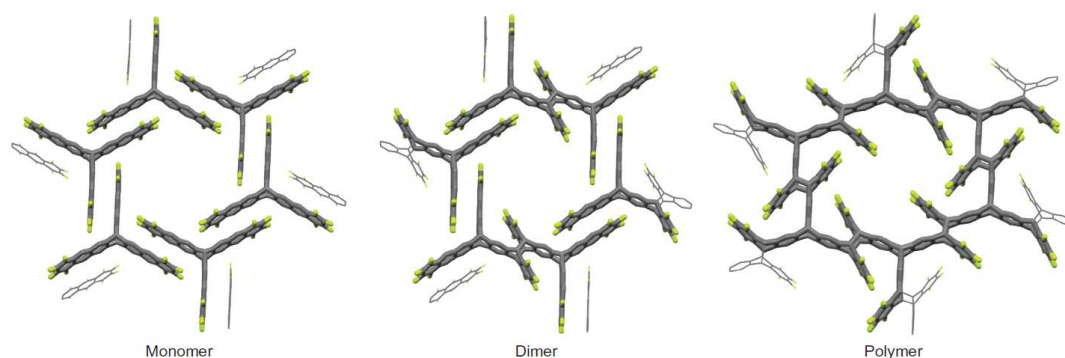


Figure 2.30: Spsc transformation from 2D monomer to 2D dimer and to 2D polymer by Kissel *et al.* Reprinted from (Kissel *et al.*)<sup>[27]</sup> with permission from the Nature Publishing Group.

Both attempts used propeller-shaped monomers that differ in the relative orientation of their anthracene units, which undergo photo-induced [4+4]-cycloaddition with adjacent monomers. The thermal backreaction/depolymerization was also documented. After polymerization, the 2DPs were exfoliated by swelling in NMP for several days and characterized with AFM and SEM. The polymer sheet sizes are basically limited by the size of the crystals.

Henceforth, the synthetic paths towards 2DPs are laid; still, the development of large scale synthesis protocols to elaborate upon the properties and applications of 2DPs needs to be addressed. It is clear that fundamental questions of 2DPs, such as the mechanical stability, stress/strain behavior, deformation, and many others remain unanswered. Possible applications are, for example, thin membranes or molecular sieves for desalination<sup>[27,41]</sup>, selective transport<sup>[228]</sup>, gas separation and storage<sup>[15]</sup>. Proceeding with the development of novel monomers for 2DP synthesis increases the chance to receive earlier answers to remaining fundamental questions.

### 3. Goal

#### Part A: Poly[n]catenane

As mentioned earlier, the synthesis of a poly[n]catenane was yet unsuccessful. With the present strategy illustrated in Figure 3.1, a new concept to synthesize a poly[n]catenane is described.

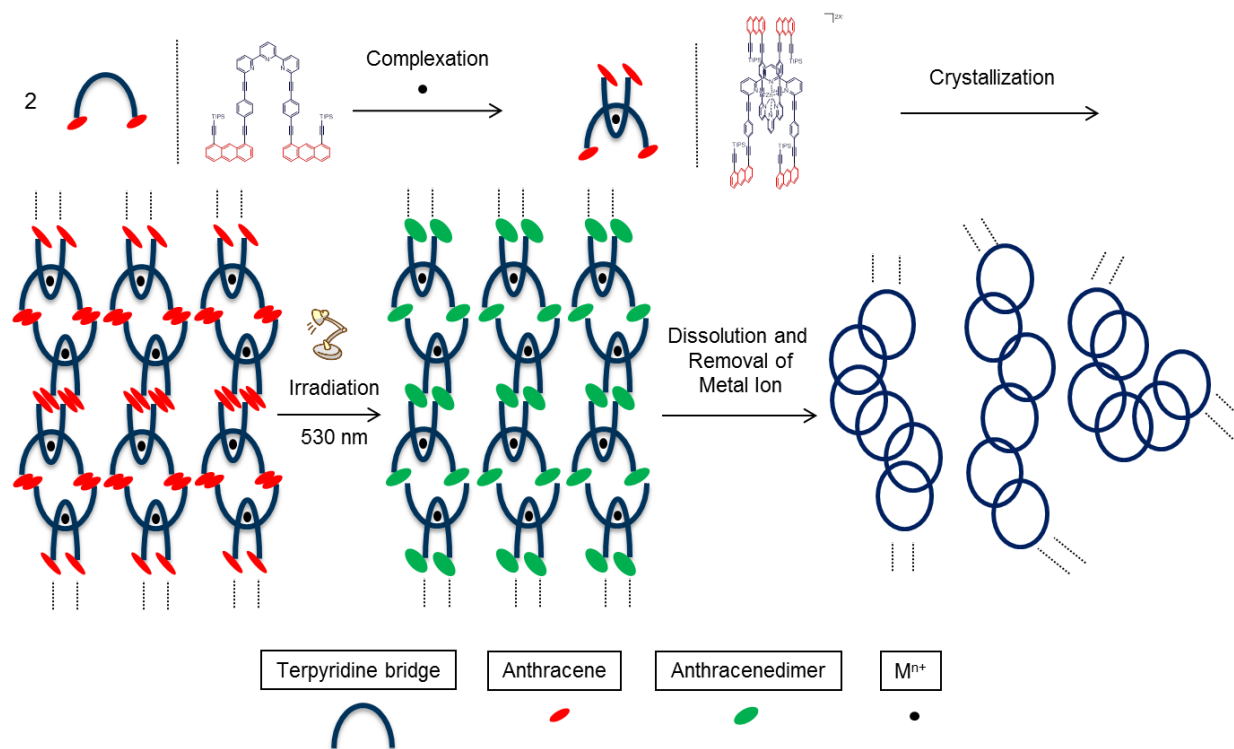


Figure 3.1: Cartoon representation of the synthesis strategy towards poly[n]catenane.

First, the U-shaped molecule **7** (terpyridine ligand) that carries two anthracene units is prepared and then interlocked with another through metal complexation to furnish a duplex U-shaped molecule **3**, which serves as monomer. The monomer's backbone is designed to be rigid in order to control its conformation, which is necessary for it to be suitable for the subsequent pre-organization. Secondly, this monomer is crystallized into a single-crystal in which the monomers are 1D-arrayed in a way that lets the anthracene parts be stacked face-to-face across the monomers. Thirdly, this 1D-array is covalently fixed by photo-induced [4+4]-cycloadditions between the anthracene pairs in the crystal. Finally, the irradiated crystal is dissolved with solvent in order to isolate the poly[n]catenane individually. The metal cations can be washed off with a competitive chelating reagent, such as HEEDTA (N-(2-Hydroxyethyl)ethylenediaminetriacetic acid).<sup>[191,194–197]</sup> The expected persistence length of the present poly[n]catenane would

### 3. Goal

be drastically altered by addition/removal of metal salts. This may suggest its application to responsive materials.

#### Part B: 2D Polymer

The present strategy to arrive at 2D polymers (2DPs) is schematically illustrated in Figure 3.2.

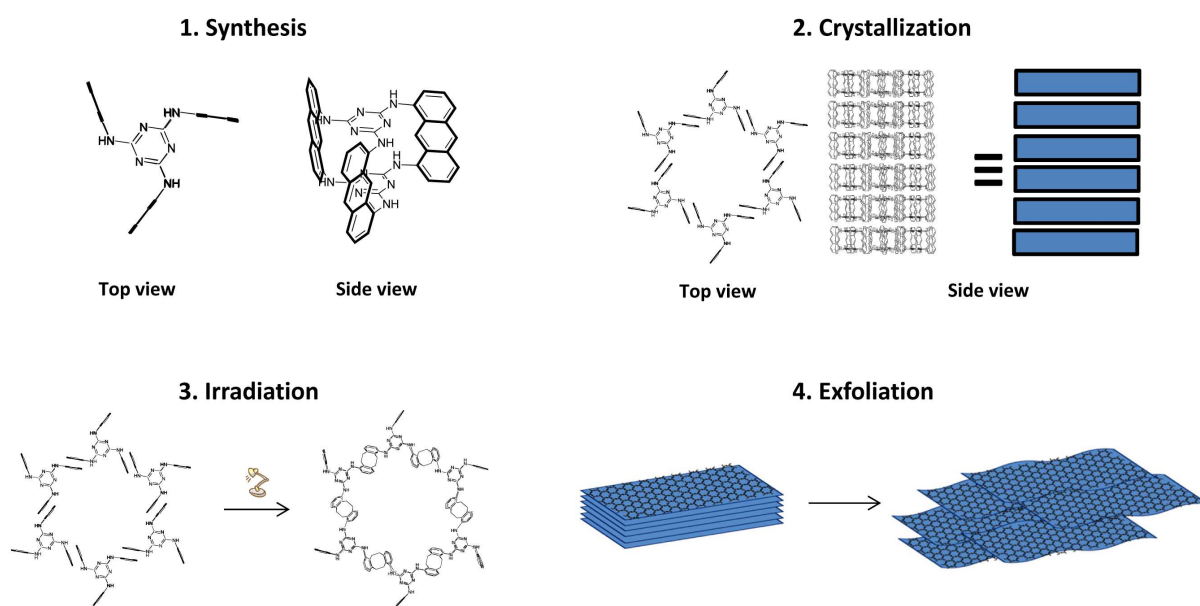


Figure 3.2: Cartoon representation of the synthesis strategy towards 2DP.

The amine-bearing triazine-based monomer **6** resembles a symmetric three-bladed rotor, which consists of stacked triazines connected by three anthracene blades via amine linkers. After synthesis of the monomer, the compound is crystallized into a single-crystal. The anthracene units should stack head-to-tail and form a hexagonal packing in 2D layers. Upon irradiation of these crystals, the anthracene blades undergo [4+4]-cycloaddition with adjacent monomers to form covalent bonds into 2DPs. The crystalline 2DPs are then exfoliated by swelling into single 2DP sheets. The protonation of the amine groups might support the exfoliation due to the resulting repulsive positive charges between the layered sheets. The 2DP sheets are then isolated.

## 4. Results and Discussion

## 4.1. Part A: Synthesis of a 2,2':6',2''-Terpyridine Ligand 7

The synthesis of the premonomer **7** is rather straightforward and was realized by using established chemistries within ca. six weeks. Parts of the premonomer synthesis, among others, were already shown in the diploma thesis.<sup>[103]</sup> In the course of the dissertation project, the reactions towards **7** were optimized and scaled-up from 250 mg to several grams.

The general synthesis path is shown in Figure 4.1. The synthesis can be divided into three building blocks, which are a 6,6''-dibromo-2,2':6',2''-terpyridine **8**, a spacer **9**, and an anthracene derivative **10**. These three compounds were synthesized in ca. 7 g scale according to literature procedures.<sup>[229–234]</sup> The target premonomer **7** was stepwise assembled from these three blocks.

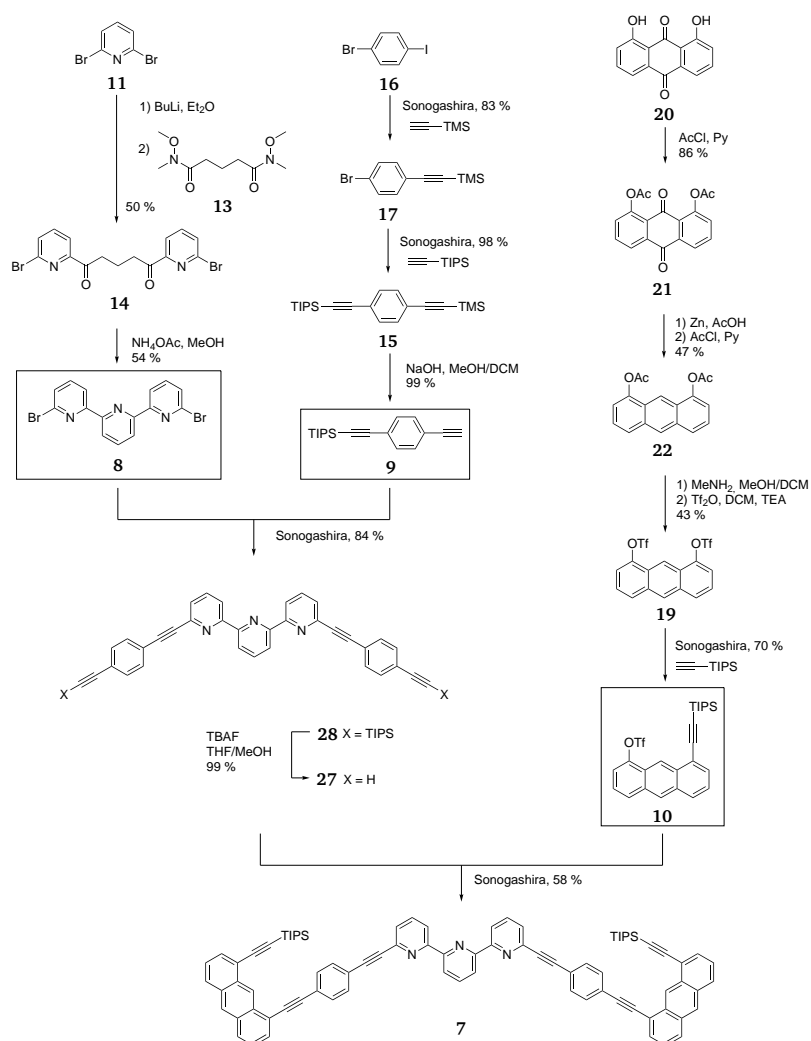


Figure 4.1: The synthetic sequence towards premonomer **7**.

## 4. Results and Discussion

### 6,6''-Dibromo-2,2':6',2''-terpyridine **8**

6,6''-Dibromo-2,2':6',2''-terpyridine **8** was chosen for the synthesis towards **7** as cross-coupling reactions can be applied to the bromide groups at the 6,6''-position. It is commercially not available and **8** was therefore synthesized by either method A, which forms the tpy via the Kröhnke<sup>[161,162]</sup> type reaction as reported by George Newkome *et al.*<sup>[229]</sup> or method B, the one-pot synthesis via phosphorus trichloride (PCl<sub>3</sub>) and lithiated 2,6-dibromopyridine **11** coupling reaction as reported by Yuzuru Uchida *et al.*<sup>[230,231]</sup>

Method A is a three step synthesis procedure (Fig. 4.2). The first reaction step was the Weinreb-Nahm ketone synthesis<sup>[235]</sup> of **12** with *N,O*-dimethylhydroxylamine hydrochloride to form the Weinreb-Nahm amide **13** in 82 - 88 % yield. This step was introduced to avoid a double substitution on the carbonyl site forming the alcohol. The second step was the substitution with monolithiated **11** to give **14** in 30 - 50 % yield, and the last step gave **8** by the Kröhnke type ring closure with NH<sub>4</sub>OAc in 52 - 54 % yield.<sup>[229]</sup> The reproducibility of the yields was not investigated.

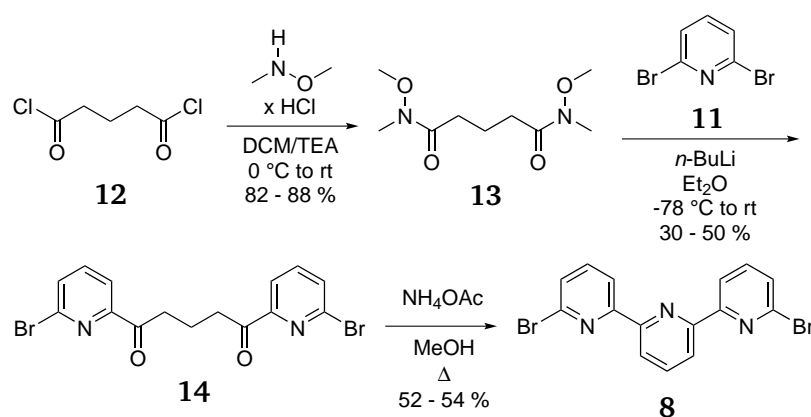


Figure 4.2: The synthetic sequence to **8** by method A.

As an alternative path, the one-pot synthesis of **8** was considered (Fig. 4.3). The PCl<sub>3</sub> serves as a coupling reagent, combining the pyridines to form **8**. Usually PCl<sub>3</sub> in combination with organometallic reagents, is used to form tertiary alkyl or aryl phosphines.<sup>[231]</sup> In the case of heteroaryllithium compounds, as for example with 2-pyridyllithium, the coupling compounds are favored over the corresponding phosphine products (Fig. 4.3).<sup>[230]</sup> The mechanism involves the formation of a pentacoordinated phosphorus intermediate, which assists the ligand coupling exchange with PCl<sub>3</sub> and the ligand coupling reaction between the pyridines to give the pyridine coupled products (Fig. 4.4).<sup>[236]</sup>

#### 4. Results and Discussion

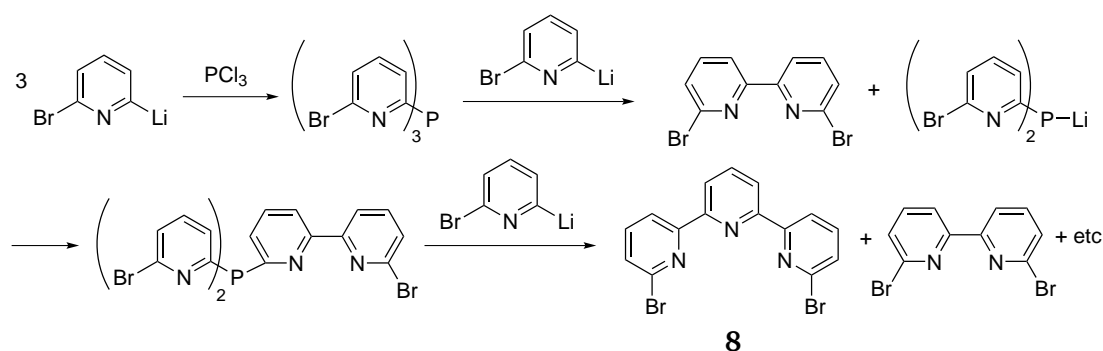


Figure 4.3: The synthetic sequence and proposed mechanism to **8** by method B. <sup>[231]</sup>

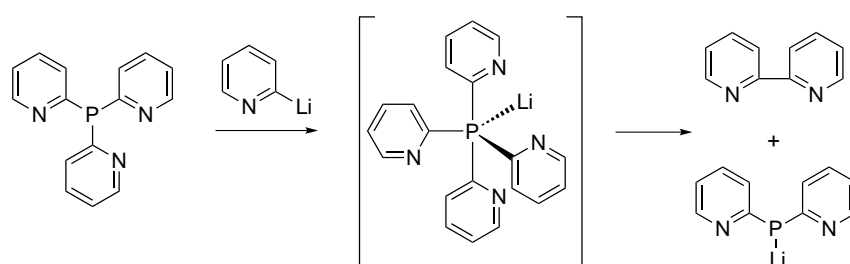


Figure 4.4: The involvement of a pentacoordinated phosphorus intermediate. <sup>[236]</sup>

The first reaction step included the lithiation of the commercially available 2,6-dibromopyridine **11** with *n*-BuLi at  $-60\text{ }^\circ\text{C}$ , followed by the addition of  $\text{PCl}_3$  at  $-40\text{ }^\circ\text{C}$ . This temperature was kept relatively constant for 20 hours without the use of a cryostat, then slowly warmed to rt over 48 hours. A substantial amount of precipitate was formed, requiring a mechanical stirrer. Since the obtained yields of **8** (11 - 20 % based on **11**) were lower than those reported in literature (39 % based on **11**)<sup>[230]</sup>, a temperature controller would be helpful. In contrast to what has been reported in specialist literature, the product did not precipitate as colorless crystals. Instead, the obtained solid was rather recrystallized from either toluene or chloroform.

Both methods were used to synthesize **8** in 5 - 8 g scale. While method B is a practical one-pot synthesis, the scale-up was less efficient in contrast to method A, which needed no special temperature control for a time course of 20 hours. In addition, the overall obtained yields and reaction time are comparable with the one-pot synthesis.

## 4. Results and Discussion

### Spacer 9

The length of the spacer **9** was important for the synthesis of premonomer **7**, with respect to the complexation towards the bis-complex **3**. Because the spacer holds the anthracene units, it needed a certain length, which would not sterically hinder the terpyridine interdigitation. Furthermore, as indicated in the Theoretical Background 2.3. (see Fig. 2.19), the  $\pi$ - $\pi$ -interactions between the benzenes from the spacer and the pyridines from the terpyridines were expected to promote stability and orientation of the spacer in the monomer **3**. The TIPS group served as a protection group for the latter reaction with **8**.

The synthesis of the spacer **9** was already reported in literature.<sup>[232,233]</sup> The reaction was performed with a double Sonogashira cross-coupling with TMS-acetylene and TIPS-acetylene in two steps. The best results were obtained, when using TMS-acetylene prior TIPS-acetylene. Eitherway, the TMS group of **15** was then deprotected under alkaline conditions to give **9**. These reactions are shown in Figure 4.5.

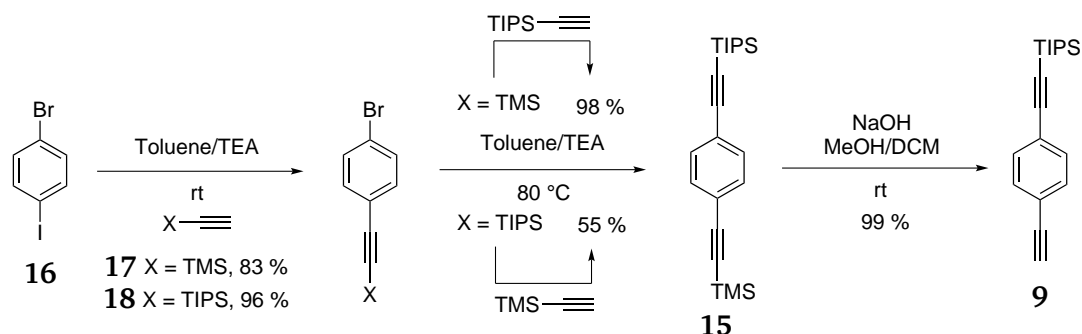


Figure 4.5: The synthetic sequence to spacer **9**.

Starting from the commercially available **16**, both **17** and **18** were synthesized using conventional Schlenk techniques within one day in approx. 10 or 20 g scales. The compounds were purified by silica gel column chromatography to separate the disubstituted side product and some remaining starting material. The reaction with TMS-acetylene at rt to afford **17** seemed smoother, even though the yields in comparison to the reaction at rt with TIPS-acetylene to give **18** were higher. TLC displayed for both reactions a disubstituted side product. The desired mono-TMS-substituted product and the di-TMS-substituted side product displayed a good separation on TLC in contrast to the TIPS parent compounds. The next reaction to give **15** via **17** and TIPS-acetylene yielded 92 - 98 %, while the reaction via **18**<sup>VIII</sup> and TMS-acetylene yielded in

<sup>VIII</sup> **18** was used without further purification.

## 4. Results and Discussion

two attempts 55 %. Both reactions mixtures were purified by silica gel column chromatography purification. The final step to synthesize **9** was easily achieved in 92 - 99 % yield under alkaline conditions.

The reaction towards the spacer is in principle very simple. The need for column chromatography however limits the accessible amount to approx. 20 g. Alternatively, the spacer could be synthesized by TMS-acetylene disubstitution of 1,4-bromobenzene, subsequent deprotection of the TMS groups and monosilylation in the presence of *n*-BuLi and TIPS-chloride, but a possible disilylated side product at the final step must be considered. [237–239]

### Anthracene derivative **10**

The anthracene unit in monomer **3** acts as connection site for the macrocyclization. The use of 1,8-disubstituted anthracenes for topochemical reactions is attractive due to the potential of retaining the crystal shape upon irradiation in single-crystal (see Fig. 2.9). Synthesis of 1,8-disubstituted anthracenes is usually complex and accessibility is still limited. [234] 1,8-Dihaloanthracenes are useful starting materials for cross-coupling reactions. The bromo, chloro and triflate derivatives are available for large scale synthesis. [234,240,241] Since the triflate **19** was extensively studied in our group [25,234], it was convenient to follow these reported procedures. The mono-TIPS-acetylene protected anthracene derivative **10** was integrated into the model compound **1** shown in Figure 1.2a. The TIPS group increases solubility in general and provides a relative stability towards silyl group deprotection. Therefore it seemed convenient to incorporate **10** into the structure of the premonomer **7** as well.

First, 1,8-dihydroxyanthraquinone **20** was protected with acetyl chloride to give **21**, then reduced with zinc, and reacylated with acetyl chloride to form **22**. Reaction with Tf<sub>2</sub>O after acetyl deprotection led to **19**, followed by a Sonogashira cross-coupling with equimolar amounts of TIPS-acetylene to give **10** (Fig. 4.6).

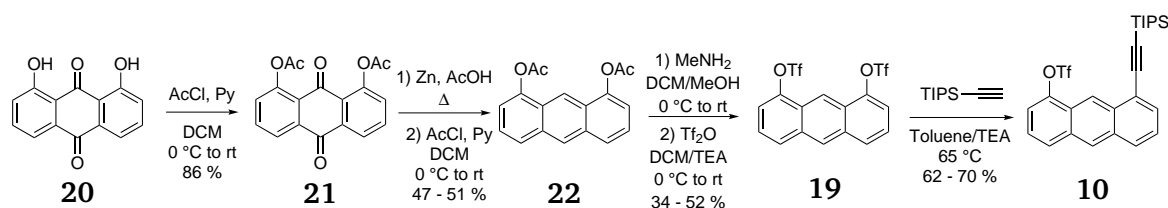


Figure 4.6: The synthetic sequence to anthracene derivative **10**.

1,8-Diacetoxyanthraquinone **21** was obtained without problems on a scale of ca. 70 g in 86 %



## 4. Results and Discussion

---

yield. The reason that 1,8-dihydroxyanthraquinone **20** was acetylated from the beginning was due to instability of 1,8-dihydroxyanthracene **23** towards oxidation in alkaline media.<sup>[44,234]</sup> The next step was usually conducted with 20 - 30 g. To the refluxing solution of **21** in AcOH, zinc dust (3.0 eq.) was added in portions over three hours. The reaction mixture was monitored by TLC to minimize over-reduction and to control starting material consumption. To the mixture was then added another equimolar amount of zinc dust. A side effect of the zinc reduction was the partial cleavage of the acetyl groups. The mixture was therefore reacylated with AcCl after a short work-up procedure. Silica gel column chromatography gave a mixture of the main product **22** in 47 - 51 % yield along with the over-reduced 1,8-diacetoxydihydroanthracene **24** side product (ca. 7 %). Both compounds eluted very close and were used without further purification. 1,8-Ditriflateanthracene **19** was isolated in 34 - 52 % yield by silica gel column chromatography, after deacetylation of **22** with MeNH<sub>2</sub> in a DCM/MeOH mixture and triflation with Tf<sub>2</sub>O at 0 °C. The ca. 5 % over-reduced 1,8-ditriflatedihydroanthracene **25** side product was carried along as well. The desymmetric ethynylation of **19** was carried out via Sonogashira cross-coupling with Pd(PPh<sub>3</sub>)<sub>4</sub> and CuI, affording 62 - 70 % yield of **10** after silica gel column chromatography purification. The dihydroanthracene side product was no longer traceable, whereas the disubstituted compound **26** could be isolated and characterized as a side product.

Silyl groups have an impact on the stability, solubility and crystal packing with regards to the premonomer **7** and monomer **3**. The larger the size of the silyl group, the more disorder and hindrance for anthracene stacking in the crystal packing is expected. More effort in growing good quality crystals suitable for XRD analysis is needed. Using a smaller silyl group, such as TMS, had already been considered for a premonomer in the diploma thesis<sup>[103]</sup>. However, it was found that the synthesis towards the premonomer via TIPS group was more efficient than with TMS. One reason for this might be the use of TEA base for the Sonogashira cross-coupling between anthracene building block and **27**, which could already deprotect TMS under the chosen reaction conditions.

### Premonomer **7**

All three building blocks were used for the stepwise assembly to the target premonomer **7** presented in Figure 4.7. The terpyridine unit **8** was reacted with the spacer **9** via Sonogashira cross-coupling reaction to gain **28**. The TIPS group was deprotected with TBAF to give **27**, which was then used for the synthesis of **7** via Sonogashira cross-coupling reaction with **10**.

## 4. Results and Discussion

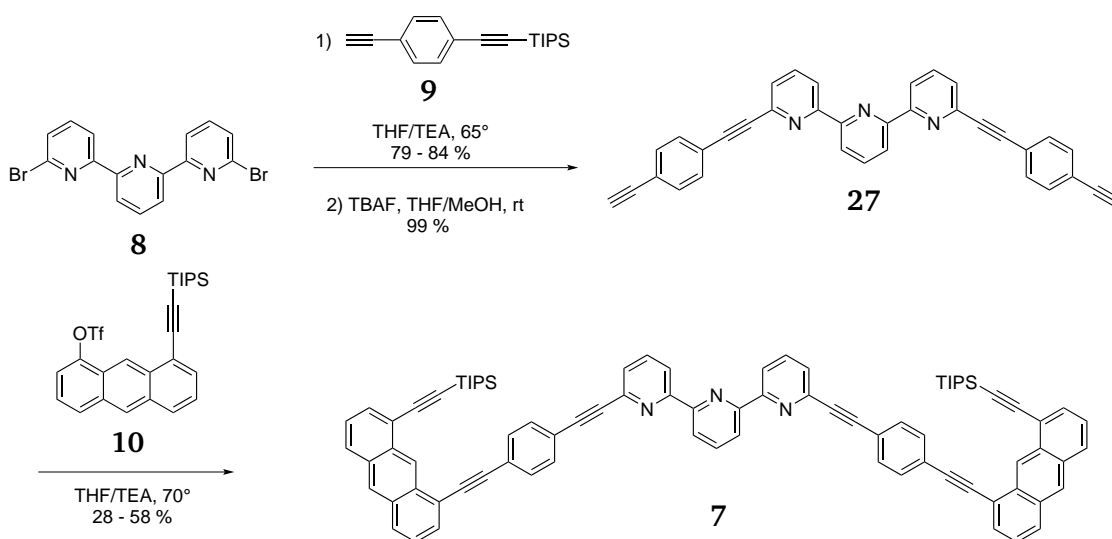


Figure 4.7: The synthetic sequence to terpyridine ligand 7.

The Sonogashira cross-coupling reaction with  $\text{Pd}(\text{PPh}_3)_4$  and  $\text{CuI}$  between spacer **9** and 6,6''-dibromo-2,2':6',2''-terpyridine **8** was performed in a THF/TEA mixture at 65 °C for usually four days. When these reactions were first explored, a copper-free Sonogashira (Heck alkynylation)<sup>[242]</sup> reaction was performed, since terpyridine compounds are known to complexate with  $\text{Cu(I)}$  and  $\text{Cu(II)}$ .<sup>[156]</sup> Nevertheless, the yields of **28** lay between 32 - 59 %<sup>[103]</sup> and were improved by using  $\text{CuI}$  as co-catalyst leading to yields of 79 - 84 %.  $\text{Cu(I)}$  seemed not to undergo complexation under the conditions used for the reaction. No significant color change for complexation was observed. If complexation had taken place, then only a small amount of tpy would have been consumed in any case, limited by the catalytical amount of  $\text{CuI}$  involved. The reaction mixture was then purified by silica gel column chromatography with an eluent mixture of hexane/ $\text{EtOAc}$ / $\text{TEA}$  (30 : 1 : 1). The amount of  $\text{TEA}$  on the one hand influenced the elution itself and on the other was necessary to elute the terpyridine system, which would strongly absorb to silica. Neutral aluminium oxide as stationary phase was not considered at this point, due to the costs involved. **28** was then dissolved in THF/ $\text{MeOH}$  (10 : 1) and TIPS was deprotected with a slight excess of TBAF per TIPS group. The reaction time lasted ca. three days with precipitation of **27** from the solution mixture. The pinkish solid was separated with a centrifuge and thoroughly washed with  $\text{MeOH}$  to remove unreacted TBAF, which would deprotect **10** in the next reaction step. Usually 99 % of the product was isolated. The solubility of **27** in organic solvents was very bad. Up to now, no  $^{13}\text{C}$ -NMR spectrum could be measured in a moderate time-frame. However,  $^1\text{H}$ -NMR spectroscopy and MS analysis (ESI) confirmed product formation. The final step to premonomer **7** was the cross-coupling of **27** with **10**. For the same reasons mentioned

## 4. Results and Discussion

in the coupling of **28**, CuI was used in small amounts (1 mol%) along with 10 mol% Pd(PPh<sub>3</sub>)<sub>4</sub> to minimize possible copper tetryridine complexation. Due to the weak solubility of **27**, the reaction scale was limited to ca. 1 g (based on **27**) with a solvent amount of ca. 400 mL in a 1 L Schlenk flask. As cross-coupled reactions are performed under oxygen exclusion and freeze-pumping is involved, the reaction flask size was the additional limitation at scale-up. After three days heating at 70 °C in a THF/TEA (3 : 1) mixture, the reaction was stopped, and filtered through a paper filter, which contained unreacted **27** (confirmed by the MS). Then the mixture was passed through a short celite column and washed with EtOAc until no fluorescence of the filtrate was observed. The mixture was then evaporated and the crude product was subjected to silica gel column chromatography with hexane/EtOAc/TEA (8 : 2 : 1) as eluent mixture. Usually ca. 1 g of **10** was regained and the yields of **7** varied between 28 - 58 % (based on the entire **27**) giving ca. 0.8 - 1.4 g, which was sufficient for complexation studies towards the monomer **3**. It is clear that the reaction conditions are still not fully optimized. One reason for this was probably the weak solubility of **27**, which perhaps would be increased with the use of DMF or DMSO as solvents. Still, the high boiling points may prove to complicate the purification process.

The premonomer was fully characterized with <sup>1</sup>H-NMR and <sup>13</sup>C-NMR spectroscopy as well as MS. With the help of COSY, HSQC, and HMBC measurements the assignment of the proton and carbon signals of the premonomer **7** in different solvents (CDCl<sub>3</sub> and DMF-*d*<sub>7</sub>) were obtained (see Experimental 6.2.). An example of the aromatic region of the premonomer **7** (Fig. 4.8) from the <sup>1</sup>H-<sup>1</sup>H-COSY spectrum in CDCl<sub>3</sub> is shown in Figure 4.9. In regards of the macrocyclization shown in Figure 1.2a, the premonomer **7** was subjected to crystallization to determine if the crystal packing is similar to Kissel's model compound **1**. A macrocycle of the premonomer would serve as the ideal model compound to assist the poly[*n*]catenane characterization. With the slow vapor diffusion of pentane into a chloroform solution of the premonomer **7**, yellow star-like crystals were obtained, but the crystal quality was not sufficient for XRD measurements. Up-to-now no other crystallization attempts gave proper crystals.

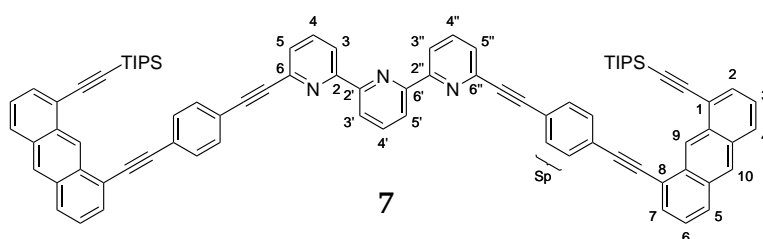


Figure 4.8: Atomic numbering of premonomer **7**.

## 4. Results and Discussion

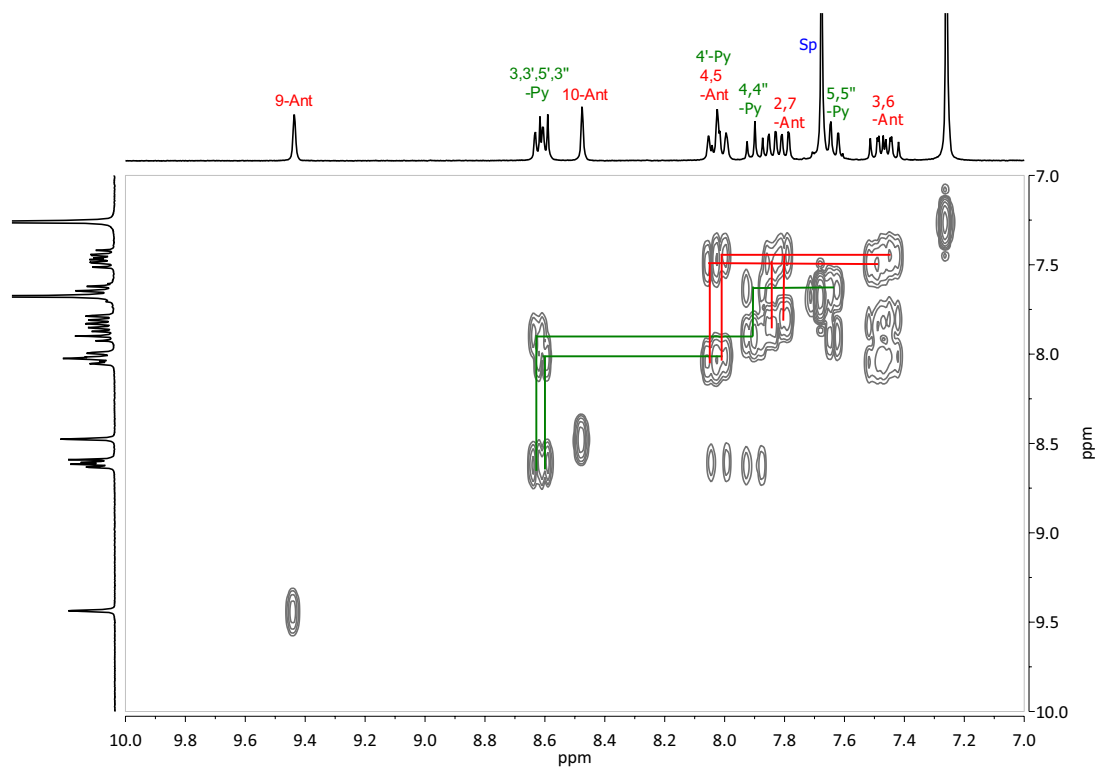


Figure 4.9: 300 MHz  $^1\text{H}$ - $^1\text{H}$ -COSY spectrum of **7** in  $\text{CDCl}_3$ .

It was considered to synthesize the premonomer **7** by two other synthetic routes (Fig. 4.10) to overcome the solubility issues given by **27** and enhance the premonomer yields.

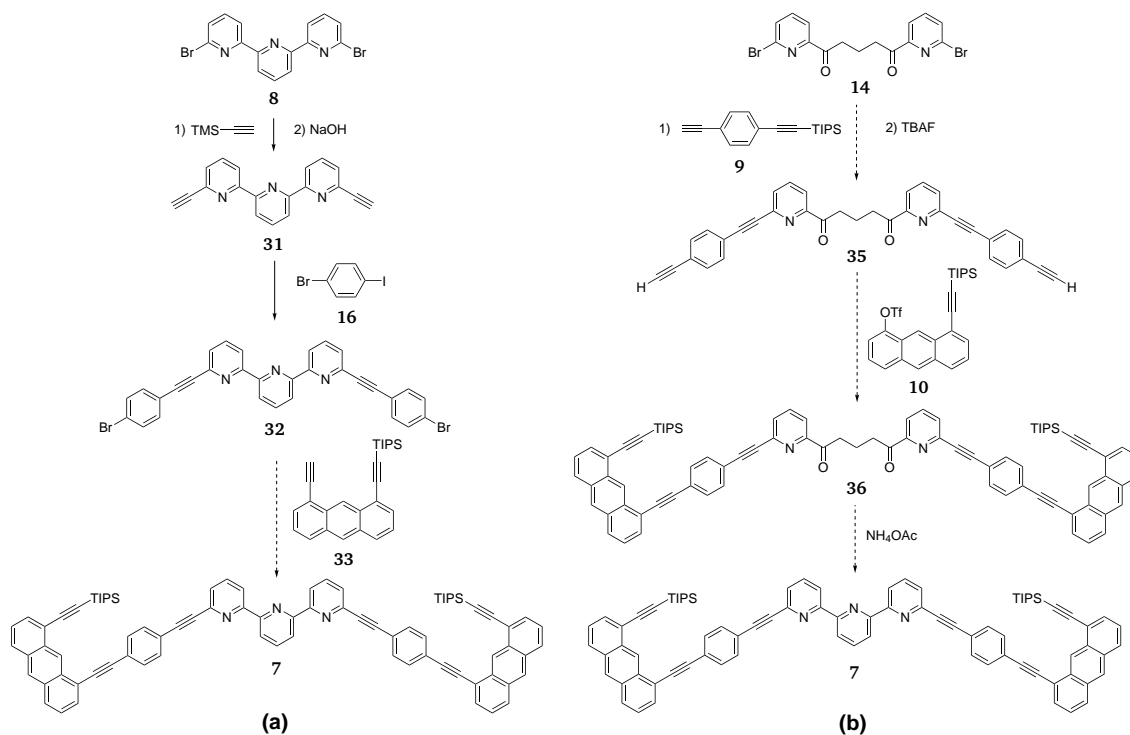


Figure 4.10: Two alternative synthetic routes towards premonomer **7**.

#### 4. Results and Discussion

---

The synthesis routes shown in Figure 4.10a assembles the premonomer by synthesizing first the tpy unit **8** and adding TMS-acetylene or TIPS-acetylene via Sonogashira cross-coupling to form **29**<sup>[243]</sup> or **30**, respectively. After deprotection of the silyl group, **31**<sup>[243,244]</sup> was cross-coupled with **16** to give **32**. The anthracene unit **33** would be synthesized according to Kissel's reported procedure<sup>[234]</sup> and subsequent TMS deprotection. Sonogashira cross-coupling of **32** with **33** would give the premonomer **7**. The reaction path was tested up to the synthesis of **32**, which showed similar solubility issues as **27** and therefore was not further considered for the premonomer **7** synthesis.

Fig. 4.10b illustrates the second alternative synthetic route, which starts from **14** by cross-coupling with the spacer **9** to form **35** after deprotection of the TIPS group from **34**. The anthracene derivative **10** would then be cross-coupled with **35** to give **36** and the premonomer **7** would be ring assembled by NH<sub>4</sub>OAc. The reaction was carried out once and up to compound **35**, which could not be isolated. Even though the reaction path seems to be productive, it is safe to assume that the ring assembly from **36** to the premonomer **7** could prove problematic due to steric demands of the long and bulky arms—which contain the spacer and anthracene unit—attached to the pyridine.

## 4. Results and Discussion

### 4.2. Part A: Complexation and Decomplexation Studies

Terpyridine compounds are known to undergo complexation upon addition of metal cations. For the purpose of this thesis, zinc metal salts were the choice, as they are known to form sufficiently stable terpyridine complexes, and are easy to remove if need arises. In this regard, the complexation of the premonomer **7** with zinc salts to give bis-complexes **3** was explored (Fig. 4.11). After synthesis and isolation of the bis-complex, a demetallation protocol was established, and the feasibility to irradiate a bis-complex was investigated in this chapter as well.

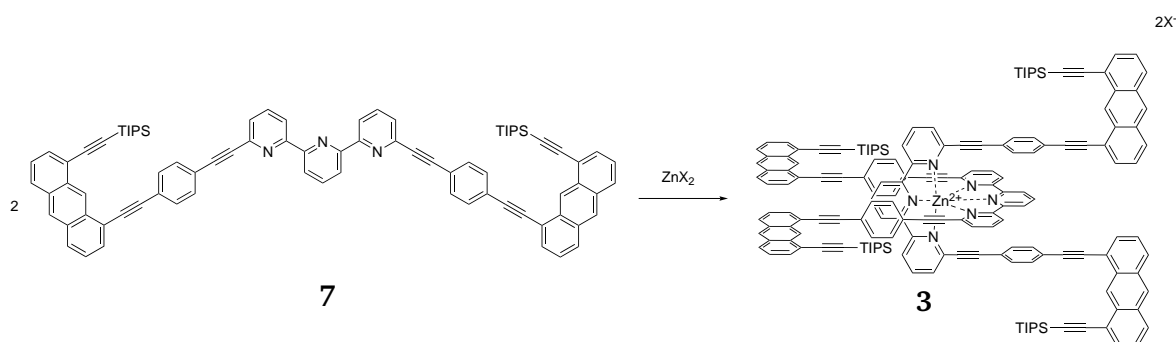


Figure 4.11: The complexation of **7** with a zinc salt to give a bis-complex **3**.

The premonomer **7** dissolved in chloroform with a yellow color and exhibited a strong blue fluorescence under 366 nm UV light. Upon the addition of 0.5 eq. of a zinc salt, such as  $\text{Zn}(\text{OTf})_2$  in acetonitrile, to the premonomer **7**, the fluorescence was quenched, and a color change of the solution to dark yellow was observed. To quantify this visual change and fluorescence quenching, the previously mentioned addition was investigated by titration experiments applying UV/Vis and fluorescence spectroscopy. The titration for both UV/Vis and fluorescence spectroscopy, was conducted as follows: the premonomer **7** was dissolved in chloroform and a spectrum was recorded. Step-wise 0.1 eq. of  $\text{Zn}(\text{OTf})_2$  in acetonitrile was added up to 1.0 eq., then the amount per addition was raised to 1.0 eq., and the zinc salt was added up to a total amount of 4.0 eq. After each addition, the solution was shaken for one minute, and a spectrum was recorded.

The fluorescence spectrum of one such titration is shown in Figure 4.12. Up to the addition of 0.5 eq. of  $\text{Zn}(\text{OTf})_2$  to the premonomer **7**, a bis-complex **3** should form and the fluorescence signal should be quenched. A further addition of  $\text{Zn}(\text{OTf})_2$  should ideally have no effect to the bis-complex **3** formation and the fluorescence signal should remain constant. Since the fluorescence signal decays at each zinc salt addition (Figure 4.12a), and reaches its maximum decay at 1.0 eq. of  $\text{Zn}(\text{OTf})_2$  to the premonomer **7**, and then remains constant, as emphasized with a red

## 4. Results and Discussion

line in Figure 4.12b, it could possibly indicate a resulting mono-complex **37** (not shown). The mono-complex **37** would be a result of the dynamic equilibrium of labile zinc terpyridine bis-complexes, which are in equilibrium with mono-complexes.<sup>[245]</sup> However, the slight decrease of the fluorescence signals was only caused by sample dilution. The result of the fluorescence spectroscopy measurement could not clarify whether a bis-complex **3** or mono-complex **37** resulted, as it was unclear why the fluorescence signal of a mono-complex **37** would be weaker.

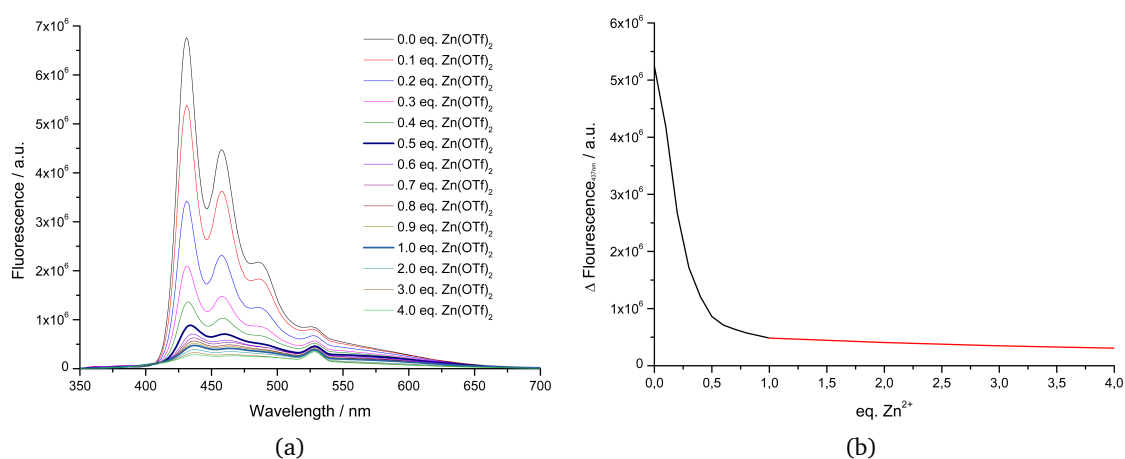


Figure 4.12: The addition of Zn(OTf)<sub>2</sub> to **7**. a) Fluorescence spectrum ( $\lambda_{em} = 264$  nm) and b) fluorescence maximum change at  $\lambda = 437$  nm for different amounts of Zn(OTf)<sub>2</sub>.

UV/Vis spectroscopy is a quantitative measure to determine if the metal cation reacted with the premonomer **7** and it would indicate if there is an equilibrium between remaining uncomplexed premonomer, mono-complex, and bis-complex. In an ideal case, the absorption bands of a terpyridine bis-complexation with the zinc salt addition from 0.0 to 0.5 eq. change and remain constant thereafter. A significant decrease at further zinc salt addition would indicate the formation of mono-complexes. A constant decrease would result, for the same reasons as in the fluorescence spectroscopy measurement (Fig. 4.12b), by sample dilution. Furthermore, the stability and the backreaction of terpyridines towards a mono-complex at an excess of metal cations would be determined. Therefore, a similar titration experiment of Zn(OTf)<sub>2</sub> to the premonomer **7** was monitored by UV/Vis spectroscopy (Fig. 4.13). The UV/Vis spectrum shown in Figure 4.13a reveals a further decrease of absorption bands upon addition of Zn(OTf)<sub>2</sub> up to ca. 0.8 - 0.9 eq., to the premonomer **7**. The observation is clearer in Figure 4.13b, which shows the changes of the 264 nm absorption band for different amounts of Zn(OTf)<sub>2</sub>. This indicates that either the bis-complexation is unfavored over the mono-complexation, or there is an equilibrium between both complexes, with a slight shift to mono-complexation. After 1.0 eq. of

## 4. Results and Discussion

the  $\text{Zn}(\text{OTf})_2$  addition, the overall equilibrium is reached, and the slight decrease of the slope is once again caused by sample dilution.

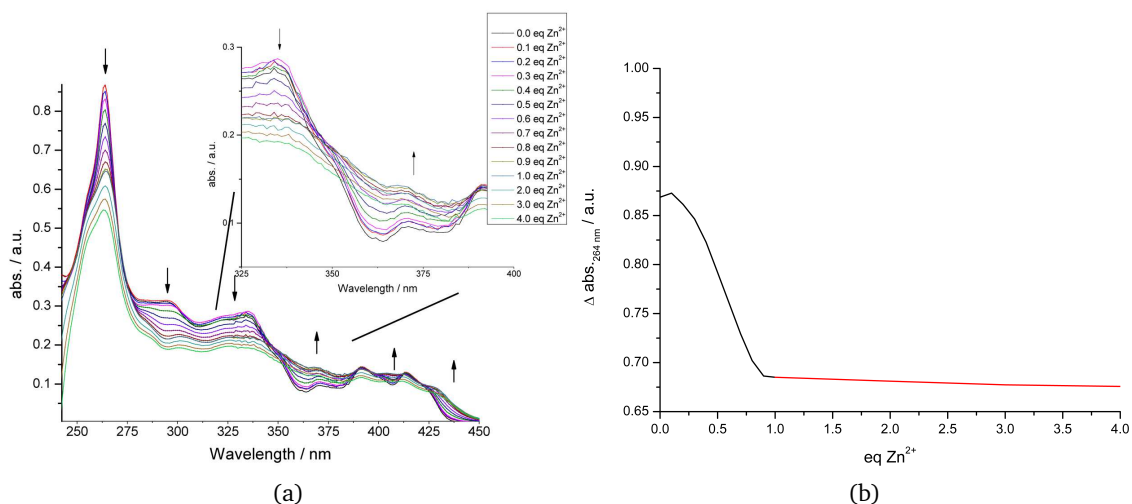


Figure 4.13: The addition of  $\text{Zn}(\text{OTf})_2$  to 7. a) UV/Vis absorption spectrum and b) absorption changes at  $\lambda = 264$  nm for different amounts of  $\text{Zn}(\text{OTf})_2$ .

The advantage of terpyridines is the easy to follow conformational change from *trans-trans* to *cis-cis* upon metal cation addition by NMR spectroscopy. The conformational change immediately affects the proton signals and causes a change of the chemical shift in the  $^1\text{H}$ -NMR spectrum.  $^1\text{H}$ -NMR spectroscopy was therefore used as an analytical tool to monitor the complexation. A simple complexation was performed: the premonomer 7 was dissolved in chloroform and mixed with an acetonitrile solution of 0.5 eq. of  $\text{Zn}(\text{OTf})_2$ . After ten minutes of stirring, the solvent was evaporated and the remaining compound was dissolved in  $\text{CDCl}_3$  to compare its  $^1\text{H}$ -NMR spectrum with the one of the metal-free premonomer 7 in  $\text{CDCl}_3$  (Fig. 4.14).

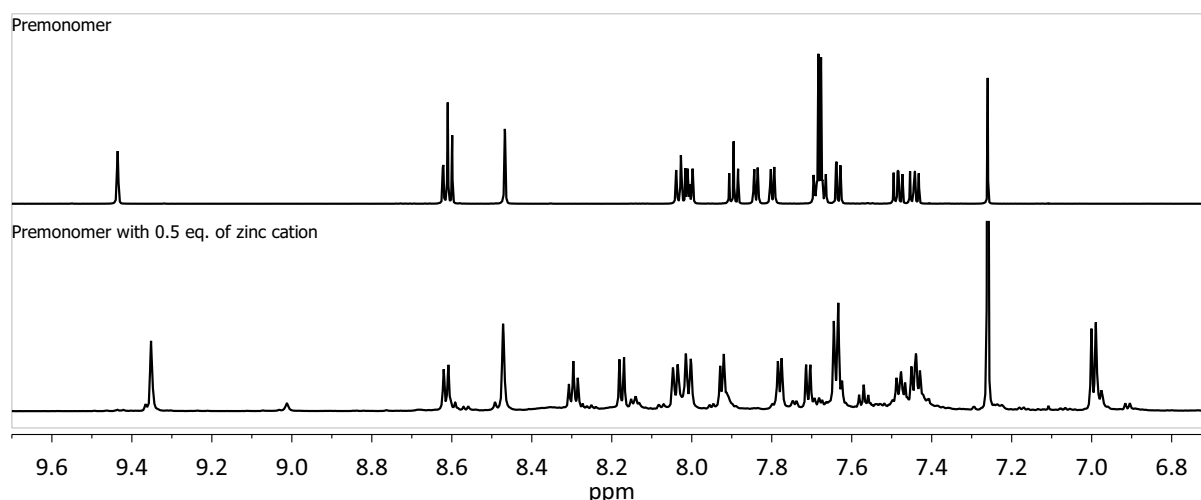


Figure 4.14: 700 MHz  $^1\text{H}$ -NMR spectra of the premonomer 7 (top) and premonomer 7/ $\text{Zn}(\text{OTf})_2$  mixture (bottom) in  $\text{CDCl}_3$ .



## 4. Results and Discussion

---

The proton signals of the premonomer **7** are clearly different to those of the premonomer **7**/ $\text{Zn}(\text{OTf})_2$  mixture from the simple complexation experiment (Fig. 4.14; bottom). A quantitative bis-complexation would show only one compound in the  $^1\text{H}$ -NMR spectrum. However, the spectrum in Figure 4.14 does not represent only one compound as shown by the observation of a mixture of many smaller proton signals independent of a larger set of signals. The large proton signals are expected to be a bis-complex **3**. According to the UV/Vis spectroscopy titration (Fig. 4.13), a mixture of bis-complex **3** and mono-complex **37** was suggested, and the  $^1\text{H}$ -NMR spectroscopy observation (Fig. 4.14) of the simple complexation experiment seemed to be in agreement. The next step was the purification of the mixture, which was dissolved in chloroform and injected into a preparative recycling GPC (rGPC), in order to isolate the main compound.

The preparative rGPC is a type of size-exclusion chromatography that separates molecules with different hydrodynamic volumes in a solution. Large molecules tend to have a large hydrodynamic volume and bypass the columns quicker, while smaller molecules usually have a small hydrodynamic volume and a longer elution time through the columns. The complex was expected to have a different hydrodynamic volume than the premonomer **7** due to its binding to a metal salt, resulting in a compact U-shaped mono-complex **37** or an U-shaped duplex bis-complex **3**.

Two main fractions were collected by the preparative rGPC with UV detection ( $\lambda = 254 \text{ nm}$ ).<sup>IX</sup> The first fraction (Fraction 1) had a shorter retention time, but a larger intensity in comparison to the second fraction (Fraction 2). Therefore, Fraction 1 should contain a "large" molecule in terms of hydrodynamic volume and presumably, due to the large intensity, could be the main compound as seen in the  $^1\text{H}$ -NMR spectrum (Fig. 4.14). In addition, the second fraction (Fraction 2) that had a longer retention time and a smaller intensity than the first fraction, could presumably reflect the compound with the smaller proton signals shown in the same  $^1\text{H}$ -NMR spectrum. Both collected fractions, the initial mixture (before preparative rGPC injection), and the premonomer **7** before zinc salt addition were compared by  $^1\text{H}$ -NMR spectroscopy in  $\text{CDCl}_3$  (Fig. 4.15).

---

<sup>IX</sup>The intensities, given by the preparative rGPC, may not correlate with the effective quantity of compound collected due to different absorption maxima and absorbances of the compounds.

## 4. Results and Discussion

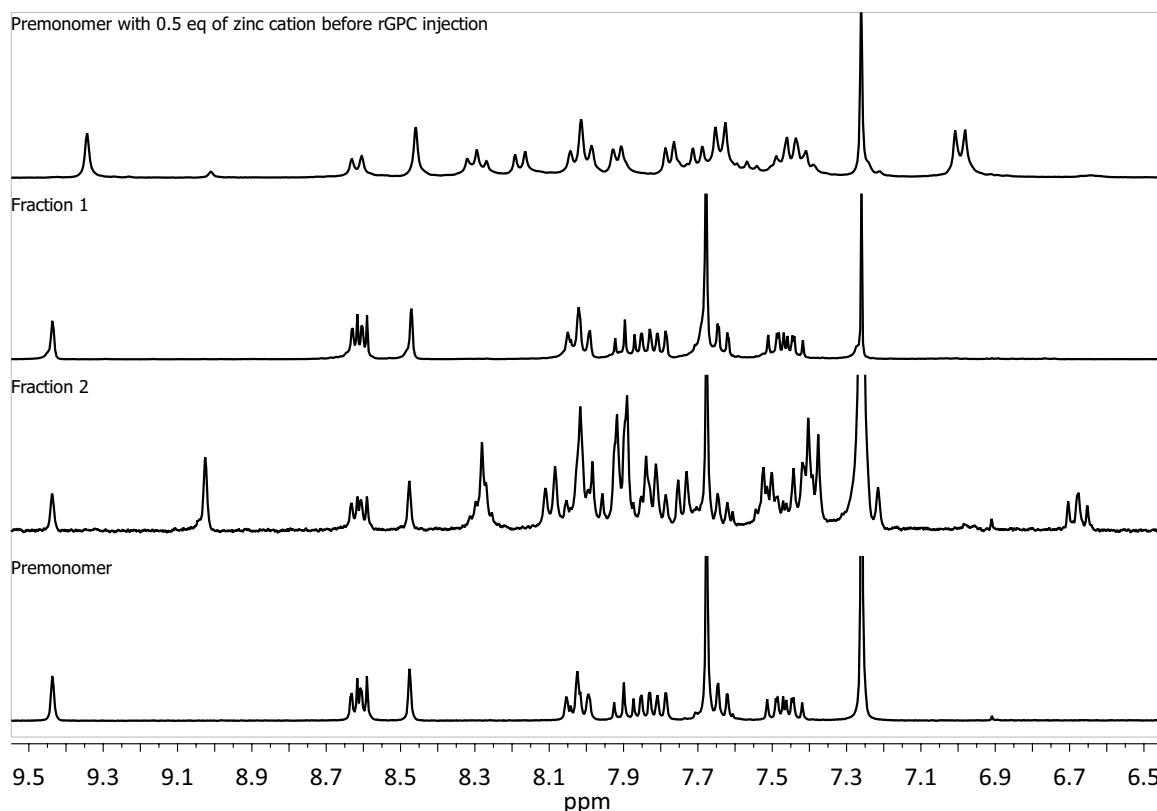


Figure 4.15: 300 MHz  $^1\text{H}$ -NMR spectra of the premonomer 7 with 0.5 eq.  $\text{Zn}(\text{OTf})_2$  before preparative rGPC injection, Fraction 1, Fraction 2, and premonomer 7 in  $\text{CDCl}_3$  (from top to bottom).

The large proton signals of the initial mixture in the  $^1\text{H}$ -NMR spectrum (Fig. 4.15; top) were absent in both collected fractions. Fraction 1 contained the identical proton signals as of the premonomer 7. Fraction 2 was a mixture that contained proton signals identical to the premonomer 7 and a new set of proton signals. Since Fraction 2 was tailing strongly during the preparative rGPC separation and no clear baseline fractionation was achieved, a mixture was in any case expected. The new set of signals in Fraction 2 are similar to those of the small proton signals in Figure 4.14 and were speculated to be caused by a mono-complex 37. This speculation was verified by the XRD crystal structure of obtained mono-complex 37 by the crystals that precipitated from  $\text{CDCl}_3$  in the NMR tube of Fraction 2 (Fig 4.16; 7.1.).

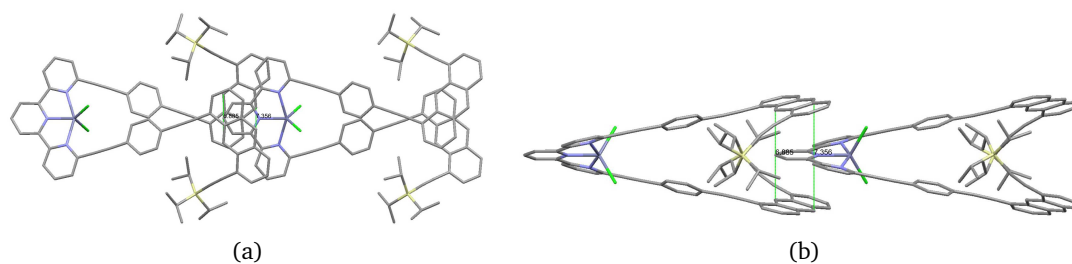


Figure 4.16: The XRD crystal structure of the mono-complex 37. a) Top view and b) side view of two mono-complexes 37. (Hydrogens and solvent molecules omitted.)

#### 4. Results and Discussion

---

Remarkably, the XRD crystal structure revealed a counterion exchange from OTf<sup>-</sup> to Cl<sup>-</sup> as well, which might be caused by a reaction between the mono-complex **37** and HCl that was released from chloroform decomposition. As these observations were considered to be special, the preparative rGPC results were reconfirmed by a second independent repeated experiment.

Since only the mono-complex **37** and premonomer **7** were found after preparative rGPC separation, it was assumed that the main proton signals, before injection into the preparative rGPC, belonged to a bis-complex **3**. This bis-complex **3** must have been partially and fully demetallated during the elution through the preparative rGPC columns. While the sample eluted through the columns, the bis-complex **3** was demetallated, probably through the interactions and shear forces with the columns, to give mono-complex **37** and premonomer **7**.<sup>[246]</sup> Demetallation of complexes caused by GPC columns was also observed by other researchers and would be reduced by using a lower flow rate.<sup>[37,246–250]</sup> Furthermore, the detection of Fraction 1 and Fraction 2 at these retention times was in agreement with their expected hydrodynamic volumes. Since the metal binds to the premonomer **7** through coordination, the resulting mono-complex **37** in Fraction 2 was more compact causing a smaller hydrodynamic volume and longer retention time, than without a metal coordinated to the premonomer **7** as observed in Fraction 1.

As the mono-complex **37** was identified through the crystal structure (Fig. 4.16), it proved to be helpful in the assignment of some unknown proton signals in the <sup>1</sup>H-NMR spectra of previously performed complexation experiments, and it supported the existence of pinched complexes (in contrast to literature; see Fig. 2.18 in Theoretical Background 2.3.). In addition, the crystal structure shows the twisting capability of the spacer from the terpyridine unit, which revealed a sandwich-like stacking between the two anthracenes and the central pyridine ring of the terpyridine unit. The twisting might be stabilized by this sandwich-like stacking. Some proton signals of the anthracene unit from the mono-complex **37** were seen at ca. 6.65 ppm in solution. These were probably shifted upfield through anthracene stacking caused by the mono-complex **37** twisting.

To generally understand the complexation process between the premonomer **7** and Zn(OTf)<sub>2</sub>, it was now decided to monitor the step-wise addition of the zinc salt to the premonomer **7** by <sup>1</sup>H-NMR spectroscopy with deuterated solvents. This addition is referred to as "NMR titration" and should clarify under which conditions the bis-complex **3**, mono-complex **37**, or both are formed

## 4. Results and Discussion

during metal salt addition. In order to favor bis-complex **3** over mono-complex **37**, the metal salt was added to the premonomer **7**, with the latter being in excess to the metal salt. A series of measurements was conducted, where a defined concentration of premonomer **7** in a  $\text{CDCl}_3$  solution was mixed with  $\text{Zn}(\text{OTf})_2$  in methanol- $d_4$  in usually 0.1 eq. steps. It was expected that the formation of a bis-complex **3** is favored upon addition of  $\text{Zn}(\text{OTf})_2$  to the premonomer **7** up to 0.5 eq., if the metal salt forms a very stable bis-complex **3**. Exceeding 0.5 eq. of metal salt should then have almost no effect on the bis-complexation. In contrast, a labile bis-complex **3** could decomplexate to a mono-complex **37** by the excess amount of zinc salts. An exemplary procedure of such titration is given in Figure 4.17 and is discussed thereafter.

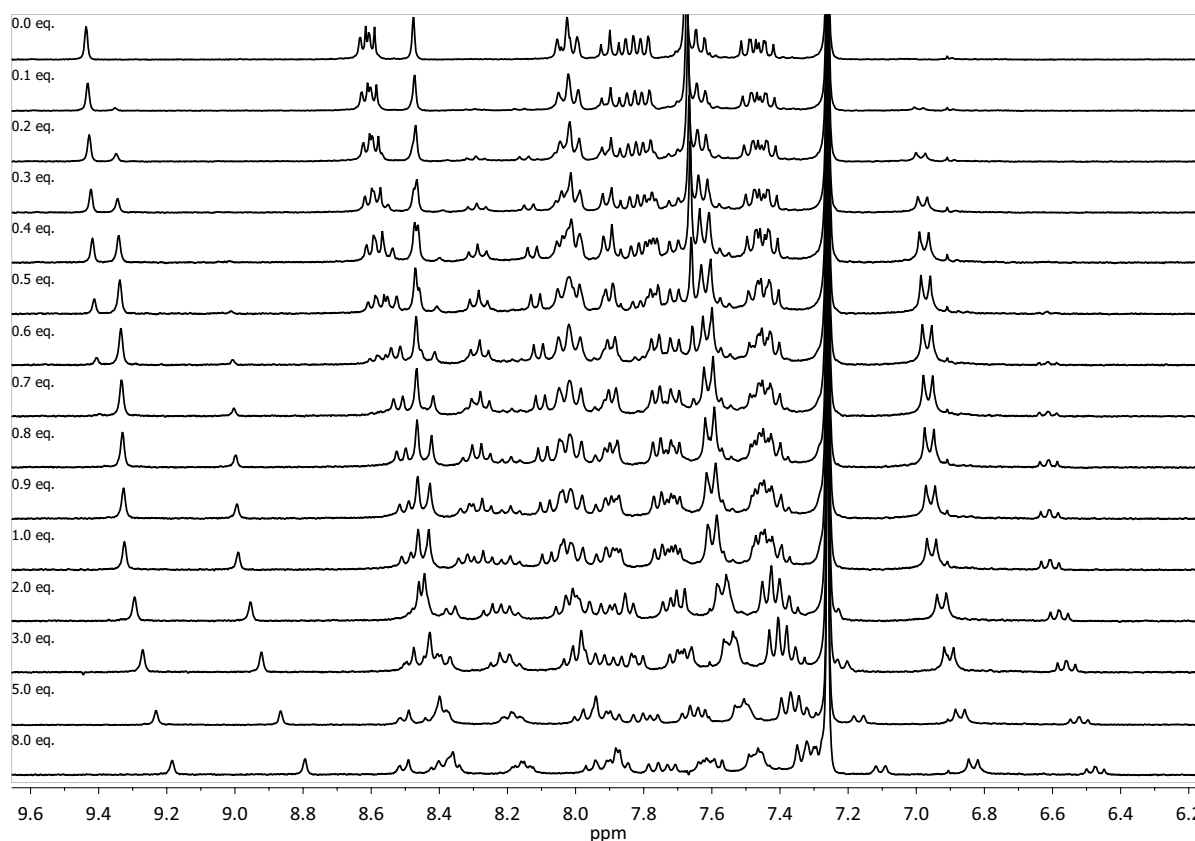


Figure 4.17: 300 MHz  $^1\text{H}$ -NMR spectra of the premonomer **7** in  $\text{CDCl}_3$  with the step-wise addition of  $\text{Zn}(\text{OTf})_2$  in methanol- $d_4$ .

First, the  $^1\text{H}$ -NMR spectrum of the premonomer **7** in  $\text{CDCl}_3$  was recorded. Then 0.1 eq. of a  $\text{Zn}(\text{OTf})_2$  solution in methanol- $d_4$  was added and the NMR tube was shaken for ca. one minute, after which another  $^1\text{H}$ -NMR spectrum was recorded. This procedure was repeated for additions of  $\text{Zn}(\text{OTf})_2$  up to 1.0 eq., then greater portions were added to the premonomer **7** up to 8.0 eq. There was a noticeable rise of a few of the signals after the first 0.1 eq. addition of  $\text{Zn}(\text{OTf})_2$ —e.g., 9.35, 8.25, 8.10, and 6.95 ppm—which was enhanced by further addition of  $\text{Zn}(\text{OTf})_2$  and

## 4. Results and Discussion

---

stagnated after ca. 1.0 eq. These signals refer to the bis-complex **3** formation. At 0.4 eq., a second set of signals slowly increased e.g., 9.00, 8.35, 8.15, and 6.60 ppm, continuously up to the addition of 8.0 eq.  $\text{Zn}(\text{OTf})_2$ . These signals refer to the mono-complex **37** formation. All proton signals were shifted upfield by each zinc salt addition to the premonomer **7** solution, which was caused by the solvent gradient of methanol- $d_4$  to  $\text{CDCl}_3$ . However, this shifting could be avoided by using the same solvent media for both zinc salt and premonomer **7**.

The cause for the mixture of bis-complex **3** and mono-complex **37** formation during titration is the labile formed bis-complex **3**, which in solution is in equilibrium with the mono-complex **37**.<sup>[245]</sup> The fact that a mono-complex **37** forms before reaching the ideal ratio of 0.5 eq. of  $\text{Zn}(\text{OTf})_2$  to premonomer **7**, also highlights that the bis-complex **3** is labile in solution. Such labile terpyridine zinc salt complexes in solution were already reported by others.<sup>[148,156,245]</sup>

Overall, the  $^1\text{H-NMR}$  spectra point out some typical characteristics observed for all titration experiments with  $\text{Zn}(\text{OTf})_2$ : the premonomer **7** signals diminish and two new sets of signals (bis-complex **3** and mono-complex **37**) appear.

### Influencing the complexation equilibrium

Using  $\text{Zn}(\text{OTf})_2$  as metal salt for the premonomer **7** titration was challenging, because only mixtures of bis-complex **3** and mono-complex **37** in solution were obtained. To influence this mixture, the equilibrium of the complexation needed to be shifted towards the bis-complex **3**. Since the complexation of metal salts to terpyridines also depends on temperature, concentration, solvent, pH, or different counterions, the variation of some parameters was investigated.<sup>[251]</sup> As a prerequisite for all experiments, further titrations did not exceed 0.5 eq. of zinc salt to premonomer **7**, in order to maintain the ideal ratio for the bis-complexation.

The temperature change showed nearly no influence on the equilibrium of a 0.5 eq. zinc salt/premonomer **7** mixture. Raising the concentration for the titration experiment was considered important, since the saturation point is reached more easily than in diluted samples. Diluted samples could prove to be a hindrance to precipitation due to reasonable solubility. Early titration experiments used concentrations of ca.  $2 \mu\text{mol/mL}$  and were then concentrated to ca.  $10 - 20 \mu\text{mol/mL}$ . In addition, it was also believed that the metal-free terpyridine would have a greater solubility than resulting complexes, which have a limited motion. Switching to other solvents could have a drastic influence on the complexation. One important criterion for the solvent of premonomer **7** and metal cation, besides the solubility of both, is the miscibility

## 4. Results and Discussion

---

of both solvents. Ideally, the titration is performed in the same solvent or solvent mixture. A stricter procedure needs to be followed with the application of a solvent gradient, since the ratio of resulting solvent mixtures may differ in their reproducibility at each titration. To follow the titration with NMR spectroscopy, deuterated solvents need to be available as well, but some uncommon deuterated solvents may be too expensive. It also needs to be considered that some solvents, such as acetonitrile, DMF, methanol, THF, and others are known to coordinate with metal cations and could compete with the terpyridine complexation itself. The counterion was considered to have the greatest influence on the complexation e.g., by either forming more or less stable complexes, or by influencing the crystal packing itself.<sup>[149]</sup> There are two possible ways to introduce different counterions: either, the complexation is performed with the appropriate zinc salt, or the reaction mixture is treated with an excess of a desired counterion to exchange the current counterion. In literature, many terpyridine complexes are purified by a counterion exchange.<sup>[36]</sup> As an example one would treat a zinc chloride terpyridine complex with an excess amount of  $\text{NH}_4\text{PF}_6$  or  $\text{AgPF}_6$ , and the resulting precipitated compound or salt is filtered, washed, and the complex is recrystallized. The precipitation of the bis-complex **3** would of course be ideal for isolation and purification.

Therefore, the complexation of premonomer **7** with different zinc salts was considered the main goal for achieving a bis-complex **3**. The following paragraphs explain the details of the other commercially available zinc salts ( $\text{Zn}(\text{OAc})_2$ ,  $\text{ZnCl}_2$ ,  $\text{Zn}(\text{ClO}_4)_2$ ,  $\text{Zn}(\text{BF}_4)_2$ , and  $\text{Zn}(\text{NTf}_2)_2$ ) used for the complexation with premonomer **7**. The complexations with these zinc salts were considered as straightforward, since the only main difference among them were the different counterions.

### **Zn(OAc)<sub>2</sub>/ZnCl<sub>2</sub>**

$\text{Zn}(\text{OAc})_2$  and  $\text{ZnCl}_2$  were used independently for titrations with the premonomer **7**. Both salts were each dissolved in methanol- $d_4$  and step-wise titrated to the premonomer **7**. The titration results for both salts were identical and were performed similarly to the earlier discussed titration shown in Figure 4.17. In this regard, an exemplary titration of  $\text{Zn}(\text{OAc})_2$  to the premonomer **7** is illustrated in Figure 4.18.

## 4. Results and Discussion

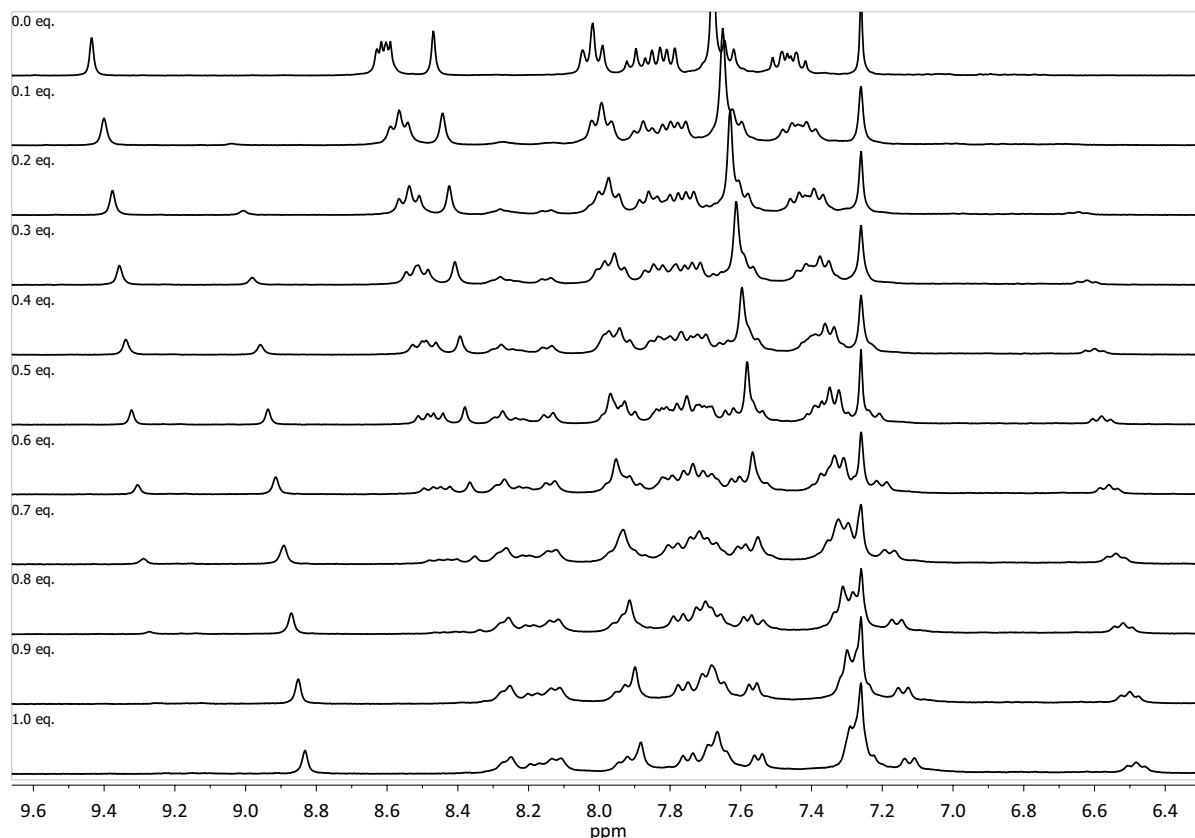


Figure 4.18: 300 MHz  $^1\text{H-NMR}$  spectra of the premonomer **7** with the step-wise addition of  $\text{Zn}(\text{OAc})_2$  in a  $\text{CDCl}_3/\text{methanol-}d_4$  mixture.

Adding  $\text{Zn}(\text{OAc})_2$  to the premonomer **7** revealed only the resulting typical proton signals of a mono-complex **37** at the  $^1\text{H-NMR}$  spectra (Fig. 4.18). The characteristic proton signals of the bis-complex **3** were missing. This could be explained by the strong binding between the zinc cation and the counterions ( $\text{OAc}^-$ ), which occupied one of two ligand positions of the premonomer **7** at the metal core, causing mono-complexation.<sup>[197]</sup> The exact same observation was made when using  $\text{ZnCl}_2$  for the titration with premonomer **7**.

Hence, none of the two zinc salts were further explored, since both only resulted in mono-complex **37**. Eventually, by changing the solvent, the bis-complex **3** formation would be enhanced.<sup>[252]</sup> Exchanging the counterion after the complexation with  $\text{PF}_6^-$  did not seem appropriate at this point, as no bis-complex **3** was observable and it is unlikely that such counterion exchange would transform a mono-complex **37** to a bis-complex **3**.

### $\text{Zn}(\text{ClO}_4)_2$

$\text{Zn}(\text{ClO}_4)_2$  contains two  $\text{ClO}_4^-$  as non-coordinating anions. Non-coordinating anions are supposed to enhance the complexation of terpyridines and shouldn't hinder the complexation of

## 4. Results and Discussion

metal cations with ligands. The titration illustrated in Figure 4.19 was performed with step-wise additions of a  $\text{Zn}(\text{ClO}_4)_2$  solution in a  $\text{CDCl}_3/\text{methanol-}d_4$  (5 : 3) mixture to the premonomer 7 solution in a  $\text{CDCl}_3/\text{methanol-}d_4$  (7 : 3) mixture. Because  $\text{Zn}(\text{ClO}_4)_2$  was insoluble in  $\text{CDCl}_3$  only, it was first dissolved in methanol- $d_4$  and then diluted with  $\text{CDCl}_3$ . The premonomer was insoluble in methanol- $d_4$  only, so it was first dissolved in  $\text{CDCl}_3$  and then diluted with methanol- $d_4$ . The solutions of both premonomer 7 and  $\text{Zn}(\text{ClO}_4)_2$  had a comparable ratio of  $\text{CDCl}_3$  to methanol- $d_4$ , which minimized the solvent shifting in the  $^1\text{H-NMR}$  spectra.

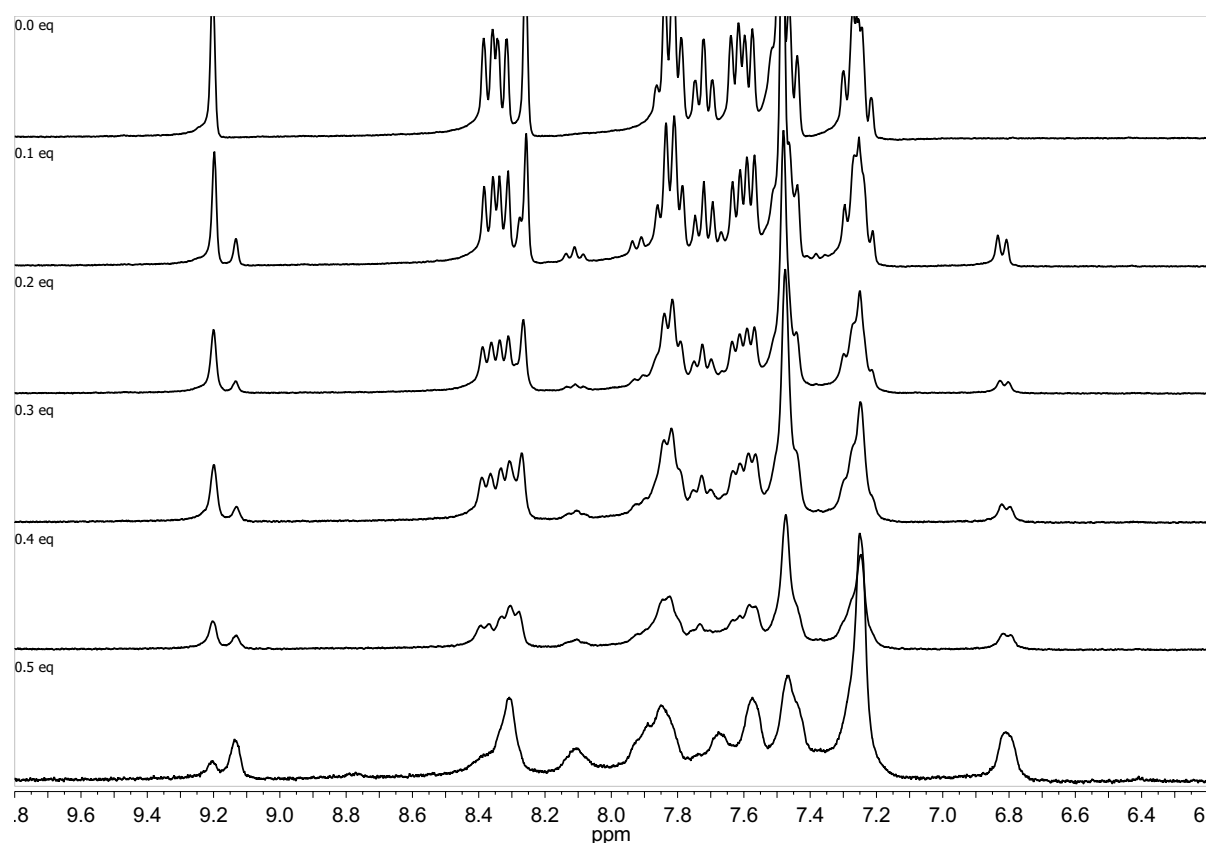


Figure 4.19: 300 MHz  $^1\text{H-NMR}$  spectra of the premonomer 7 with the step-wise addition of  $\text{Zn}(\text{ClO}_4)_2$  in a  $\text{CDCl}_3/\text{methanol-}d_4$  (7 : 3) mixture.

After each addition of  $\text{Zn}(\text{ClO}_4)_2$  to the premonomer 7, a new set of proton signals appeared in the spectrum and the signals broadened significantly with the appearance of a yellow solid, which precipitated from the solvent. In general, solid particles in a solution NMR spectroscopy measurement distort the homogeneity of the magnetic field, which causes line broadening of the NMR signals. The precipitated solid was redissolved by heat, but it reprecipitated within a minute. Nevertheless, the titration was continued up to the addition of 0.5 eq. of  $\text{Zn}(\text{ClO}_4)_2$ , at which the proton spectrum indicated resulting bis-complex 3 and some remaining premonomer 7 signals. The yellow solid was separated by paper filtration and washed with methanol, then



## 4. Results and Discussion

analyzed by  $^1\text{H-NMR}$  spectroscopy in a  $\text{CDCl}_3/\text{methanol-}d_4$  (5 : 1) mixture. The  $^1\text{H-NMR}$  spectrum is seen in Figure 4.20 and reveals the expected proton signals of bis-complex **3**. The characterization will be described later in this chapter. In addition, the yellow solid was examined under the OM and observed as tiny oval crystals (16 x 40  $\mu\text{m}$ ).

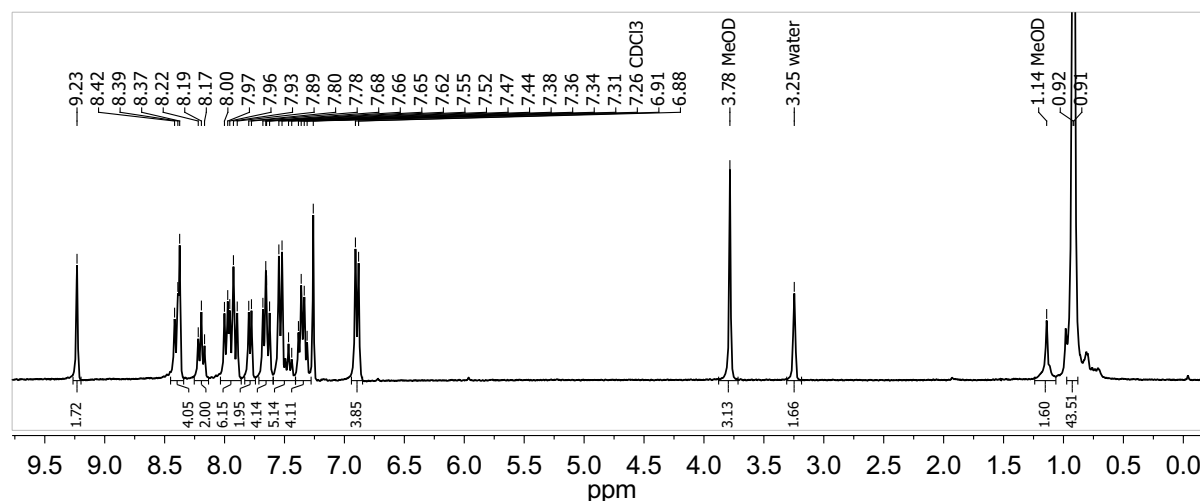


Figure 4.20: 300 MHz  $^1\text{H-NMR}$  spectrum of bis-complex **3** ( $X = \text{ClO}_4^-$ ) in a  $\text{CDCl}_3/\text{methanol-}d_4$  (5 : 1) mixture.

### $\text{Zn}(\text{BF}_4)_2/\text{Zn}(\text{NTf}_2)_2$

$\text{Zn}(\text{BF}_4)_2$  and  $\text{Zn}(\text{NTf}_2)_2$  both contain non-coordinating anions. Of the two anions,  $\text{NTf}_2^-$  is bulkier and its salts are supposed to have a high solubility in non-polar organic solvents,<sup>[253]</sup> which was considered important to finding new solvents for the complexation that would lead to crystals with a suitable crystal packing for a poly[n]catenane monomer. The titration of either,  $\text{Zn}(\text{BF}_4)_2$  or  $\text{Zn}(\text{NTf}_2)_2$ , to the premonomer **7** was performed in the same two-solvent media: a mixture of  $\text{CDCl}_3/\text{methanol-}d_4$  (2 : 1). Using the same solvent media prevented the proton signal shifting, which was observed for earlier titrations (Fig. 4.17 & Fig. 4.18), and had the advantage of experimental reproducibility for repetition of titrations. As a remark, the proton signals of the metal-free premonomer **7** in  $\text{CDCl}_3/\text{methanol-}d_4$  (2 : 1) were strongly dependent on the concentration of the methanol- $d_4$  content. Methanol- $d_4$  and other alcohols are weak acids and could therefore act as proton donors.<sup>[251]</sup> The protons could complexate with terpyridines and cause a shift of the terpyridine proton signals.

The use of  $\text{Zn}(\text{BF}_4)_2$  as the salt for the premonomer **7** titration minimized the mono-complex **37** formation, and caused precipitation of the bis-complex **3** from the reaction mixture in the form of crystals. A very similar result was obtained by using  $\text{Zn}(\text{NTf}_2)_2$  instead. The typical

## 4. Results and Discussion

titration of  $\text{Zn}(\text{BF}_4)_2$  to the premonomer **7** in a  $\text{CDCl}_3/\text{methanol-}d_4$  (2 : 1) mixture is shown in Figure 4.21 and represents the nearly ideal case for the titration towards a bis-complex **3**.

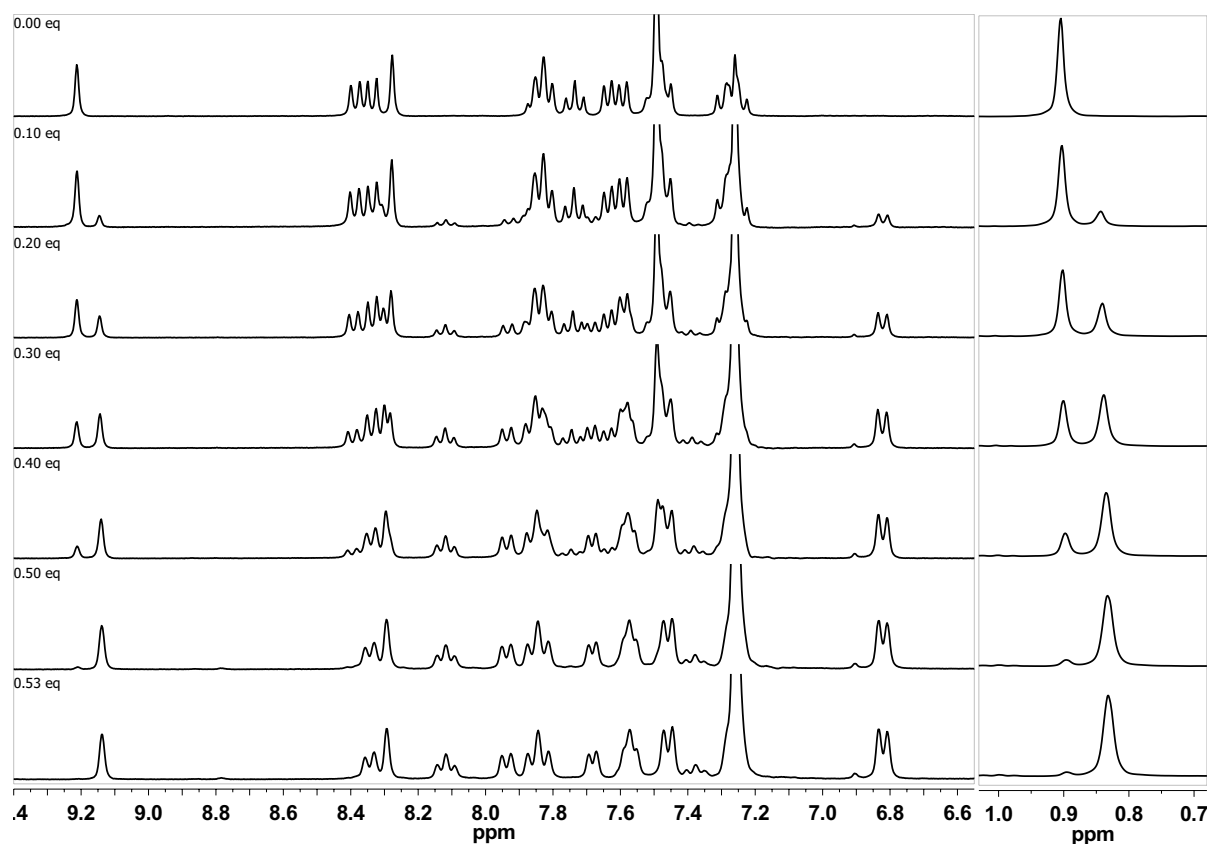


Figure 4.21: 300 MHz  $^1\text{H}$ -NMR spectra of the premonomer **7** with the step-wise addition of  $\text{Zn}(\text{BF}_4)_2$  in a  $\text{CDCl}_3/\text{methanol-}d_4$  (2 : 1) mixture.

The proton signals in the  $^1\text{H}$ -NMR spectra (Fig. 4.21) clearly show the rise of the bis-complex **3** and the decrease of the premonomer **7**. Since the proton spectrum at 0.5 eq. of  $\text{Zn}(\text{BF}_4)_2$  revealed remaining premonomer **7** signals, the  $\text{Zn}(\text{BF}_4)_2$  addition was continued in smaller additions until the premonomer **7** signals completely disappeared at 0.53 eq. of  $\text{Zn}(\text{BF}_4)_2$ . The cause for necessitating a slight excess could be the inaccurate amount of water contained in the commercially available  $\text{Zn}(\text{BF}_4)_2^{\text{X}}$ . The small signal observed at ca. 8.8 ppm could be resulting mono-complex **37**, caused by the slight excess of  $\text{Zn}(\text{BF}_4)_2$  used, but since the bis-complex **3** precipitated out of the reaction mixture and was isolated by filtration, the mono-complex **37** formation was disregarded from this point onwards. As a consequence of the bis-complex **3** precipitation, other complexation experiments were not necessarily followed by  $^1\text{H}$ -NMR titration anymore. Instead of performing a titration, a solution of 0.5 eq. of zinc salt was now added at once to a solution of premonomer **7**, and the resulting bis-complex **3** precipitate

<sup>X</sup>According to Strem it contained ca.  $4 \cdot \text{H}_2\text{O}$  per  $\text{Zn}(\text{BF}_4)_2$

## 4. Results and Discussion

was isolated by filtration.

The NMR spectra of both, premonomer **7** and isolated bis-complex **3** in CDCl<sub>3</sub>, were compared. The proton spectra are shown in Figure 4.22a and the carbon spectra in Figure 4.22b. The signals of 9-Ant, 3,3''-Py, and 3',5'-Py, as well as the spacer (Sp) signal splitting caused by the complexation of premonomer **7** to the bis-complex **3** are highlighted in the NMR spectra.

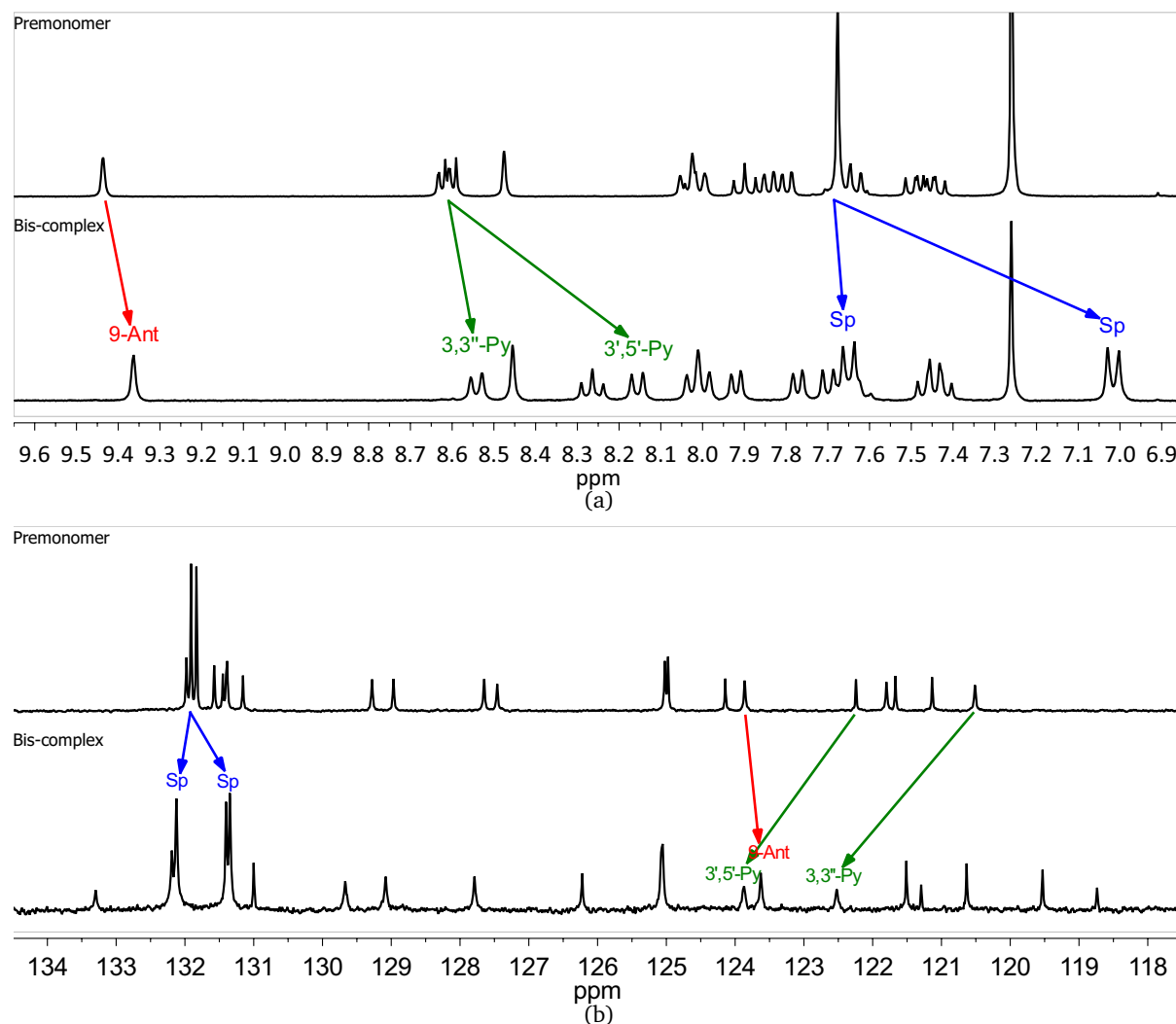


Figure 4.22: a) 300 MHz <sup>1</sup>H-NMR spectra and b) 126 MHz <sup>13</sup>C-NMR spectra of the premonomer **7** (top) in comparison with the bis-complex **3** (bottom) in CDCl<sub>3</sub>.

Upon complexation of the premonomer **7** with the zinc salt, many terpyridine proton signals are shifted due to the change from a *trans-trans* to a *cis-cis* conformation (Fig. 4.22a). The spacer protons are also split into two signals, as one part is more influenced by the metal cation than the other. For the same reason, many anthracene signals are chemically shifted due to the influence of the cation on the aromatic ring current. Since the 9-anthracene proton signal is not overlapping with other signals, the slight change is distinctive. Also, the carbon spectra of

## 4. Results and Discussion

both, premonomer **7** and bis-complex **3**, were chemically shifted for similar arguments as for the proton signals. The interconnection between neighboring proton signals within the bis-complex **3** were determined by the  $^1\text{H}$ - $^1\text{H}$ -COSY spectrum (Fig. 4.23). All proton and carbon signals of the bis-complex **3** could be characterized as shown in the Experimental 6.2..

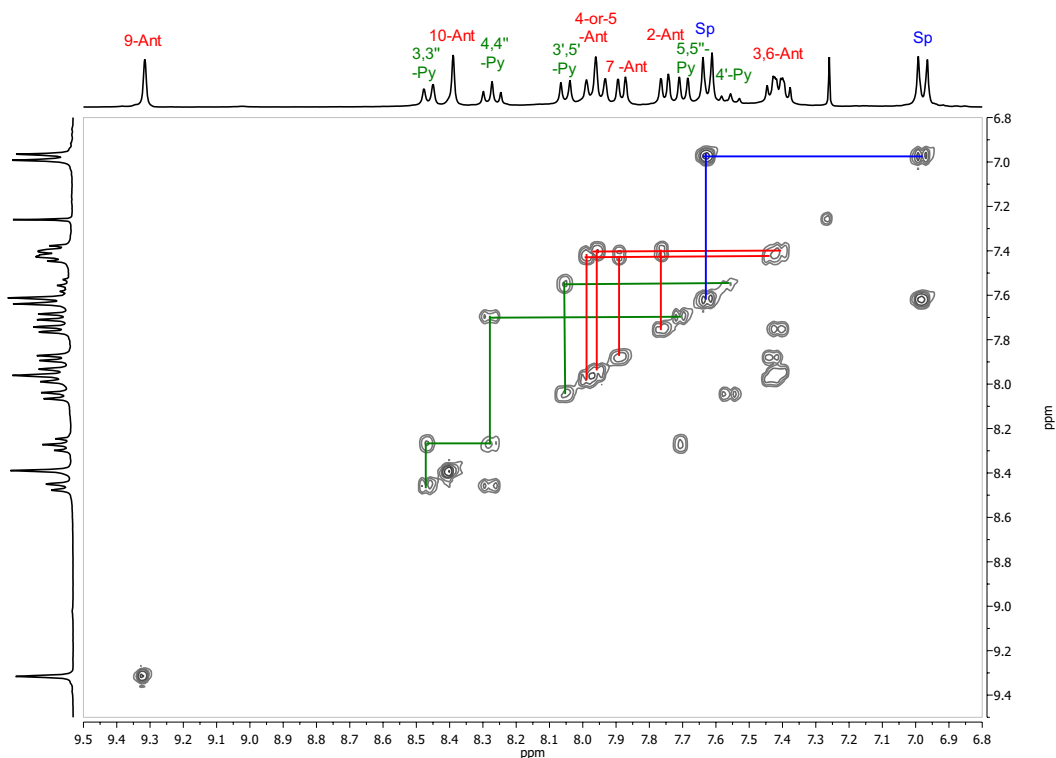


Figure 4.23: 500 MHz  $^1\text{H}$ - $^1\text{H}$ -COSY spectrum of **3** in  $\text{CDCl}_3$ .

Summarizing all the spectral discussions above, it can be concluded that the premonomer **7** undergoes complexation with zinc salts. Mono-complexes **37** are formed by using  $\text{Zn}(\text{OAc})_2$  or  $\text{ZnCl}_2$  at the complexation with the premonomer **7**. Bis-complexes **3** precipitate in the form of crystals if one of these zinc salts,  $\text{Zn}(\text{ClO}_4)_2$ ,  $\text{Zn}(\text{BF}_4)_2$ , or  $\text{Zn}(\text{NTf}_2)_2$ , are used for the complexation with the premonomer **7**.

### Decomplexation of the bis-complex **3**

For the final step to poly[n]catenanes, a decomplexation/demetallation protocol needed to be established. By using the bis-complex **3** itself as a model compound, several decomplexation methods were tested according to procedures that recommended using acids (HCl, HEEDTA, and TFA)<sup>[195–198,246,254]</sup> and bases (1,8-Diazabicyclo[5.4.0]undec-7-en<sup>[255]</sup>, NaOH<sup>[246,256,257]</sup> and  $\text{K}_2\text{CO}_3$  in DMF<sup>[258]</sup>). Of these methods, the HEEDTA was observed to perform well under ambient conditions (Fig. 4.24), keeping the TIPS group intact. It was therefore decided to

## 4. Results and Discussion

use this method for further decomplexation of the metallated poly[n]catenanes, once they had been obtained. Other reagents, such as cyclen<sup>[199]</sup>, CN<sup>-</sup>, pentetic acid, Li<sub>2</sub>S<sup>[259]</sup>, and tetraethyl ammonium chloride<sup>[259]</sup> are also potential decomplexation agents.

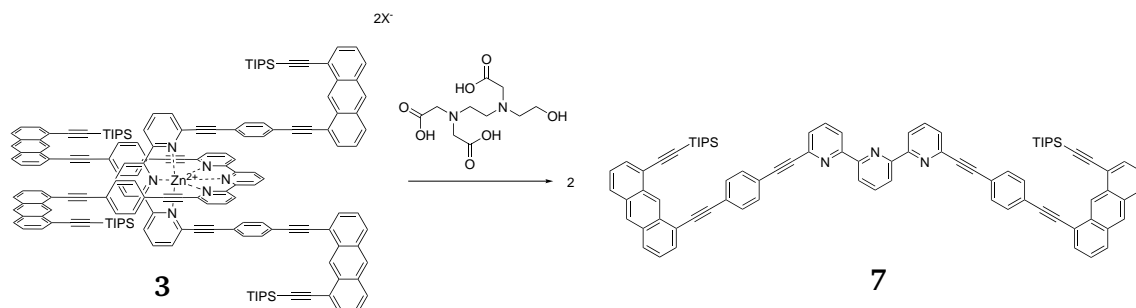


Figure 4.24: Decomplexation of **3** with HEEDTA.

Surprisingly, the <sup>1</sup>H-NMR spectrum of the bis-complex **3** in DMF-*d*<sub>7</sub> revealed proton signals nearly identical with the ones from the premonomer **7**. DMF was found to act as a competitor to the terpyridine complexation and demetallated the bis-complex **3**. To confirm this, a time-course experiment was conducted (Fig. 4.25) in which a proton spectrum of the bis-complex **3** in DMF-*d*<sub>7</sub> was measured at specific points of time for two hours.

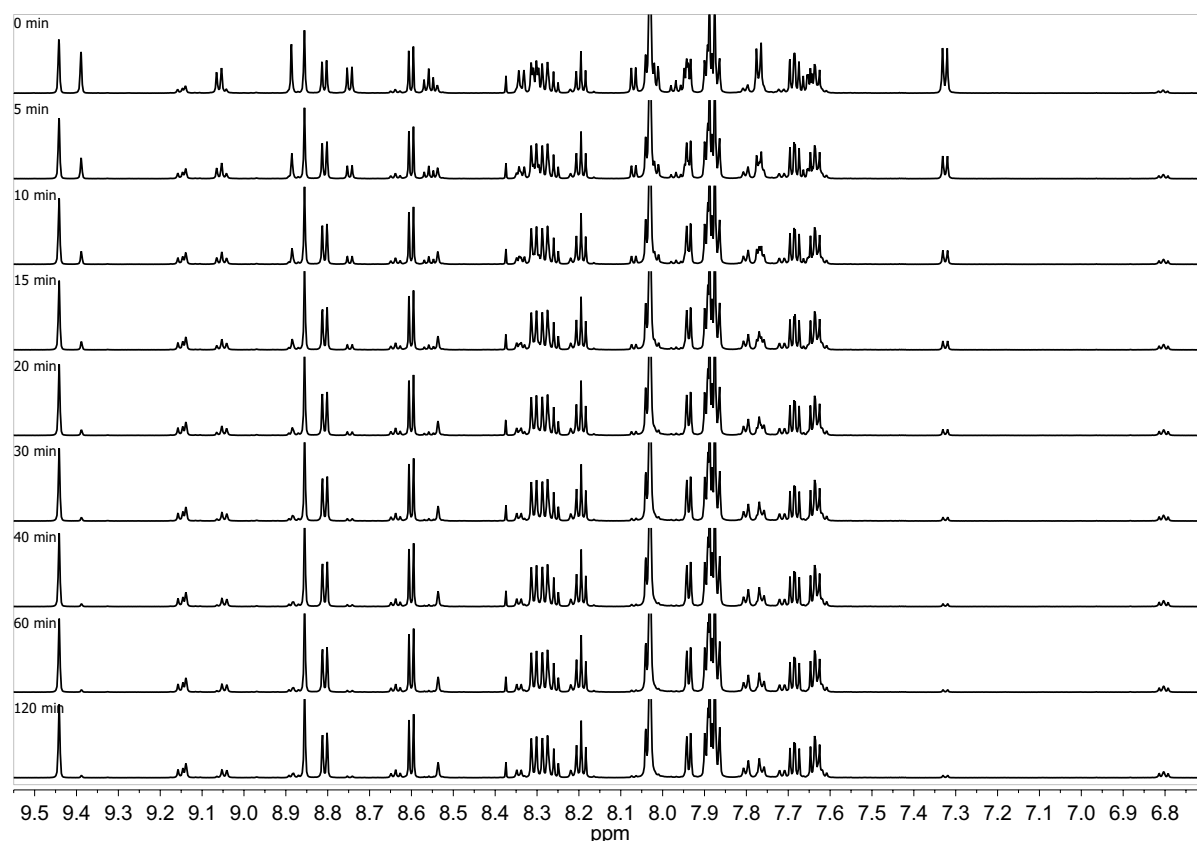


Figure 4.25: 700 MHz <sup>1</sup>H-NMR spectra of the time-course decomplexation of bis-complex **3** at rt in DMF-*d*<sub>7</sub>.

## 4. Results and Discussion

The bis-complex **3** was quickly dissolved in DMF- $d_7$  and subsequently the first proton NMR was measured after 105 seconds. Therefore, the first spectrum beginning at "0 minutes" in Figure 4.25 shows the equilibrium of bis-complex **3**, mono-complex **37**, and premonomer **7** at the average measured scans from the first 105 seconds. Over time, the bis-complex **3** proton signals decreased, while the premonomer **7** and mono-complex **37** proton signals increased. The changes over time was monitored and are shown in Figure 4.26. Therein, chloroform was used as a reference compound to compare the different ratios between characteristic bis-complex **3**, mono-complex **37**, and premonomer **7** proton signals (highlighted at inset in Fig. 4.26). The curves show a time-dependent proton signal decrease of the bis-complex **3**, as well as the increase of the mono-complex **37** and premonomer **7**.

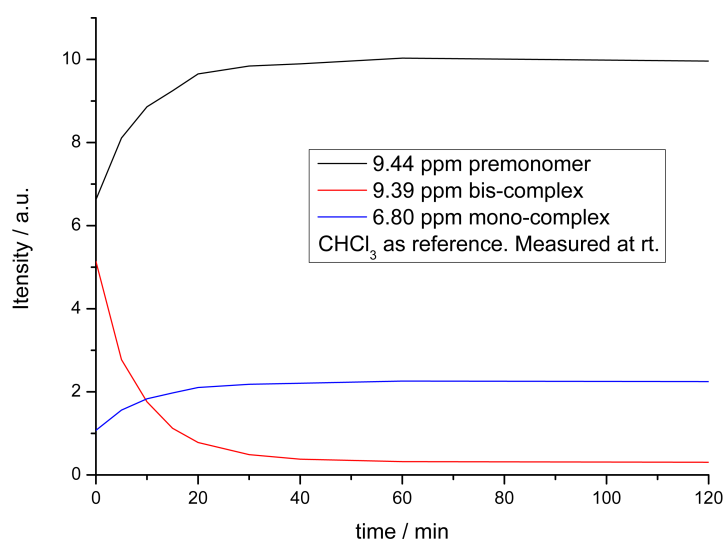


Figure 4.26: Time-course decomplexation of characteristic proton signals of premonomer **7**, bis-complex **3**, and mono-complex **37**, with CHCl<sub>3</sub> as the reference compound at rt in DMF- $d_7$ .

Overall, the time-course decomplexation revealed that over a time frame of 120 minutes, the equilibrium of all three compounds was reached after ca. 20 minutes. This proved the feasible demetallation with DMF by simply adding the solvent to the bis-complex **3** within a time-frame of 20 minutes. A similar time-course decomplexation experiment was repeated with fresh samples of bis-complex **3** at 50 °C and at 90 °C. At these temperatures the equilibrium was reached within five minutes of the <sup>1</sup>H-NMR measurement, proving a fast decomplexation in DMF at high temperatures. However, to isolate a fully demetallated compound, there is still the need of an additional treatment to remove the remaining zinc salt from the solution.

The proton spectra of premonomer **7**, bis-complex **3** after start, and bis-complex **3** after 120 minutes at rt in DMF- $d_7$  were compared in Figure 4.27 to characterize the observed proton sig-

## 4. Results and Discussion

nals. Figure 4.27 also shows the interconnection of the proton signals of each compound within in the spectrum, in which the terpyridine signals were connected with a line on top of each spectrum, while anthracene signals are connected with a line below each spectrum. The spacer proton signals are marked as Sp. The 2,3,4,5,6,7-Ant signals in the bis-complex **3** spectrum were difficult to distinguish, therefore only the range is marked with a short line to indicate where the signals are expected to appear. For clarification, the TIPS group of each compound is not shown in the spectrum. The TIPS group of the premonomer **7** and the mono-complex **37** would appear at 1.12 ppm, while the TIPS group of the bis-complex would appear at 1.06 ppm. The strong singlet at 8.38 ppm corresponds to the chloroform reference.

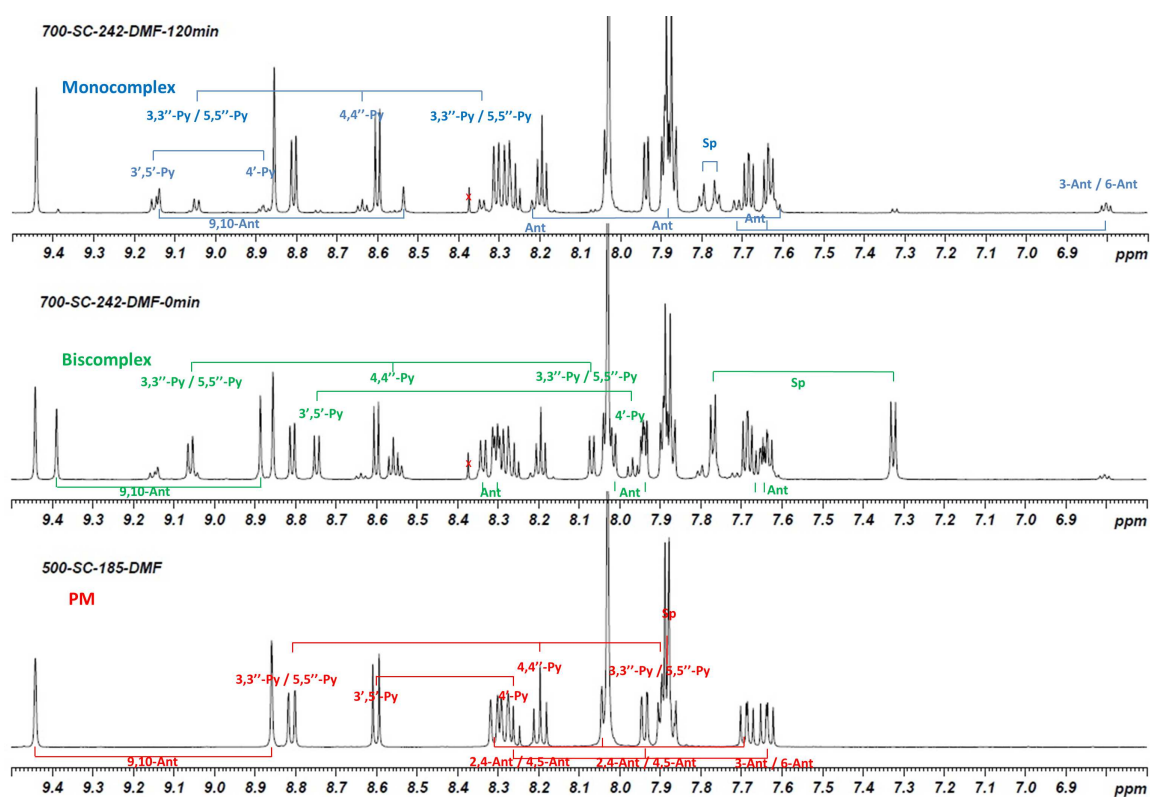


Figure 4.27: <sup>1</sup>H-NMR spectra of the bis-complex **3** after 120 minutes, the bis-complex **3** at the beginning, and the premonomer **7** at rt in DMF-d<sub>7</sub> (from top to bottom).

### UV/Vis and fluorescence analysis of the bis-complex **3** and the reference compound **38**

Before attempting crystallization or irradiation experiments, the bis-complex **3** was analyzed by UV/Vis and fluorescence spectroscopy measurements to guarantee the capability for a photoreaction to take place, and to make sure that the bis-complex **3** does not absorb the excitation energy for processes other than photodimerizations upon irradiation. In this regard, UV/Vis absorption and fluorescence emission spectra were measured on both bis-complex **3** (X = NTf<sub>2</sub><sup>-</sup>)

## 4. Results and Discussion

and a reference compound **38**<sup>XI</sup>, in solution (Fig. 4.28).

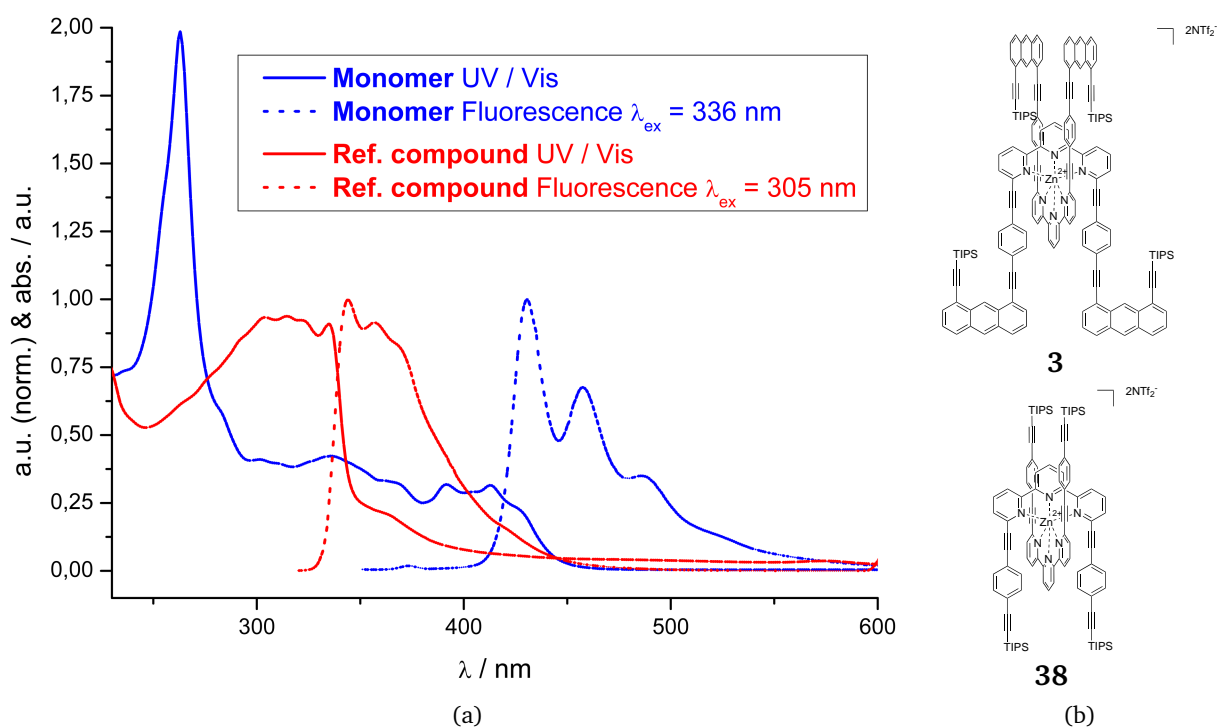


Figure 4.28: UV/Vis absorption and fluorescence emission spectra of bis-complex **3** ( $X = NTf_2^-$ ) and a reference compound **38**.

The spectra of the reference **38** represents the UV/Vis absorption and fluorescence emission (Fig. 4.28) from the parts other than anthracenes in the structure of **3** ( $X = NTf_2^-$ ). The comparison of both absorption spectra shows that zinc-complexation of the terpyridine parts generate no MLCT band, which would typically appear above 500 nm with other metal cations, such as  $Fe^{2+}$ . In addition, the absorption bands of the anthracene moieties are rendered at the lowest energy levels and well separated with the other absorption bands. These results confirm the following: a) the anthracene moieties of **3** can be selectively excited by light with the wavelengths of the absorption tail (430 - 460 nm); b) there is no competing chromophore group which can possibly trap the energy absorbed by the anthracenes; c) the excited anthracenes can undergo the subsequent processes which include not only fluorescence emission (broken blue line in Figure 4.28) and thermal deactivation to the ground state, but also the photochemical reaction of the present interest.

<sup>XI</sup>For the spectroscopy measurements, the reference compound **38** was prepared by adding a dissolved solution of 0.5 eq. of  $Zn(NTf_2)_2$  in methanol to the premonomer **7** in a chloroform solution.



### 4.3. Part A: Crystals and Irradiation

This subchapter discusses the processes of crystallization of the bis-complex **3**, the irradiation of its crystals, the characterization and the demetallation of the photoproducts obtained.

Having succeeded in the synthesis of the bis-complex **3**, the compound had to be crystallized, and the crystal structure had to be determined—which presents a crucial step for the proposed solid-state photoirradiation towards a poly[n]catenane. For a proper photoreaction to take place, the anthracene units of the bis-complex **3** need to stack face-to-face between adjacent bis-complexes within a distance of ca. 4 Å. It would only be feasible to use crystal structures of a bis-complex **3** with exactly these features as a monomer for photoirradiation. As indicated previously, the complexations of the premonomer **7** with  $\text{Zn}(\text{ClO}_4)_2$ ,  $\text{Zn}(\text{BF}_4)_2$ , and  $\text{Zn}(\text{NTf}_2)_2$  resulted in bis-complexes **3** that precipitated out of the reaction mixture in the form of crystals. As a point of departure, an XRD analysis of these crystals was performed.

Since the process of crystallization is complex, a number of factors can confound the process. For example, crystals that precipitate out too quickly could potentially be of lower quality due to the reduced time for nucleation and growth into a crystal. These inferior crystals would be hard to define with XRD analysis, especially with the use of conventional X-ray generators<sup>XII</sup>. To avoid measurements of low quality crystals, and to determine the average size and shape of the samples, the crystals were examined under the OM before submitting them to the crystallographer. The observation of birefringence—which is an optical property of anisotropic crystals—with the inspected material under the POM can be considered a sign of crystalline order.

The probability of growing crystals with a quality suitable for XRD analysis can be enhanced in two ways: by focusing on the precipitation process itself, or by using the precipitated crystals for recrystallization to regrow higher quality crystals. Additionally, the precipitate could be used to recrystallize the bis-complex **3** in other solvents, potentially resulting in a different crystal packing. The crystallization process itself can be affected by a number of factors, including time, temperature, vessel shape, and solvent mixture.

#### *Crystallization methods using good solvents*

The bis-complex **3** was first screened for solubility in a variety of organic solvents. Solvents such as a butanone, chloroform/methanol mixture, *o*-chlorophenol, cyclohexanone, ODCB, 1,2-

---

<sup>XII</sup>For example a synchrotron light source would allow a better resolution than in-house X-ray generators.

#### 4. Results and Discussion

---

dichloroethane, DCM, 1,4-dioxane, DMF<sup>XIII</sup>, NMP, TCE, and THF all qualified for evaporation, vapor diffusion, and liquid/liquid diffusion crystallization because of their good solubility.

Particularly slow evaporation is suitable for organic solvents marked by not too low boiling points (bps), or high vapor pressures at rt. While the solvent is evaporating, the dissolved compound becomes more concentrated over time until saturation is reached, at which point it precipitates out in the form of crystals or solid. If low bp solvents are used, then the time frame for crystallization is shorter at rt and the potential crystal precipitation may produce the aforementioned lower quality crystals. Therefore, these solvents should be used at low temperatures to slow the process of evaporation.

Vapor diffusion makes use of two separate solvents in a closed vessel. The desired compound is dissolved in a good solvent (inner solvent) and transferred to a small vial which is placed in a larger vessel. This large vessel is filled with a solvent (outer solvent) in which the compound has little to no solubility (bad solvent). In addition, the outer solvent usually has a lower bp. The large vessel is then sealed to prevent evaporation of both solvents. Slowly, the outer solvent vapor diffuses into the small vial, leading to a saturation of the compound in the solution and subsequent precipitation. For this to be successful, both solvents should also be miscible.

The third technique, liquid/liquid diffusion (layering technique), makes use of two solvents with different specific densities. Here, the compound is dissolved in a good solvent and the bad solvent is carefully layered on top of it, provided that it has a lower density than the good solvent. It is important that the solvents are not added rapidly to allow a good separation of the layers. Over time, the solvents gradually mix and the compound has a chance to precipitate.

These are standard techniques for crystallization in good solvents. Other techniques, such as crystallization by heating and cooling are suitable if the compound is insoluble or slightly soluble in the solvent at rt, but soluble at high temperatures near the bp. In this case, the solution can be slowly cooled to rt to allow slow precipitation. In some cases, ideal solvent mixtures are determined by adding a bad solvent to the dissolved compound until it precipitates, heating the mixture until it dissolves, then recooling to rt. This method can be used to find ideal solvents for vapor diffusion as well. A final method to purify and ideally crystallize a compound is through sublimation. Here, the solid is heated in a flask with a cold-finger in high vacuum. If the compound is volatile, then over time it deposits onto the cooled cold-finger.

---

<sup>XIII</sup>DMF is not being used as a solvent for crystallization, due to decomplexation ability.

## 4. Results and Discussion

---

With all of these techniques in mind, the crystallization of a compound can be addressed. Generally, the crystal structure of a compound is more easily solved with high crystal quality. However, some solvents, which are very often good solvents to organic compounds, are integrated into the crystal packing upon crystallization of a compound and are often not crystallographically well resolved. When using chloroform, for example, disorder is the frequent result.

### *Applying crystallization methods to the synthesized complexes*

Rather than recrystallization of a pre-prepared bis-complex **3**, it was more ideal for the complexation to occur in the same solvent as the crystallization would take place, as a one-pot procedure.

Towards this end, the solubility of the premonomer **7** was screened and solvents such as chloroform, cyclohexanone, ODCB, 1,2-dichloroethane, DCM, DMF, DMSO, 1,4-dioxane, fluorobenzene, NMP, TCE, THF, toluene, and *p*-xylene showed good solubility. The solubility of zinc salts in alcohols and ethers were generally good. Therefore, the premonomer **7** was dissolved in one of the solvents and the zinc salt, dissolved in another (miscible) solvent, was added at once.

Other considerations included the purity of the compound, as high purity is sometimes important for good crystallization. Additionally, the vials used for slow evaporation, vapor diffusion, and liquid/liquid diffusion should have no scratches to avoid unwanted nucleation sites for the precipitation and dust particles should be avoided as well. On the other hand, one has to keep in mind that sometimes compounds need such "defect" sites in order to nucleate at all. Vials were kept undisturbed in the dark with occasional inspections.

With all of these methods and solvents in mind, the crystallization attempts and subsequent XRD analysis of obtained crystals are described in the following paragraphs. The descriptions do not necessarily follow the order in which the experiments were performed. It must be remarked that as soon as the first XRD crystal structure (7.1.) of the bis-complex **3** ( $X = \text{BF}_4^-$ ) was obtained, the focus was shifted to explore bis-complexes **3** with  $\text{BF}_4^-$  as counterion. At a later stage of the thesis  $\text{NTf}_2^-$  was used as the counterion in the bis-complex **3**. Since the XRD crystal structure (7.1.) of bis-complex **3** ( $X = \text{NTf}_2^-$ ) was suitable for the aim of a poly[n]catenane via solid-state photoreaction, the focus was then shifted to this particular counterion.

## 4. Results and Discussion

### Crystals of bis-complex **3** ( $X = \text{ClO}_4^-$ )

At the titration of the  $\text{Zn}(\text{ClO}_4)_2$  solution into the premonomer **7** solution, the bis-complex **3** ( $X = \text{ClO}_4^-$ ) precipitated out, but the quality of the crystals was insufficient for an XRD measurement since they did not scatter enough. The crystals were then dissolved by heating and the solution was slowly cooled to rt, in order to give the compound more time to crystallize. With this method, the crystal size changed from ca.  $30 \mu\text{m}$  to ca.  $300 \mu\text{m}$  (Fig 4.29). However, the crystals were again not suitable for XRD measurements for the same reasons as before.

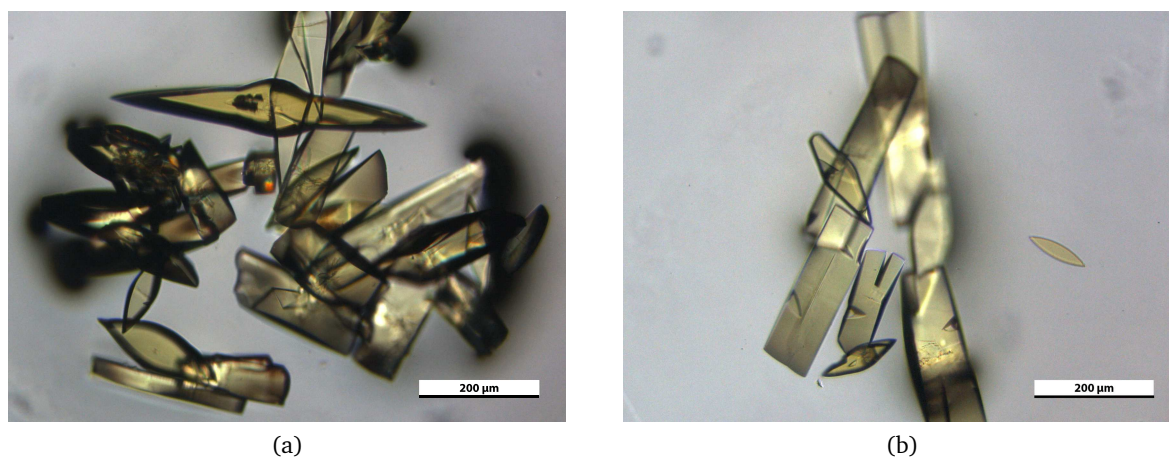


Figure 4.29: Optical micrographs showing crystals of **3** ( $X = \text{ClO}_4^-$ ) from chloroform/methanol.

Vapor diffusion of an alcohol (outer solvent), to a dissolved bis-complex **3** ( $X = \text{ClO}_4^-$ ) mixture of ODCB with the corresponding alcohol (inner solvent) resulted in precipitation of crystals. Using other outer solvents for the vapor diffusion resulted in a variety of bis-complex **3** crystals within two days: *n*-butanol resulted in yellow needles, methanol resulted in yellow squares & plates, and ethanol resulted in yellow squares. The XRD pattern of the latter crystals, from the ethanol to ODCB/ethanol vapor diffusion mixture, could not be precisely solved, due to the low quality and the disorder of the crystals. However, the preliminary solved structure (not shown) indicated that the bis-complex **3** ( $X = \text{ClO}_4^-$ ) was not forming 1D arrays.

Other attempted solvent mixtures for crystallization of  $\text{Zn}(\text{ClO}_4)_2$  salts did not yield crystals suitable for XRD measurements up to this point. Since the crystals were identified as bis-complex **3** by  $^1\text{H-NMR}$  spectroscopy, the crystal could, as a general principle, be irradiated without the knowledge of the actual crystal structure. During the course of the dissertation, other counterions led to bis-complexes **3** as well; the investigation was then expanded to include all other counterions, in order to achieve crystals of a higher quality suitable for XRD analysis.

## 4. Results and Discussion

### Crystals of bis-complex **3** ( $X = \text{BF}_4^-$ )

In some cases the titration of  $\text{Zn}(\text{BF}_4)_2$  to the premonomer **7** in a chloroform/methanol solution resulted in precipitation of crystals within minutes. These crystals were yellow, transparent, and had a plate-like shape (Fig. 4.30). Usually the size of these crystals were between 0.1 - 0.5 cm in length and 0.05 - 0.12 cm in width. To synthesize a large amount of crystals, the addition of  $\text{Zn}(\text{BF}_4)_2$  to the premonomer **7** was performed in one shot, as opposed to a series of measured additions (titration). In this addition, 0.5 eq. of zinc salt was dissolved in a chloroform/methanol (2 : 1) mixture and was added directly at once to the premonomer **7** in a chloroform/methanol (2 : 1) mixture. Depending on the concentration, the crystals formed between minutes and days.

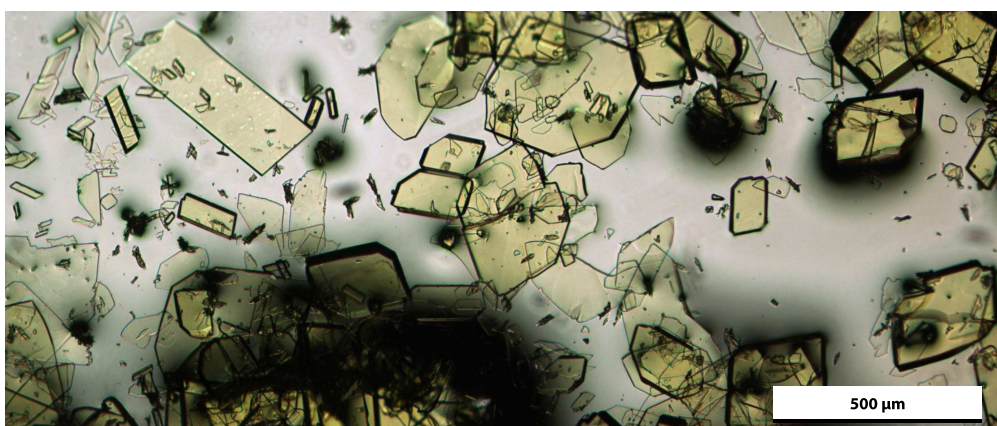


Figure 4.30: Optical micrograph showing crystals of **3** ( $X = \text{BF}_4^-$ ) in chloroform/methanol.

The crystals were examined with OM and POM (Fig. 4.31). When rotating the sample by  $45^\circ$  under the POM, the crystals showed birefringence, which is a sign of crystalline order, through the visual disappearance and reappearance of the crystals.

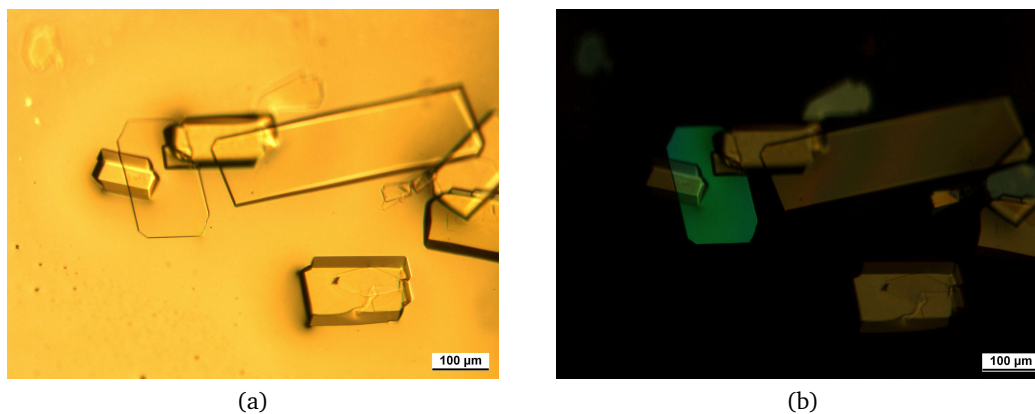


Figure 4.31: a) Optical and b) polarized optical micrographs showing crystals of **3** ( $X = \text{BF}_4^-$ ) in chloroform/methanol.

## 4. Results and Discussion

The XRD crystal structure (7.1.) of these crystals were determined (Fig. 4.32).

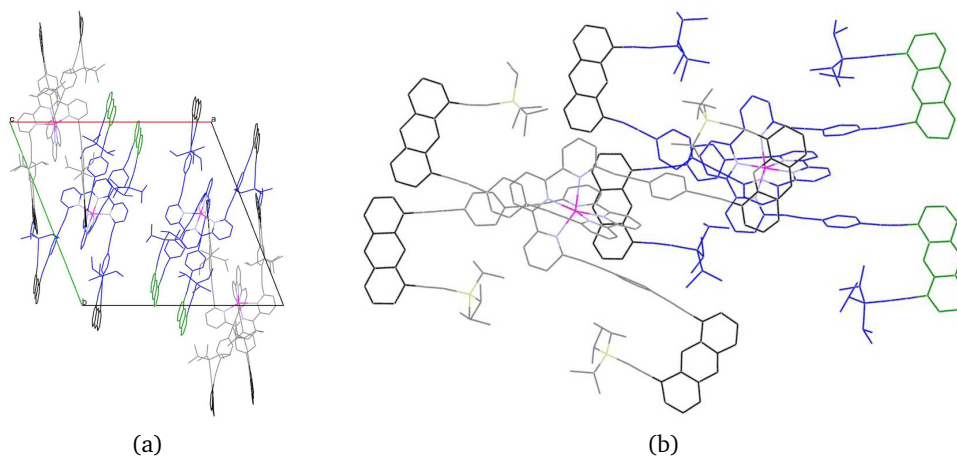


Figure 4.32: XRD crystal structure of **3** ( $X = \text{BF}_4^-$ ). (Hydrogens, counterions, and solvent molecules omitted.)

The crystal structure shows two independent bis-complexes within the unit cell and incorporates at least five chloroform (partially disordered) and one methanol solvent molecule. The two types of bis-complexes differ structurally slightly from each other (Fig. 4.32b). The grey colored bis-complex has a lower priority for the following discussion, as no anthracene (colored in black) stacking between adjacent bis-complexes is visible. The other blue colored bis-complex shows no anthracene stacking between adjacent bis-complex on the one side (anthracenes in black). On the other side, the anthracene units do stack face-to-face though, and are colored in green. The anthracene stackings of the blue colored bis-complexes are shown in Figure 4.33.

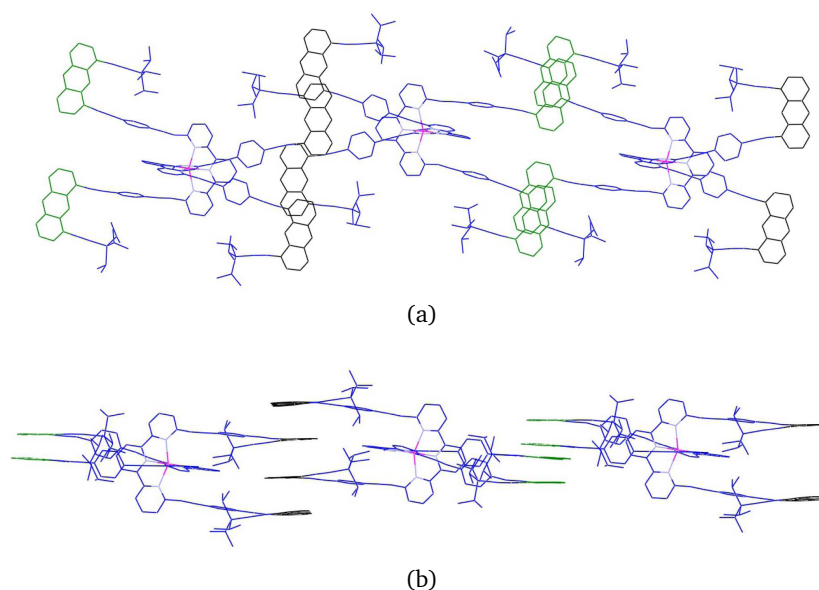


Figure 4.33: XRD crystal structure of **3** ( $X = \text{BF}_4^-$ ) a) top view and b) side view. (Hydrogens, counterions, and solvent molecules omitted.)

## 4. Results and Discussion

---

The green colored anthracene units of the blue colored bis-complex stack face-to-face with an adjacent bis-complex in a distance of 3.6 - 3.8 Å between the 9,10:9',10'-positions, which is sufficient for the [4+4]-cycloaddition dimerization. The other black anthracene units of the bis-complex show a distance of 5.6 - 5.9 Å between the 9,10:9',10'-positions with the adjacent bis-complex, which is in principle too far apart to allow a dimerization.

Overall, these crystals upon solid-state photoirradiation would most likely only lead to a bis-complex dimer. The other grey colored bis-complex is projected to show no dimerization due to the lack of anthracene stacking with adjacent bis-complex anthracene units. It is, however, safe to argue that the synthesis of a macrocycle upon irradiation and removal of the metal salts is possible with this type of crystal structure. This impact is elaborated on later in this chapter.

Other solvent mixtures and techniques to adjust the crystal structure were considered. Mixtures of premonomer **7** in chloroform with  $\text{Zn}(\text{BF}_4)_2$  in a variety of alcohols (MeOH, EtOH, iPrOH, PrOH, or *n*-BuOH) gave all crystalline precipitate. Unfortunately, only the resulting crystals from a chloroform/methanol mixture were suitable for XRD analysis. A mixture of ODCB/MeOH was promising for yielding yellow, clear, and rectangular crystals. In turn, a mixture of 1,4-dioxane/MeOH produced equally promising yellow, opaque crystals. Needles were obtained by vapor diffusion of a solution of a bis-complex **3** ( $\text{X} = \text{BF}_4^-$ ) in TCE/ethanol (inner solvents) and ethanol (outer solvent). The described process yielded crystals, which were, unfortunately, too low in quality to be measured by XRD. Within a few days, a slow evaporation in DCM at 5 °C resulted in crystals as well, which did not scatter well enough for an XRD analysis. Still, the determined unit cell was similar to the one of the chloroform/methanol mixture, and was therefore not further considered. In the case that the unit cell determination resulted in the same unit cell as with the crystal shown in Figure 4.32, which proved unsuitable, then the XRD measurement was not taken into consideration due to the limited amount of time slots available for measurements. It was therefore decided, in consultation with the crystallographer, that it was more feasible to determine an alternate process of crystal packing.

### Irradiation of the bis-complex **3** ( $\text{X} = \text{BF}_4^-$ ) crystals

Although the bis-complex **3** ( $\text{X} = \text{BF}_4^-$ ) did not show a crystal packing ideal for poly[n]catenation (Fig. 4.33), it could be used as a test compound to probe irradiation experiments, demetallations, and characterizations of resulting products. Using such a complex, which comprises anthracene units, for solid-state photoreactions is a new approach in context of terpyridine com-

## 4. Results and Discussion

plexes. In this context, it became of interest to further explore the impact of irradiation on a bis-complex **3** ( $X = \text{BF}_4^-$ ) crystal. The obtained results would then be valuable for other bis-complex crystals that are suitable for poly[n]catenation.

The first irradiation experiment with crystals of the bis-complex **3** ( $X = \text{BF}_4^-$ ) were performed between two glass slides at 465 nm for ca. 24 hours with no special set-up. The yellow color of the crystals changed to orange (Fig. 4.34) and the crystals were no longer soluble in chloroform at rt and bp. The color change may have been caused by oxidation to an anthrone. This oxidation was indicated by the IR spectroscopy measurement, through a broad band at  $1704 \text{ cm}^{-1}$ , which is characteristic for a C=O bond bounded to two aromatic moieties.<sup>[28]</sup> Further verification of an oxidation process occurring during the bis-complex **3** ( $X = \text{BF}_4^-$ ) irradiation was neglected. It was thus evident that some reaction in the crystal had taken place.

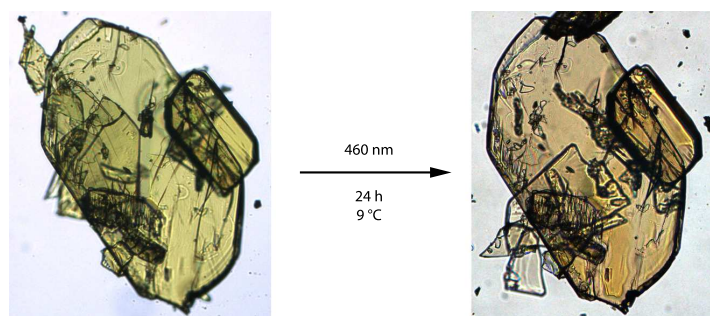


Figure 4.34: Optical micrograph showing the bis-complex **3** ( $X = \text{BF}_4^-$ ) crystals before and after irradiation (left to right).

A few irradiation experiments followed, with two of them using crystal samples with ca. 40 mg and 47 mg for the irradiation process. The irradiation of the samples took place in vials (at argon atmosphere), in the fridge (ca.  $10 \text{ }^\circ\text{C}$ ) at 465 nm for ca. two days. These crystals changed in color from yellow to orange as well. Some of the crystals were used for  $^1\text{H-NMR}$  spectroscopy measurements in  $\text{DMF-}d_7$ . This solvent nearly dissolved all of the crystals. The other insoluble part was only a fraction of the crystals' total mass; it was not quantified and up-to-now it is not clear what this insoluble part constitutes. The parts that dissolved in  $\text{DMF-}d_7$  (irradiated bis-complex) were analyzed by  $^1\text{H-NMR}$  spectroscopy. In consideration of the XRD crystal structure (7.1.) of the bis-complex **3** ( $X = \text{BF}_4^-$ ) shown earlier (Fig. 4.32 & 4.33), one would expect that only the blue colored bis-complex undergoes a dimerization between the green anthracenes upon irradiation with an adjacent blue colored bis-complex. As a result, only two anthracene units out of the eight should react with adjacent anthracenes to result in a "closed" macrocycle. In principle, the formation of an "open" macrocycle in which only one anthracene pair dimerizes,



## 4. Results and Discussion

with the other still unreacted, is feasible as side product. Provided that a quantitative reaction leading to a macrocycle took place, the  $^1\text{H-NMR}$  spectrum of the irradiated bis-complex **3** ( $X = \text{BF}_4^-$ ) should therefore reveal proton signals of the anthracene bridge-head as well as remaining anthracenes in a relative ratio of 1 : 3 (reacted : remaining). The proton spectra of the bis-complex **3** ( $X = \text{BF}_4^-$ ), the premonomer **7** (Fig. 4.35), and the irradiated bis-complex **3** ( $X = \text{BF}_4^-$ ) are seen in Figure 4.35.

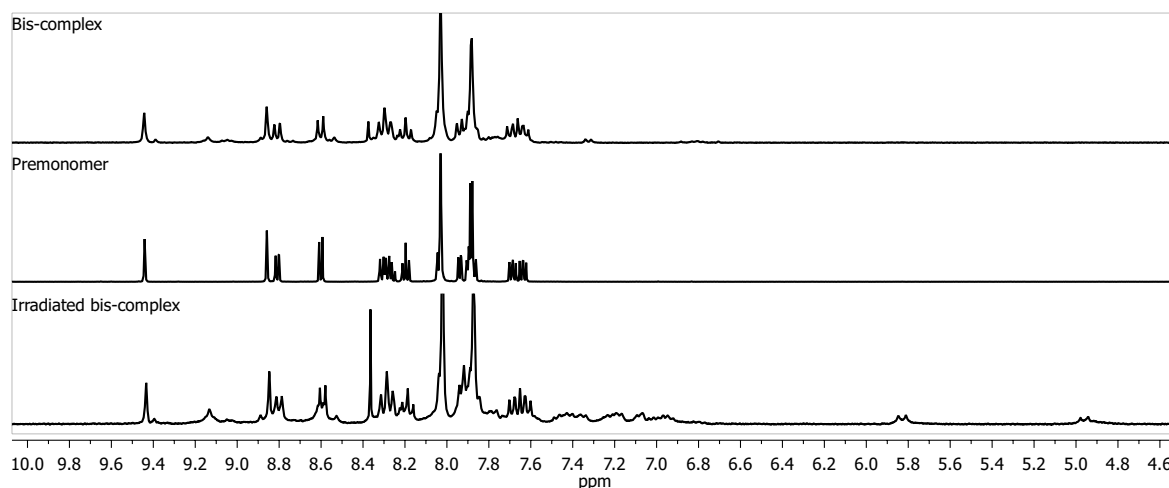


Figure 4.35: 300 MHz  $^1\text{H-NMR}$  spectra of bis-complex **3** ( $X = \text{BF}_4^-$ ) (top), premonomer **7** (middle), and irradiated bis-complex **3** ( $X = \text{BF}_4^-$ ) (bottom) in  $\text{DMF-}d_7$ .

The appearance of new anthracene bridge-head signals in the  $^1\text{H-NMR}$  spectra of the irradiated bis-complex **3** ( $X = \text{BF}_4^-$ ) at 4.95 and 5.85 ppm, and aromatic signals between 7.5 - 6.5 ppm, caused by the anthracene dimerization, are remarkable. However, the ratio between reacted and remaining anthracenes proton signals is about 1 : 1. This may indicate that some of the anthracene units have reacted to other products, such as through oxidation to anthracene endoperoxides or anthrones. Since the characteristic 9,10-dihydro singlet proton signal of an anthracene endoperoxide did not show up at ca. 6.0 ppm<sup>XIV</sup> in the  $^1\text{H-NMR}$  spectrum,<sup>[87,260]</sup> the endoperoxide formation was excluded. Anthrones could not be confirmed by  $^{13}\text{C-NMR}$  spectroscopy, due to the low signal-to-noise ratio of the measured spectrum. Although IR spectroscopy confirmed the observation of  $\text{C=O}$  bands, the total amount of oxidized irradiated bis-complex **3** ( $X = \text{BF}_4^-$ ) could not be determined. Perhaps the anthracenes that were stacking with distances greater than ca. 4 Å dimerized after all. In addition, the proton signals of the irradiated bis-complex **3** ( $X = \text{BF}_4^-$ ) are in general broadened, which could indicate resulting large molecules that cause this signal broadening due to their limited motion, or the signal broadening is a sign of nearly superimposing chemical shifts in solution. Remaining insoluble compound could also

<sup>XIV</sup>Reference measured in  $\text{CDCl}_3$ .

## 4. Results and Discussion

be the cause of signal broadening.

Since the  $^1\text{H-NMR}$  spectrum (Fig. 4.35) of the irradiated bis-complex **3** ( $X = \text{BF}_4^-$ ) appeared to be very similar to that of the premonomer **7** rather than of the non-irradiated bis-complex **3** ( $X = \text{BF}_4^-$ ), it was concluded that spontaneous self-decomplexation had occurred. This was possibly spurred by the solvent, DMF. This decomplexation would explain the multiplet proton signal at ca. 9.15 ppm, which is assigned to a mono-complex-type conformation. In summary, the  $^1\text{H-NMR}$  spectrum of the irradiated bis-complex **3** ( $X = \text{BF}_4^-$ ) shows anthracene dimer signals, and therefore reveals some successful photoirradiation. Simultaneously, the remaining 9,10-anthracene proton signals confirm that not all anthracene units have reacted.

Another tool to characterize the photoproducts was the MS analysis. The uncalibrated mass spectrum of the irradiated bis-complex **3** ( $X = \text{BF}_4^-$ ) is shown in Figure 4.36.

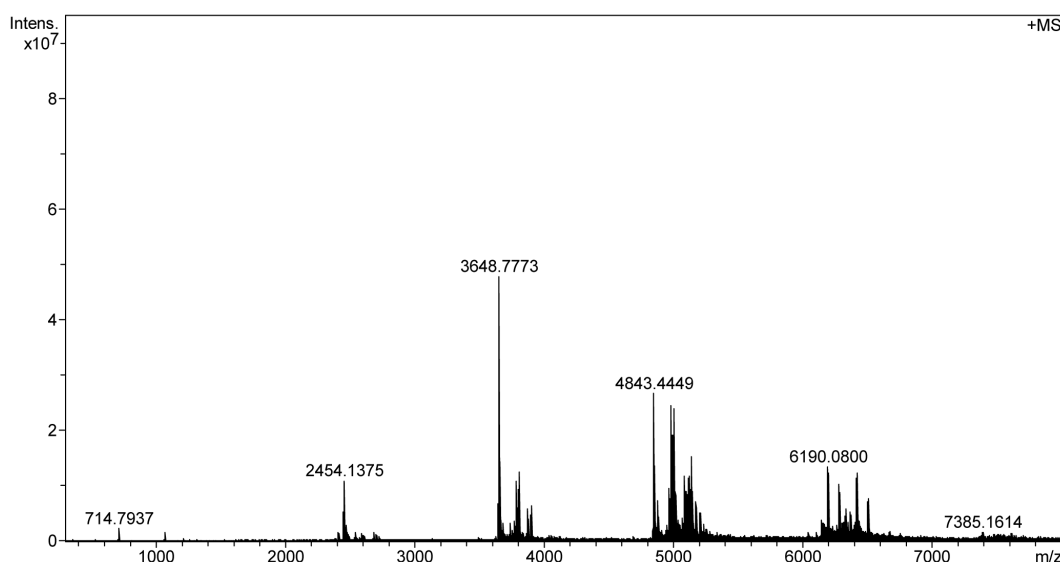


Figure 4.36: The high resolution MALDI MS of irradiated crystals of bis-complex **3** ( $X = \text{BF}_4^-$ ).

The MS of the irradiated bis-complex **3** ( $X = \text{BF}_4^-$ ) was expected to reveal the masses of a bis-complex and a dimerized bis-complex. Since the laser power of the MALDI could in principle degrade the complexation, the dimerized bis-complex minus a premonomer, a mono-complex, and a premonomer, were also expected. These compounds would then also be detected without counterions or zinc cations. Larger complexes that exceed the masses of two bis-complexes were, due to the crystal packing of the bis-complex **3** ( $X = \text{BF}_4^-$ ), not expected.

The first set of signals ( $m/z = 2454$ ) in the mass spectrum (Fig. 4.36) corresponds to the bis-complex (without counterions), the second set of signals ( $m/z = 3649$ ) corresponds to the

## 4. Results and Discussion

premonomer ( $M = 1195$  g/mol) that is connected to the bis-complex (without counterions), and the third set of signals ( $m/z = 4843$ ) corresponds to two bis-complexes (without counterions and one missing zinc cation). The larger set of signals ( $m/z = 6190$ ) could not be assigned. The detection of these signals clearly show that the bis-complex did undergo a reaction with another bis-complex. As well the set of signals are well separated with gaps of about the mass of a premonomer ( $m/z = 1195$ ). However, the formation of the larger set of signals at ca.  $m/z = 6190$  is still inexplicable.

### *Removal of the zinc salts*

The zinc salts needed to be removed for the next step to isolate the potential formed macrocycle. Since HEEDTA was still under inspection for efficiency of bis-complex **3** demetallation, a very crude method to remove the zinc cation was applied to the irradiated bis-complex **3** ( $X = \text{BF}_4^-$ ). The irradiated bis-complex **3** ( $X = \text{BF}_4^-$ ) was treated with a HCl/methanol mixture in chloroform, then was washed with water, and heated in TEA. After another water washing process, the organic part was analyzed by  $^1\text{H-NMR}$  spectroscopy in  $\text{CDCl}_3$ . Surprisingly, the mixture after HCl/TEA work-up was now soluble in chloroform. The rise of its solubility could be caused by the increase of motion of the compound, which was restricted through the zinc complexation. In addition, the solution showed a strong fluorescence under 366 nm UV light. The recurrence of fluorescence is another indication of zinc removal. The  $^1\text{H-NMR}$  spectrum of the premonomer **7** in comparison with the HCl/TEA treated mixture is shown in Figure 4.37.

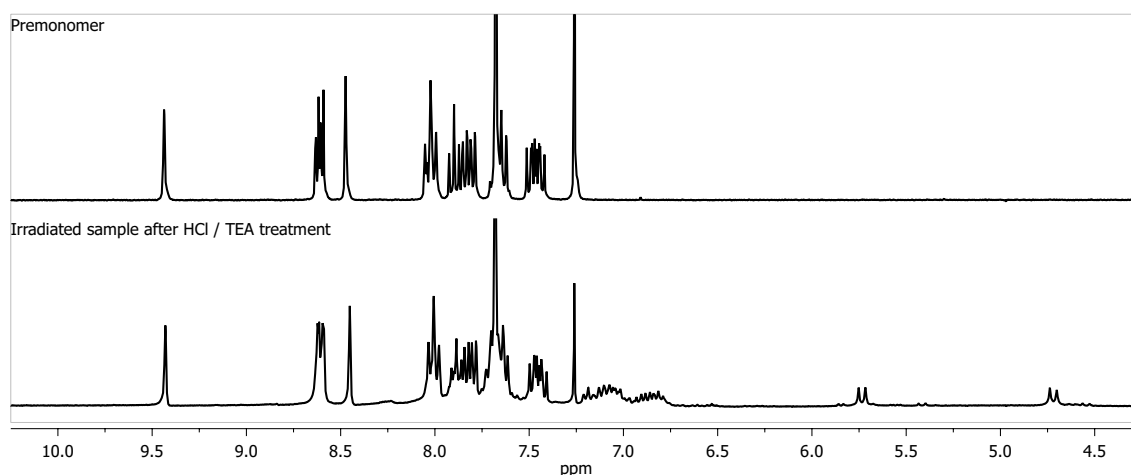


Figure 4.37: 300 MHz  $^1\text{H-NMR}$  spectra of premonomer **7** (top) and the HCl/TEA treated irradiated bis-complex mixture (bottom) in  $\text{CDCl}_3$ .

The spectrum of the irradiated bis-complex after HCl/TEA treatment should give a mixture of premonomers **7**, macrocycles, and potentially "open" macrocycles caused by incomplete dimer-

## 4. Results and Discussion

ization. Without the involvement of zinc salts, the spectrum shouldn't show any complex degradation caused by the MALDI laser. The proton spectrum (Fig. 4.37) clearly shows the 9,10-anthracene proton signals, which are in agreement with the premonomer **7** signals. The characteristic dimer bridge-head proton signals at 4.7 and 5.7 ppm are also observed, and the corresponding anthracene proton signals other than the 9,10-anthracene signals appear between 7.2 and 6.7 ppm as well. Once again, the spectrum of the HCl/TEA treated mixture indicates a successful photoirradiation. However, some weaker signals near the anthracene bridge-head proton signals mark side products within the mixture. To further investigate the photoproducts, a new mass spectrum measurement was conducted (Fig. 4.38; uncalibrated).

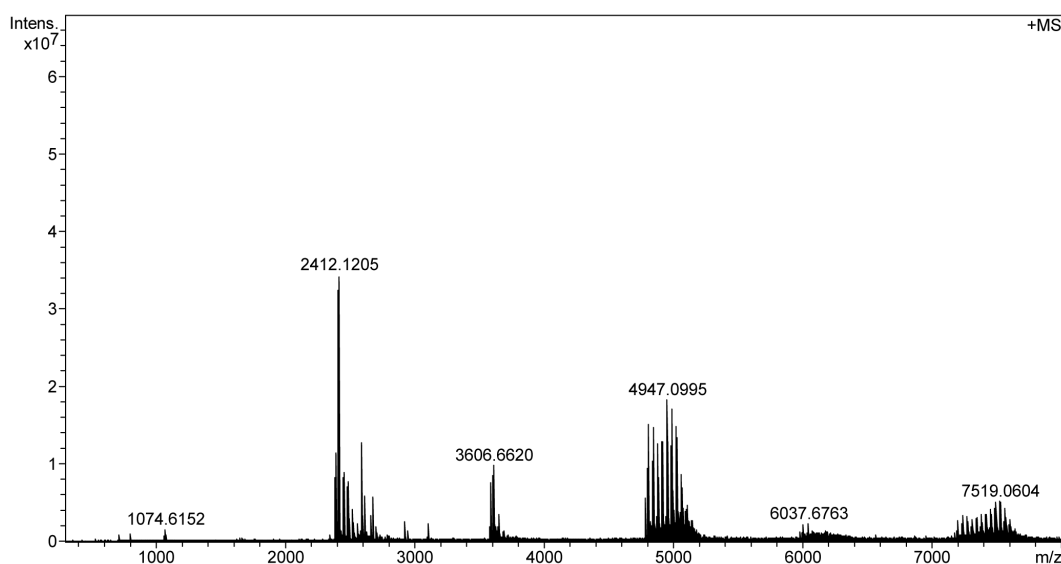


Figure 4.38: The high resolution MALDI MS of HCl/TEA treated irradiated bis-complex **3** ( $X = \text{BF}_4^-$ ).

As of now, the zinc salts have been successfully removed from the irradiated bis-complex, its MS (Fig. 4.38) should show similar masses than the previously measured MS (Fig. 4.36) minus the masses of zinc cations and counterions. Basically, the ratio of premonomer **7** to macrocycle of **3** : **1** should be found for the same reasons as described earlier. According to the XRD crystal structure (Fig. 4.33), the mass of a macrocycle should be found if dimerization of the green colored anthracenes took place. In addition, the mass of premonomer **7** should largely be found as well, due to the decomplexation of the grey bis-complex (Fig. 4.32), which is not expected to undergo a dimerization with adjacent anthracenes, and the blue bis-complex should also release a remaining premonomer.

The three sets of signals within the MS at  $m/z = 2410$ ,  $3604$ , and  $4797$  were confirmed by their specific isotope distribution as  $\text{C}_{170}\text{H}_{150}\text{N}_6\text{NaSi}_4$ ,  $\text{C}_{255}\text{H}_{225}\text{N}_9\text{NaSi}_6$ , and  $\text{C}_{340}\text{H}_{300}\text{N}_{12}\text{NaSi}_8$ ,

## 4. Results and Discussion

which correspond to a dimer, trimer, and tetramer of the premonomer with  $\text{Na}^+$ . While the premonomer dimer mass is equal to the macrocycle and an "open" macrocycle, the main product between those two could not be distinguished with MS only. Although it can be considered a good sign that all these compounds were traceable in the mixture because that confirmed the feasibility of a photoreaction. The presence of a trimer and tetramer masses, and the absence of premonomer mass were not expected with the present crystal structure. Traces of a trimer signal in the mixture would be difficult to consolidate with the characteristics of the bis-complex **3** ( $\text{X} = \text{BF}_4^-$ ) crystal packing (Fig. 4.33) that is marked by a dimerization between the 9,10:,9',10'-anthracene of the blue colored bis-complex in forming of a macrocycle. Given these circumstances, there is no way a third premonomer can react with the remaining anthracenes of the macrocycle to form a trimer, except if it is somehow complexated with a terpyridine unit of the macrocycle and remaining zinc salt. This adduct was, however, not found.

A possible explanation for the existence of a trimer signal in the MS would be deducible from the assumption that not only a 9,10:9',10'-anthracene dimerization is taking place, but also a dimerization of a 1,4:5',8'-anthracene or 1,4:9',10'-anthracene. These dimerizations are very rare<sup>[79,92-94]</sup> and such anthracene stackings are illustrated in Figure 4.39. The distances between these possible reactive sites are in an appropriate range, between 3.6 - 4.1 Å, for dimerization. The tetramer could also only be explained by these unusual dimerizations. One also needs to keep in mind that the MS characterization is generally not ideal for conversion relations, because of the difference in individual ionizations. Other methods for molar mass determination were not considered due to the initial situation with the crystal structure and the parallel successful crystal structure determination of the bis-complex with  $\text{NTF}_2^-$  as counterion.

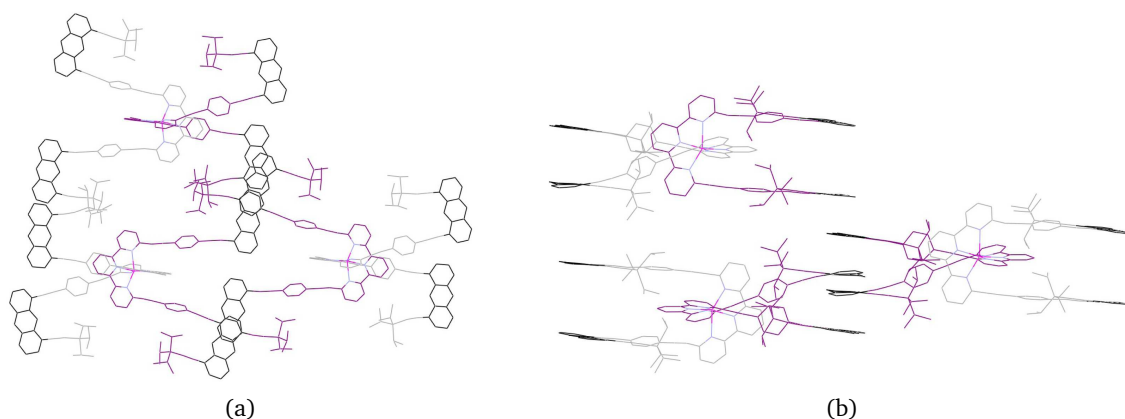


Figure 4.39: XRD crystal structure of bis-complex **3** ( $\text{X} = \text{BF}_4^-$ ) with potential reactive sites other than the 9,10:9',10'-anthracene dimerization. a) Top view and b) side view.

## 4. Results and Discussion

### Irradiation of the premonomer 7 in solution

To further study the photoproducts of the bis-complex **3** irradiation in solid-state, the irradiation of the premonomer **7** in solution was investigated to compare the photoproducts of both solid-state and solution with each other later in the chapter. The photoproducts of the premonomer **7** were expected to show similar anthracene bridge-head proton signals in comparison to the demetallated solid-state photoirradiated bis-complex **3**. Potentially the bis-complex **3** could have been used for solution irradiation as well, but its photoproducts were more likely to precipitate out of the solution due to their rigidity and limited motion caused by the zinc complexation. Therefore, the premonomer **7** was dissolved in degassed  $\text{CDCl}_3$ , to avoid the formation of anthracene peroxides, and irradiated in solution at 525 nm for nine days. The chosen irradiation wavelength lies in a very low absorption range of the premonomer **7** in solution, to cause a slow reaction that is easy to monitor by  $^1\text{H-NMR}$  spectroscopy over time (Fig. 4.40).

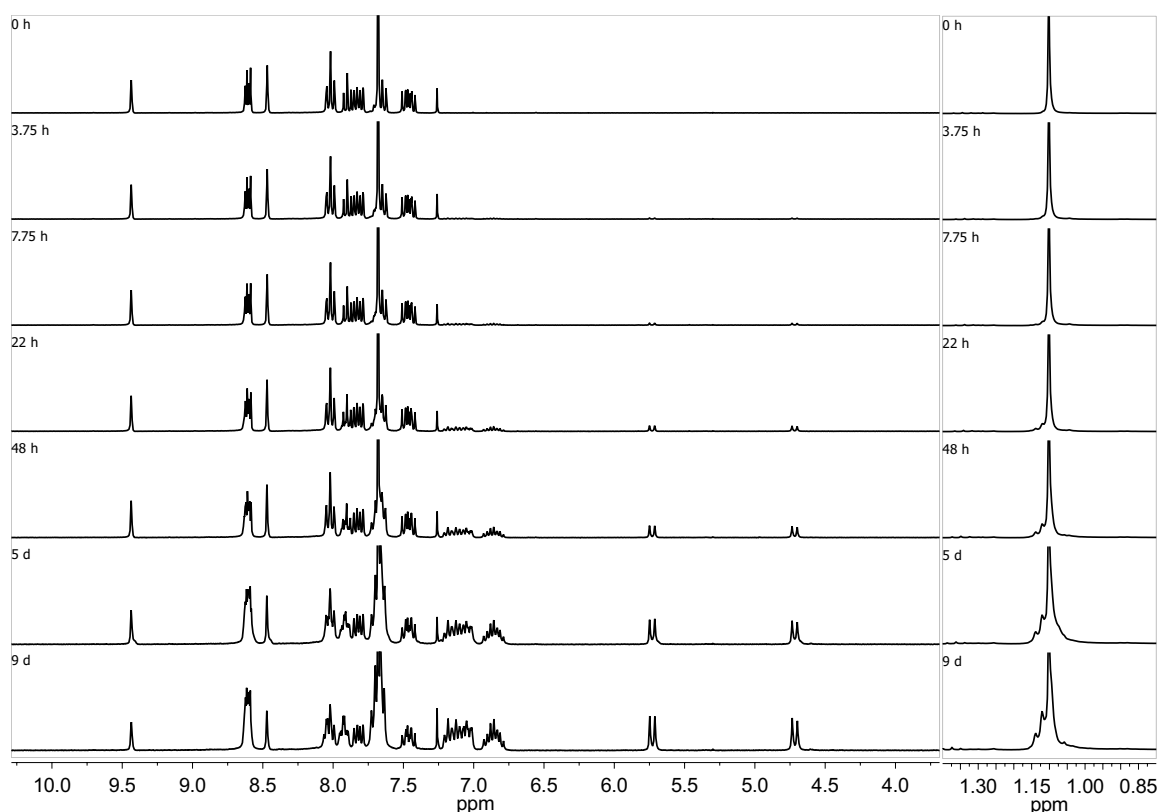


Figure 4.40: 300 MHz  $^1\text{H-NMR}$  spectra of premonomer **7** in  $\text{CDCl}_3$  recorded at different irradiation times.

Since the premonomer **7** includes two photoreactive anthracene groups, both are suitable to propagate in one dimension acting as a monomer for polymerization. The distinctive proton signals that should evolve during irradiation are the resulting anthracene bridge-head proton signals, and the other anthracene signals that are shifted due to the 9,10-anthracene dimer-

## 4. Results and Discussion

ization, besides remaining unreacted anthracene signals due to the chain ends of the formed oligomers/polymers. The proton spectra (Fig. 4.40) show an increase of a set of proton signals over time, which correspond to the aforementioned signals. Remarkable are the signals that arise at 4.7 and 5.7 ppm, which are both assigned to the anthracene bridge-head signals of dimerized anthracenes. The other aromatic signals that evolve through the anthracene dimerization (2,3,4,5,6,7-Ant) are located between 7.25 - 6.75 ppm. As expected, unreacted anthracene signals were still significantly present in the solution. This may be because of the unreacted chain ends or because of incompleting reaction. However, the photoproduct mixture was injected into the preparative rGPC (UV detection at  $\lambda = 254$  nm) to isolate any photoproduct. The elution curve is seen in Figure 4.41 and the isolated photoproducts in Figure 4.42.

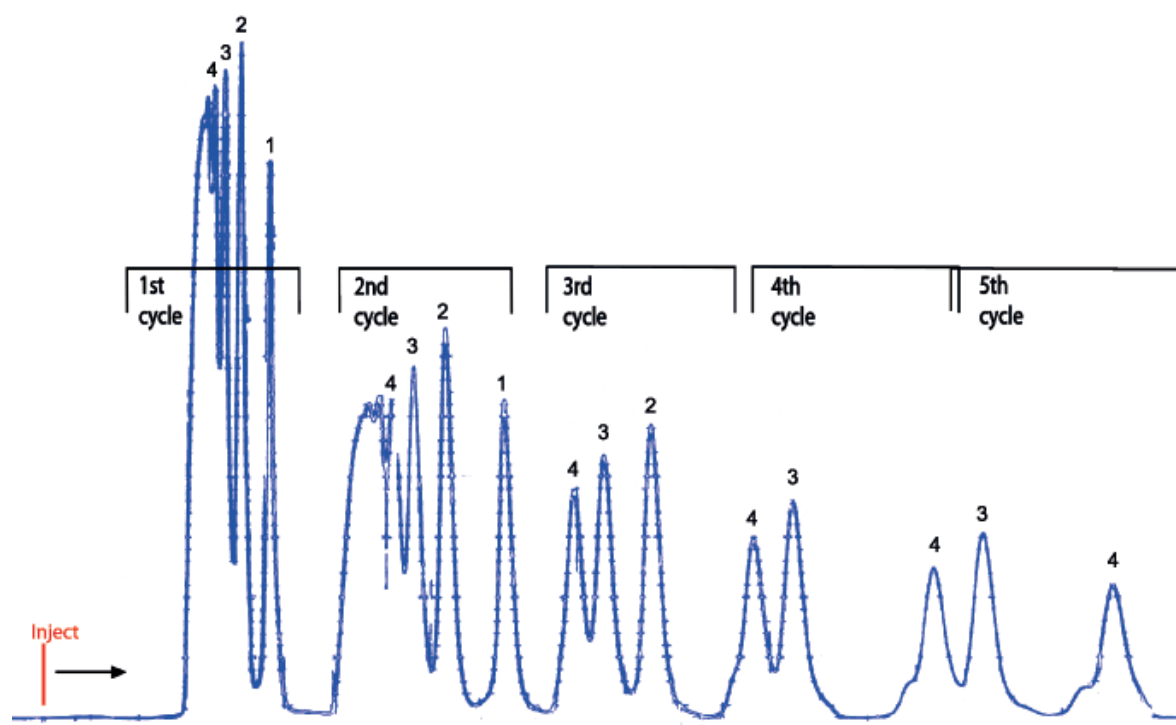


Figure 4.41: Elution curve from the preparative rGPC showing five full cycles of the mixture of the solution irradiation of premonomer 7.

The elution curve shows the separation of the different kinds of photoproducts during five full cycles. As the signals in the elution curve quickly overlapped, the individual signals could not be ideally separated. Consequentially, partial mixtures of the fractions were in any case expected. Additional purification or a second injection of the fractionated products would be required for improved separation. A further purification was, however, unnecessary for the purposes of this experiment. Also, since the elution curve seemed to reveal no high polymeric compound,

## 4. Results and Discussion

the injection into the analytical GPC was neglected. The isolated photoproducts (premonomer, dimer, trimer, and tetramer) from the preparative rGPC were fractionated and are shown next to their  $^1\text{H}$ -NMR spectrum in Figure 4.42. Due to the low concentration  $^{13}\text{C}$ -NMR spectra were not measured.

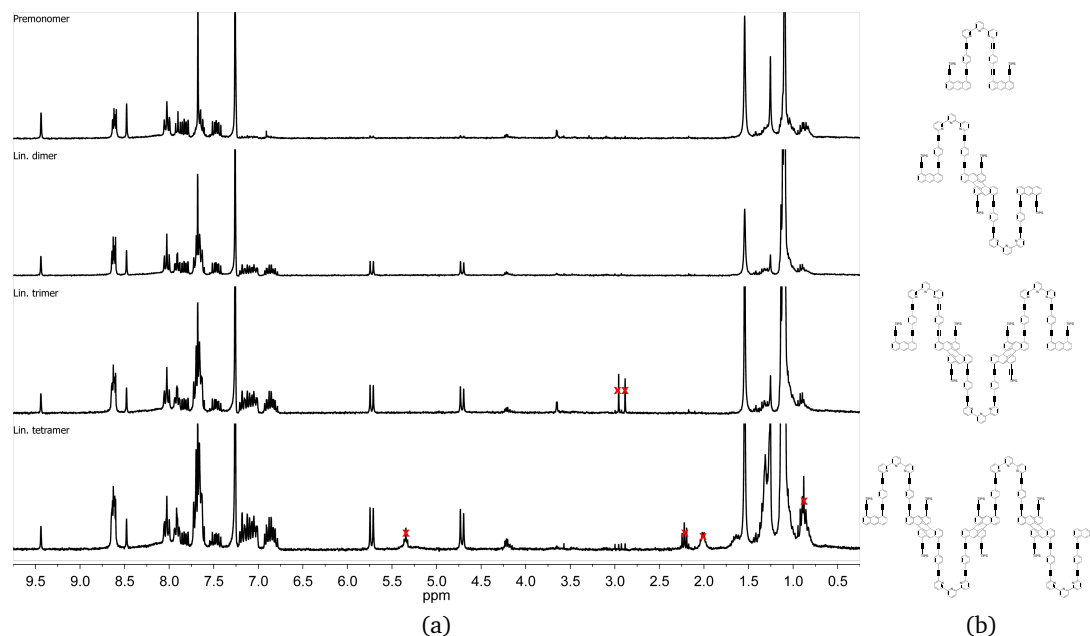


Figure 4.42: a) 300 MHz  $^1\text{H}$ -NMR spectra of isolated fractions from the solution irradiation of the premonomer **7** in  $\text{CDCl}_3$ . b) The chemical structure of corresponding photoproducts (only the anti dimerized product is shown).

The integration (not shown) of the proton signals of each isolated compound confirmed the corresponding photoproduct. For example, the tetramer was overlapping at the elution curve with the signals of the trimer and higher oligomers, therefore the integration of the proton signals was not precise. But the ratio between the 9,10-anthracene chain end proton signals in comparison to the reacted 9,10-anthracene bridge-head signals within the spectrum (Fig. 4.42) are clearly shifted towards the bridge-head signals. In addition, the MS of each isolated photoproduct would give a further confirmation. Unfortunately, the MS of the isolated photoproducts only detected the premonomer **7** mass signal. Either the concentration was too low, or the photoproducts were unstable under the MS determination conditions. It seems, however, unlikely that the photoproducts from the solution irradiation are unstable due to the detection of similar compounds from earlier MS measurements e.g., as shown in Fig. 4.38.

The solution irradiation of the premonomer **7** should also reveal a mixture of cis and anti dimerization in contrast to the solid-state irradiation that only allows a dimerization, which is given by the crystal structure. This differentiation will be addressed later in the chapter.



**Crystals of the bis-complex  $\mathbf{3}$  ( $X = \text{NTf}_2^-$ )**

The crystals of the bis-complex  $\mathbf{3}$  ( $X = \text{NTf}_2^-$ ) formed during titration of  $\text{Zn}(\text{NTf}_2)_2$  to the premonomer  $\mathbf{7}$  in a chloroform/methanol (2 : 1) mixture. These crystals were yellow and plate-like (Fig. 4.43) and they showed birefringence under POM. Large star-like crystals (up to 3 mm) were grown by using a low concentration of premonomer  $\mathbf{7}$  and  $\text{Zn}(\text{NTf}_2)_2$  mixture. These large crystals needed to be cut for the XRD crystal structure determination (7.1.). Usually the crystals formed over a time frame of hours to days. Using seed crystals from a batch of a solved XRD crystal structure helped to speed up the crystallization process and maintain the required crystal structure for the crystallization of newer batches.

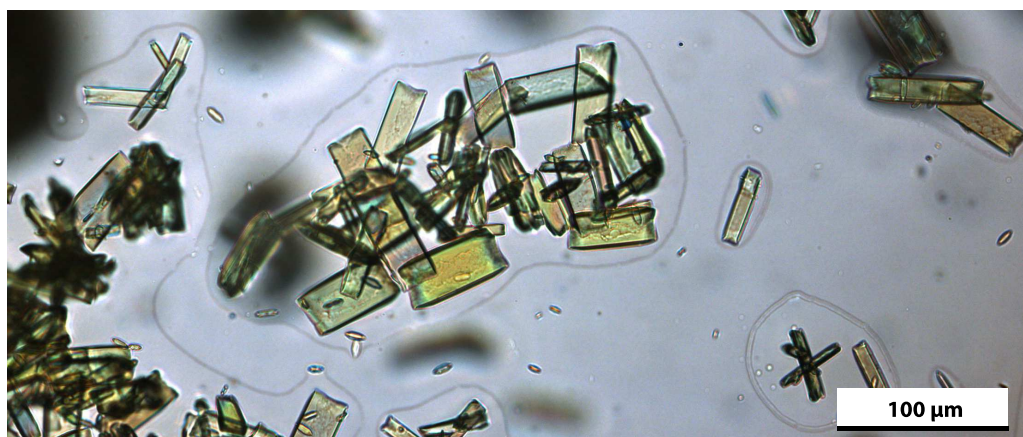


Figure 4.43: Optical micrograph showing the crystals of the bis-complex  $\mathbf{3}$  ( $X = \text{NTf}_2^-$ ) from chloroform/methanol.

The unit cell of the XRD crystal structure of the bis-complex  $\mathbf{3}$  ( $X = \text{NTf}_2^-$ ) is shown in Figure 4.44. It comprises four bis-complexes  $\mathbf{3}$  ( $X = \text{NTf}_2^-$ ) colored in blue, and its anthracene units are marked in green and light green.

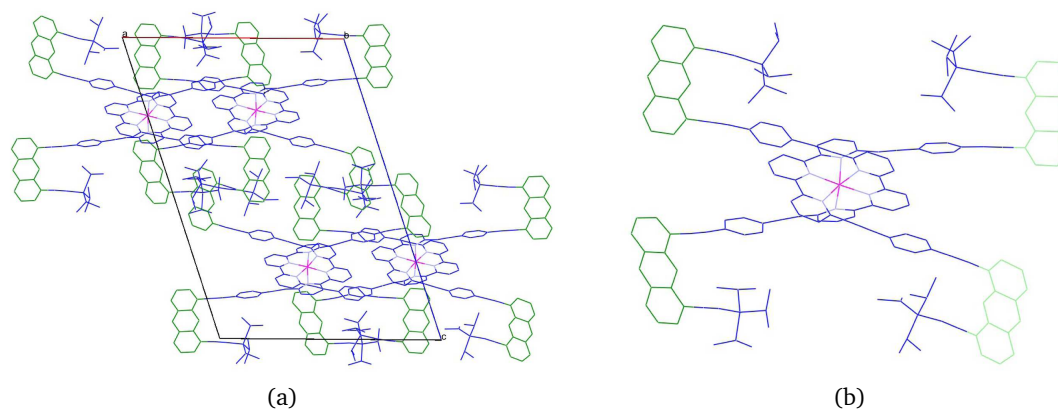


Figure 4.44: XRD crystal structure of the bis-complex  $\mathbf{3}$  ( $X = \text{NTf}_2^-$ ). (Hydrogens, counterions, and solvent molecules omitted.)

## 4. Results and Discussion

The stacking of the anthracene units of adjacent bis-complexes **3** ( $X = \text{NTf}_2^-$ ) is illustrated in Figure 4.45. These anthracene units stack face-to-face with a distance between the 9,10:9',10'-positions in a range of 3.5 - 3.8 Å, which makes the [4+4]-cycloaddition feasible. While one anthracene adjacent pair is stacked with a slightly twisted torsion angle of 7.3°, the other is significantly twisted by a torsion angle of 24.6°. However, the crystal was composed of 1D arrays of the bis-complexes and therefore represents a promising molecular arrangement for the potential synthesis of a poly[n]catenane by solid-state photoirradiation. The face indexing of the crystal (Fig. 4.46 & 4.47) revealed that the 1D arrays are situated along the thickness (height) of the crystals, which were usually very thin.

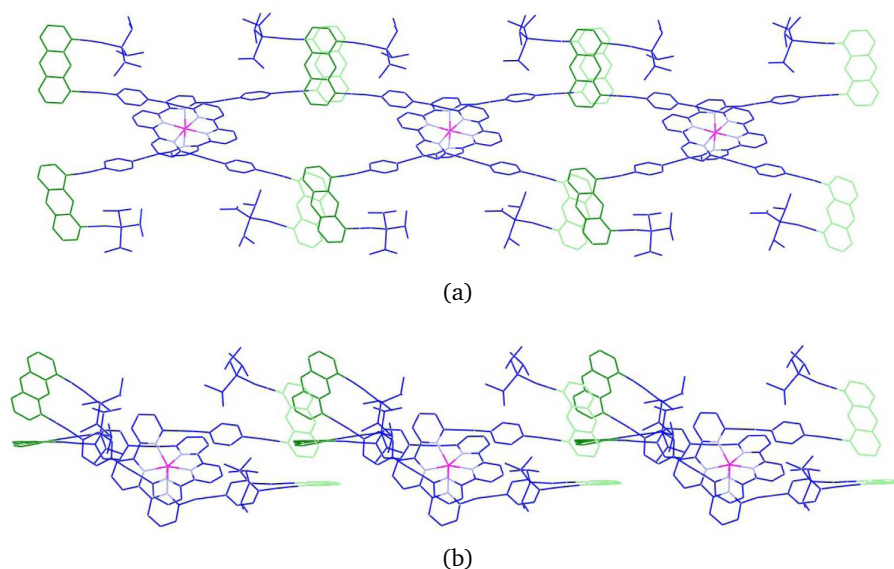


Figure 4.45: XRD crystal structure of **3** ( $X = \text{NTf}_2^-$ ) a) top view and b) side view. (Hydrogens, counterions, and solvent molecules omitted.)

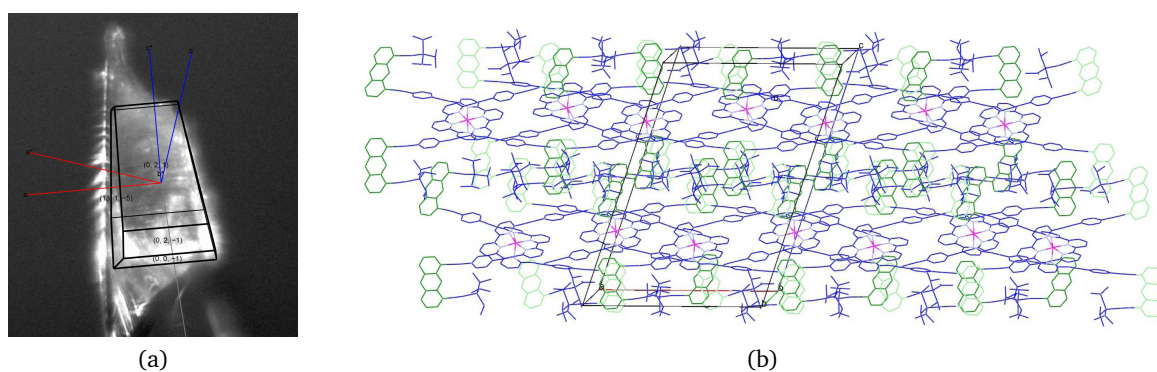


Figure 4.46: Face indexing of the crystal of bis-complex **3** ( $X = \text{NTf}_2^-$ ). a) Crystal along b-axis and b) its XRD crystal structure along the b-axis.

## 4. Results and Discussion

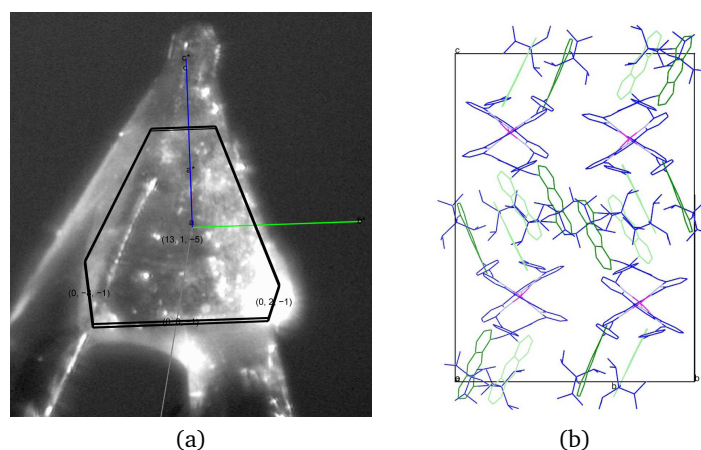


Figure 4.47: Face indexing of the crystal of bis-complex **3** ( $X = \text{NTf}_2^-$ ). a) Crystal along a-axis and b) its XRD crystal structure along the a-axis.

The crystals of bis-complex **3** ( $X = \text{NTf}_2^-$ ), which resulted from chloroform/methanol, revealed a very promising XRD crystal structure. Since both solvents have a low boiling point and potentially could evaporate during an irradiation process, other solvent mixtures were still considered and some resulted in crystals as well.

Yellow needle crystals of the bis-complex **3** ( $X = \text{NTf}_2^-$ ) in 1,4-dioxane/diethylene glycol monomethyl ether were grown within hours by mixing premonomer **7** in 1,4-dioxane with 0.5 eq. of  $\text{Zn}(\text{NTf}_2)_2$  in diethylene glycol monomethyl ether (Fig 4.48a). These crystals are anisotropic and show birefringence (Fig 4.48b). The XRD crystal structure (7.1.) of these crystals are shown in Figure 4.49.

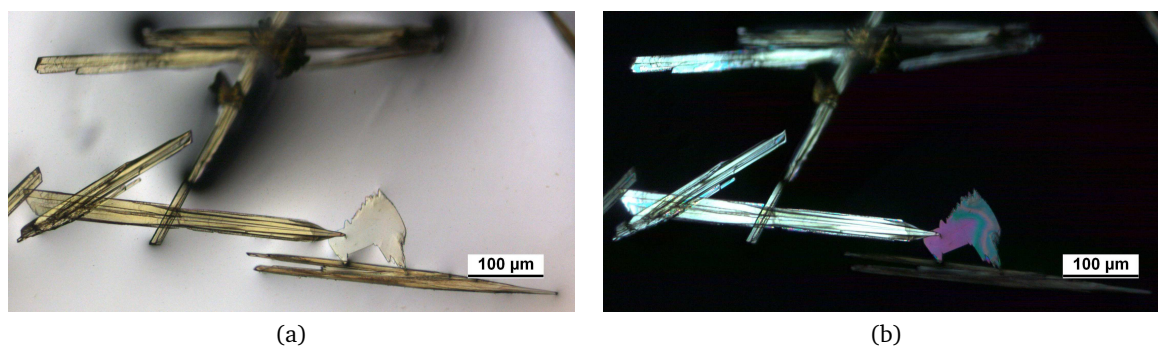


Figure 4.48: Optical micrographs showing the crystals of **3** ( $X = \text{NTf}_2^-$ ) from 1,4-dioxane/diethylene glycol monomethyl ether. a) Under OM and b) under POM.

## 4. Results and Discussion

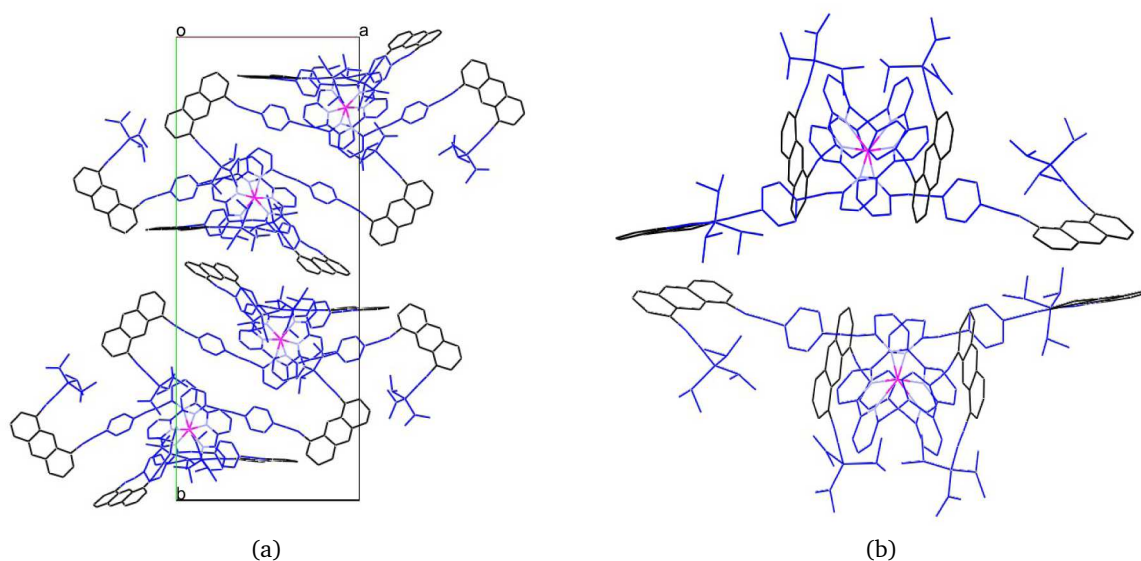


Figure 4.49: XRD crystal structure of **3** ( $X = \text{NTf}_2^-$ ) from 1,4-dioxane/diethylene glycol monomethyl ether. (Hydrogens, counterions, and solvent molecules omitted.)

The unit cell consists of four blue colored bis-complexes, while the anthracene units are colored black. There is no stacking between adjacent bis-complexes and no possibility for a [4+4]-cycloaddition. This solvent mixture was a good example of the solvent's influence on the crystal structure, in that it strongly differs from the crystal structure as seen in the solvent mixture of chloroform/methanol (Fig. 4.44). Therefore, this crystal underlines that it is not necessary to change the counterion, but to vary instead the solvent mixtures in order to obtain crystals with different crystal structures.

Bis-complex **3** ( $X = \text{NTf}_2^-$ ) mixtures were prepared in the same manner as for the 1,4-dioxane/diethylene glycol monomethyl ether crystals, but with mixtures of 1,4-dioxane and either diethylene glycol dimethyl ether, glycol, 1,2-dimethoxyethane, or diethylene glycol monoethyl ether, which resulted in needles with similar unit cell parameters. The mixture in 1,4-dioxane/2-methoxy ethanol, at first, resulted in yellow needle crystals, but during the recrystallization, however, yellow rectangular crystals were obtained. These crystals had a similar unit cell as the chloroform/methanol crystals (7.1.), but the crystal quality was not as favorable for an XRD analysis, since it did not scatter well enough. Further crystallization attempts did not improve the crystal quality and, up-to-now, no other promising XRD crystal structures were discovered.

### Irradiation of the bis-complex **3** ( $X = \text{NTf}_2^-$ ) crystals

The XRD crystal structure of the bis-complex **3** ( $X = \text{NTf}_2^-$ ) from the chloroform/methanol mixture (Fig. 4.44 & Fig. 4.45) was promising. The anthracene units of the bis-complex were stacking with adjacent bis-complex anthracenes with a distance below 4 Å in 1D arrays across the crystal (Fig. 4.46b). This crystal packing raised expectations for the formation of a poly[n]catenate upon irradiation of such crystals and after demetallation a poly[n]catenane.

The ideal case for the proposed poly[n]catenane synthesis would be as follows: upon irradiation of the yellow crystals, the anthracenes of the bis-complexes undergo dimerizations forming poly[n]catenates in a single-crystal-to-single-crystal (scsc) transformation, which allows a subsequent XRD analysis of intact and resulting colorless crystals. The scsc transformation would only slightly change the unit cell parameters. In addition, the irradiated crystals would be less soluble due to the high rigidity and restricted free motion caused by the metal coordinated backbone. These irradiated crystals would need to be demetallated to gain access to poly[n]catenanes and it is expected that the solubility would raise due to the metal removal. The poly[n]catenane would then be fully characterized in terms of molecular weight, yield, and many other aspects. The molecular weight would not only be limited by the reaction time and conversion, but also by the crystal size (with consideration of crystal defects). However, the simplicity of such a reaction on paper is not reflected by the reality. The actual experimental outcome of many attempted photoirradiations was more complex and did not reflect the expected results. Therefore, this part of the thesis elaborates upon the significant results among the irradiation experiments.

Photoirradiations of different single crystals of bis-complex **3** ( $X = \text{NTf}_2^-$ ) mounted onto a goniometer head of a diffractometer, and each externally cooled with a nitrogen stream at specific temperatures (at -100 °C, -55 °C, and -20 °C) over a period of ca. 24 hours, were conducted. The crystals were irradiated with either one or two 470 nm fiber-coupled LEDs. Unfortunately, the crystal structure did not change upon irradiation and no photoreaction could be determined. The quality of the crystals deteriorated as the temperatures increased, which was probably caused by the partial cracking of the crystals.

A series of irradiation experiments with crystals of bis-complex **3** ( $X = \text{NTf}_2^-$ ) at different reaction conditions under argon atmosphere followed. The conditions for the experiments, summarized in Table 1, were varied in quantity, wavelength, temperature as well as temperature control, reaction container, time, and type.

#### 4. Results and Discussion

#	Type	Quantity	$\lambda$ / nm	Temp. Control	Container	Temp. / C	Time
<b>Irrad1</b>	Crude	6 mg	525	Fridge	Vial	25°	106 h
<b>Irrad2</b>	Crude	5 mg	465	Fridge	Vial	25°	117 h
<b>Irrad3</b>	Crude	5 mg	525	Fridge	Vial	25°	117 h
<b>Irrad4</b>	Crude	5 mg	465	Fridge	Vial	25°	132 h
<b>Irrad5</b>	Dispersion	76 mg	525	Fridge	Schlenk tube	40°	24 d
<b>Irrad6</b>	Dispersion	72 mg	525	Fridge	Schlenk tube	40°	21 d
<b>Irrad7</b>	Dispersion	141 mg	525	Fridge	Schlenk tube	25°	24 d
<b>Irrad8<sup>XV</sup></b>	Dispersion	91 mg	465	Fridge	Schlenk tube	85°	6 d
<b>Irrad9</b>	Dispersion	118 mg	465	External	Schlenk tube	13°	21 d
<b>Irrad10</b>	Dispersion	200 mg	525	Fridge	Schlenk tube	18°	22 d
<b>Irrad11<sup>XVI</sup></b>	Dispersion	200 mg	525	External	Schlenk tube	13°	28 d

Table 1: Overview of irradiation conditions for the crystals of bis-complex **3** ( $X = \text{NTf}_2^-$ ) from chloroform/methanol.

The irradiation experiments, presented in Table 1, all have in common a visible color change and a solubility change from the starting material to the photoreacted material. Due to the solubility change,  $^1\text{H-NMR}$  spectra were measured in  $\text{DMF-}d_7$  at rt. Not all experiments showed a simple rise of anthracene bridge-head signals and a complete decrease of 9,10-anthracene signals caused by the anthracene dimerization, but also included other new unknown signals at  $^1\text{H-NMR}$  spectroscopy. Experiments that showed characteristic features of the photoirradiations will be discussed further on in more detail.

Solid-state photoreactions of crystals are usually fast<sup>XVII</sup> within hours or sometimes up to a few days.<sup>[28,47]</sup> However, the prolonged reaction time of the different photoreactions stands out. The reason for prolonging the irradiation time was the observation of significant remaining 9,10-anthracene proton signals in the mixture, determined by samples that were taken out over time during irradiation, suggesting an incomplete reaction. To ensure a comparability of the different experiments, the irradiation time was kept as constant as possible.

Crystals of bis-complex **3** ( $X = \text{NTf}_2^-$ ) were dispersed in perfluoropolyether and photoirradiated at 465 nm for 60 hours. The yellowish color of the crystals virtually disappeared. Still, birefringence was observed, which suggests a retained crystalline order inside. The crystals, however, were cracked along the length, but maintained their overall rectangular shapes. Similar observations were made across the various experiments. Optical and polarized optical images of the crystals before and after irradiation are shown in Figure 4.50.

<sup>XV</sup>Due to overheating of the LEDs (85 °C), the reaction was aborted after 6 days

<sup>XVI</sup>These crystals were still wet at weight determination.

<sup>XVII</sup>The power of the light source has an impact to the reaction time.

## 4. Results and Discussion

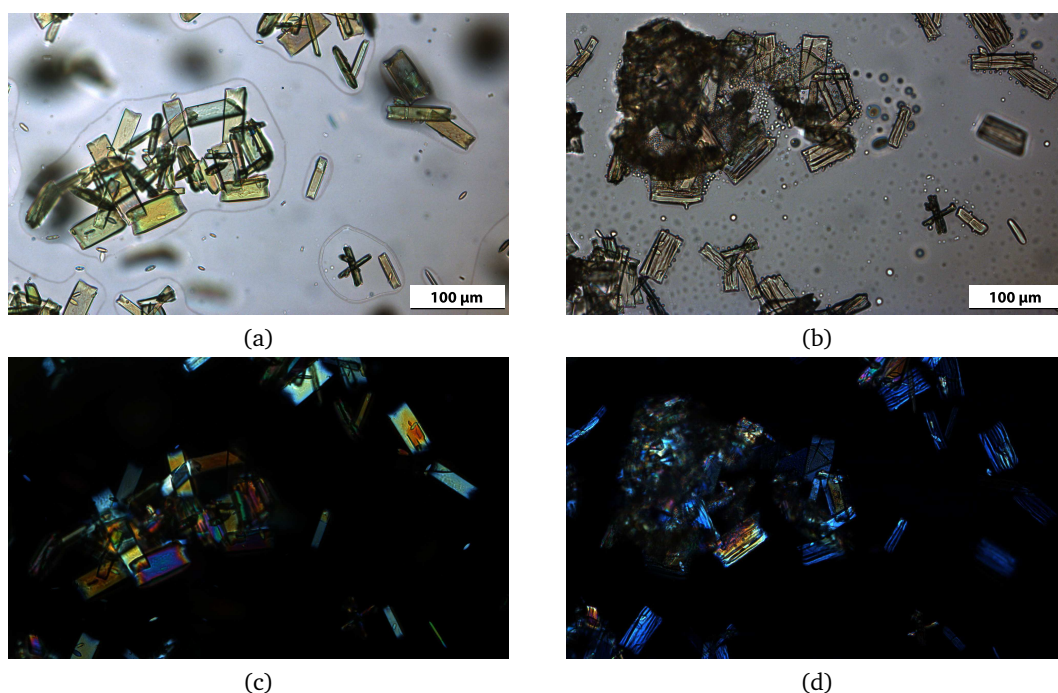


Figure 4.50: Optical micrographs showing the crystals of **3** ( $X = \text{NTf}_2^-$ ) from chloroform/methanol mixture. a) Before irradiation under OM, b) after irradiation under OM, c) before irradiation under POM, and d) after irradiation under POM.

A homogeneous reaction is supported by using a wavelength in the absorption tail of the photoreactive material (Fig. 2.5).<sup>[35,58,77,78]</sup> The probability to retain the crystal during irradiation is then enhanced. Therefore, the absorption of the bis-complex **3** ( $X = \text{NTf}_2^-$ ) was measured with solid-state UV/Vis spectrometry. Its absorption spectrum is shown in Figure 4.51, which highlights the ideal wavelength of ca. 530 nm for a tail irradiation. The absorption maximum is at ca. 470 nm.

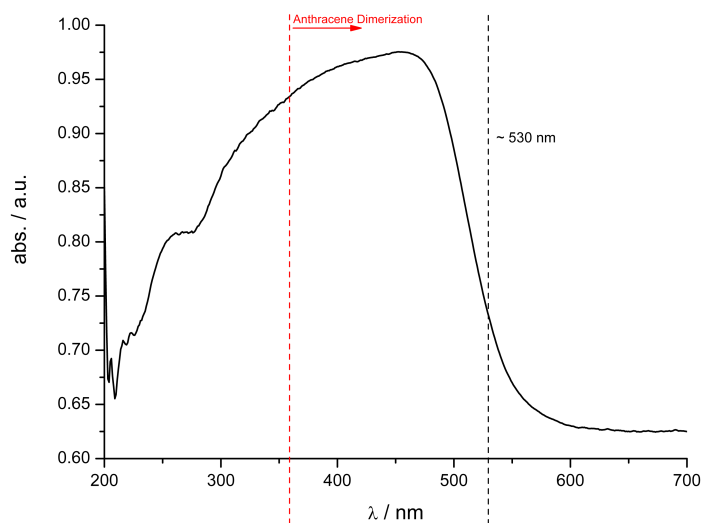


Figure 4.51: Solid-state UV/Vis spectrum of **3** ( $X = (\text{NTf}_2^-)$ ).

#### 4. Results and Discussion

In order to guarantee a uniform irradiation among all the crystals, it was decided to perform further experiments in dispersion. The preparation for these experiments was as follows: the crystals of the bis-complex **3** ( $X = \text{NTf}_2^-$ ) from the mother solution were filtered on paper in the fridge and washed with cold MeOH before transferring them to a Schlenk tube. After gently exchanging the atmosphere with argon, the crystals were dispersed with an argon purged water/methanol mixture (8 : 5). The specific mixture of water/methanol was chosen carefully to allow the crystals to float rather than to sediment to the flask bottom. An argon balloon was attached to the Schlenk tube to maintain the argon atmosphere during irradiation. An example of such dispersion irradiation at 525 nm over time is shown in Figure 4.52.

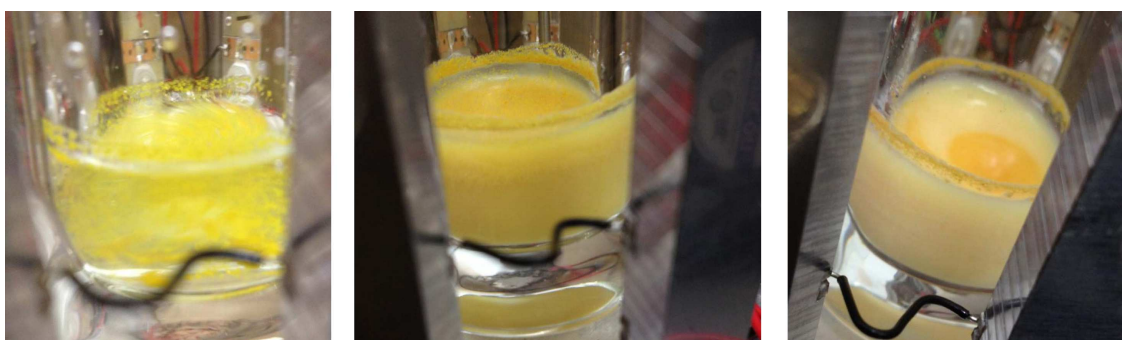


Figure 4.52: The color change of the crystals of bis-complex **3**: before, after one day, and after seven days of dispersion irradiation at 465 or 525 nm (From left to right).

The yellow dispersed crystals changed their color to light yellow over time, while crystals that were closer to the liquid surface appeared orange. In addition the crystals were broken into smaller pieces during irradiation by collisions with the stirring bar. However, the advantage of such irradiation in dispersion is the absorption of heat through the liquid medium, which is uniform over the whole sample. As a result, the sample is more easily cooled than it would be during a crude reaction at atmosphere. It was believed that the temperature was crucial for the irradiation, as chloroform and MeOH are present in the crystal structure, and would slowly vaporize if the temperatures overheat, causing disruption of the crystals. A disadvantage of a dispersion with stirring is clearly the shrinkage of crystals due to the stirring bar. In consequence, the small crystals are not suitable for a subsequent XRD determination anymore. Since the temperature of the dispersion medium increased (up to 40 °C) at some experiments e.g., "Irrad5" & "Irrad6", due to the heat of the light source, it was decided to cool further reactions externally by a doubled-walled Schlenk tube with continuous water cooling.

Once the dispersion irradiation was stopped, the mixture was transferred to a centrifuge tube



## 4. Results and Discussion

to separate the liquid from the remaining solids. These solids were then washed twice with water/methanol and dried at high vacuum. The experiment of "Irrad6" was performed in the described way. Some of the solids from "Irrad6" were used for comparison with the non-irradiated bis-complex **3** ( $X = \text{NTf}_2^-$ ) by  $^{13}\text{C}$  CP/MAS NMR spectroscopy (Fig. 4.53).

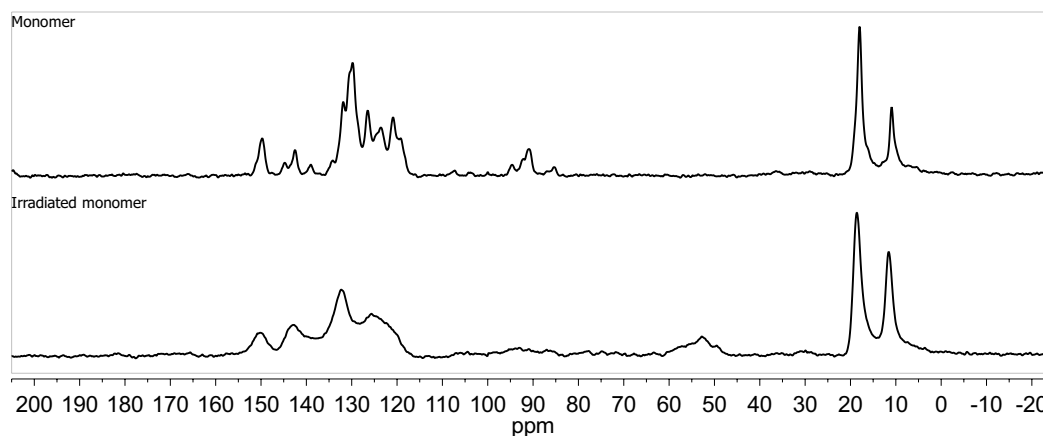


Figure 4.53: 176 MHz  $^{13}\text{C}$  CP/MAS NMR spectra of non-irradiated bis-complex **3** ( $X = \text{NTf}_2^-$ ) (top) and the irradiated bis-complex from experiment "Irrad6" (bottom).

The  $^{13}\text{C}$  CP/MAS NMR spectrum of the irradiated bis-complex **3** ( $X = \text{NTf}_2^-$ ) "Irrad6" in comparison to the non-irradiated bis-complex **3** ( $X = \text{NTf}_2^-$ ) shows the rise of possible anthracene bridge-head signals at 50 - 60 ppm, and the decrease of signals from the acetylene groups between 80 - 100 ppm. The bridge-head signals are a good indication for a succeeded photoreaction in contrast to the decreased acetylene signals that are more likely to be caused by other side reactions. It is however possible that the acetylenes' signals could have been only weak in comparison to the other signals, due to the protons in proximity to the acetylenes. In addition, the relative ratios in a spectrum are not necessarily proportional. The observable decrease in signal strength could also have been reduced due to disorder caused by the irradiation within the crystal. The general signal smoothness of the irradiated sample could have been caused by the smaller crystals resulting from the dispersion irradiation.

The bis-complex **3** ( $X = \text{NTf}_2^-$ ) compound after irradiation was almost completely soluble in DMF, except for ca. 1 % remaining insoluble parts that were separated.<sup>XVIII</sup> The proton spectra of the bis-complex **3** ( $X = \text{NTf}_2^-$ ) and the irradiated bis-complex **3** ( $X = \text{NTf}_2^-$ ) sample of "Irrad10" in  $\text{DMF-}d_7$  are shown in Figure 4.54.

<sup>XVIII</sup>These insoluble solids were washed with little amounts of DMF, then dried, and analyzed by IR spectroscopy. The spectrum revealed no relevant bands of either starting or reacted material.

## 4. Results and Discussion

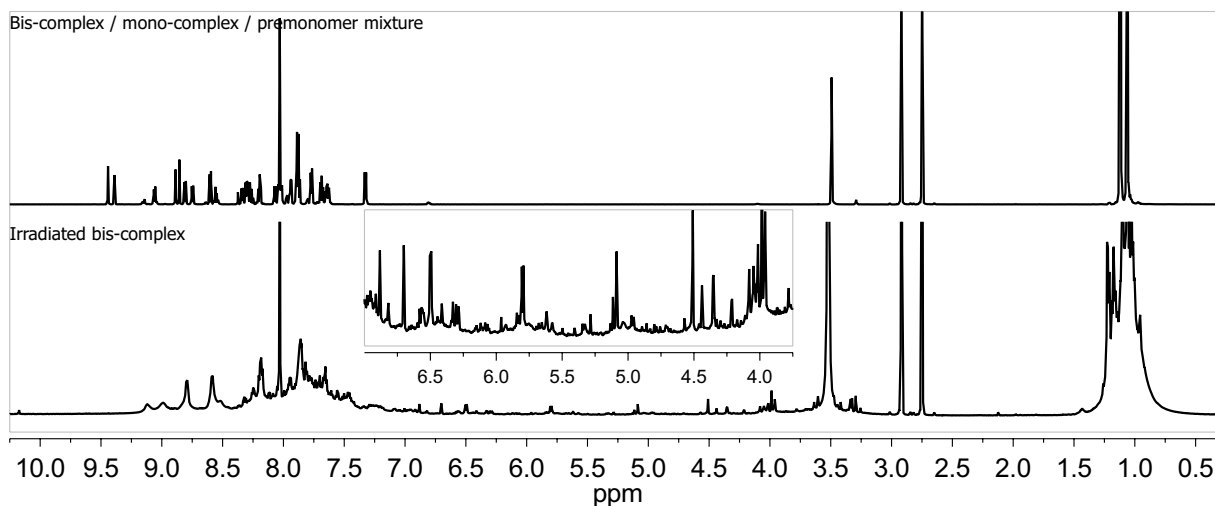


Figure 4.54: 700 MHz  $^1\text{H}$ -NMR spectra of bis-complex **3** ( $X = \text{NTf}_2^-$ ) (top) and the irradiated bis-complex **3** "Irrad10" (bottom) in  $\text{DMF-}d_7$ .

The proton spectrum of the irradiated bis-complex **3** ( $X = \text{NTf}_2^-$ ) sample "Irrad10" (Fig. 4.54) features the appearance of characteristic anthracene bridge-head signals (see Fig. 4.35) at 4.95 and 5.85 ppm, and the disappearance of the 9,10-anthracene signals at 8.85 and 9.45 ppm. In addition, it shows a number of unknown signals across the spectrum. The  $^1\text{H}$ - $^1\text{H}$ -COSY spectrum in Figure 4.55 gives a closer insight to the numerous proton relationships.

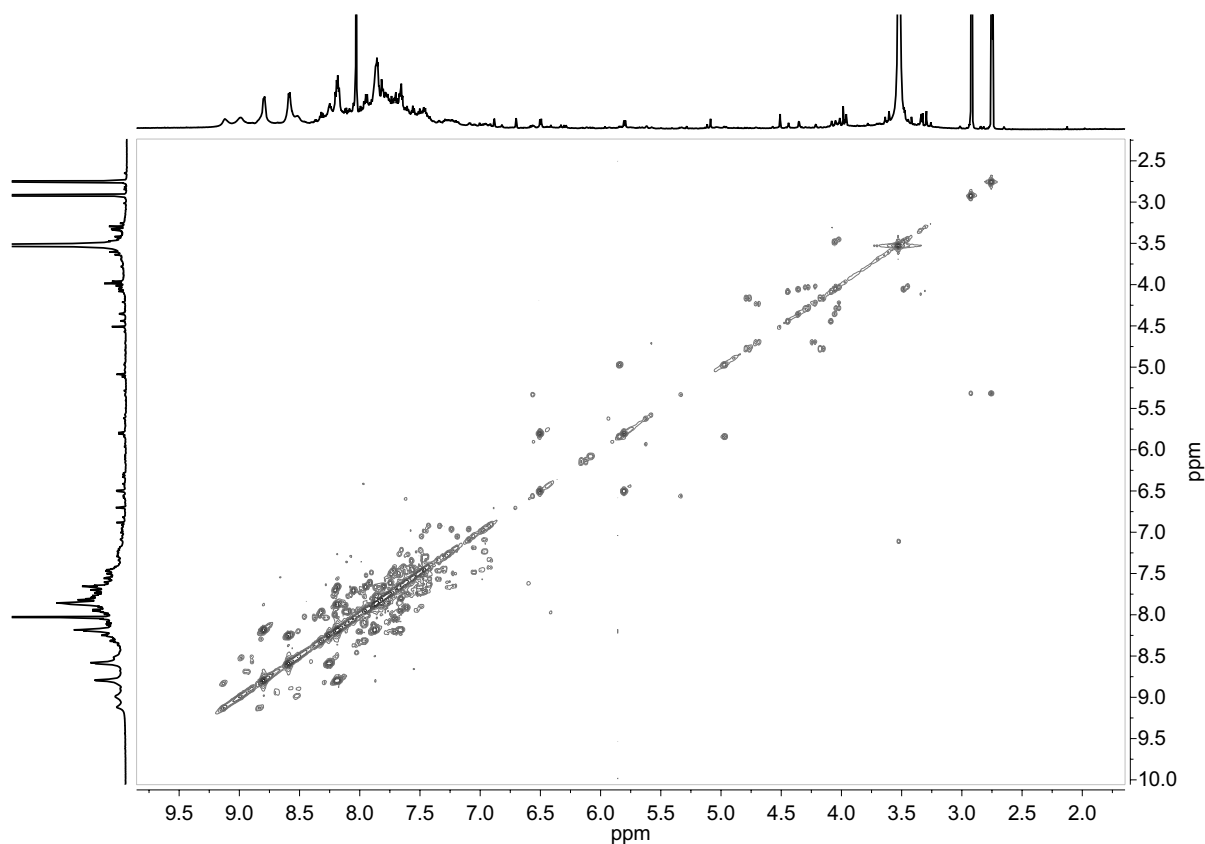


Figure 4.55: 700 MHz  $^1\text{H}$ - $^1\text{H}$ -COSY spectrum of irradiated bis-complex **3** ( $X = \text{NTf}_2^-$ ) "Irrad10" in  $\text{DMF-}d_7$ .

## 4. Results and Discussion

The  $^1\text{H}$ - $^1\text{H}$ -COSY spectrum generally reveals the expected proton relationships of the anthracene bridge-head signals at 4.95 and 5.85 ppm, but also other proton relationships e.g., in the region between 4 - 7 ppm such as at 5.8 and 6.5 ppm, are seen. The chaos of this spectrum is clearly an indication of processes that go beyond photoreactions to 9,10:9',10'-anthracene dimers only. The carbon spectrum of the premonomer **7** in comparison with the irradiated bis-complex **3** ( $X = \text{NTf}_2^-$ ) of "Irrad6" in  $\text{DMF-}d_7$  is shown in Figure 4.56.<sup>XIX</sup>

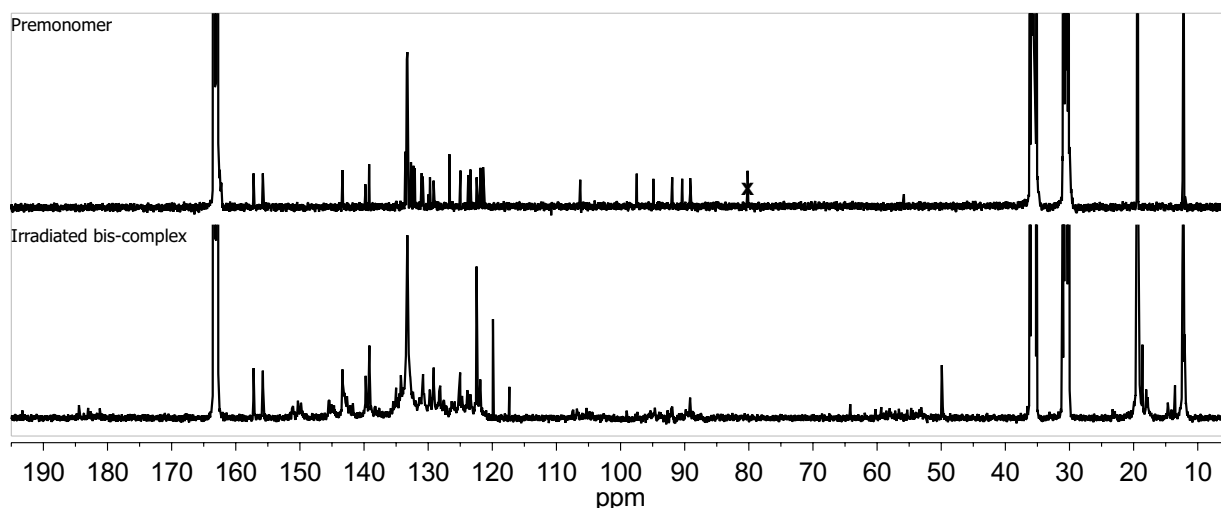


Figure 4.56: 126 MHz  $^{13}\text{C}$ -NMR spectra of premonomer **7** (top) and the irradiated bis-complex **3** ( $X = \text{NTf}_2^-$ ) "Irrad6" (bottom) in  $\text{DMF-}d_7$ .

Comparing the carbon solution NMR spectra of both, premonomer **7** and irradiated bis-complex **3** ( $X = \text{NTf}_2^-$ ) "Irrad6", revealed on the one hand the presence of some identical signals and on the other many new signals that relate to anthracene reactions. Noticeable are the generally broadened signals for the irradiated sample, which could be caused by the same reasons as mentioned earlier at the bis-complex **3** ( $X = \text{BF}_4^-$ ) irradiations, because of possible resulting large molecules. In this carbon spectrum (Fig. 4.56), all acetylene signals (85 - 110 ppm) of the irradiated bis-complex **3** ( $X = \text{NTf}_2^-$ ) were reduced and new signals in this region appeared. In the range of 50 - 65 ppm, the region expected for anthracene bridge-head signals to appear, many relatively small signals were seen. Since there are many signals in both mentioned regions, one could conclude that these might be caused through other bridge-head-type signals or reactions with acetylenes. Although 45 mg were used for the carbon measurement, which needed up to a few days, the signal-to-noise ratio is low, and a clear differentiation from the background noise is hard to conclude. Oxidation towards an anthrone/anthraquinone derivative is indicated by the small signals at 180 - 185 ppm in the spectrum of irradiated bis-complex **3** ( $X = \text{NTf}_2^-$ ), which could also be the cause for some of the "new" acetylene signals.

<sup>XIX</sup>Since  $\text{DMF}$  demetallates the bis-complex **3** mostly to the premonomer **7**; its spectrum was used for comparison.

## 4. Results and Discussion

### *Time-course irradiation experiment*

To get a closer insight into the reaction progress, a time-course irradiation experiment "Irrad10" was performed in which samples were taken at different points in time and analyzed by powder XRD, as well as IR, and NMR spectroscopy. About 200 mg of crystals were used for this experiment in a dispersion of water/methanol (8 : 5) for irradiation at 525 nm under argon atmosphere. The first sample was taken as prepared; the second was taken out after 24 hours stirring in the dispersion without irradiation. Then, irradiation was started and sample probes were taken: after 1 hour, 2 hours, 4 hours, 8 hours, 12 hours, 24 hours, 36 hours, 48 hours, 72 hours, 4 days, 6 days, 9 days, 13 days, 17 days, and 22 days of irradiation. Each sample was about 6 - 8 mg of solid after evaporation, which was sufficient to measure powder XRD (Fig. 4.57), IR (Fig. 4.58 & 4.59), and  $^1\text{H}$ -NMR spectroscopy (Fig. 4.54).

The powder XRD pattern of the irradiated crystals are shown in Figure 4.57<sup>XX</sup> in which only the time-frames where a significant transitional change was observed, is shown.

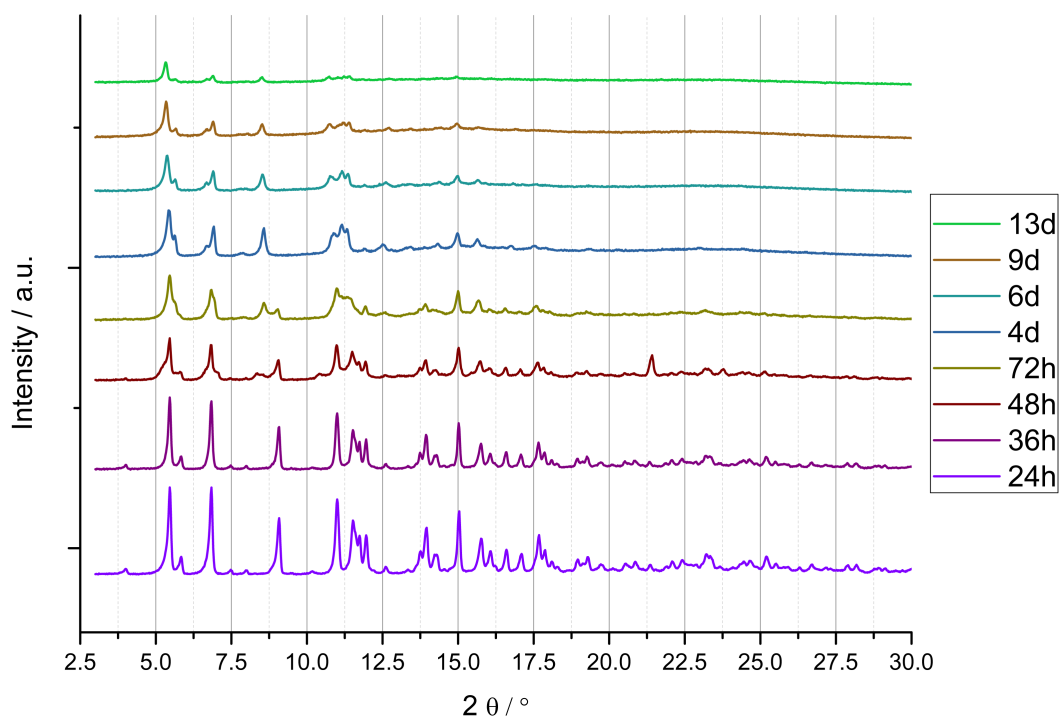


Figure 4.57: The powder XRD pattern of experiment "Irrad10" between 24 hours and 13 days.

Up to the irradiation time to 36 hours, no relevant signal change is seen. After 48 hours, new signals, such as at  $5.8^\circ$ ,  $8.5^\circ$ , and  $11.3^\circ$  increased, while signals, such as at  $6.8^\circ$  and  $9.1^\circ$ , de-

<sup>XX</sup>The measurement at 48 hours contains an artifact at  $21.25^\circ$ .

#### 4. Results and Discussion

creased. After four days, the  $9.1^\circ$  signal disappeared, while the signal at  $6.8^\circ$  decreased to a low signal. A clear conclusion cannot be drawn from these measurements. The fact that a transition from one XRD pattern to another began after 48 hours is, however, significant. By this time, the signal broadened and the intensity decreased, both of which are a result of the small crystals brought about the stirring of the dispersion at irradiation. In addition, the simulated powder XRD pattern (not shown) from the XRD crystal structure was not in accordance with the experimental powder XRD pattern. An explanation for this might be that the crystals used for the XRD determination were not from the same batch as for the powder XRD measurement. Not every XRD crystal structure in those batches of crystal was determined, but the unit cell parameters were usually confirmed. Keeping in mind that a large number of chloroform solvent molecules are incorporated into the crystal structure of the bis-complex **3** ( $X = \text{NTf}_2^-$ ), it is likely that the crystals were not equal in their crystal structure in every batch. These solvent molecules could have slowly evaporated, leading to a change of crystal packing, and causing a differently simulated powder XRD pattern than for the measured experimental pattern.

The IR absorption spectra of the irradiated crystals are shown in Figure 4.58 with an inset of bands between  $1825 - 1525 \text{ cm}^{-1}$  and the time-frame between 24 hours and 13 days.

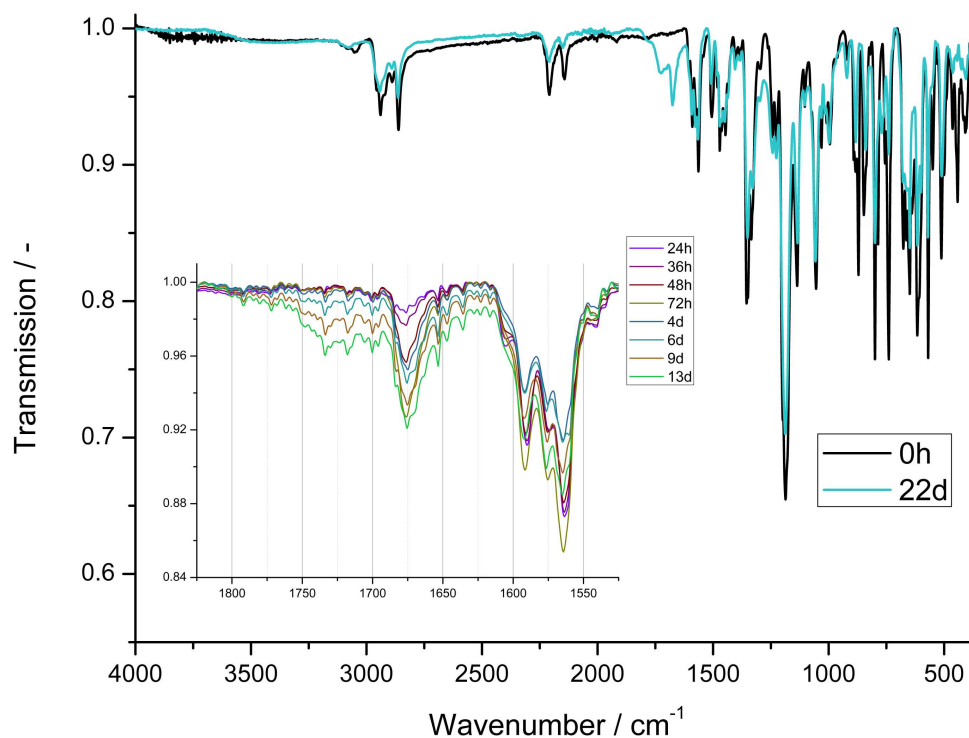


Figure 4.58: The IR absorption spectra of experiment "Irrad10" before and after 22 days. The inset shows bands between  $1825 - 1525 \text{ cm}^{-1}$  during the 24 hours and 13 days of irradiation.

## 4. Results and Discussion

The significant rise of a band at ca.  $1670\text{ cm}^{-1}$  in the IR spectra stands out, which occurs already after 24 hours. Another broader band between  $1750 - 1700\text{ cm}^{-1}$  rises significantly after four days. Both bands could have been caused by oxidation of the anthracenes, since similar oxidation bands during anthracene irradiation have been reported before,<sup>[28]</sup> as well as reports of bands at ca.  $1670\text{ cm}^{-1}$  known for C=O band of anthraquinones.<sup>[261]</sup> Even though the samples were argon-purged and irradiated under an argon atmosphere, unintentional oxidation could have take place, considering the prolonged reaction time for these experiments.

In the range of  $900 - 400\text{ cm}^{-1}$  (Fig. 4.59) the bands of the bis-complex **3** ( $X = \text{NTf}_2^-$ ) at 893, 871, 848, 786, 757, 607, 550, and  $441\text{ cm}^{-1}$  disappear, while a new band forms during 22 days at  $770\text{ cm}^{-1}$ , and another band at  $739\text{ cm}^{-1}$  significantly decreases. The band at  $871\text{ cm}^{-1}$  could be the out-of-plane stretch of the 9,10-anthracene positions that decreases over time and changes to possibly form the anthracene bridge-head band at  $770\text{ cm}^{-1}$ . Once again, a clear conclusion cannot be drawn from these measurements except the obvious transformation to a different product.

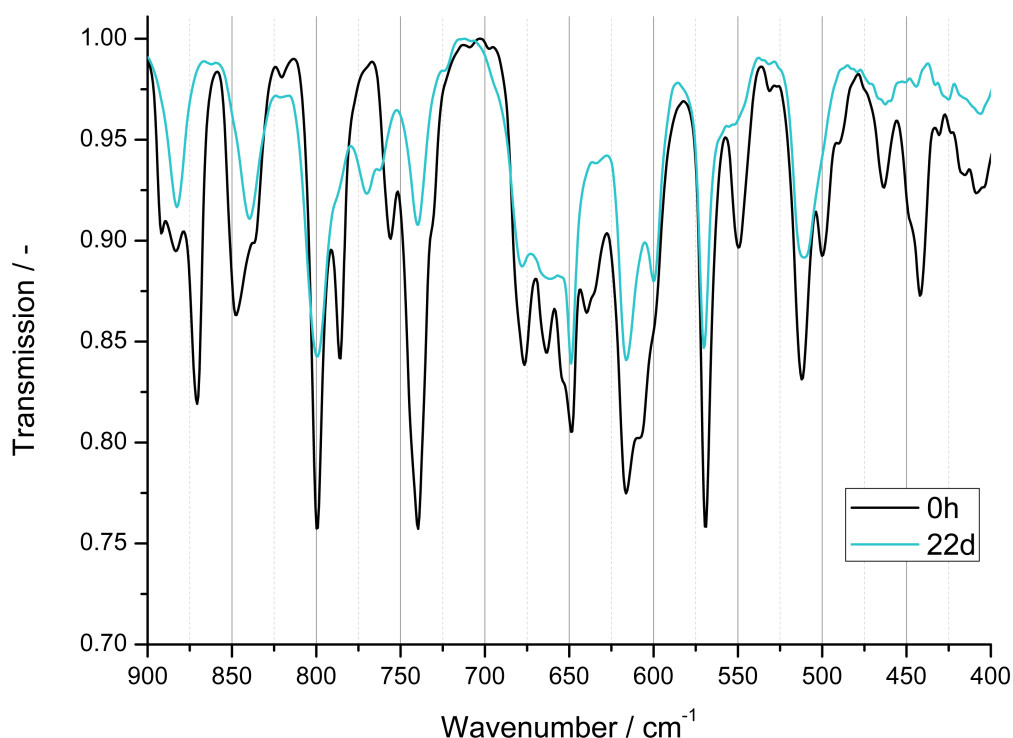


Figure 4.59: The IR absorption spectrum between  $900 - 400\text{ cm}^{-1}$  before and after 22 days of irradiation.

Overall, the time-course experiment could reveal the change of the bis-complex **3** ( $X = \text{NTf}_2^-$ ) to another compound over time. The XRD pattern and IR spectra revealed that a transition after ca. four days is taking place. There are indications of successful [4+4]-cycloadditions of the

## 4. Results and Discussion

---

anthracenes as well occurring oxidation during irradiation, which seem to become dominant after four days. The long reaction time of 22 days is most likely not necessary.

### *Removal of the zinc salts*

Although some irradiation experiments, listed in Table 1, were already partially demetallated by the DMF- $d_7$  that was used for the NMR spectroscopy analysis, the zinc salts were still present in the DMF solution. These needed to be washed out to guarantee a full demetallation.

In order to remove the zinc salts, two different methods were applied: either the irradiated bis-complex **3** ( $X = \text{NTf}_2^-$ ) was treated with the complexation competitor HEEDTA, or it was repeatedly precipitated into MeOH by a concentrated DMF solution.

The first method was the mixing of HEEDTA (dissolved in water) with the irradiated bis-complex **3** ( $X = \text{NTf}_2^-$ ) in DMF. A short work-up included evaporation of the DMF, extraction with chloroform, and washing with water. The demetallated sample was found in the chloroform phase. The advantage of HEEDTA treatment was the simple separation. Still, traces of the compound were always caught in between the water/organic solvent boundary of the separation funnel, thereby distorting a clear separation.

The other method made use of the precipitation of the dissolved irradiated bis-complex **3** ( $X = \text{NTf}_2^-$ ) from DMF into MeOH. One has to keep in mind that DMF does not fully demetallate the bis-complex sample, but rather gives an equilibrium of mono-complex and premonomer. Therefore, the zinc salts would be dragged along into further fractions. The precipitation process could also be seen as a dilution of the zinc salts. A quick method to check whether the zinc salt had been successfully removed from the solution, was by measuring a  $^{19}\text{F}$ -NMR spectrum, since the counterion  $\text{NTf}_2^-$  contains fluorines. Although, the absence of fluorines would only indicate the removal of the counterion. It would be likely that the salt is then successfully removed, except if there had been a counterion exchange somehow before. The drastic increase of solubility in chloroform accompanied with the strong fluorescence under UV light was another indication of successful metal salt removal. Due to the increased solubility in chloroform, the compound could now be analyzed using NMR spectroscopy in  $\text{CDCl}_3$ .

An example that adequately represents the demetallation process of the irradiated bis-complex **3** ( $X = \text{NTf}_2^-$ ) by HEEDTA is the experiment "Irrad6". The  $^1\text{H}$ -NMR spectrum of the HEEDTA treated irradiated bis-complex **3** ( $X = \text{NTf}_2^-$ ) is shown in Figure 4.60, and compared with the

## 4. Results and Discussion

premonomer **7**, and non-irradiated bis-complex **3** ( $X = \text{NTf}_2^-$ ) in  $\text{CDCl}_3$ .

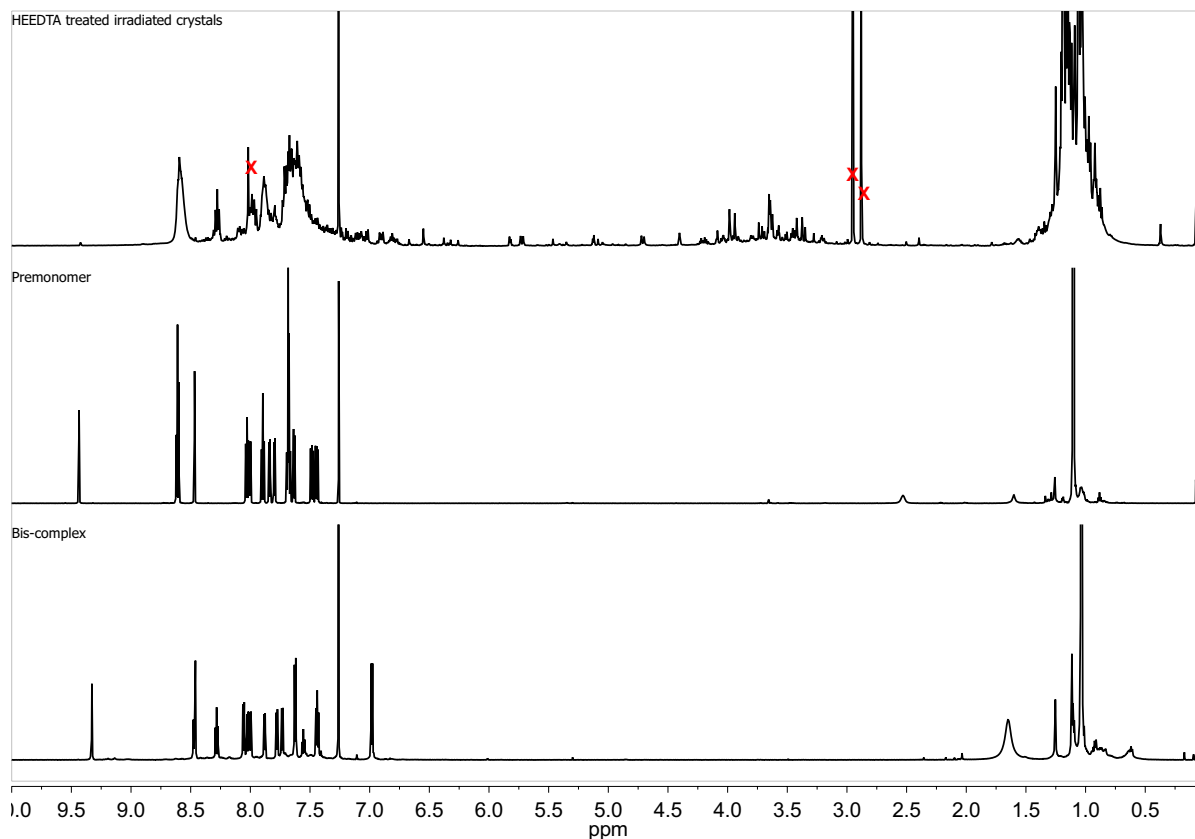


Figure 4.60: 500/700 MHz  $^1\text{H-NMR}$  spectra of the demetallated irradiated sample "Irrad6" (top), premonomer **7** (middle), and bis-complex **3** ( $X = \text{NTf}_2^-$ ) (bottom) in  $\text{CDCl}_3$ .

The proton spectrum of the HEEDTA treated irradiated bis-complex **3** ( $X = \text{NTf}_2^-$ ) reveals the decrease of 9,10-anthracene signals (8.45 and 9.35 ppm) and the resulting anthracene bridge-head signals (4.70 and 5.70 ppm) are seen instead. However, these are relatively weak in comparison to other aromatic signals in the spectrum. The characteristic spacer signals that were split at the bis-complex **3** ( $X = \text{NTf}_2^-$ ) spectrum at ca. 7.6 and 7.0 ppm were not split at 7.6 ppm in the HEEDTA treated irradiated bis-complex **3** ( $X = \text{NTf}_2^-$ ) sample. This is similar to the premonomer **7** spectrum and is an indication that the zinc salts were not involved anymore. The  $^{19}\text{F-NMR}$  spectrum (not shown) of the irradiated bis-complex also revealed the absence of the fluorine signal that would appear through the counterion ( $\text{NTf}_2^-$ ). It could therefore be concluded that the demetallation was successful. However, the HEEDTA treated sample revealed many other unknown proton signals that were scattered across the spectrum (Fig. 4.60), which complicated a precise characterization and would suggest that not only anthracene dimerization took place.

All three compounds mentioned in the proton spectra were also compared by their carbon spec-



## 4. Results and Discussion

tra in Figure 4.61).

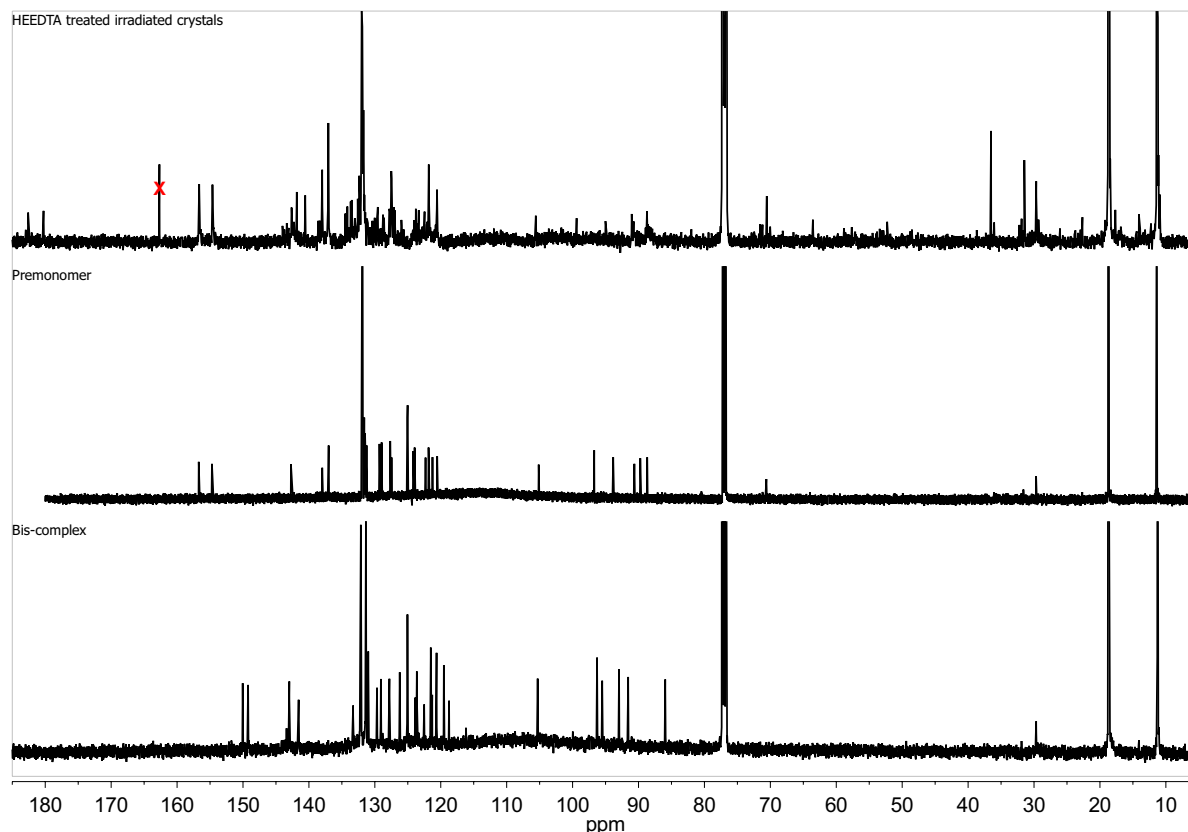


Figure 4.61: 126/176 MHz <sup>13</sup>C-NMR spectra of the demetallated irradiated sample "Irrad6" (top), premonomer 7 (middle), and bis-complex 3 (bottom) in CDCl<sub>3</sub>.

The similarities between the HEEDTA treated irradiated bis-complex 3 ( $X = \text{NTf}_2^-$ ) "Irrad6" and the premonomer 7 carbon signals were greater than in comparison to the bis-complex 3 signals. The two characteristic terpyridine signals around 155 ppm, for both, premonomer 7 and HEEDTA treated irradiated bis-complex 3 ( $X = \text{NTf}_2^-$ ) "Irrad6", indicate a similar metal free conformation. This is another hint of a successful zinc salt removal. However, the carbon spectra also revealed that the demetallated sample had either been impure and/or had been soiled with side products due to the many signals observed. In addition, the two signals above 180 ppm are typical for C=O signals and therefore confirm as well that an oxidation process during irradiation took place. The resulting C=O signals would also be the cause of decreasing 9,10-anthracene signals.

### *Comparison between demetallated irradiated bis-complex and premonomer solution irradiation*

As the <sup>1</sup>H- & <sup>13</sup>C-NMR spectra of the HEEDTA treated sample "Irrad6" was very complex (Fig. 4.60 & 4.61), it was decided to inject the mixture into the preparative rGPC in order to separate different compounds. Four fractions were collected, of which fraction 2 represents the oligomeric

## 4. Results and Discussion

part of the peak with the shortest elution time, fraction 3 the second largest intensity peak, and fraction 4 represents the largest intensity peak with the longest retention time. The elution curves of five full cycles from the solid-state irradiation (red)<sup>XXI</sup> and the solution irradiation (blue) in Figure 4.62 were deliberate overlapped with the purpose of allowing for a comparison of the isolated fractions from the solid-state irradiation with isolated fractions from the premonomer solution irradiation (Fig. 4.42) at the end of this chapter.

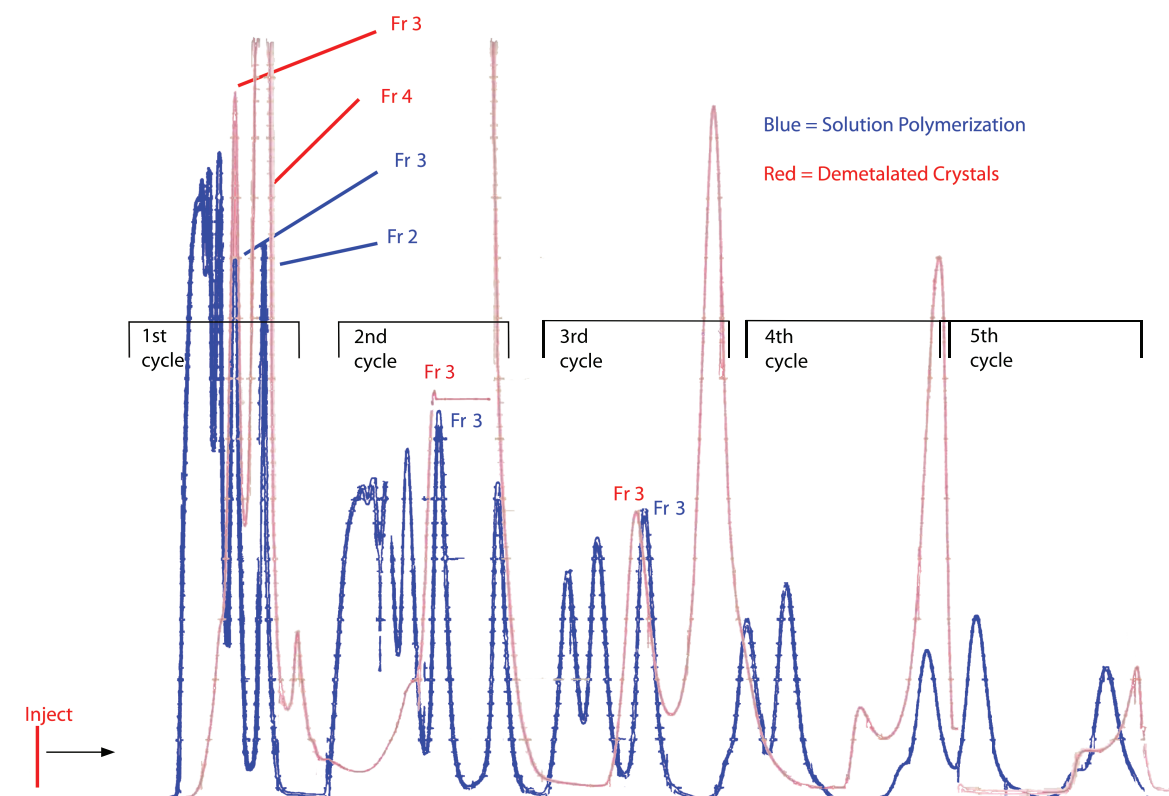


Figure 4.62: Elution curve from the preparative rGPC showing five full cycles of the solution irradiation of the premonomer **7** (blue) overlaid with the demetallated irradiated sample "Irrad6" (red).

Fraction 3 of the blue elution curve was identified earlier as the linear dimer **39**. Fraction 3 from the red elution curve was speculated to be a macrocyclic ring. Both fractions, fraction 3 of the blue elution curve and fraction 3 of the red elution curve, had a comparable retention time. Similar retention time would indicate a compound that has a similar hydrodynamic volume, which is the measure for the separation of a preparative rGPC. In this context, one could relate a linear dimer of the premonomer **39** with a potential macrocyclic ring (a closed linear dimer).

The isolated fractions 2, 3, and 4 of the red curve were also compared with the linear dimer

<sup>XXI</sup>The red elution curve shows a straight line at the 2nd cycle due to the pen of the analog output that for unknown reasons got stuck.

## 4. Results and Discussion

**39**, which was isolated from the solution irradiation of the premonomer **7** (4.3.), by  $^1\text{H-NMR}$  spectroscopy in  $\text{CDCl}_3$  (Fig. 4.63).

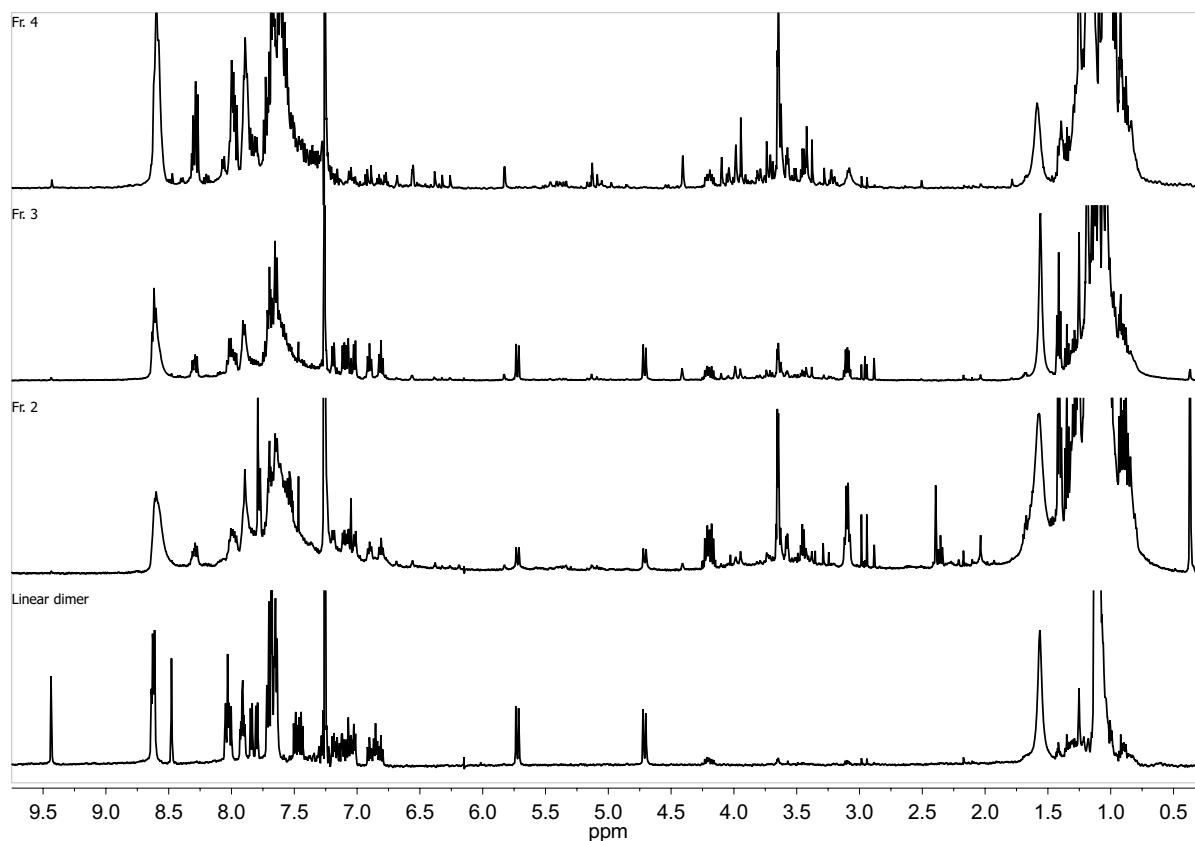


Figure 4.63: 500 MHz  $^1\text{H-NMR}$  spectra of Fr. 4, 3, 2, and linear dimer **39** in comparison in  $\text{CDCl}_3$  (from top to bottom).

It is, once again, quite easy to see the absence of 9,10-anthracene signals as well as other unknown signals across the  $^1\text{H-NMR}$  spectra of the HEEDTA treated samples (Fr. 2, 3, and 4). Fraction 4, in addition, reveals no anthracene bridge-head proton signals and could be representing an oxidized compound, but this was not confirmed. Fraction 2, 3, and linear dimer **39** have the similar anthracene bridge-head proton signals in common.

Upon irradiation of the premonomer **7** in solution (Fig. 4.42), four different dimerization constellations are possible (random dimerization), whereas only one kind of dimerization is feasible for the solid-state irradiation of bis-complex **3** ( $X = \text{NTf}_2^-$ ) given by its crystal structure. All possible constellations are illustrated in Figure 4.64.

## 4. Results and Discussion

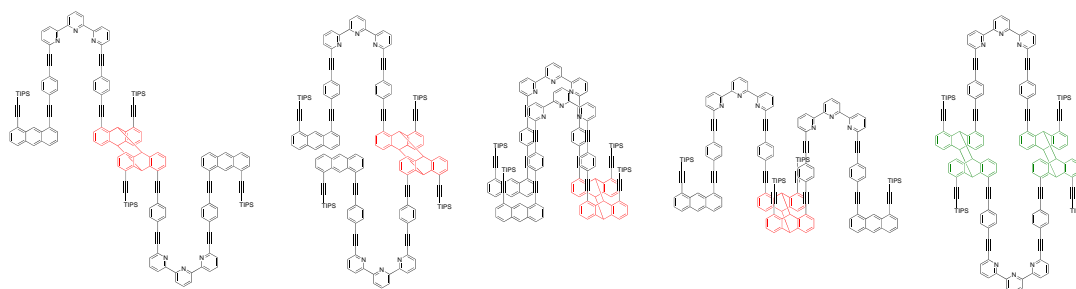


Figure 4.64: All constellations of photoproducts by solution (red) and solid-state (green) irradiation.

Comparing the  $^1\text{H-NMR}$  spectra of fraction 3 from the solution with fraction 3 of the solid-state irradiation should reveal a slight variation of photoproducts that are caused by the anthracene dimerizations. The difference between the solution and solid-state irradiation is highlighted in the proton spectra in Figure 4.65 in the range of 7.20 - 6.80 ppm (on top and below of the spectra), which show the anthracene signals, other than the 9,10-position that are shifted by the dimerization. The red spectrum of the solution irradiation reveals more overlapping signals, due to the mixture of head-to-head and head-to-tail photoproducts, than the green spectrum of the solid-state irradiation, which shows less signals due to the only possible head-to-tail photoproduct.

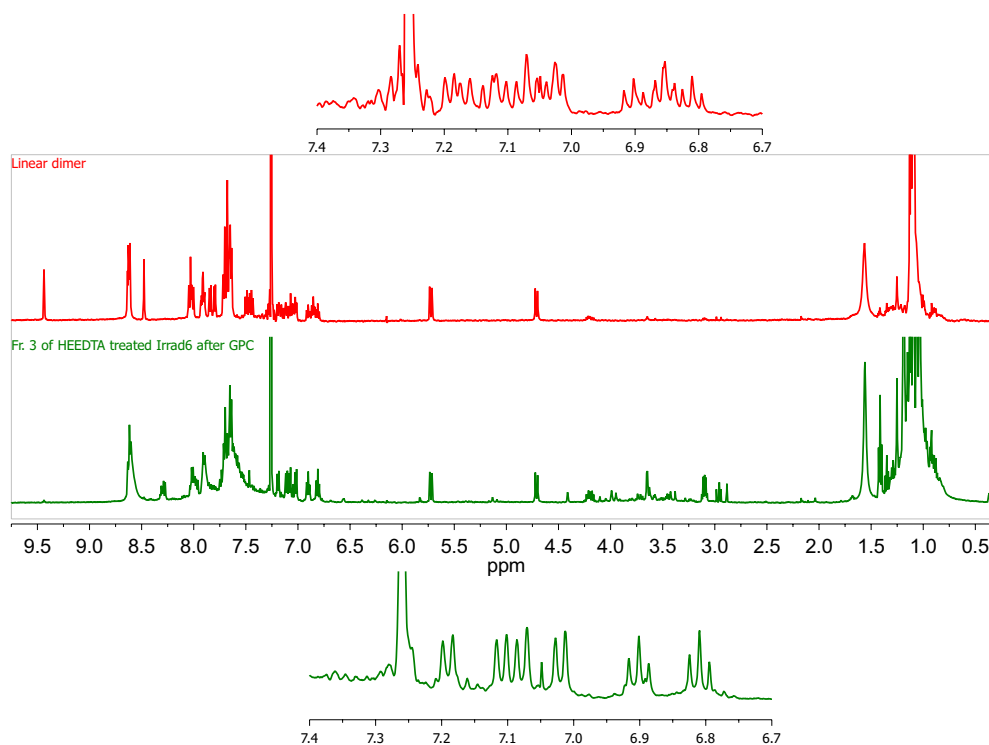


Figure 4.65: 500 MHz  $^1\text{H-NMR}$  spectra of the linear dimer (top) and Fr. 3 of the demetallated irradiated sample after preparative rGPC separation (bottom) in  $\text{CDCl}_3$ .

## 4. Results and Discussion

---

### *Conclusions*

The  $^1\text{H-NMR}$  spectra comparison (Fig. 4.65) of the linear dimer and the potential macrocyclic ring is a good support for a successful solid-state irradiation, but there are still many questions remaining. If the overlaid elution curves (Fig. 4.62) are examined more closely, then one notices that the solid-state photoirradiated sample generally has a larger retention time in comparison to the solution irradiation sample. This could mean that products from the solid-state photoirradiation are not polymeric. It is also possible that the actual polymeric part, which was the aim of this irradiation, was simply filtered off by the PTFE filter that is used before the sample had been injected into the preparative rGPC. Perhaps at the HEEDTA demetallation process and the use of a separation funnel, the material between the layers of water/chloroform that was separated, could have been a high molar mass compound, and had already been excluded before it was injected into the preparative rGPC. It is possible that the irradiation did not form polymers at all due to an incomplete photoreaction or during irradiation the crystal structure had been gradually deformed by the many dimerization processes to an extent, which made a photoreaction through 1D array impossible.

If the solid-state reaction to polymers had not been complete, then oligomers would have formed, and a larger amount of free premonomers **7** (after demetallation) should have been traceable as well. None of the irradiation experiments yielded any premonomer **7**. Perhaps the premonomer **7** was always oxidized during the irradiation and therefore could not be found as such.

Many of the observations presented here clearly indicated that the starting material (bis-complex **3**) had changed. Still, the fact that it remains impossible to prove a polymeric material with simple analytical tools, presents a crucial missing link in the process of synthesizing a poly[n]catenane. Since the expectation to achieve a poly[n]catenane was simple: irradiation of the bis-complex **3** ( $X = \text{NTf}_2^-$ ) crystal, then dissolving the crystals, and washing off the metal cation, one would rather have such a simple process. The novel strategy towards the synthesis of a poly[n]catenane via solid-state photopolymerization could have these legitimate obstacles, but on the other hand, time was the limiting factor for this approach, and this final missing step still needs further investigation.

## 4. Results and Discussion

### 4.4. Part B: Synthesis of a Monomer 6 for 2D Polymerization

The different synthetic paths leading to the monomer **6** are illustrated in Figure 4.66. The first path uses Kory's five-step synthesis of the oxygen-bearing monomer **4** as a point of departure.<sup>[44]</sup> In the present approach, synthesizing the amine-bearing monomer **6** involves a six step synthesis procedure with the stepwise addition of 1,8-diaminodihydroanthracene units **40** to the mono-blade **41**.<sup>[44,262–266]</sup> The process is finalized by oxidizing the tri-blade **42** with DDQ.<sup>[44]</sup> This reaction towards the tri-blade **42** was, however, not straightforward, and an alternate path was therefore attempted.

The alternative path presents the second approach to the synthesis of the monomer **6**. This second approach included adding three 1,8-diaminoanthracene units **48** to a *s*-triazine **43** core, and closing the resulting precursor **44** with another *s*-triazine **43** cap.<sup>[262,267,268]</sup>

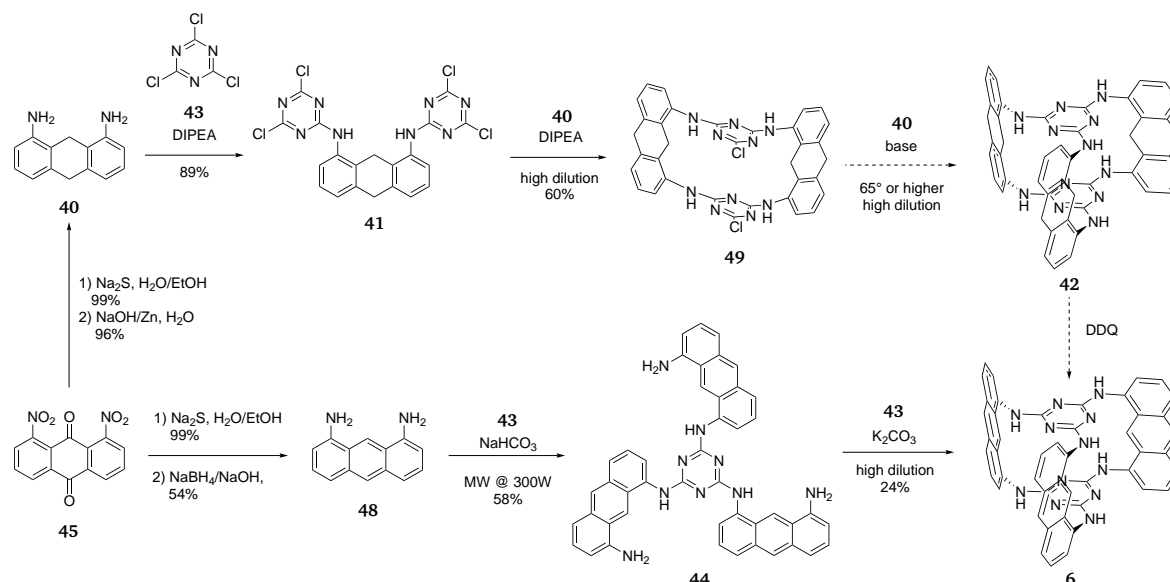


Figure 4.66: The synthetic sequence towards the amine-bearing monomer **6**.

The chemistry involved is based on the nucleophilic substitution reactions of cyanuric chloride **43** with amines or alcohols. Which of the chlorides is being selected for substitution depends on the applied temperature.<sup>[269,270]</sup> As a rule of thumb, the first substitution of cyanuric chloride **43** occurs at a temperature of 0 °C, the second at 25 °C, and the third at 65 °C.<sup>[270]</sup>

Already in the 1930s many reactions of cyanuric chloride **43** were explored.<sup>[271]</sup> In the 1950s a series of derivative syntheses were published by the Stamford Research Laboratories of the American Cyanamid Co.<sup>[272]</sup> Today, cyanuric chloride derivatives (*s*-triazines) are used as pesticides, herbicides, dyes, bleaches, and cross-linking agents.<sup>[269,273]</sup> *s*-Triazines capabilities for molecular recognition (coordination, hydrogen bonding,  $\pi$ - $\pi$ -interactions, and others) is ideal

## 4. Results and Discussion

for applying it in supramolecular chemistry. The low costs of cyanuric chloride make it an attractive starting component for dendrimer syntheses.<sup>[269,270,274-276]</sup>

### Monomer 6 via Kory's path

The synthesis towards the oxygen-bearing monomer **4** was already established by Kory *et al.*, who used the crystals for photoirradiation to achieve one of the very first successful scsc transformed 2DP crystals.<sup>[28]</sup> Kory's monomer **4** was synthesized in five steps—without any column chromatography purification. The yields were high, and the starting materials used were cheap.<sup>[28,44]</sup> The synthetic route of the oxygen-bearing monomer **4** presented a remarkable example for the synthesis of the amine-bearing monomer **6**. For the reaction described in this thesis, the 1,8-dihydroxyanthraquinone **20** used in Kory's synthetic route<sup>[44]</sup> was replaced with the 1,8-dinitroanthraquinone **45** for a starting material.

The reactions towards 1,8-diaminodihydroanthracene **40** are seen in Figure 4.67. Two slightly different paths were followed to achieve the product **40**. These paths included either a one-step reaction of 1,8-dinitroanthraquinone **45** with zinc under basic media to give **40** in 28 - 61 % yield,<sup>[265]</sup> or a two-step reaction via 1,8-diaminoanthraquinone **46** to give **40** in a 57 - 95 % yield in total.<sup>[262]</sup>

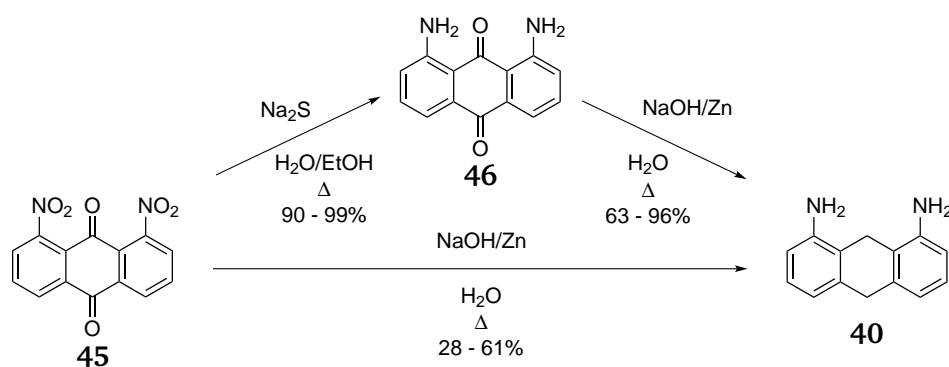


Figure 4.67: The synthetic sequence to **40**.

The one-step reaction was quicker to walk through, but involved two side products—the hydrazobenzene derivative **47** (Fig. 4.68a) and 1,8-diaminoanthracene **48**—which formed during the reaction. The latter anthracene side product **48** is generally expected as intermediate of the zinc reduction of anthraquinones to dihydroanthracenes. The former side product **47** probably emerged from the known side reactions of nitro/nitroso compound with base metals.<sup>[277]</sup> In this regard, the reduction in basic media is slowed, allowing the resulting reduction intermediates—nitroso compound and hydroxylamine—to undergo the dominant competitive

## 4. Results and Discussion

reaction that yielded an azoxybenzene as well as other intermediates shown in Figure 4.68b. [277]

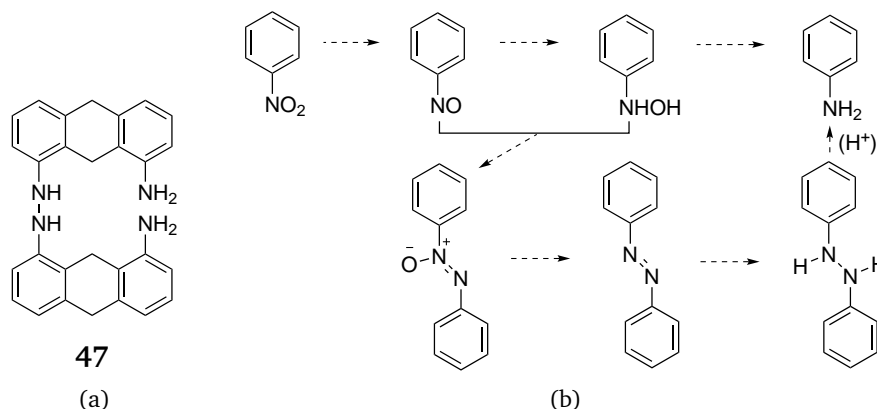


Figure 4.68: a) The side product **47** and b) the reduction of nitrobenzene with base metals [277].

The anthracene side product **48** has a similar elution as **40** and is not easily removed without the help of further purification. To confirm the anthracene compound, **48** was synthesized for purposes of comparison. Its synthesis is discussed later in this chapter. At the same time, the hydrazobenzene derivative **47** was isolated by column chromatography purification from the reaction mixture of **40**. The <sup>1</sup>H-NMR spectra in Figure 4.69 illustrate the reaction mixture of the one-step reaction to show the identified side products—**47** and **48**—within the mixture.

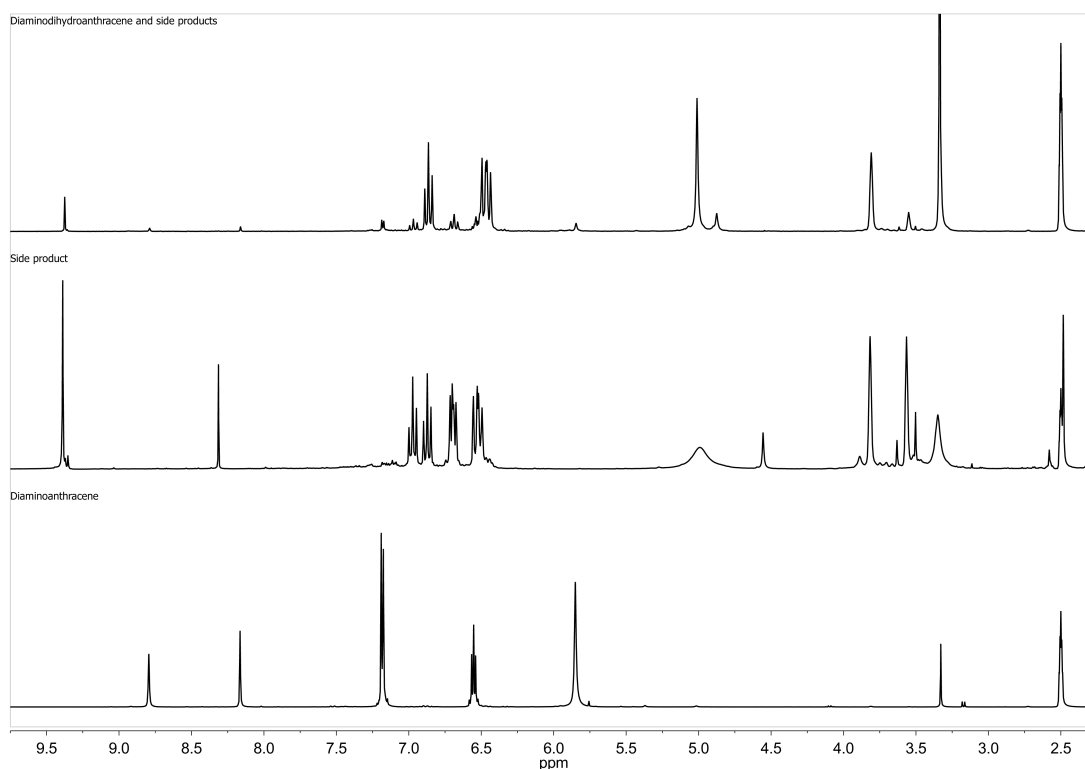


Figure 4.69: 300 MHz <sup>1</sup>H-NMR spectra in DMSO-*d*<sub>6</sub> of the one-step reaction mixture, the hydrazobenzene derivative **47**, and the 1,8-diaminoanthracene **48** in comparison (from top to bottom).



## 4. Results and Discussion

The  $^1\text{H-NMR}$  spectrum of the one-step reaction mixture confirms the resulting side products—**47** and **48**—within the mixture of the expected product **40**.

The first step of the two-step reaction of 1,8-dinitroanthraquinone **45** involved a Zinin reaction through the reduction of the nitro group to the amino group with sodium sulfide to achieve 1,8-diaminoanthraquinone **46** in 90 - 99 % yield.<sup>[262,278,279]</sup> The second step followed a similar procedure as the one-step reaction described earlier, by reducing 1,8-diaminoanthraquinone **46** with zinc under basic media to give 1,8-diaminodihydroanthracene **40** in 63 - 96 % yield.

Comparing the one-step and the two-step reactions, the latter was accompanied by an increased overall yield of **40**, as well as an suppression of the involved hydrazobenzene derivative side product **47**. However, the two-step reaction requires an additional day of work, due to the detour via 1,8-diaminoanthraquinone **46**. The process of purification of the product **40** was for both paths the same. After isolation of 1,8-diaminodihydroanthracene **40**, the compound was purified by silica gel column chromatography, and crystallized from EtOH to give greyish needles<sup>XXII</sup> in a 11 - 17 g scale.

Reactions towards di-blade **49** via mono-blade **41**, using 1,8-diaminodihydroanthracene **40** as starting material, are illustrated in Figure 4.70.

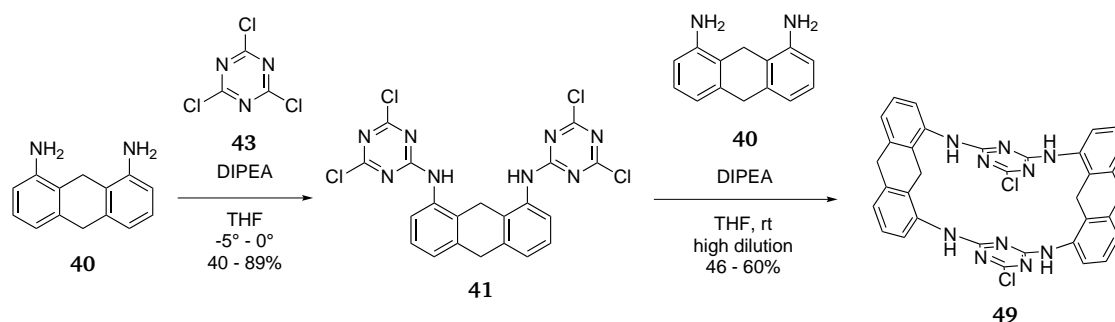


Figure 4.70: The synthetic sequence to **49**.

1,8-Diaminodihydroanthracene **40** with DIPEA was added dropwise to an excess solution of cyanuric chloride **43** in THF at ca.  $0^\circ\text{C}$  within three hours. After TLC confirmed the consumption of all the starting material **40**, the reaction was stopped, and the solvent evaporated. The remaining solid was washed with water to remove the excess of cyanuric chloride **43**, and identified as mono-blade **41** by NMR spectroscopy and MS analysis. The  $^1\text{H-NMR}$  spectrum of the product **41** is shown in Figure 4.71 in comparison to the starting material **40**.

<sup>XXII</sup>The crystals appeared greenish, if the ratio of the side product **48** was high.

## 4. Results and Discussion

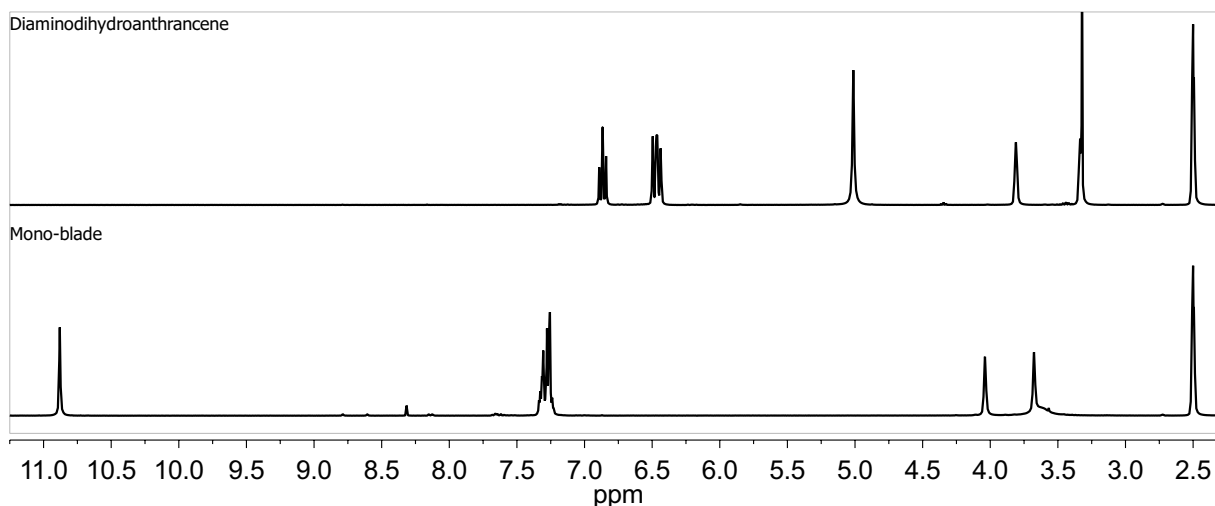


Figure 4.71: 300 MHz <sup>1</sup>H-NMR spectra of 1,8-diaminodihydroanthracene **40** (top) and mono-blade **41** (bottom) in DMSO-*d*<sub>6</sub>.

The proton spectrum of mono-blade **41** clearly shows the downfield shift of all proton signals in comparison to the starting material **40**. There was also an observable downfield shift of the amino group from 5.0 to 10.9 ppm, as well as the emergence of small amounts of an anthracene derivative **50** of mono-blade **41** as a side product (ca. 2.5 %). The cause of the side reaction is explained by the 1,8-diaminoanthracene's **48** impurity inherited from the synthesis of 1,8-diaminodihydroanthracene **40**. For purposes of comparison, the side product **50** was also synthesized separately through the oxidation of mono-blade **41** with DDQ. In addition, the general feasibility to oxidize such an amino-based *s*-triazine compound—which is detrimental for the proposed oxidation of tri-blade **42** to the monomer **6**—was explored. In addition, **50** was recrystallized from ODCB to give crystals suitable for XRD analysis (7.1.). The XRD crystal structure revealed a stacking of the anthracene units within a distance of 3.7 Å between the 9,10:9',10'-positions.

The product **41** was obtained as a white solid with 40 - 89 % yield between 1 and 11 g scale. Single-crystals suitable for XRD analysis were obtained by recrystallization from acetone (7.1.). The XRD crystal structure revealed hydrogen bonds between the amino groups and the nitrogens of the *s*-triazine from adjacent **41**.

The reaction towards di-blade **49** was performed in high dilution (ca. 2.5 mmol/L), which prolonged the reaction time (up to weeks), with a mixture of 1,8-diaminodihydroanthracene **40**, mono-blade **41**, and DIPEA in THF at rt. The high dilution conditions were chosen to favor intramolecular reaction over intermolecular reaction for the ring closing of the di-blade product **49**.<sup>[126,127]</sup> Already within a few days, the product **49** precipitated out of the reaction

## 4. Results and Discussion

mixture, but to maximize the product yield the reaction was continued up to ca. three weeks. The precipitate was collected by centrifugation, washed with methanol, and a water/methanol mixture to give **49** as a whitish solid in 46 - 60 % yield at 0.5 - 3.8 g scale. The remaining filtrate still contained dissolved product **49** and some starting material of mono-blade **41**, but none of the other starting material 1,8-diaminodihydroanthracene **40**. It was therefore assumed that **40** had already reacted with one of the *s*-triazines in **41**, but didn't undergo the intramolecular reaction to form **49** yet (Fig. 4.78). Presumably, the proton signals to identify such an intermediate were superimposed by the other compounds. Prolonging the reaction time or concentrating the reaction mixture over time could increase the yield of di-blade **49**. The  $^1\text{H-NMR}$  spectra of **49** is shown in Figure 4.72 and compared with mono-blade **41**.

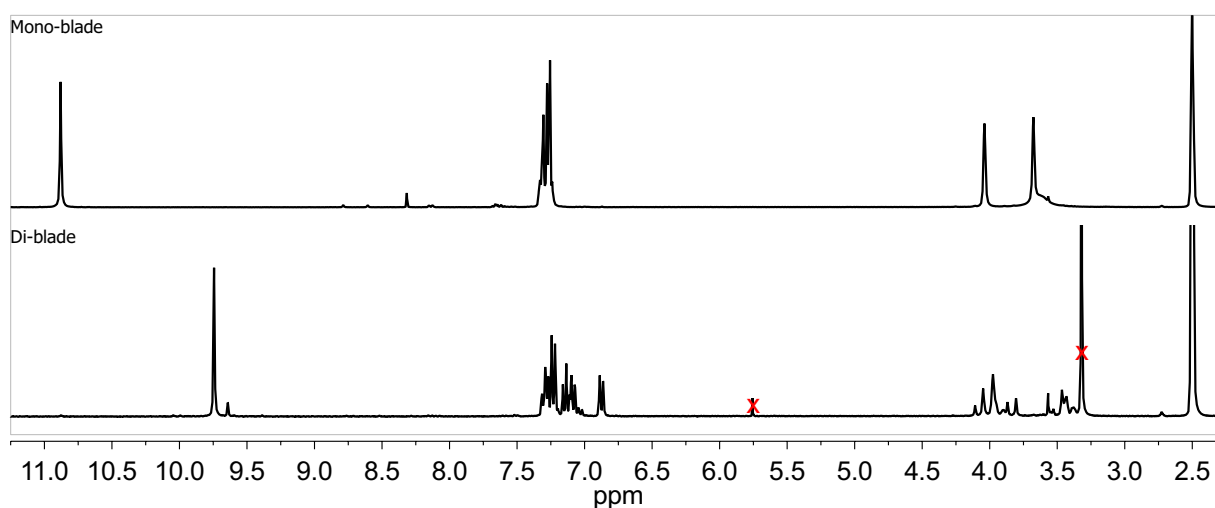


Figure 4.72: 300 MHz  $^1\text{H-NMR}$  spectra of mono-blade **41** (top) and di-blade **49** (bottom) in  $\text{DMSO-d}_6$ .

The difference between the mono-blade starting material **41** and the product di-blade **49** is clearly seen in the  $^1\text{H-NMR}$  spectra. The amino proton signals of the mono-blade **41** are shifted upfield from 10.9 to 9.8 ppm in comparison to the di-blade **49**. As well the aromatic proton signals of mono-blade **41** around 7.3 ppm are distributed for di-blade **49** between 7.3 to 6.8 ppm, and the two dihydroanthracene proton signals 4.0 & 3.7 ppm in the aliphatic range of mono-blade **41** are split for di-blade **49** to a group of signals ranging between 4.2 to 3.3 ppm.

In solution, the di-blade **49** is in an equilibrium between different conformations and flips back and forth depending on the solvent. These different conformations are illustrated from a top view onto the di-blade **49** in Figure 4.73 and are described by two symmetric forms (I. & III.) as well by one asymmetric form (II.).

## 4. Results and Discussion

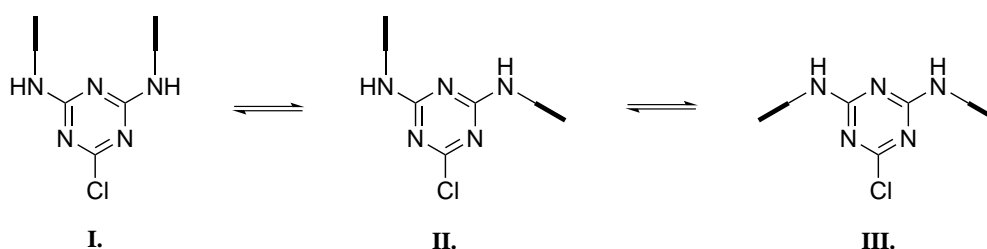


Figure 4.73: Simplified illustration of the di-blade **49** flipping from conformation I. to II. to III.

These possible conformations might explain the small amine proton signal at 9.65 ppm in the  $^1\text{H-NMR}$  (Fig. 4.72) of the di-blade **49**, which is probably caused by one of these conformers. In addition, the small amine proton signal should be accompanied by the other resulting shifted proton signals of its neighboring signals of the di-blade **49**, but probably these are superimposed by the main proton signals of the preferred conformation. The preferred conformation in  $\text{DMSO-}d_6$  is the II. asymmetric form, which is indicated by the proton spectrum (Fig. 4.72) and  $^1\text{H-}^1\text{H-COSY}$  spectrum (not shown). The analysis of the spectra revealed a difference between the 2,7-anthracene signals from one dihydroanthracene of the di-blade **49**, and the 2',7'-anthracene signals from the other, second dihydroanthracene (Fig. 4.74).

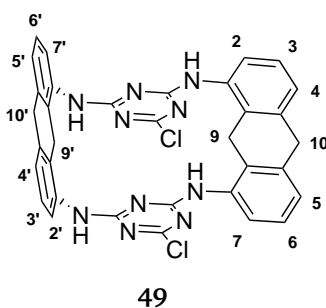


Figure 4.74: Atomic numbering of di-blade **49**.

The carbon spectrum supports the asymmetric conformation preference in  $\text{DMSO-}d_6$  solution as well. This carbon spectrum includes a total amount of 19 carbon signals that were assigned to 12 aromatic, 4 dihydro, and 3 triazine carbon signals. In contrast, the symmetric forms would presumably show only 10 carbon signals (6 aromatic, 2 dihydro, and 2 triazine signals).

A  $^1\text{H-NMR}$  spectrum of the di-blade **49** in  $\text{DMF-}d_7$  (not shown) revealed three equal amino proton signals in which the compound's flipping seems more balanced among the different conformations. Therefore it shows no particular conformational preference than as in the solvent  $\text{DMSO-}d_6$ . The equilibrium of the different conformations of **49** generates a mixture of the conformers, which have different chemical shifts of signals in the NMR spectrum.

## 4. Results and Discussion

The preferred conformation in solid-state was determined by the XRD crystal structure of di-blade **49**. The crystals of di-blade **49** were obtained by crystallization from DMSO, which gave clear cubic crystals suitable for XRD analysis (7.1.). The XRD crystal structure of the di-blade **49** is shown in Figure 4.75a&b and Figure 4.76.

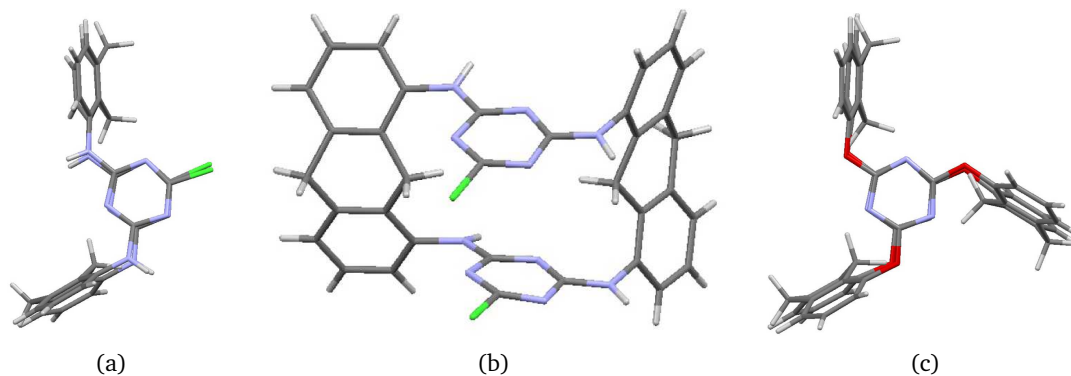


Figure 4.75: The XRD crystal structure of di-blade **49** a) top view & b) side view, and c) the XRD crystal structure of oxygen-bearing tri-blade by Kory *et al.* [44] (top view). (Solvents omitted.)

The XRD crystal structure of di-blade **49** (Fig. 4.75a&b) shows the preferred asymmetric conformation II. (Fig. 4.73). The reaction of di-blade **49** with another 1,8-diaminodihydroanthracene blade **40** is projected to result in a similar symmetric rotor shaped tri-blade **42** as seen in the XRD crystal structure (Fig. 4.75c) of the oxygen-bearing tri-blade, synthesized by Kory and coworkers. [44] Figure 4.76 shows the hydrogen bonds between the *s*-triazines and amino groups of adjacent di-blades **49**.

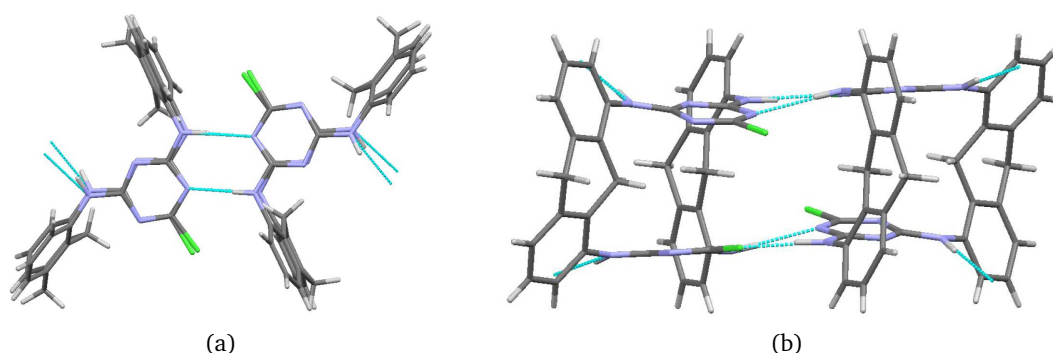


Figure 4.76: The XRD crystal structure of adjacent di-blades **49** and their hydrogen bonds (light blue). a) Top view and b) side view. (DMSO solvent omitted.)

The crystals of di-blade **49** from DMSO crystallization were only partially soluble in boiling DMSO. This was probably the result of these hydrogen bonds between the *s*-triazines and amino groups. The MS analysis of the di-blade **49** revealed an unexpected result as seen in Figure 4.77.

## 4. Results and Discussion

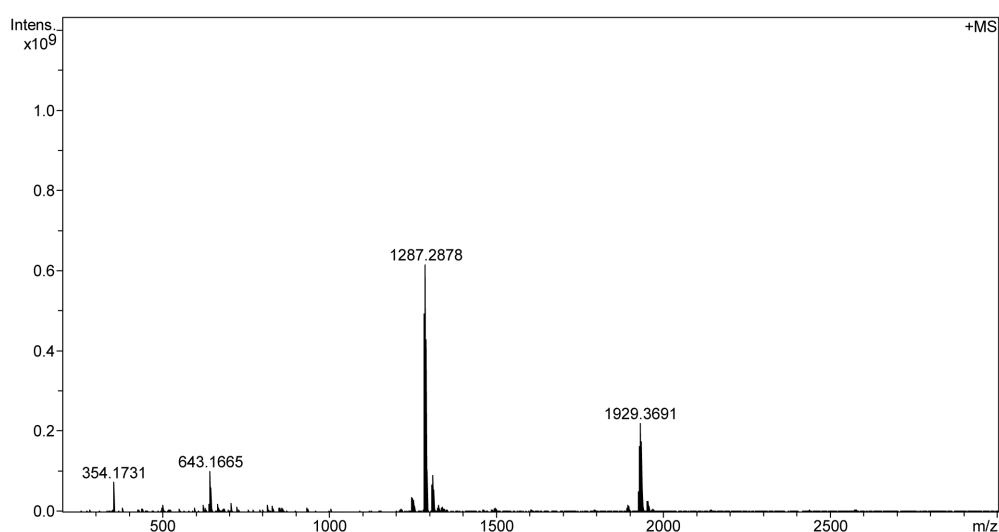


Figure 4.77: The high resolution MALDI MS of di-blade **49**.

Surprisingly, the MS shows only small amounts of di-blade **49** ( $m/z = 643$ ) in comparison to the two additional larger signals that correspond to the mass of a dimer ( $m/z = 1287$ ) and trimer ( $m/z = 1929$ ) of di-blade **49**. The reason for the occurrence of dimer and trimer signals might be that two or three di-blades **49** are held together by the aforementioned hydrogen bonds as seen in the crystal structure of the di-blade **49** (Fig.4.76), and withstand the conditions applied at the MS analysis. A different reason for the dimer and trimer mass detection might be that these are side product impurities. These impurities could have been the result of intermolecular reactions at the di-blade **49** synthesis. Figure 4.78 illustrates these intermolecular reactions that would lead to compounds with the mass of a dimer and trimer.

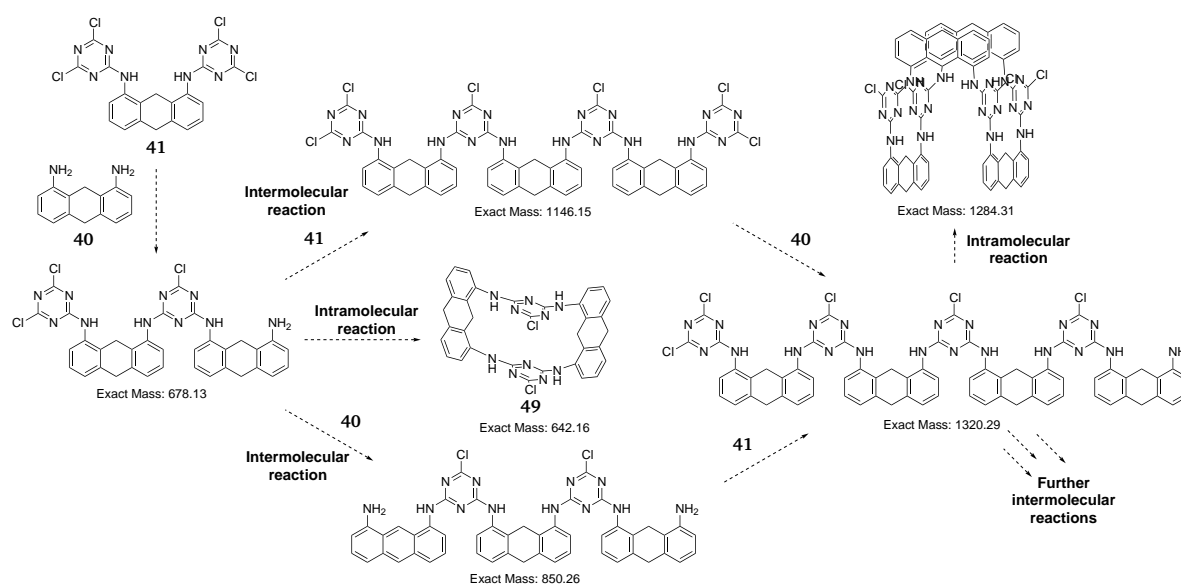


Figure 4.78: Synthetic sequence towards **49**, including intermediates, and possible side reactions.

## 4. Results and Discussion

The synthetic sequence in Figure 4.78 shows the intermolecular and intramolecular reactions between mono-blade **41** and 1,8-diaminodihydroanthracene **40**. Many intermediates should form during these reactions and should be traceable with the MS analysis of a crude reaction sample. However, the only mass that was found during the synthesis towards the di-blade **49** was the di-blade **49** itself. In addition, a proton spectrum of the crude sample revealed remaining 1,8-diaminodihydroanthracene **40** as well as di-blade **49**.

A further immediate intermolecular reaction should produce a dimer mass. The intermolecular reactions beyond this should, in turn, result in a trimer mass. Even though the high dilution conditions chosen for the di-blade **49** synthesis, which supports intramolecular reactions, makes such a result unlikely. It is likely that the dimer/trimer mass signals, which were found in the MS (Fig. 4.77), were the result of the hydrogen bonds between the *s*-triazines and amino groups of two/three di-blades **49**. However, the di-blade **49** was expected to be suitable for further reactions in solution.

The next reaction step was the synthesis of the tri-blade **42**, as shown in Figure 4.79, with the expected intermediate **51** that forms prior to the intramolecular reaction. Once again, the reaction towards tri-blade **42** was following Kory's oxygen-bearing tri-blade synthetic protocol.<sup>[44]</sup> The tri-blade **42** would ideally precipitate during the reaction—such as in Kory's approach.

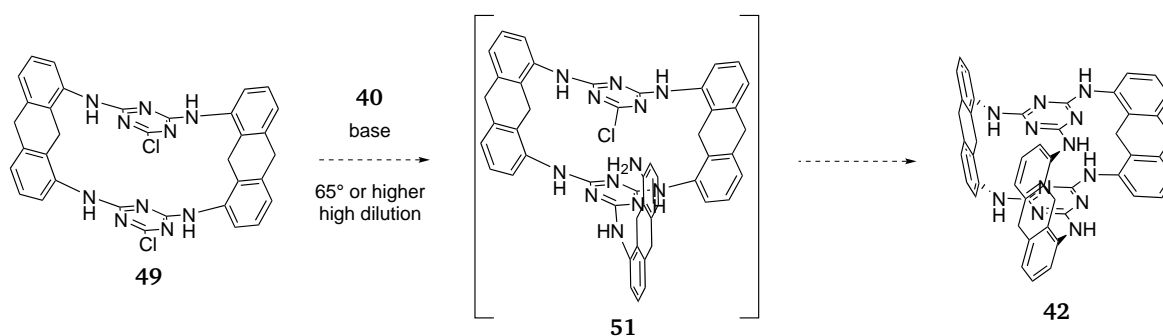


Figure 4.79: The synthetic sequence to **42**.

The suspension of di-blade **49** in THF was added to a refluxing high diluted (1.3 mmol/L) solution of 1,8-diaminodihydroanthracene **40** with  $K_2CO_3$  in THF. After five days of reaction, the mixture was analyzed by  $^1H$ -NMR spectroscopy and MS, which both revealed that di-blade **49** did not yield any product of tri-blade **42**—probably due to the low solubility of **49** in THF. Therefore, the general solubility of di-blade **49** was screened to find the ideal solvent first, before further reactions towards tri-blade **42** were attempted. A variety of solvents were screened, in which  $\gamma$ -butyrolactone, cyclohexanone, DMA, DMF, DMSO, 1,4-dioxane, NMP, or pyridine

## 4. Results and Discussion

showed good solubility of di-blade **42** at slight heating. The reaction conditions were then examined by varying not only solvents, but also bases (DIPEA,  $K_2CO_3$ , NaOH, pyridine,  $Na_2CO_3$ ,  $NaHCO_3$ , NaOAc, and HCOONa), temperatures (65 - 125 °C), and concentrations (0.27 mmol/L to 1.6 mmol/L). The most promising conditions were found to be by using 1,4-dioxane at high dilution (1.6 mmol/L) as solvent with  $K_2CO_3$  at 125 °C. The usefulness of these conditions were supported by the detected product tri-blade **42** signals at the MS analysis of the 1,4-dioxane phase from the crude reaction mixture, as seen in Figure 4.80 ( $m/z = 781.3259$  corresponds to the specific isotope distribution of tri-blade + H). The  $^1H$ -NMR spectrum of the same sample revealed, however, too many impurities.

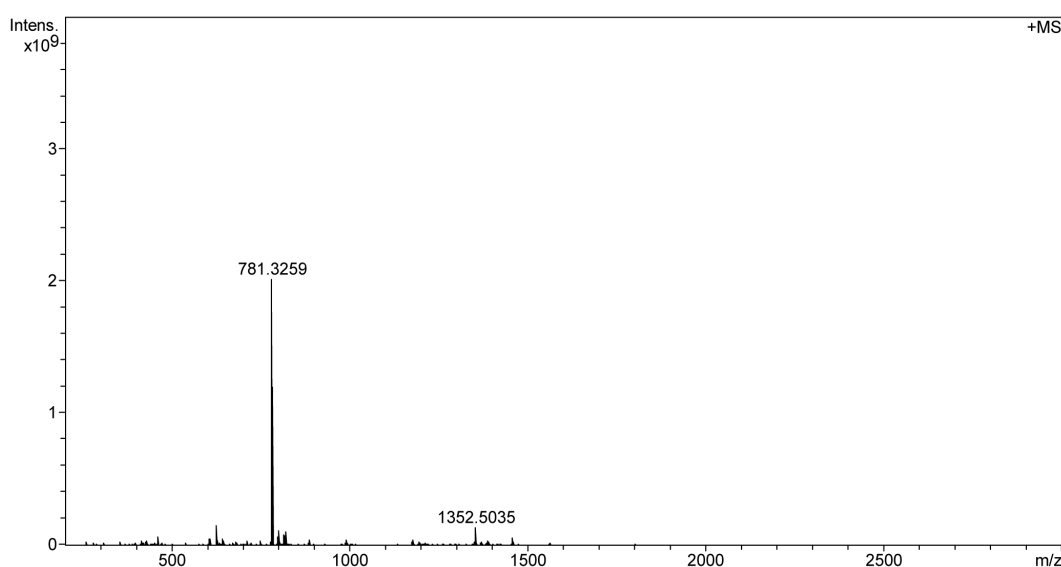


Figure 4.80: The high resolution MALDI MS of the 1,4-dioxane phase of the tri-blade **42** reaction.

The conditions that seemed most promising, mentioned also above, were applied to another series of experiments towards the tri-blade **42**. Usually the amount of di-blade **49** for each experiment varied between 20 - 200 mg. One of these experiments will be described in all detail in the following. The di-blade **49** was dissolved in 1,4-dioxane at 125 °C and high dilution (1.6 mmol/L), then  $K_2CO_3$  and 1,8-diaminodihydroanthracene **40** were added. Within 30 minutes the reaction mixture became already turbid by the precipitation of a whitish solid. However, the reaction was continued for several days and samples were taken to monitor the reaction process. The ratio between the di-blade **49**, the intermediate **51**, and the tri-blade **42** were inspected through MS analysis.<sup>XXIII</sup> It was expected that the ratio changes over time and that it would shift towards the tri-blade **42** product. After several days, the reaction was stopped and the precipitated solid was separated from the 1,4-dioxane phase by centrifugation. Both the

<sup>XXIII</sup>The actual ratio at MS analysis might be different, since compounds could be ionized differently.



## 4. Results and Discussion

---

solid and the 1,4-dioxane phase were analyzed by MS. Surprisingly, the tri-blade product **42** was found exclusively in the 1,4-dioxane phase, while the solid was identified as the di-blade **49**. Therefore, the precipitate that formed within 30 minutes was the starting material di-blade **49**. Obviously, the product tri-blade **42** remained in the solvent phase as a mixture of some dissolved di-blade **49**, 1,8-diaminodihydroanthracene **40**, and other side products, due to its good solubility. Although these reaction conditions did result in the tri-blade **42**, as seen in the MS (Fig. 4.80), it could not be isolated from the reaction mixture.

The precipitation of the di-blade **49** is generally problematic, because the 1 : 1 ratio of di-blade **49** to 1,8-diaminodihydroanthracene **40** at the tri-blade **42** synthesis would shift towards an excess of 1,8-diaminodihydroanthracene **40** that would cause other side products.

To understand the precipitation of di-blade's **49** during the reaction towards tri-blade **42** in 1,4-dioxane, the precipitate was examined more carefully. Under the OM, the precipitate revealed crystallinity, but these crystals were too small for in-house XRD analysis. It is likely that the di-blade **49** was recrystallized by the 1,4-dioxane at heating. Similar to the crystals obtained by DMSO crystallization, these crystals were only partially soluble upon heating in 1,4-dioxane. Heating the di-blade **49** in 1,4-dioxane without the other reactants and reagents resulted in the same precipitation within 30 minutes. It is therefore that these reactants and reagents could be excluded as the cause for precipitation during the reaction towards tri-blade **42**.

Since the XRD crystal structure of the di-blade **49** (Fig. 4.76) revealed hydrogen bonds between the *s*-triazines and amino groups of adjacent di-blades **49**, it was assumed that the same coordination bonds are formed in the crystals from 1,4-dioxane. Further investigations to confirm this assumption by measuring the XRD crystal structure of crystals of di-blade **49** from 1,4-dioxane recrystallization were not pursued due to the too small resulting crystals, which were not suitable for XRD measurements.

Hence, the solvent 1,4-dioxane, which was used for the reactions of di-blade **49** towards tri-blade **42**, was not ideal. Other solvents such as DMA, DMF, DMSO, and NMP were considered, since they kept the di-blade **49** in solution. All of the MS analysis and <sup>1</sup>H-NMR spectrum was barely able to find traces of the tri-blade **42** product. In addition, the reaction mixtures in these solvents turned red during reaction, which might hint at unintentional reaction. Presently, the cause and result of this color change remains unclear, and reactions in one of these solvents were not further considered. Since the reactions of di-blade **49** in 1,4-dioxane at least revealed tri-blade **42** product, it is necessary to optimize the reaction conditions.

#### 4. Results and Discussion

The amount of di-blade **49** that precipitated from 1,4-dioxane was filtered and weighed. Those parts of the di-blade **49**, which were still dissolved in the filtrate could then be calculated and the reaction would be continued by adjusting the amounts of the other reactants and reagents needed for the reaction towards tri-blade **42**. To determine to what extent the precipitate was forming, the temperature and concentration for different reaction mixtures were varied. However, this approach would extend the reaction time by an even higher dilution. In addition, the tri-blade **42** after reaction would still need a purification step, since the product **42** was expected to remain in solution. The problem that arose with this attempt was the inconsistency of the di-blade **49** solubility, and the amount of di-blade **49** that precipitated varied among the different experiments. In addition, the results of different di-blade **49** batches were inconsistent. As a consequence, the reactions towards tri-blade **42** were discontinued.

Since it was the di-blade **49** which proved to be a hindrance in the reaction towards tri-blade **42**, it was considered to synthesize anthracene derivatives of **49**, such as **52** and **53** (Fig. 4.81).

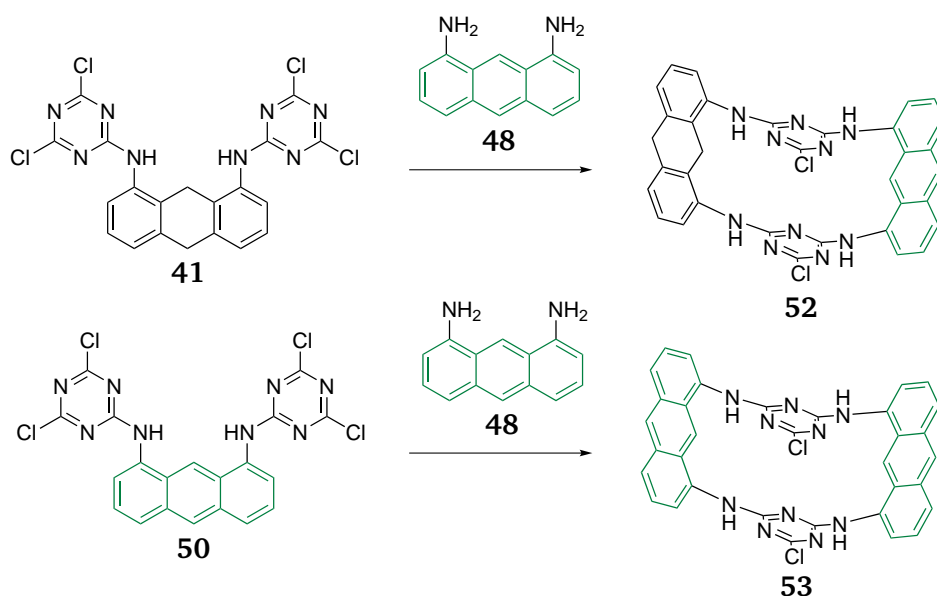


Figure 4.81: The **52** and **53** derivatives of di-blade **49**.

The idea to use either one or the other derivative (**52** or **53**) was grounded in the expectation of an increased solubility for the reaction towards a tri-blade derivative. As well as in preventing a hydrogen bond formation between the *s*-triazines and amino groups of adjacent di-blade derivatives that might cause precipitation. In addition, by using the anthracene derivatives instead of dihydroanthracenes, the final oxidation reaction step would no longer be needed.

The reaction towards **52** and **53** were performed similar to the di-blade **49** synthesis. At the

## 4. Results and Discussion

**52** synthesis, mono-blade **41** was mixed with 1,8-diaminoanthracene **48** in THF and DIPEA at rt. Within a few days a light green precipitate formed, which was isolated by centrifugation. Unfortunately, the solid of **52** was less soluble in common organic solvents than in comparison to the di-blade **49**. The  $^1\text{H-NMR}$  spectrum of **52** was complex and eventually contained signals of other side products that had formed during reaction. In Figure 4.82, the proton spectrum is compared with the spectrum of **49**.

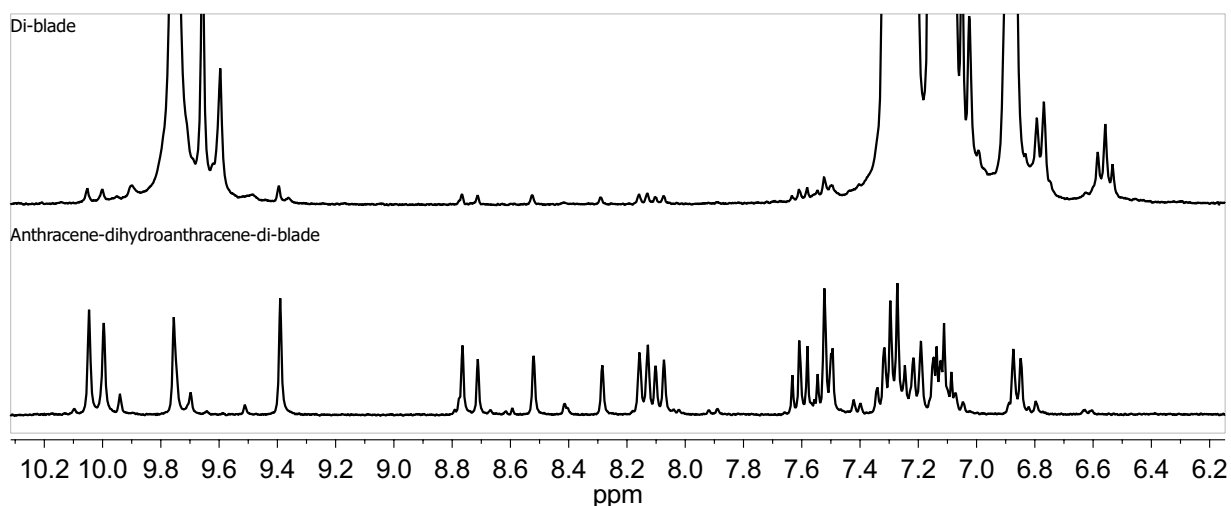


Figure 4.82: 300 MHz  $^1\text{H-NMR}$  spectra of di-blade **49** (top) and **52** (bottom) in  $\text{DMSO-}d_6$ .

Since the spectrum of **52** was very complex it was difficult to correctly assign the proton signals to the compound. However, the comparison between **52** and **49** showed that the spectrum of di-blade **49** included the di-blade derivative **52** as an impurity. This was due to the **50** or **48**, which was dragged along during the synthesis towards **49** as impurity. The MS analysis identified the light green solid as the product of **52**.

Performing the reaction towards **53** with similar reaction conditions by mixing **50** with **48** in THF and a base at rt, a yellow solid of **53** precipitated during the reaction. This solid also showed bad solubility in common organic solvents. The  $^1\text{H-NMR}$  spectrum (not shown) was again complex and unclear.

To conclude, both di-blade derivatives, **52** and **53**, did not show an enhanced and proper solubility suitable for reactions towards tri-blade derivatives. Therefore, further reactions with these derivatives were discontinued and the focus of the monomer **6** synthesis was shifted to the alternative synthesis approach.

## 4. Results and Discussion

### Monomer 6 via alternative path

The reactions towards the precursor **44** are seen in Figure 4.83. First, 1,8-Dinitroanthraquinone **45** was reduced in a two-step reaction via 1,8-diaminoanthraquinone **46** to yield 1,8-diaminoanthracene **48**.<sup>[262,267]</sup> An excess of 1,8-diaminoanthracene **48** was then used in reaction with cyanuric chloride **43** in the microwave reactor to form the precursor **44**.<sup>[268]</sup>

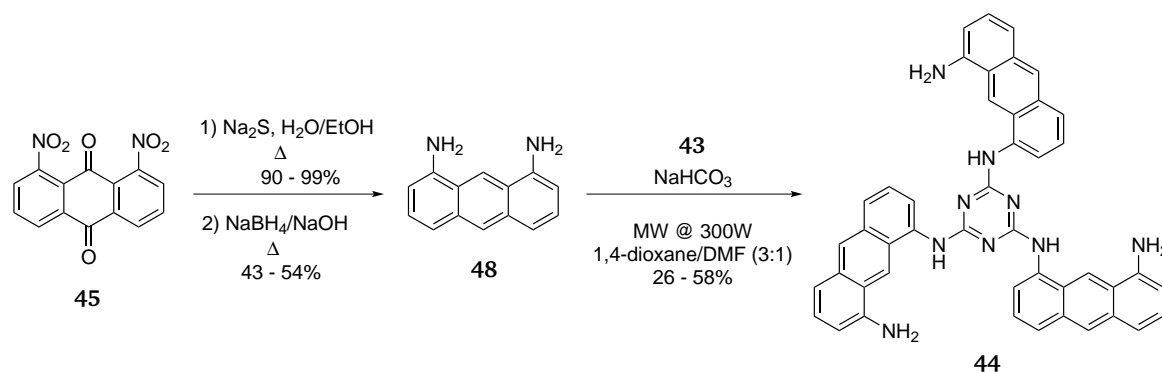


Figure 4.83: The synthetic sequence towards **44**.

1,8-Dinitroanthraquinone **45** was reduced by sodium sulfide via the Zinin reaction to the 1,8-diaminoanthraquinone **46** in 90 - 99 % yield, as described earlier.<sup>[262,278,279]</sup> The next step involved a one-step reduction of 1,8-diaminoanthraquinone **46** via  $\text{NaBH}_4$ ,<sup>[262]</sup> which resulted in 1,8-diaminoanthracene **48** in 43 to 54 % yield after silica gel column chromatography purification at 1 - 20 g scale. Alternatively, a two-step reduction was attempted via the intermediate 1,8-diamino-9-anthrone **54**, which was reduced with aqueous ammonium, and then further reduced with  $\text{NaBH}_4$  to synthesize 1,8-diaminoanthracene **48** without column chromatography purification.<sup>[267]</sup> However, the two-step reduction gave a mixture of 1,8-diaminoanthracene **48** and 1,8-diaminodihydroanthracene **40** in a molar ratio of 1.0 : 0.37 (determined by  $^1\text{H-NMR}$ ), which was too impure for further consideration.

1,8-Diaminoanthracene **48** was then used in a fivefold excess to react with cyanuric chloride **43**. The fivefold excess of 1,8-diaminoanthracene **48** was chosen to avoid disubstitution of two cyanuric chlorides **43** with one 1,8-diaminoanthracene **48**, as seen at the mono-blade **41** synthesis in Figure 4.70. Therefore, the solution of 1,8-diaminoanthracene **48** in a 1,4-dioxane/DMF (3 : 1) mixture with  $\text{NaHCO}_3$  was cooled to ca.  $-20\text{ }^\circ\text{C}$ , then cyanuric chloride **43** was added dropwise within 10 minutes to the slowly solidified reaction mixture. Subsequently, the reaction mixture was set into a microwave reactor and heated to  $160\text{ }^\circ\text{C}$  for 15 minutes.<sup>[268]</sup> The reaction mixture was purified by silica gel column chromatography with an eluent mixture of

## 4. Results and Discussion

$\text{CHCl}_3/\text{MeOH}/\text{TEA}$  (19 : 1 : 1) to give precursor **44** in 26 - 58 % yield at 0.1 - 0.6 g scale. TEA was an important eluent for the purification, since the amines would strongly absorb to silica. This approach had a clear disadvantage: the resulting TEA salt impurities accompanied the precursor **44** samples, which then made an additional washing procedure necessary. Alternatively, the TEA salts could be avoided by using  $\text{CHCl}_3$  stabilized with amylene instead of  $\text{CHCl}_3$  stabilized with ethanol, as eluent at the chromatography purification.

Generally, the purification by silica gel column chromatography was straightforward due to the good separation of the product **44** and 1,8-diaminoanthracene **48**. In addition, the separation was easy to trace, because of the yellow fluorescence of the product **44** and green fluorescence of the unreacted anthracenes **48** under the 366 nm UV light. The latter could also be recovered in 52 - 73 %. Crystals of the precursor **44** would have been ideal for purification and for curiosity, but unfortunately no crystals were yet obtained.

The precursor **44** was characterized by MS analysis and NMR spectroscopy. Its carbon spectrum in  $\text{DMSO}-d_6$  revealed the expected 15 carbon signals (Fig. 4.84). The single peak of the *s*-triazine core at ca. 165 ppm was particularly significant. Most of the other carbon signals could be assigned as seen in the experimental part of the thesis.

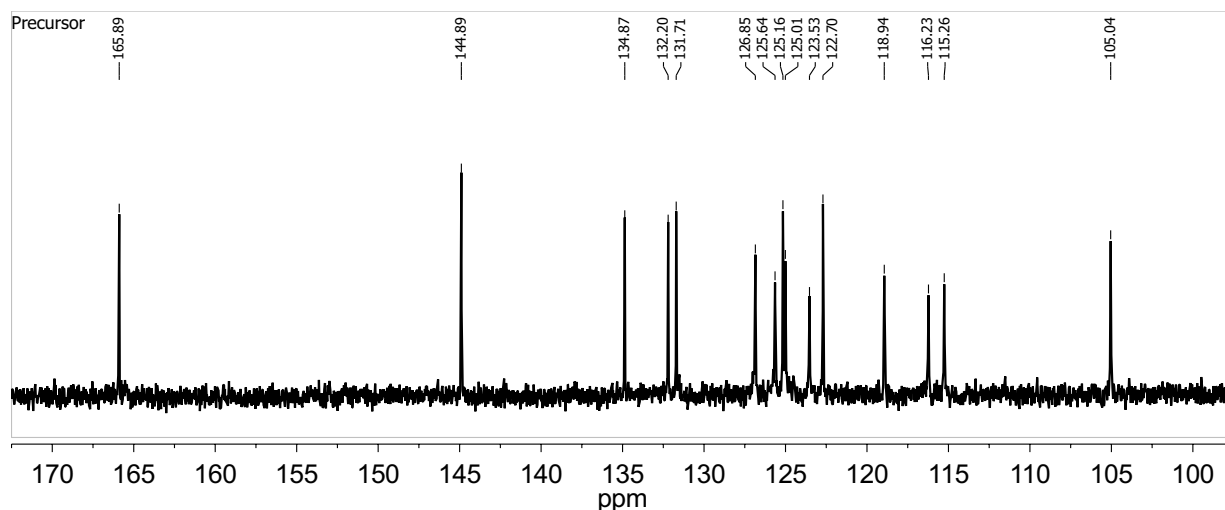


Figure 4.84: 76 MHz  $^{13}\text{C}$ -NMR spectrum of precursor **44** in  $\text{DMSO}-d_6$ .

## 4. Results and Discussion

The synthesis of monomer **6** is shown in Figure 4.85.

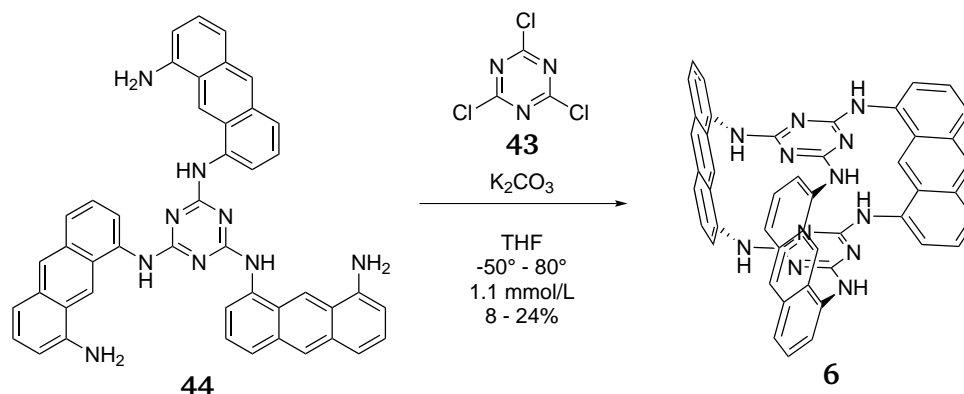


Figure 4.85: The synthetic scheme of **6**.

The precursor **44** and cyanuric chloride **43** were dissolved in a 1 : 1 ratio at  $-50^{\circ}\text{C}$  in distilled THF<sup>XXIV</sup> with  $\text{K}_2\text{CO}_3$ . Subsequently, the reaction mixture was transferred to a  $85^{\circ}\text{C}$  preheated oil bath to react at the same temperature for ca. two days in the dark. The reaction mixture was monitored by MS analysis and NMR spectroscopy. In addition, the fluorescence color change from green<sup>XXV</sup> to blue under 366 nm UV light over time was significant and a good indicator for reaction completion. The MS analysis of the reaction mixture is shown in Figure 4.86).

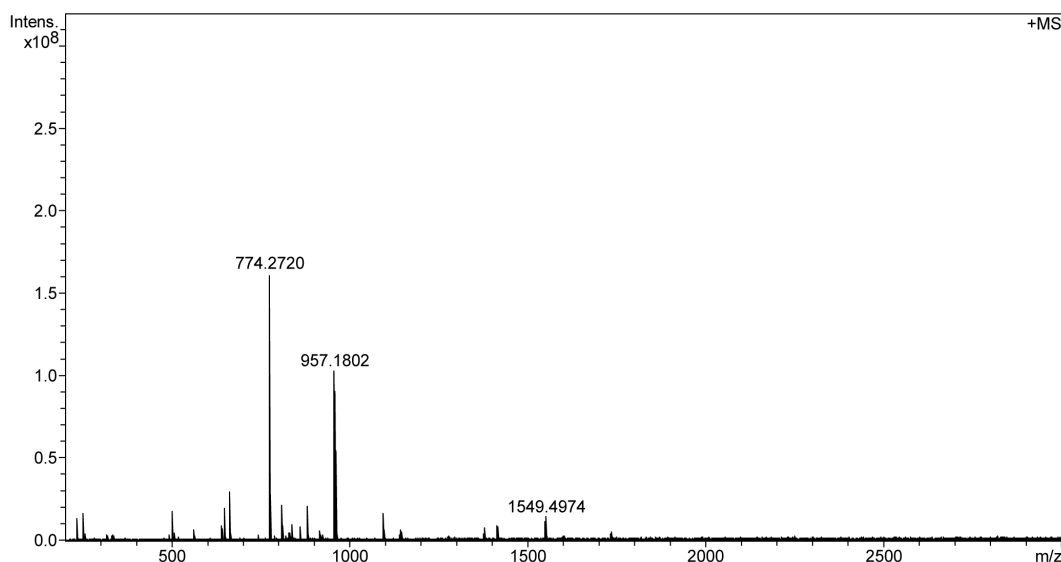


Figure 4.86: The high resolution MALDI MS of the reaction mixture towards the monomer **6**.

Since the precursor **44** and cyanuric chloride **43** have each three reactive groups, the reaction would not only afford the product **6**, but also other side products. The signal at  $m/z = 774.27$

<sup>XXIV</sup>THF was distilled to remove the stabilizer BHT, which otherwise showed up as a significant impurity.

<sup>XXV</sup>The fluorescence of **44** in THF was green, while in  $\text{CHCl}_3/\text{MeOH}/\text{TEA}$  (19 : 1 : 1) it was yellow.

## 4. Results and Discussion

corresponds to the specific isotope distribution of the monomer **6**. Another strong signal at  $m/z = 957.18$  corresponds to a precursor **44** that reacted with two cyanuric chlorides **43** and underwent an intramolecular reaction. The signal at  $m/z = 1549.49$  corresponds to a dimer of the monomer **6**. All identified and significant side products ( $m/z = 810, 957, \text{ and } 1549$ ) are illustrated in Figure 4.87.

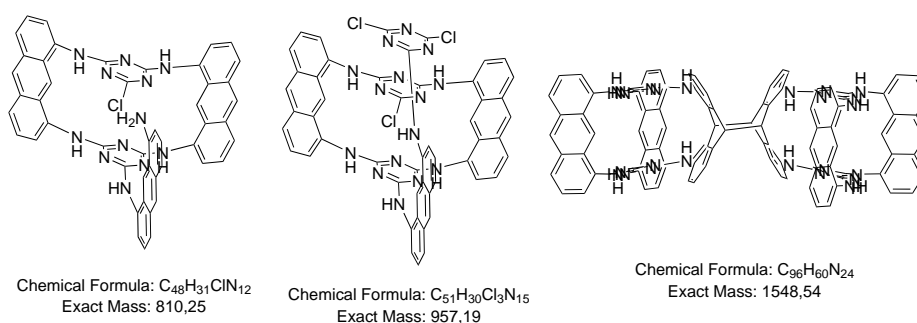


Figure 4.87: The side products of the reaction mixture towards **6** identified from the MS.

The reaction mixture was purified by silica gel column chromatography to yield the monomer **6** in 8 - 24 % at a scale of ca. 0.1 g. However, the monomer **6** was still contaminated by an unknown side product, which was seen in the proton spectrum by the broad signal that superimposed the aromatic signals of the monomer **6**. With the use of the preparative rGPC the monomer **6** could be further purified in a few mg scale. The low amounts of the monomer **6** were somewhat disappointing. Perhaps, the general low solubility of the monomer **6** in chloroform, which is the solvent used for the preparative rGPC, was one reason for the low amounts achieved. It is also possible that the statistical nature of the reaction in the alternate path can only yield low amounts. Other attempts to optimize the reaction conditions, such as a parallel and slow addition of both **44** and **43** to a base/THF mixture, or the reaction of **43** with **44** to be in a slight excess, yielded the same results (Fig. 4.86).

Another possible approach towards the monomer **6** would be following the same reaction procedure as shown in Figure 4.83 with the use of the 1,8-diaminodihydroanthracene **40** instead of the 1,8-diaminoanthracene **48** to yield a dihydroanthracene-type precursor. Perhaps, this dihydroanthracene-type precursor might give higher yields towards a tri-blade **42** molecule, due to increased flexibility by the dihydroanthracenes. This tri-blade **42** would then be oxidized towards the monomer **6**.

The small amounts of the monomer **6**, which were achieved by preparative rGPC, were on the one hand sufficient for simple characterizations, such as MS analysis and  $^1\text{H-NMR}$  spectroscopy,

## 4. Results and Discussion

but on the other not ideal for crystallization. The  $^1\text{H}$ - $^1\text{H}$ -COSY of the monomer **6** in  $\text{DMSO-}d_6$  illustrates the interconnection and shows the assigned proton signals (Fig.4.88).

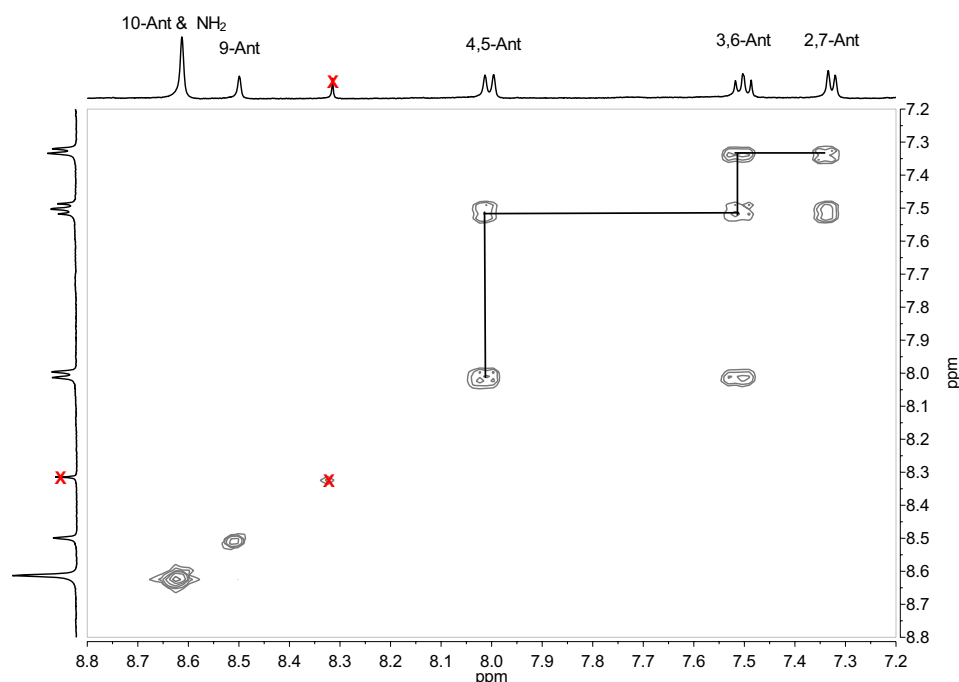


Figure 4.88: 500 MHz  $^1\text{H}$ - $^1\text{H}$ -COSY spectrum of monomer **6** in  $\text{DMSO-}d_6$ .

The next steps, which involve crystallization of the monomer **6**, polymerization of the resulting crystals into 2DP crystals, and exfoliation are still in progress. Since the amount of the monomer **6** was limited, and its solubility was acceptable, a test for the polymerization on the air/water interface seemed appropriate.

### Preliminary experiments of the monomer **6** on the air/water interface

The monomer **6** was spread to the air/water interface from a chloroform/methoxyethanol solution (20 : 1) (Fig. 4.89a). For an ideal polymerization the monomer **6** is compressed to a surface pressure, which allows the monomers to retain their lateral mobility. This allows for the rearrangement that is needed for the polymerization and to hinder possible contraction of the resulting polymer. The surface pressure of 29 mN/m (Fig. 4.89b) was determined as ideal by isotherm measurements. At constant pressure the monomer **6** was polymerized by UV irradiation ( $\lambda = 365$  nm) overnight (16 hours). The formed film was then transferred to a TEM mesh copper grid and analyzed with SEM (Fig. 4.90a). The SEM image shows films that are spanned on the TEM grids. Some parts of the film are ruptured and show folded edges.

A second "control" experiment was performed to test if the irradiation was in fact the cause for the film formation. Once again, the monomer **6** was spread to the air/water interface from a



#### 4. Results and Discussion

chloroform/methoxyethanol solution (20 : 1) and compressed to the pressure of 29 mN/m, but at constant pressure no irradiation was applied to the monomer **6** overnight. The sample was then transferred to a TEM grid and analyzed with SEM. As seen in the Figure 4.90b no film is observed on the TEM grids. It was therefore concluded that the monomer **6** polymerized by irradiation, which resulted in film formation.

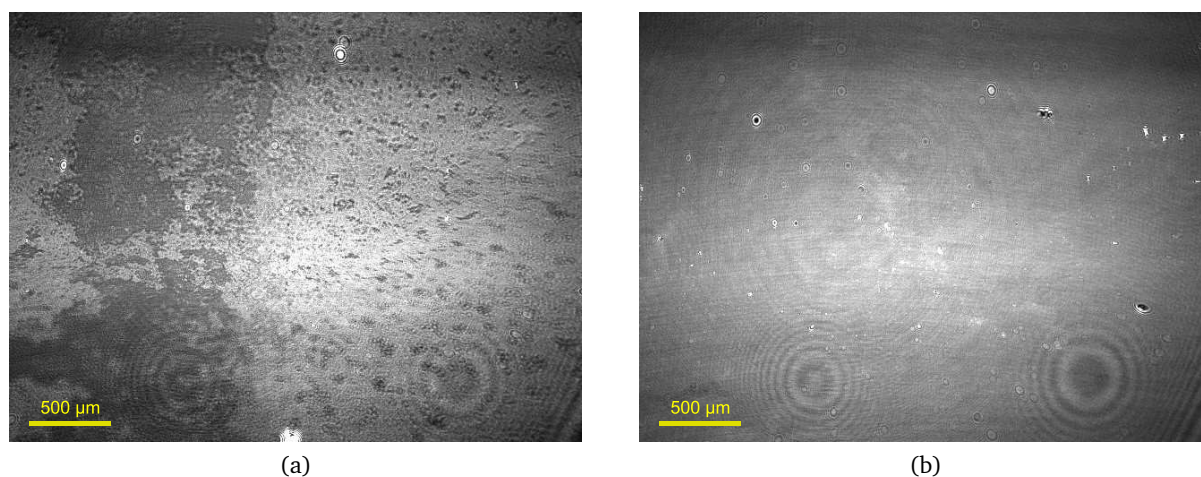


Figure 4.89: Brewster angle microscopy images of **6** on the air/water interface. a) At start and b) at constant pressure.

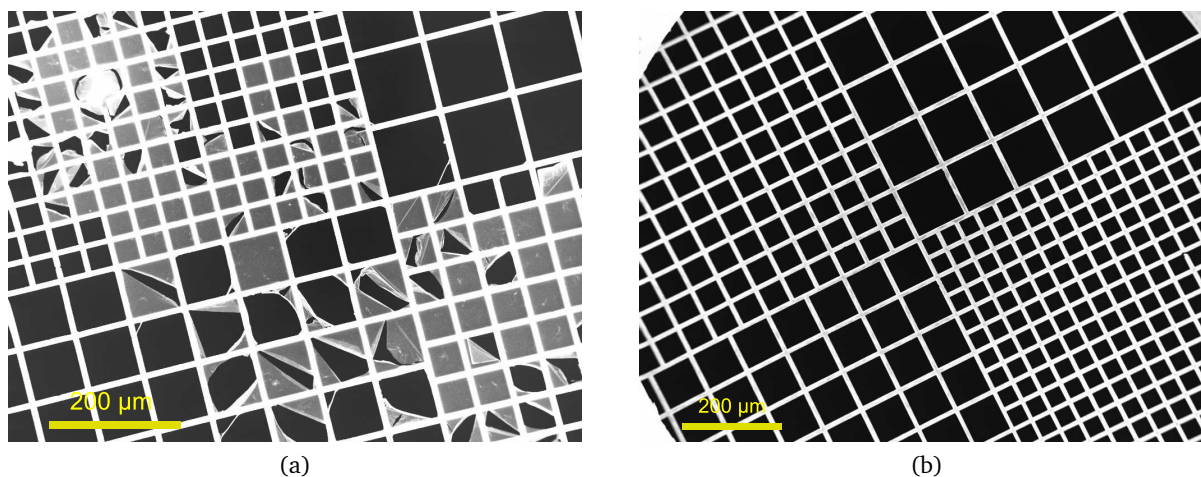


Figure 4.90: SEM images of **6** transferred from the air/water interface onto a TEM mesh copper grid. a) The irradiated sample and b) the non-irradiated sample.

After film formation, the polymerized film needed to be further inspected, by, for example, AFM, to determine the thickness of the film in order to prove the one monomer unit thick layer. Since the monomer **6** is not amphiphilic, it would as well be possible that it forms networks instead of a one monomer unit thick layer. The correct (monolayer) thickness would be an important feature towards claiming two-dimensional polymerization to have occurred.

### 5. Summary and Outlook

#### 5.1. Summary

In the first part of this thesis, a new approach towards poly[n]catenanes by solid-state photopolymerization was introduced. The first chapter includes the iterative organic synthesis of the anthracene-bearing terpyridine-based premonomer **7**, which, as shown in the second chapter, was successfully interlocked through metal complexation with zinc salts, such as  $\text{Zn}(\text{BF}_4)_2$ ,  $\text{Zn}(\text{NTf}_2)_2$ , and  $\text{Zn}(\text{OCl}_4)_2$ , furnishing a bis-complex **3**. In addition, the demetallation of the bis-complex **3** to the premonomer **7** was also achieved. The third chapter describes crystallizations and irradiations of bis-complexes with different counterions. Two of them, the bis-complexes **3** with  $\text{Zn}(\text{BF}_4)_2$  and  $\text{Zn}(\text{NTf}_2)_2$ , were crystallized from a chloroform/methanol mixture and characterized by XRD crystal structure determination as well as NMR spectroscopy and MS analysis. Eventually, the crystals of the bis-complex **3** with  $\text{Zn}(\text{NTf}_2)_2$  revealed a structure, in which the anthracenes of adjacent bis-complexes aligned in 1D arrays across the crystal, allowing the compound to be used as a monomer for the solid-state photopolymerization. Photoirradiation experiments of the monomer **3** in solid-state indicated anthracene dimerizations by the typical resulting anthracene bridge-head signals, which were seen by NMR spectroscopy. Masses that correspond with dimers of the monomer **3** were detected through MS analysis, which could only be explained by a photoreaction of the anthracene moieties. However, the crystals disintegrated upon irradiation and could not be used for XRD analysis after irradiation. Further demetallation of the irradiated crystals indicated once again anthracene dimerization, but a polymer was not traceable.

The second part of the present thesis describes the successful synthesis of the amine-bearing triazine-based compound **6** to be used as monomer for the solid-state photopolymerization towards 2DPs. The obtained amount of the monomer **6** was still low and its crystals have yet to be achieved. As a preliminary result, the photoirradiation of the monomer **6** was probed on the air/water interface and resulted in a film formation, which would indicate a photopolymerization. Further characterization of the film thickness and internal order is still in progress.

### 5.2. Outlook

Both topics presented in this thesis rely on the XRD crystal structure of their monomers to be used for solid-state photopolymerization. The synthesis of the monomers is one obstacle, but crucial is also the crystallization of the monomers itself. Therefore, the monomers need to be carefully designed and ideally synthesized in a large scale. A large quantity of monomers allow a considerable number of crystallization experiments and in long term provide a considerable amount of material for their polymer characterization, and properties determination.

#### Part A: Towards Poly[n]catenanes

In order to establish poly[n]catenanes, the evidence and characterization of a polymer is detrimental. The poly[n]catenane approach presented in this thesis, makes use of the solid-state photopolymerization of crystals of the monomer **3**. A successful irradiation of these crystals would lead to a photochemical conversion of monomers to poly[n]catenanes. These poly[n]catenanes would still be, in terms of their rotation and mobility, restricted due to remaining metal complexations. The final step, which would lead to poly[n]catenanes, is the removal of the metal cations. Afterwards, the poly[n]catenanes would be analyzed by standard polymer analytics, such as analytical GPC, MALDI, and light scattering, to prove it as a polymer. Therefore, this approach needs to aim at crystals which have the suitable XRD crystal structure and allow the crystals to retain its structural integrity upon irradiation. This would allow to prove the conversion from a monomer to a polymer through XRD analysis.

The crystals used in this thesis could, unfortunately, not be analyzed by XRD after irradiation due to partial disruption or shrinkage. There are three possible ways to continue using the same premonomer **7** for the complexations that result in a bis-complex used as a monomer: 1. the bis-complex **3** is recrystallized in a different solvent than the ones tested in this thesis; 2. other counterions, such as  $\text{PF}_6^-$ ,  $\text{Al}(\text{OC}(\text{CF}_3)_3)_4^-$ ,  $\text{B}(\text{C}_6\text{F}_5)_4^-$ , and others, which were not tested in the thesis, should be considered; 3. the use of other metal cations, such as  $\text{Fe}^{2+}$ ,  $\text{Co}^{2+}$ ,  $\text{Ni}^{2+}$ ,  $\text{Pb}^{2+}$ ,  $\text{Cd}^{2+}$ , and  $\text{Cu}^{2+}$ , which are removable, should be considered as well.

Alternatively, other terpyridine derivatives should be explored. The premonomer **7** used in this thesis was build up by three building blocks, which could in principle all be replaced by derivatives of the building blocks or replaced by other compounds that would lead to a variety of potential ligands for the bis-complexation (Fig. 5.1). Provided that these crystallize in a way suitable for a photopolymerization, the potential of this approach is still viable.

## 5. Summary and Outlook

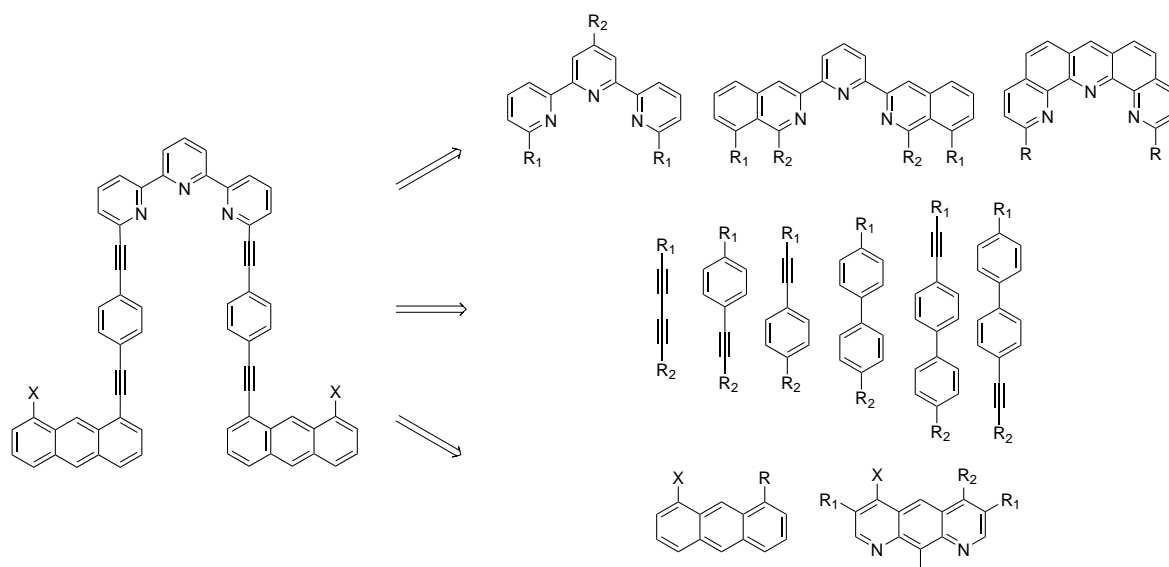


Figure 5.1: The premonomer and potential building blocks for the synthesis of premonomer derivatives.

### Part B: Towards Two-dimensional Polymers

The reaction conditions towards the monomer **6** via the precursor **44**, and its purification need to be optimized. Since the reaction is of statistical nature—due to the three reactive groups of the precursor **44** and the cyanuric chloride **43**—the conditions that need to be found should favor the intramolecular reaction. The purification of the monomer **6** would be easier if a solvent was used that dissolved the monomer **6** even more—such as DMF or THF—and if subsequently an open GPC or a preparative rGPC was used with the suitable solvent.

The idea to synthesize "hybrids" of the monomer **6** was created in the course of this thesis, since the hydrogen bonds of the di-blade **49** at the tri-blade **42** synthesis turned out to be problematic and hindered the continuation of Kory's synthetic path.<sup>[44]</sup> Instead of synthesizing an all amine-bearing monomer, a mixture of oxy- and amine-linked blades within the structure was envisioned and preliminary investigated by the di-blade-hybrid synthesis shown in Figure 5.2.

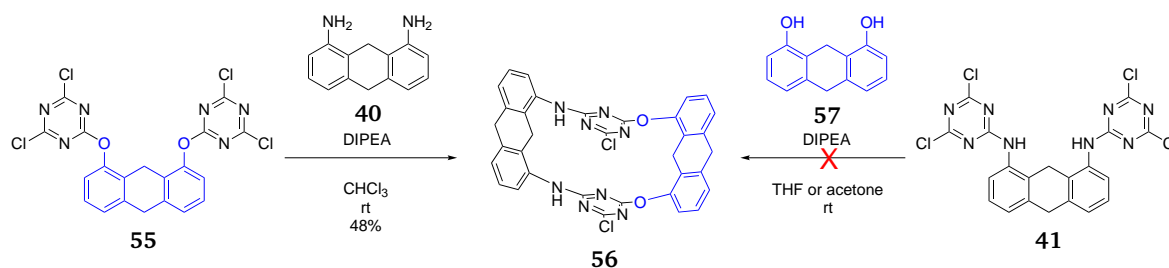


Figure 5.2: The synthetic sequence towards the hybrid **56**.

The di-blade-hybrid **56** was synthesized by using **55** following the procedure by Kory *et al.*<sup>[44]</sup>

## 5. Summary and Outlook

Using **41** as the starting material did not give the di-blade-hybrid **56** product, probably due to the disability of deprotonation of the **57** in a mixture with **41**. This observation needs to be considered for further reactions. This di-blade-hybrid **56** product was recrystallized from DMSO (Fig. 7.8 in 7.1.) and showed no hydrogen bonds, as it was seen in the di-blade **49** XRD crystal structure (Fig. 4.76). Therefore, further reactions towards monomer derivatives as seen in Figure 5.3 could be candidates for the 2D polymerization.

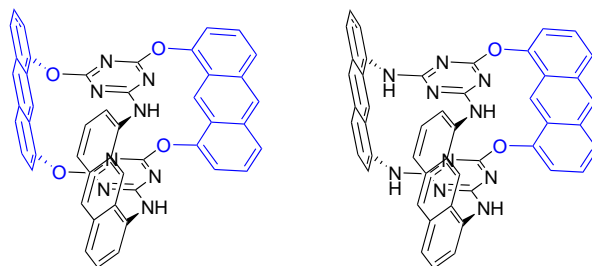


Figure 5.3: Potential tri-blade derivatives.

These monomer derivatives, however, would probably not give a  $C_{3h}$  symmetric conformation, such as seen earlier in Kory's oxygen-bearing monomer **4**,<sup>[44]</sup> due to the different angles from the oxy and amine linkers.

Another synthetic approach towards an amphiphilic hybrid of the monomer is shown in Figure 5.4.

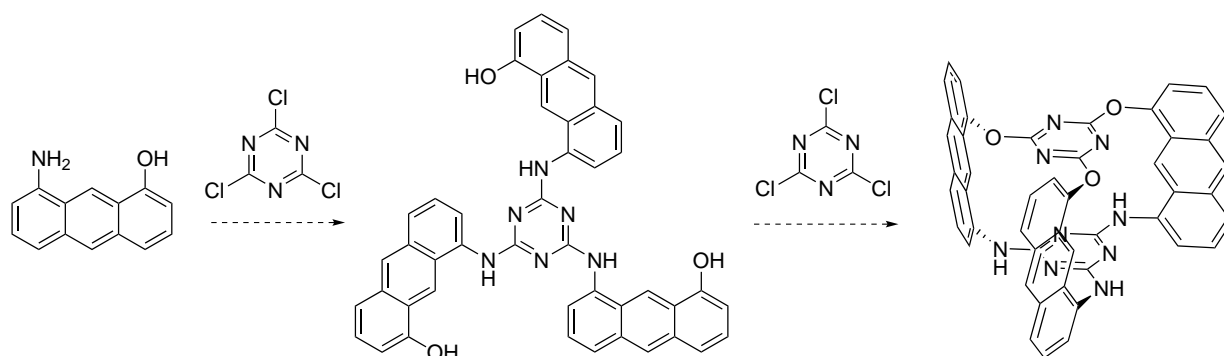


Figure 5.4: The synthetic sequence towards a monomer derivative.

This monomer and its resulting polymer would allow functionalization by chemical modification of the amine groups. The monomer would also serve as an amphiphilic monomer for the air/water interface approach.

## 6. Experimental

### 6.1. Materials and Methods

#### Chemicals and general remarks

All reactions were carried out as described in the experimental procedure. Solvents were only purified if specifically mentioned. Palladium catalyst was prepared following the literature procedure<sup>[280]</sup> and stored under N<sub>2</sub>. Palladium catalyzed reactions were performed under nitrogen or argon by using standard Schlenk techniques. All chemicals were purchased from ABCR, Acros, Aldrich, AlfaAesar, CIL, Fluka, Fluorochem, Merck, Strem, or TCI, and used without further purification. *n*-BuLi was used as a 1.6 M solution in *n*-hexane.

#### Nuclear magnetic resonance (NMR) spectroscopy

Solution NMR spectra were recorded with Bruker AVANCE 200 (<sup>1</sup>H: 200 MHz, <sup>13</sup>C: 50 MHz), Bruker AVANCE 300 (<sup>1</sup>H: 300 MHz, <sup>13</sup>C: 76 MHz), Bruker AVANCE 500 (<sup>1</sup>H: 500 MHz, <sup>13</sup>C: 126 MHz), and Bruker AVANCE 700 (<sup>1</sup>H: 700 MHz, <sup>13</sup>C: 176 MHz) at room temperature (or as mentioned) using CDCl<sub>3</sub>, DMF-*d*<sub>7</sub>, DMSO-*d*<sub>6</sub>, and methanol-*d*<sub>4</sub>. The solvent signal was used as internal standard (<sup>1</sup>H:  $\delta$  = 7.26 ppm, <sup>13</sup>C:  $\delta$  = 77.00 ppm for CDCl<sub>3</sub>; <sup>1</sup>H:  $\delta$  = 8.03 ppm, <sup>13</sup>C:  $\delta$  = 163.15 ppm for DMF-*d*<sub>7</sub>; <sup>1</sup>H:  $\delta$  = 2.50 ppm, <sup>13</sup>C:  $\delta$  = 38.52 ppm for DMSO-*d*<sub>6</sub>; <sup>1</sup>H:  $\delta$  = 4.78 ppm, <sup>13</sup>C:  $\delta$  = 49.15 ppm for methanol-*d*<sub>4</sub>). <sup>13</sup>C CP/MAS NMR spectra were recorded on Bruker AVANCE spectrometer operating at 176 MHz for <sup>13</sup>C. The sample rotation frequency was 20 or 25 kHz using a 2.5 mm rotor.

#### Mass spectrometry (MS)

High resolution mass spectrometry (HRMS) analyses were performed by the MS-service of the laboratory for organic chemistry at ETH Zurich with spectrometers (MALDI-ICR-FTMS: IonSpec Ultima Instrument, MALDI-TOF: Bruker Ultraflex II) and electrospray-ionization (ESI) MS spectrometer with a Quadrupole-Time-of-flight tandem mass analyzer (Q-TOF) (Bruker Daltonics maXis). Either 3-hydroxypicolinic acid (3-HPA) or trans-2-[3-(4-tert-butylphenyl)-2-methyl-2-propenylidene]malononitrile (DCTB) was used as matrix in the presence of silver triflate for the latter.

Note that the signals of the terpyridine complexes were [M]<sup>+</sup>, while doubly positively charged were expected for the zinc complexes. During the desorption process at MALDI, electrons emerge and the effected compound is partially neutralized, and survives the longest as singly positive charged.<sup>[36]</sup> Furthermore zinc terpyridine complexes are weak and often signals of

## 6. Experimental

---

free ligands are accompanied due to the destruction of the complex during the measuring process.<sup>[148]</sup>

### **Optical (OM) and polarized microscope (POM)**

OM and POM was carried out with a Leica DMRX polarizing microscope equipped with a Leica DFC 480 Camera (Leica Microsystems, Heerbrugg, Switzerland) or with a Leica DM4000M optical microscope (Leica Microsystems GmbH, Wetzlar, Germany).

### **Infrared spectroscopy (IR)**

Infrared spectroscopic analyses were carried out using an attenuated total reflection (ATR) - Fourier transform infrared (FTIR) spectrometer (Bruker Optics Alpha system with a built-in diamond ATR). OPUS 6 from Bruker was used as software. The data represent the average of 128 scans in the wavenumber range between 4000 – 375  $\text{cm}^{-1}$  at a resolution of 2  $\text{cm}^{-1}$ .

### **Preparative recycling gel permeation chromatography (rGPC)**

Preparative recycling GPC was performed with high pressure liquid chromatography apparatus (Japan Analytical Industry Co. Ltd.) using chloroform as eluent at room temperature. Small scale separations (below 300 mg) used a LC-9101 apparatus equipped with a pump (Hitachi L-7110, flow rate 3.5 mL/min or 4 mL/min), a degasser (GASTORR-702), an RI detector (Jai RI-7), a UV detector (Jai UV-3702), and two columns (Jaigel 2H and 2.5H, 20 × 600 mm for each). Large scale separations (below 1 g) used a LC-9204 apparatus equipped with a pump (Jai PI-60, flow rate 14 mL/min), a UV detector (Jai UV-310B), and two columns (Jaigel 2H and 2.5H, 40 × 600 mm for each).

### **Chromatography**

Column chromatography for purification was performed by using Fluka silica gel 60 (particle size 40 - 63  $\mu\text{m}$ ; 230 - 400 mesh) as solid phase and common organic solvents as mobile phase.

### **Microwave reactor**

The CEM Discover microwave ( $P_{max} = 300 \text{ W}$ ) single mode reactor was equipped with a 80 mL sealed vessel accessory including thermowell (fiber optic temperature control). The microwave reactor was connected to a Schlenk line in order to perform reactions under nitrogen atmosphere.

### **Light emitting diode (LED) reactor**

The LED reactors were built in-house by Dr. T. Schweizer (D-MATL).

## 6. Experimental

---

465 nm (blue): The photoreactor was equipped with 16 LEDs, (from Seoul Semiconductors) each at 22 lm.

525 nm (green): The photoreactor was equipped with 16 LEDs, (from Seoul Semiconductors) each at 70 lm.

### UV/Vis spectrometry

UV/Vis absorption spectroscopy was performed on a Lambda 20 spectrometer (PerkinElmer, USA). Solution spectra were recorded in a quartz cell (Hellma, d: 10 mm, spectral range: 200 - 2500 nm).

The solid-state UV/Vis absorption spectrum was recorded on a JASCO V-660 UV-VIS-NIR Spectrophotometer (Jasco Inc., Tokyo, Japan) equipped with a 150 mm integrating sphere (ILN-725, Jasco Inc., Tokyo, Japan) using a powder holder against a white barium sulphate standard.

### Fluorescence spectrometry

For solutions, fluorescence spectra were recorded using a Spex Fluorolog 2 spectrophotometer from Jobin Yvon (United Kingdom) using a quartz cell with a path length of 1 cm.

### Centrifuge

BHG Hermle Z320K was used for centrifuge separation at room temperature.

### Scanning electron microscopy (SEM)

Scanning electron microscopy was carried out on a FEG-SEM, Zeiss (LEO Gemini 1530 Germany) microscope with an in-lens detector using Quantifoil TEM grids, which were placed on a holder (PLANO, G3662). Images were recorded at low beam energy (1 - 3 kV) to avoid damaging of the thin films. For imaging, a chloroform/methoxyethanol (20 : 1) suspension of the sample was deposited onto a Quantifoil TEM grid (R2/2, Cu 400 mesh, Quantifoil Micro Tools GmbH, Grosslöbichau, Germany), which was placed with the carbon side up on a Kimwipe tissue, so that the solvent would pass through the grid and be absorbed by the tissue. The sample was dried over a few hours under ambient conditions.

### Langmuir experiments

Two Langmuir trough set ups were used. One was a KSV 2000 System 2 and the other system was a KSV Minitrough. Both systems are equipped with a platinum Wilhelmy plate and a dipper. Trough is made out of Teflon and the barriers are made of Delrin. Cleaning of the troughs was done by rinsing them with millipore water followed by cleaning with chloroform, ethanol,



## 6. Experimental

and again chloroform by the use of dust-free papers. The monomer was dissolved in a chloroform/methoxyethanol (20 : 1) mixture with the concentration of 0.25 mg/mL and spread at the air/water interface by using air/tight micro-syringe. The volume spread on the KSV 2000 system 2 was 300  $\mu$ L while the amount applied to the second trough was 100  $\mu$ L. Forty-five minutes time was given to both of the systems in order to let the solvent evaporate from the interface. The compression rate for the barriers was 3 mm/min and 2 mm/min for KSV 2000 and Minitrough, respectively.

Brewster's angle microscope (BAM) was a KSV MicroBAM which is operating a 659 nm laser.

### X-ray diffraction (XRD)

Crystallographic data was collected by the X-ray analysis service of the laboratory for inorganic chemistry, Small Molecule Crystallography Center (SMoCC), D-CHAB at ETH Zurich.

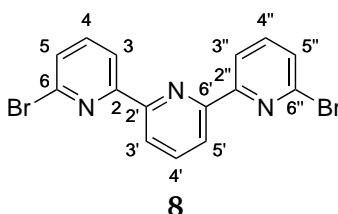
### Powder XRD

Wide-angle powder X-ray diffraction patterns were recorded with a STOE STADI P diffractometer and a position sensitive detector. A copper X-ray tube was used as a radiation source (wavelength  $\lambda = 1.54056 \text{ \AA}$ ) and Ge(111) as a monochromator. The substance was filled into a glass capillary (diameter 0.7 mm) and measured over a  $2\theta$ -range of  $3^\circ$  to  $90^\circ$  with a step size of  $0.02^\circ$  and an exposure time of 90 s per  $0.1^\circ$ .

## 6.2. Synthesis Part A

Parts of Part A have already been characterized and reported in the diploma thesis.<sup>[103]</sup>

### 6,6''-Dibromo-2,2':6',2''-terpyridine **8**



Method A<sup>[229]</sup>:

Compound **14** (14.8 g, 35.8 mmol),  $\text{NH}_4\text{OAc}$  (76.0 g, 986 mmol), and MeOH (750 mL) were heated to  $75^\circ\text{C}$  for 62 hours, then cooled to rt. Sat. aq.  $\text{Na}_2\text{CO}_3$  was added until pH reached 7 - 8, followed by the addition of water (750 mL). The reaction mixture was then extracted with

## 6. Experimental

$\text{CHCl}_3$ . The organic solvent was concentrated *in vacuo* and the residue was recrystallized from  $\text{CHCl}_3$  to give **8** (7.57 g, 53.7 %) as light brown crystals.

Method B<sup>[230,231]</sup>:

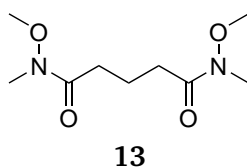
A suspension of 2,6-dibromopyridine **11** (50.1 g, 211 mmol) in  $\text{Et}_2\text{O}$  (420 mL) under  $\text{N}_2$  was cooled to  $-60\text{ }^\circ\text{C}$  (acetonitrile/dry ice bath) for 45 minutes. To this suspension  $n\text{-BuLi}$  (218 mmol) in  $n\text{-hexane}$  (136 mL) was added within one hour and stirred for another two hours at  $-45\text{ }^\circ\text{C}$ . A solution of  $\text{PCl}_3$  (4.65 mL, 53.3 mmol) in  $\text{Et}_2\text{O}$  (200 mL) was added dropwise to the reaction mixture within 2.5 hours. The reaction mixture was cooled to  $-78\text{ }^\circ\text{C}$  (acetone/dry ice bath) and stirred for 10 hours, followed by 24 hours of stirring between  $-40$  to  $-60\text{ }^\circ\text{C}$ , and slowly warming to rt for another 48 hours. The mixture was poured and stirred in water (400 mL) for one hour. The precipitate was filtered through a glass filter and dried under air. The residue was then stirred at  $85\text{ }^\circ\text{C}$  in toluene (1 L) for 30 minutes, filtered hot through a paper filter on top of a short silica gel column, and washed with cold toluene. The solvent was evaporated and the residue was recrystallized from toluene, followed by drying the white powder of **8** (5.38 g, 19.5 % based on **11**.) *in vacuo*.

$^1\text{H-NMR}$  (700 MHz,  $\text{CDCl}_3$ ):  $\delta$  [ppm] = 8.54 (d,  $^3J_{\text{H,H}} = 7.6\text{ Hz}$ , 2H, 3,3''-Py-H), 8.47 (d,  $^3J_{\text{H,H}} = 7.6\text{ Hz}$ , 2H, 3',5'-Py-H), 7.96 (t,  $^3J_{\text{H,H}} = 7.6\text{ Hz}$ , 1H, 4'-Py-H), 7.71 (t,  $^3J_{\text{H,H}} = 7.6\text{ Hz}$ , 2H, 4,4''-Py-H), 7.52 (d,  $^3J_{\text{H,H}} = 7.6\text{ Hz}$ , 2H, 5,5''-Py-H).

$^{13}\text{C-NMR}$  (176 MHz,  $\text{CDCl}_3$ ):  $\delta$  [ppm] = 157.20 (2,2''-Py), 153.84 (2',6'-Py), 141.64 (6,6''-Py), 139.13 (4,4''-Py), 138.11 (4'-Py), 128.12 (5,5''-Py), 121.98 (3',5'-Py), 119.73 (3,3''-Py).

**HRMS** (ESI/MALDI-FTICR, DCTB):  $m/z$  calcd for  $\text{C}_{15}\text{H}_{10}\text{Br}_2\text{N}_3$   $[\text{M}+\text{H}]^+$  389.9236, found 389.9236.

### ***N,N'*-Dimethoxy-*N,N'*-dimethyl Glutaramide **13****<sup>[281]</sup>



A suspension of *N,O*-dimethylhydroxylamine hydrochloride (100 g, 1.03 mol) in DCM (1.4 L) was stirred for 40 minutes at  $0\text{ }^\circ\text{C}$  (ice/water bath) under  $\text{N}_2$ . Within 1.5 hours TEA (290 mL, 2.08 mol) was added dropwise, followed by the dropwise addition of glutaryl chloride **12**

## 6. Experimental

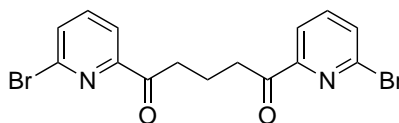
(53.0 mL, 415 mmol) within two hours. The temperature was slowly warmed to rt and the stirring was continued for three days. The mixture was then washed twice with water (300 mL), 1M HCl (300 mL), sat. aq. NaHCO<sub>3</sub> (300 mL), and brine (300 mL). The organic layers were collected, dried with Na<sub>2</sub>SO<sub>4</sub>, and mixed with charcoal followed by paper filtration. The solvent was evaporated and the purple liquid dried *in vacuo* to give **13** (79.6 g, 87.9 %).

<sup>1</sup>H-NMR (300 MHz, CDCl<sub>3</sub>): δ [ppm] = 3.64 (s, 6H, O-CH<sub>3</sub>), 3.13 (s, 6H, N-CH<sub>3</sub>), 2.47 (t, <sup>3</sup>J<sub>H,H</sub> = 7.1 Hz, 4H, -C(O)-CH<sub>2</sub>-), 1.93 (qu, <sup>3</sup>J<sub>H,H</sub> = 7.2 Hz, 2H, -CH<sub>2</sub>-).

<sup>13</sup>C-NMR (76 MHz, CDCl<sub>3</sub>): δ [ppm] = 173.97 (C=O), 61.06 (O-CH<sub>3</sub>), 32.05 (N-CH<sub>3</sub>), 30.92 (-C(O)-CH<sub>2</sub>-), 19.34 (-CH<sub>2</sub>-).

HRMS (ESI/MALDI-FTICR, 3-HPA): m/z calcd for C<sub>9</sub>H<sub>19</sub>N<sub>2</sub>O<sub>4</sub> [M+H]<sup>+</sup> 219.1339, found 219.1339.

### 1,5-Bis(6-bromopyridin-2-yl)pentane-1,5-dione **14**<sup>[282]</sup>



**14**

2,6-Dibromopyridine **11** (74.5 g, 314 mmol) was dissolved in Et<sub>2</sub>O (700 mL) and cooled to -78 °C (acetone/dry ice bath). Dropwise a 1.6 M solution of *n*-BuLi in *n*-hexane (100 mL, 160 mmol) was added within 1.5 hours, followed by stirring at the same temperature for another 0.5 hours. Then a solution of **13** (31.4 g, 144 mmol) in Et<sub>2</sub>O (60 mL) was added dropwise to the reaction mixture within 1.5 hours. The stirring was continued overnight for 20 hours, while it was allowed to slowly warm to rt. A 5 % aq. HCl (200 mL) solution was added and the mixture was extracted with Et<sub>2</sub>O (x4). The solvent was evaporated under reduced pressure and the compound was recrystallized three times from abs. EtOH. The mixture was kept in the fridge, then filtered through glass filter, and dried at air to afford **14** (29.8 g, 50.2 %) as light brown crystals.

<sup>1</sup>H-NMR (300 MHz, CDCl<sub>3</sub>): δ [ppm] = 7.99 (dd, <sup>3</sup>J<sub>H,H</sub> = 7.3 Hz, <sup>4</sup>J<sub>H,H</sub> = 1.5 Hz, 2H, 3-Py-H), 7.74–7.61 (m, 4H, 4,5-Py-H), 3.32 (t, <sup>3</sup>J<sub>H,H</sub> = 7.2 Hz, 4H, -C(O)-CH<sub>2</sub>-), 2.16 (qu, <sup>3</sup>J<sub>H,H</sub> = 7.2 Hz, 2H, -CH<sub>2</sub>-)

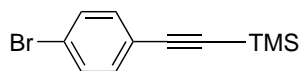
<sup>13</sup>C-NMR (76 MHz, CDCl<sub>3</sub>): δ [ppm] = 199.84 (C=O), 154.06 (2-Py), 141.29 (6-Py), 139.11

## 6. Experimental

(4-Py), 131.70 (5-Py), 120.50 (3-Py), 36.92 (-C(O)-CH<sub>2</sub>-), 17.71 (-CH<sub>2</sub>-).

**HRMS** (ESI/MALDI-FTICR, DCTB): *m/z* calcd for C<sub>15</sub>H<sub>13</sub>Br<sub>2</sub>N<sub>2</sub>O<sub>2</sub> [M+H]<sup>+</sup> 410.9338, found 410.9337.

### **((4-Bromophenyl)ethynyl)trimethylsilane 17**<sup>[283]</sup>

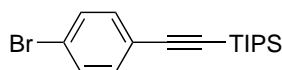


**17**

1-Bromo-4-iodobenzene **16** (10.0 g, 35.4 mmol), TEA (40 mL), and toluene (40 mL) were stirred at rt and TMS-acetylene (5.5 mL, 38.9 mmol) was added. The reaction mixture was degassed by three freeze-pump-thaw cycles, and Pd(PPh<sub>3</sub>)<sub>4</sub> (228 mg, 197 μmol) and CuI (75 mg, 390 μmol) were then added under N<sub>2</sub>, followed by another freeze-pump-thaw cycle. After 16.5 hours of stirring, the solvent was evaporated, and the residue was purified by silica gel column chromatography (hexane) to give **17** (7.43 g, 82.9 %) as a white solid.

<sup>1</sup>H-NMR (300 MHz, CDCl<sub>3</sub>): δ [ppm] = 7.46–7.39 (m, 2H, Ar-H), 7.35–7.29 (m, 2H, Ar-H), 0.24 (s, 9H, Si-(CH<sub>3</sub>)<sub>3</sub>).

### **((4-Bromophenyl)ethynyl)triisopropylsilane 18**<sup>[283]</sup>



**18**

1-Bromo-4-iodobenzene **16** (20.9 g, 70.7 mmol), TEA (80 mL), and toluene (80 mL) were stirred at rt and TIPS-acetylene (17.4 mL, 77.8 mmol) was added. The reaction mixture was degassed by three freeze-pump-thaw cycles, then Pd(PPh<sub>3</sub>)<sub>4</sub> (860 mg, 744 μmol) and CuI (260 mg, 1.38 mmol) were added under N<sub>2</sub>, followed by another freeze-pump-thaw cycle. After ca. 18 hours of stirring, the reaction mixture was passed through a short column, and washed with hexane. The solvent was evaporated and the residue was used without further purification for the next reaction step. According to <sup>1</sup>H-NMR analysis **18** contained 2 % of the disubstituted adduct.

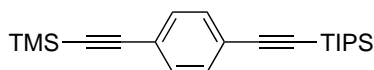
<sup>1</sup>H-NMR (300 MHz, CDCl<sub>3</sub>): δ [ppm] = 7.46–7.40 (m, 2H, 2,6-Ar-H), 7.36–7.30 (m, 2H, 3,5-Ar-H), 1.12 (s, 21H, Si-(CH(CH<sub>3</sub>)<sub>2</sub>)<sub>3</sub>).

## 6. Experimental

$^{13}\text{C-NMR}$  (76 MHz,  $\text{CDCl}_3$ ):  $\delta$  [ppm] = 133.42 (3,5-Ar), 131.39 (2,6-Ar) 122.44<sup>xxvi</sup> (1,4-Ar), 105.81 (C=C-TIPS), 92.04(C=C-TIPS), 18.60 (TIPS), 11.23 (TIPS).

**HRMS** (EI):  $m/z$  calcd for  $\text{C}_{17}\text{H}_{25}\text{BrSi}$   $[\text{M}]^+$  336.0904, found 336.0905.

### Triisopropyl((4-((trimethylsilyl)ethynyl)phenyl)ethynyl)silane **15**



**15**

Method A via **17**:

A 250 mL Schlenk flask was charged with **17** (14.6 g, 57.5 mmol), TIPS-acetylene (14.0 mL, 62.4 mmol), toluene (80 mL), and TEA (40 mL). The solution was degassed by three freeze-pump-thaw cycles. Between the first and second cycle,  $\text{Pd}(\text{PPh}_3)_4$  (330 mg, 286  $\mu\text{mol}$ ) and  $\text{CuI}$  (50.0 mg, 263  $\mu\text{mol}$ ) were added under  $\text{N}_2$ . The mixture was stirred at 80 °C in the dark for 10 days, then slowly cooled to rt. The reaction mixture was passed through a short celite pad, washed off with EtOAc, and the solvent was evaporated. The oilish residue was purified with silica gel column chromatography (hexane) to give **15** (20.0 g, 98.0 %) as a highly viscous slightly yellow oil.

Method B via **18**:

Compound **18** (26.2 g, 70.7 mmol) was dissolved in a toluene/TEA mixture (160 mL; 1 : 1) and TMS-acetylene (10.9 mL, 77.8 mmol) was added. After three freeze-pump-thaw cycles,  $\text{Pd}(\text{PPh}_3)_4$  (817 mg, 710  $\mu\text{mol}$ ) and  $\text{CuI}$  (269 mg, 1.41 mmol) were added, another freeze-pump-thaw cycle was performed before the mixture was heated to 80 °C for three days in the dark. The reaction mixture was cooled to rt, the solvent was evaporated, and the crude product was purified by silica gel column chromatography (hexane) to give **15** (13.9 g, 55 %) as a green oil.

$^1\text{H-NMR}$  (300 MHz,  $\text{CDCl}_3$ ):  $\delta$  [ppm] = 7.39 (s, 4H, Ar-H), 1.12 (s, 21H,  $\text{Si}-(\text{CH}(\text{CH}_3)_2)_3$ ), 0.25 (s, 9H,  $\text{Si}-(\text{CH}_3)_3$ ).

$^{13}\text{C-NMR}$  (76 MHz,  $\text{CDCl}_3$ ):  $\delta$  [ppm] = 131.80 (2,6-or-3,5-Ar), 131.71 (2,6-or-3,5-Ar), 123.56 (Ar), 122.97 (Ar), 106.58 (C=C), 104.64 (C=C), 96.12 (C=C-TMS), 92.77 (C=C-TIPS), 18.65

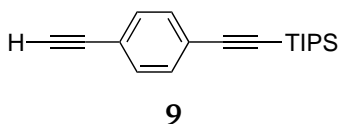
<sup>xxvi</sup>The reference by Türp *et al.* [284] showed 8 C signals, probably the signal at 122.44 ppm was superimposed. HMBC measurement indicates two signals in this range.

## 6. Experimental

(TIPS), 11.31 (TIPS), -0.09 (TMS).

**HRMS** (EI):  $m/z$  calcd for  $C_{22}H_{34}Si_2$   $[M]^+$  354.2194, found 354.2196.

### (2-(4-Ethynylphenyl)ethynyl)triisopropylsilane = Sp 9



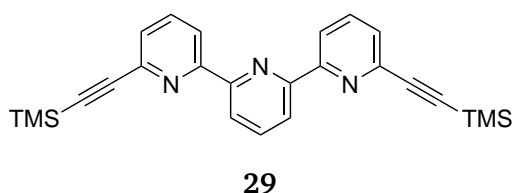
A solution of **15** (13.4 g, 37.8 mmol) in a DCM/MeOH mixture (220 mL; 1 : 1) was mixed with 2M NaOH (4 mL) and stirred at rt. The reaction was completed after 15 hours (determined by  $^1\text{H-NMR}$  analysis), then the reaction mixture was passed through a short celite pad with hexane. The organic solvent was evaporated, and the remaining compound was mixed with DCM, and washed with brine. After removal of the solvent, **9** (10.6 g, 99.2 %) was obtained as a yellowish oil.

$^1\text{H-NMR}$  (300 MHz,  $\text{CDCl}_3$ ):  $\delta$  [ppm] = 7.43 (s, 4H, Ar-H), 3.16 (s, 1H, Ethynyl-H), 1.22–1.06 (m, 21H,  $\text{Si}-(\text{CH}(\text{CH}_3)_2)_3$ ).

$^{13}\text{C-NMR}$  (76 MHz,  $\text{CDCl}_3$ ):  $\delta$  [ppm] = 131.88 (2,3,5,6-Ar), 123.98, 121.92, 106.39 ( $\text{C}=\text{C}$ ), 92.97 ( $\text{C}=\text{C}$ ), 83.26 ( $\text{C}=\text{C}$ ), 78.83 ( $\text{C}=\text{C-H}$ ), 18.64 (TIPS), 11.29 (TIPS).

**HRMS** (ESI/MALDI-FTICR, DCTB):  $m/z$  calcd for  $C_{19}H_{26}NaSi$   $[M+Na]^+$  305.1696, found 305.1696.

### TpyTMS **29**<sup>[243]</sup>



6,6''-Dibromo-2,2':6',2''-terpyridine **8** (500 mg, 1.28 mmol) was dissolved in TEA (40 mL) and THF (40 mL), and the mixture was degassed by three freeze-pump-thaw-cycles. Then  $\text{Pd}(\text{PPh}_3)_4$  (73.8 mg, 64.0  $\mu\text{mol}$ ), CuI (12.2 mg, 64.0  $\mu\text{mol}$ ), and TMS-acetylene (450  $\mu\text{L}$ , 3.20 mmol) were added, and another freeze-pump-thaw-cycle was performed. The reaction mixture was heated at 60 °C overnight. After TLC confirmed the consumption of the starting material and revealed a single spot, the reaction mixture was cooled to rt. The mixture was passed through a short

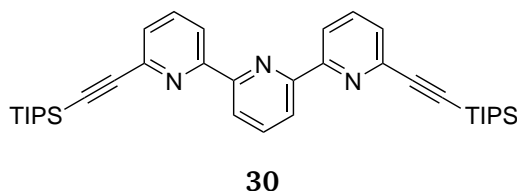
## 6. Experimental

column and washed with EtOAc and DCM. The solvent was evaporated and the light yellow solid was used without further purification for the next reaction step. The yield was not determined.

**<sup>1</sup>H-NMR** (300 MHz, CDCl<sub>3</sub>): δ [ppm] = 8.58–8.50 (m, 4H, 3,3',5',3''-Py-H), 7.94 (t, <sup>3</sup>J<sub>H,H</sub> = 7.9 Hz, 1H, 4'-Py-H), 7.80 (t, <sup>3</sup>J<sub>H,H</sub> = 7.9 Hz, 2H, 4,4''-Py-H), 7.52 (dd, t, <sup>3</sup>J<sub>H,H</sub> = 7.7 Hz, <sup>4</sup>J<sub>H,H</sub> = 0.9 Hz, 2H, 5,5''-Py-H), 0.31 (s, 18H, Si-(CH<sub>3</sub>)<sub>3</sub>).

**HRMS** (ESI/MALDI-FTICR, 3-HPA): m/z calcd for C<sub>25</sub>H<sub>28</sub>N<sub>3</sub>Si<sub>2</sub> [M+H]<sup>+</sup> 426.1816, found 426.1816.

### TpyTIPS 30<sup>[243]</sup>



6,6''-Dibromo-2,2':6',2''-terpyridine **8** (1.00 g, 2.56 mmol) was dissolved in TEA (80 mL) and THF (80 mL), and the mixture was degassed by three freeze-pump-thaw-cycles. Then Pd(PPh<sub>3</sub>)<sub>4</sub> (148 mg, 130 μmol), CuI (24.0 mg, 130 μmol), and TIPS-acetylene (900 μL, 4.01 mmol)<sup>xxvii</sup> were added, and another freeze-pump-thaw-cycle was performed. The reaction mixture was heated at 60 °C overnight. After TLC confirmed the consumption of the starting material and revealed a single spot, the reaction mixture was cooled to rt. The mixture was purified by silica gel column chromatography (DCM/hexane; 2 : 1). The solvent was evaporated and the remaining solid was recrystallized from iPrOH to give **30** (744 mg, 49.0 %) as a white solid.

**<sup>1</sup>H-NMR** (700 MHz, CDCl<sub>3</sub>): δ [ppm] = 8.57–8.52 (m, 4H, 3,3',5',3''-Py-H), 7.95 (t, <sup>3</sup>J<sub>H,H</sub> = 7.8 Hz, 1H, 4'-Py-H), 7.79 (t, <sup>3</sup>J<sub>H,H</sub> = 7.8 Hz, 2H, 4,4''-Py-H), 7.50 (dd, <sup>3</sup>J<sub>H,H</sub> = 7.6 Hz, <sup>4</sup>J<sub>H,H</sub> = 0.9 Hz, 2H, 5,5''-Py-H), 1.20–1.16 (m, 42H, Si-(CH(CH<sub>3</sub>)<sub>2</sub>)<sub>3</sub>).

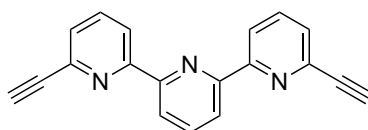
**<sup>13</sup>C-NMR** (176 MHz, CDCl<sub>3</sub>): δ [ppm] = 156.33, 154.59, 142.75, 137.86, 136.76, 127.82, 121.78, 120.36, 106.33 (C≡C), 91.25 (C≡C), 18.69(TIPS), 11.32 (TIPS).

**HRMS** (ESI/MALDI-FTICR, DCTB): m/z calcd for C<sub>37</sub>H<sub>52</sub>N<sub>3</sub>Si<sub>2</sub> [M+H]<sup>+</sup> 594.3694, found 594.3693.

<sup>xxvii</sup>The shortage of TIPS-acetylene was unintentional.

## 6. Experimental

### TpyD 31<sup>[244]</sup>



**31**

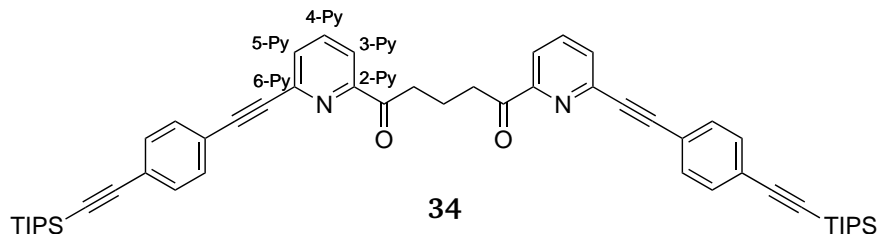
Compound **30** (740 mg, 1.81 mmol) was dissolved in a THF/MeOH mixture (55 mL; 10 : 1) and 1M TBAF solution in THF (3.75 mL, 3.75 mmol) was added. The solution was stirred at rt overnight. The mixture was then passed through a short silica gel column and the solvent was evaporated. The crude mixture was heated in EtOH and filtered through glass wool. The remaining filtrate was then mixed DCM and kept in the fridge at 5 °C. After a few hours, the mixture was concentrated and filtered through a glass filter to give **31** (187 mg, 53.2 %) as a grey solid.

<sup>1</sup>H-NMR (700 MHz, CDCl<sub>3</sub>): δ [ppm] = 8.65–8.48 (m, 4H, 3,3',5',3''-Py-H), 7.94 (t, <sup>3</sup>J<sub>H,H</sub> = 7.7 Hz, 1H, 4'-Py-H), 7.83 (t, <sup>3</sup>J<sub>H,H</sub> = 7.7 Hz, 2H, 4,4''-Py-H), 7.53 (d, <sup>3</sup>J<sub>H,H</sub> = 7.6 Hz, 2H, 5,5''-Py-H), 3.20 (s, 2H, Ethynyl-H).

<sup>13</sup>C-NMR (176 MHz, CDCl<sub>3</sub>): δ [ppm] = 156.52, 154.42, 141.64, 137.94, 137.03, 127.53, 121.80, 120.96, 83.03 (C=C), 76.86 (C=C).

HRMS (ESI/MALDI-FTICR, 3-HPA): m/z calcd for C<sub>19</sub>H<sub>12</sub>N<sub>3</sub> [M+H]<sup>+</sup> 282.1026, found 282.1026.

### DioneSp 34



A solution of **14** (500 mg, 1.21 mmol) and **9** (760 mg, 2.69 mmol) in a THF/TEA mixture (40 mL; 3 : 1) was degassed by three freeze-pump-thaw-cycles. Then Pd(PPh<sub>3</sub>)<sub>4</sub> (59.0 mg, 48.0 μmol) and CuI (10.0 mg, 48.0 μmol) were added, followed by another freeze-pump-thaw-cycle. The reaction mixture was heated at 65 °C for four days, then cooled to rt, and filtered



## 6. Experimental

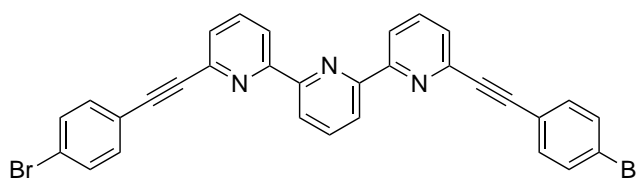
through a short silica gel column. The solvent was evaporated and the remaining solid was recrystallized in *i*PrOH to give **34** (560 mg, 56.8 %) a light brown crystals.

<sup>1</sup>H-NMR (700 MHz, CDCl<sub>3</sub>): δ [ppm] = 7.98 (d, <sup>3</sup>J<sub>H,H</sub> = 7.8 Hz, 2H, 3-Py-H), 7.81 (t, <sup>3</sup>J<sub>H,H</sub> = 7.8 Hz, 2H, 4-Py-H), 7.66 (d, <sup>3</sup>J<sub>H,H</sub> = 7.6 Hz, 2H, 5-Py-H), 7.55 (d, <sup>3</sup>J<sub>H,H</sub> = 8.0 Hz, 4H, Ar-H), 7.48 (d, <sup>3</sup>J<sub>H,H</sub> = 8.0 Hz, 4H, Ar-H), 3.42 (t, <sup>3</sup>J<sub>H,H</sub> = 7.2 Hz, 4H, -C(O)-CH<sub>2</sub>-), 2.20 (quint, <sup>3</sup>J<sub>H,H</sub> = 7.3 Hz, 2H, -CH<sub>2</sub>-), 1.14 (s, 42H, Si-(CH(CH<sub>3</sub>)<sub>2</sub>)<sub>3</sub>).

<sup>13</sup>C-NMR (176 MHz, CDCl<sub>3</sub>): δ [ppm] = 201.04 (C=O), 153.76, 142.61, 137.03 (4-Py), 132.00 (Ar), 131.89 (Ar), 130.48 (5-Py), 124.33, 121.78, 120.76 (3-Py), 106.41 (C≡C), 93.46 (C≡C-TIPS), 89.87 (C≡C-Py), 89.24 (C≡C), 37.07 (-C(O)-CH<sub>2</sub>-), 18.65 (TIPS), 17.84 (-CH<sub>2</sub>-), 11.29 (TIPS).

HRMS (ESI/MALDI-FTICR, DCTB): *m/z* calcd for C<sub>53</sub>H<sub>63</sub>N<sub>2</sub>O<sub>2</sub>Si<sub>2</sub> [M+H]<sup>+</sup> 815.4423, found 815.4417.

### TpyBrphenyl **32**



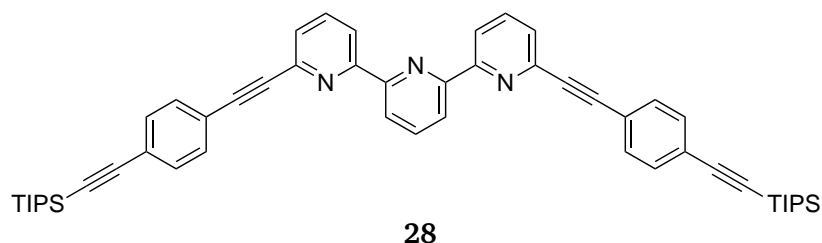
**32**

A 100 mL Schlenk flask was charged with **31** (187 mg, 665 μmol), 1-bromo-4-iodobenzene **16** (422 mg, 1.49 mmol), THF (30 mL), and TEA (15 mL). The solution was degassed by three freeze-pump-thaw cycles, then Pd(PPh<sub>3</sub>)<sub>4</sub> (47.0 mg, 40.7 μmol) was added under N<sub>2</sub> and another freeze-pump-thaw cycle was performed. The reaction mixture was stirred at rt in the dark for 15 hours, then heated to 40 °C for four days. Then the mixture was filtered through a glass filter and the solvent was evaporated *in vacuo*. The remaining brown solid was still impure and very insoluble. The yield was not determine.

HRMS (ESI/MALDI-FTICR, DCTB): *m/z* calcd for C<sub>31</sub>H<sub>18</sub>Br<sub>2</sub>N<sub>3</sub> [M+H]<sup>+</sup> 589.9862, found 589.9861.

## 6. Experimental

### TpySp-TIPS 28



6,6''-Dibromo-2,2':6',2''-terpyridine **8** (6.88 g, 17.6 mmol) and **9** (10.9 g, 38.7 mmol) were suspended in a mixture of THF/TEA (500 mL; 1 : 1). The suspension was degassed by three freeze-pump-thaw cycles. Between the first and second cycle, Pd(PPh<sub>3</sub>)<sub>4</sub> (880 mg, 762 μmol) and CuI (220 mg, 1.16 mmol) were added under N<sub>2</sub>. The reaction mixture was stirred at 65 °C for four days, then cooled to rt, and passed through a short celite pad. The solvent was removed under reduced pressure. The crude residue was purified by silica gel column chromatography (hexane/EtOAc/TEA; 30 : 1 : 1) and the eluent was evaporated to give **28** (11.8 g, 84.2 %) as a light brown solid.

<sup>1</sup>H-NMR (300 MHz, CDCl<sub>3</sub>): δ [ppm] = 8.65–8.49 (m, 4H, 3,3',5',3''-Py-H), 7.98 (t, <sup>3</sup>J<sub>H,H</sub> = 7.8 Hz, 1H, 4'-Py-H), 7.86 (t, <sup>3</sup>J<sub>H,H</sub> = 7.9 Hz, 2H, 4,4''-Py-H), 7.66–7.54 (m, 6H, Ar-H and 5,5''-Py-H), 7.53–7.45 (m, 4H, Ar-H), 1.14 (s, 42H, Si-(CH(CH<sub>3</sub>)<sub>2</sub>)<sub>3</sub>).

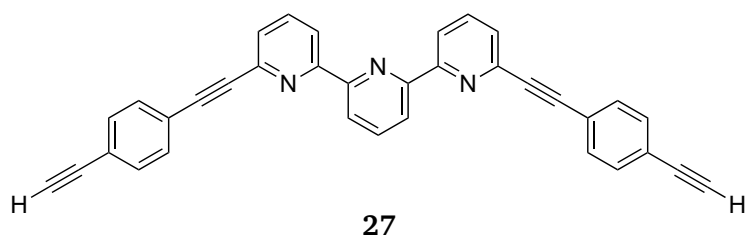
<sup>13</sup>C-NMR (176 MHz, CDCl<sub>3</sub>): δ [ppm] = 156.66 (2,2''-Py), 154.67 (2',6'-Py), 142.66 (6,6''-Py), 137.90 (4'-Py), 136.94 (4,4''-Py), 131.98 (Ar), 131.86 (Ar), 127.34 (5,5''-Py), 124.13, 122.21, 121.80 (3',5'-Py), 120.48 (3,3''-Py), 106.56 (C≡C), 93.29 (C=C-TIPS), 90.64 (C=C-Py), 88.56 (C≡C), 18.65 (TIPS), 11.33 (TIPS).

IR (ATR):  $\tilde{\nu}$  [cm<sup>-1</sup>] = 2941, 2889, 2863, 2216, 2151, 1560, 1506, 1498, 1461, 1429, 881, 835, 793. 786.

HRMS (ESI/MALDI-FTICR, DCTB): m/z calcd for C<sub>53</sub>H<sub>60</sub>N<sub>3</sub>Si<sub>2</sub> [M+H]<sup>+</sup> 794.4320, found 794.4317.

## 6. Experimental

### TpySpD 27



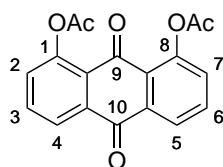
Compound **28** (8.17 g, 10.3 mmol) was dissolved in a THF/MeOH mixture (330 mL; 10 : 1), followed by the addition of a 1M TBAF solution in THF (22.5 mL, 22.5 mmol). The reaction mixture was diluted after two hours with a THF/MeOH mixture (110 mL; 10 : 1) and stirred for three days at rt. The formed precipitate was separated by centrifugation and washed with MeOH to give **27** (4.90 g, 98.9 %) as a pinkish solid.

$^1\text{H-NMR}$  (700 MHz,  $\text{DMF-}d_7$ ):  $\delta$  [ppm] = 8.78 (d,  $^3J_{\text{H,H}} = 7.9$  Hz, 2H, 3,3''-Py-H or 5,5''-Py-H), 8.57 (d,  $^3J_{\text{H,H}} = 7.6$  Hz, 2H, 3',5'-Py-H), 8.24 (t,  $^3J_{\text{H,H}} = 7.8$  Hz, 1H, 4'-Py-H), 8.17 (t,  $^3J_{\text{H,H}} = 7.7$  Hz, 2H, 4,4''-Py-H), 7.86 (dd,  $^3J_{\text{H,H}} = 7.6$  Hz,  $^4J_{\text{H,H}} = 0.7$  Hz, 2H, 3,3''-Py-H or 5,5''-Py-H), 7.77–7.74 (m, 4H, Ar-H), 7.67–7.65 (m, 4H, Ar-H) 4.40 (s, 2H, Ethynyl-H).

**IR** (ATR):  $\tilde{\nu}$  [ $\text{cm}^{-1}$ ] = 3412, 3271, 2960, 2875, 1562, 1497, 1432, 829, 793, 544.

**HRMS** (ESI):  $m/z$  calcd for  $\text{C}_{35}\text{H}_{20}\text{N}_3$  [ $\text{M}+\text{H}$ ] $^+$ : 482.1652, found 482.1649.

### 1,8-Diacetoxy-9,10-anthraquinone **21** [234,285]



**21**

1,8-Dihydroxy-9,10-anthraquinone **20** (69.5 g, 289 mmol) was mixed with DCM (1.3 L) and pyridine (140 mL), and stirred for 30 minutes, then cooled down to 0 °C (ice/water bath). Dropwise, acetyl chloride (62.0 mL, 877 mmol) was added within 50 minutes. The reaction mixture was diluted with DCM (100 mL) and slowly warmed to rt overnight and the solvent was evaporated *in vacuo*. The residue was heated in EtOH (1.3 L) at 80 °C for three hours. After raising the temperature to 95 °C and heating for another three hours, the reaction mixture was then filtered hot. The remaining solid was transferred to another flask and the three hour

## 6. Experimental

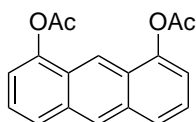
heating procedure was repeated with EtOH (500 mL). The solid was dried *in vacuo* to give **21** (80.8 g, 86.1 %) as a yellow powder.

<sup>1</sup>H-NMR (300 MHz, CDCl<sub>3</sub>): δ [ppm] = 8.23 (dd, <sup>3</sup>J<sub>H,H</sub> = 7.8 Hz, <sup>4</sup>J<sub>H,H</sub> = 0.8 Hz, 2H, 4,5-Ar-H), 7.77 (t, <sup>3</sup>J<sub>H,H</sub> = 7.8 Hz, 2H, 3,6-Ar-H), 7.41 (dd, <sup>3</sup>J<sub>H,H</sub> = 8.1 Hz, <sup>4</sup>J<sub>H,H</sub> = 0.8 Hz, 2H, 2,7-Ar-H), 2.45 (s, 6H, -CH<sub>3</sub>).

<sup>13</sup>C-NMR (76 MHz, CDCl<sub>3</sub>): δ [ppm] = 181.90(C=O), 180.79 (C=O), 169.36 (O=C-CH<sub>3</sub>), 150.02 (C-O-C=O), 134.61 (3,6-Ar), 134.41, 130.21 (2,7-Ar), 125.59, 125.42 (4,5-Ar), 21.05 (-CH<sub>3</sub>).

HRMS (ESI/MALDI-FTICR, DCTB): m/z calcd for C<sub>18</sub>H<sub>12</sub>NaO<sub>6</sub> [M+Na]<sup>+</sup> 347.0526, found 347.0526.

### 1,8-Diacetoxyanthracene **22**<sup>[234]</sup>



**22**

A 2 L two-neck flask was charged with **21** (28.6 g, 88.2 mmol), AcOH (1 L), and flushed with N<sub>2</sub>. The reaction mixture was heated to reflux under N<sub>2</sub>. After 75 minutes zinc (17.3 g, 265 mmol) was added in portions within three hours. After 15 hours at reflux, another two portions of zinc (5.94 g, 91 mmol) were added within 30 minutes. The reaction mixture was stirred for another six hours at reflux. Between the zinc additions, the reaction was monitored with TLC (DCM/MeOH; 40 : 1). The reaction mixture was cooled to rt and passed through a short silica gel column with EtOAc. The solvent was evaporated to complete dryness. The remaining solid was mixed with pyridine (470 mL) and cooled to 0 °C (ice/water bath) under N<sub>2</sub>. Acetyl chloride (13.5 mL, 190 mmol) was added within five minutes and the mixture was allowed to heat to rt overnight in the dark. The solvent was evaporated and the crude solid dried *in vacuo* in the dark. The product was purified by silica gel column chromatography (DCM) to yield a brown/yellow solid of **22** as a mixture with 1,8-Diacetoxydihydroanthracene **24** (13.1 g, molar ratio 1 : 0.08 determined by <sup>1</sup>H-NMR). The yield of **22** was calculated as 46.9 %.

<sup>1</sup>H-NMR (300 MHz, CDCl<sub>3</sub>): δ [ppm] = 8.51 (s, 1H, 10-Ant-H), 8.46 (s, 1H, 9-Ant-H), 7.91 (d, <sup>3</sup>J<sub>H,H</sub> = 8.5 Hz, 2H, 4,5-Ant-H), 7.51–7.43 (m, 2H, 3,6-Ant-H), 7.30 (d, <sup>3</sup>J<sub>H,H</sub> = 7.2 Hz, 2H,

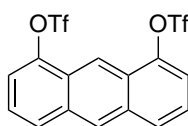
## 6. Experimental

2,7-Ant-H), 2.53 (s, 6H, -CH<sub>3</sub>).

<sup>13</sup>C-NMR (76 MHz, CDCl<sub>3</sub>): δ [ppm] = 169.10 (O=C-CH<sub>3</sub>), 146.59 (1,8-Ant), 132.73, 127.00 (9-Ant), 126.18 (4,5-Ant), 125.58, 125.05 (3,6-Ant), 117.38 (2,7-Ant), 113.71 (10-Ant), 20.96 (-CH<sub>3</sub>).

HRMS (ESI/MALDI-FTICR, DCTB): m/z calcd for C<sub>18</sub>H<sub>14</sub>O<sub>4</sub> [M]<sup>+</sup> 294.0887, found 294.0887.

### 1,8-Di(trifluoromethanesulfonyl)oxyanthracene **19**<sup>[234]</sup>



**19**

A 1 L Schlenk flask was charged with a solution of the mixture of **22** and **24** (13.1 g, 44.6 mmol, molar ratio 1 : 0.08) in DCM (200 mL) and MeOH (100 mL). The mixture was degassed by three freeze-pump-thaw cycles and cooled to 0 °C (ice/water bath) under N<sub>2</sub>. With a syringe, MeNH<sub>2</sub><sup>XXVIII</sup> (27.0 mL, 265 mmol) was added within 30 minutes in the dark. The reaction mixture was allowed to stir at the same temperature and slowly warmed to rt. The solvent was evaporated and the residue dried *in vacuo* in the dark overnight. Dry DCM (300 mL) and TEA (50 mL, 359 mmol) was added to the residue and the reaction mixture was cooled with an ice/water bath. Then Tf<sub>2</sub>O (22.5 mL, 134 mmol), diluted in dry DCM (90 mL), was added dropwise within 100 minutes. After addition, the reaction mixture was stirred and slowly warmed over time to rt for two days. The solvent was evaporated and the crude compound was purified with silica gel column chromatography (hexane/DCM; 10 : 3) to give light green crystals of **19** as a mixture with 1,8-ditriflatedihydroanthracene **25** (9.48 g, molar ratio 1 : 0.05 determined by <sup>1</sup>H-NMR). The yield of **19** was calculated as 42.6 %.

<sup>1</sup>H-NMR (300 MHz, CDCl<sub>3</sub>): δ [ppm] = 8.90 (s, 1H, 9-Ant-H), 8.62 (s, 1H, 10-Ant-H), 8.11–8.05 (m, 2H, 4,5-Ant-H), 7.62–7.52 (m, 4H, 2,3,6,7-Ant-H).

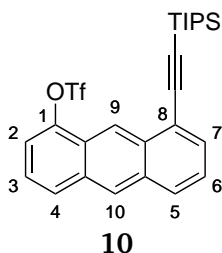
<sup>13</sup>C-NMR (76 MHz, CDCl<sub>3</sub>): δ [ppm] = 145.49 (1,8-Ant), 132.92, 128.70 (4,5-Ant), 127.70 (10-Ant), 125.36, 125.21 (3,6-Ant), 118.80 (q, <sup>1</sup>J<sub>C,F</sub> = 320.6 Hz, CF<sub>3</sub>), 118.25 (2,7-Ant), 113.93 (9-Ant).

HRMS (ESI/MALDI-FTICR, DCTB): m/z calcd for C<sub>16</sub>H<sub>8</sub>F<sub>6</sub>O<sub>6</sub>S<sub>2</sub> [M]<sup>+</sup> 473.9661, found 473.9660.

<sup>XXVIII</sup>Containing 40 %wt MeOH.

## 6. Experimental

### 1-(Trifluoromethanesulfonyl)oxy-8-(triisopropylsilyl)ethynylantracene **10**



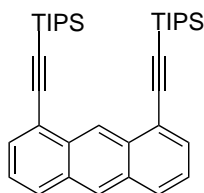
To a solution of the mixture of **19** and **25** (9.40 g, 19.8 mmol, molar ratio 1 : 0.05) in a toluene/TEA mixture (140 mL; 1 : 1), TIPS-acetylene (4.45 mL, 19.9 mmol) was added. The reaction mixture was degassed by three freeze-pump-thaw cycles. In between the first and second cycle, Pd(PPh<sub>3</sub>)<sub>4</sub> (560 mg, 485 μmol) and CuI (50.0 mg, 263 μmol) were added under N<sub>2</sub>. The reaction mixture was heated at 65 °C for two days, then cooled to rt, passed through a short celite pad, and washed with EtOAc. The solvent was evaporated and purified with silica gel column chromatography (hexane/DCM; 10 : 2) to give **10** (7.06 g, 70.3 %) as a yellow solid.

<sup>1</sup>H-NMR (700 MHz, CDCl<sub>3</sub>): δ [ppm] = 9.23 (s, 1H, 9-Ant-H), 8.48 (s, 1H, 10-Ant-H), 8.02–7.97 (m, 2H, 4,5-Ant-H), 7.83 (d, <sup>3</sup>J<sub>H,H</sub> = 6.9 Hz, 1H, 7-Ant-H), 7.53 (d, <sup>3</sup>J<sub>H,H</sub> = 7.4 Hz, 1H, 2-Ant-H), 7.50–7.44 (m, 2H, 3,6-Ant-H), 1.26–1.22 (m, 21H, Si-(CH(CH<sub>3</sub>)<sub>2</sub>)<sub>3</sub>).

<sup>13</sup>C-NMR (176 MHz, CDCl<sub>3</sub>): δ [ppm] = 146.30 (C-OTf), 132.59, 132.31, 131.82, 128.80, 128.61, 127.52, 125.90, 124.95, 124.22, 122.05, 119.76, 119.09, 117.93, 116.84, 104.23 (C≡C), 97.63 (C≡C), 18.74 (TIPS), 11.36 (TIPS).

HRMS (ESI/MALDI-FTICR, DCTB): m/z calcd for C<sub>26</sub>H<sub>29</sub>F<sub>3</sub>O<sub>3</sub>SSi [M]<sup>+</sup> 506.1553, found 506.1557.

### 1,8-Bis((triisopropylsilyl)ethynyl)anthracene **26**



Compound **26** was isolated as a side product from the reaction of **10**.

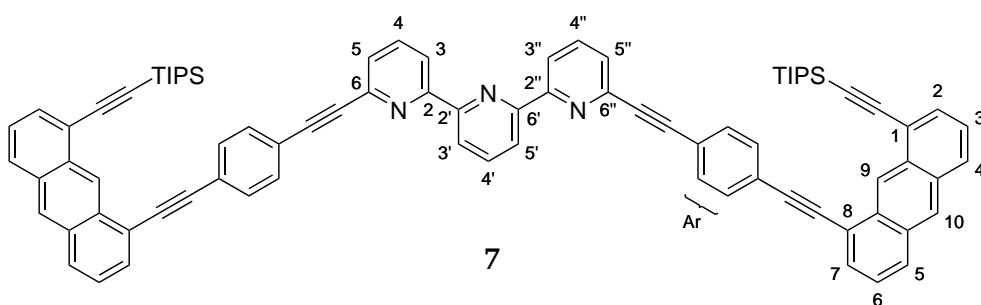
## 6. Experimental

$^1\text{H-NMR}$  (300 MHz,  $\text{CDCl}_3$ ):  $\delta$  [ppm] = 9.29 (s, 1H, 9-Ant-H), 8.41 (s, 1H, 10-Ant-H), 7.97 (d,  $^3J_{H,H} = 8.6$  Hz, 2H, 4,5-Ant-H), 7.83 (dd,  $^3J_{H,H} = 6.9$  Hz,  $^4J_{H,H} = 0.9$  Hz, 2H, 2,7-Ant-H), 7.48–7.36 (m, 4H, 3,6-Ant-H), 1.33–1.13 (m, 42H,  $\text{Si}-(\text{CH}(\text{CH}_3)_2)_3$ ).

$^{13}\text{C-NMR}$  (76 MHz,  $\text{CDCl}_3$ ):  $\delta$  [ppm] = 133.36 (2,7-Ant), 131.42, 131.09, 129.06 (4,5-Ant), 127.77 (10-Ant), 124.91 (3,6-Ant), 123.72 (9-Ant), 121.81 (1,8-Ant), 105.94 ( $-\text{C}\equiv\text{C-TIPS}$ ), 96.77 ( $-\text{C}\equiv\text{C-TIPS}$ ), 18.89 (TIPS), 11.69 (TIPS).

HRMS (ESI/MALDI-FTICR, DCTB):  $m/z$  calcd for  $\text{C}_{36}\text{H}_{50}\text{Si}_2$   $[\text{M}]^+$  538.3446, found 538.3445.

### TpySpA-TIPS = PM 7



Compound **27** (1.03 g, 2.14 mmol) and **10** (2.29 g, 4.52 mmol) were suspended in a THF/TEA mixture (400 mL; 3: 1). The suspension was degassed by three freeze-pump-thaw cycles. Between the first and second cycle,  $\text{Pd}(\text{PPh}_3)_4$  (275 mg, 238  $\mu\text{mol}$ ) and  $\text{CuI}$  (5.00 mg, 26.0  $\mu\text{mol}$ ) were added under  $\text{N}_2$ . The reaction mixture was heated at 70  $^\circ\text{C}$  for three days in the dark and then cooled to rt. The reaction mixture was passed through a paper filter and a short celite pad with EtOAc. The solvent was evaporated and the residue was subjected to silica gel column chromatography (hexane/EtOAc/TEA; 8 : 2 : 1) to afford **7** (1.47 g, 57.5 %) as a yellow solid.

$^1\text{H-NMR}$  (700 MHz,  $\text{CDCl}_3$ ):  $\delta$  [ppm] = 9.44 (s, 2H, 9-Ant-H), 8.63–8.59 (m, 4H, 3,3',5',3''-Py-H), 8.47 (s, 2H, 10-Ant-H), 8.05–7.99 (m, 5H, 4,5-Ant-H & 4'-Py-H), 7.90 (t,  $^3J_{H,H} = 7.7$  Hz, 2H, 4,4''-Py-H), 7.84 (dd,  $^3J_{H,H} = 6.8$  Hz,  $^4J_{H,H} = 0.9$  Hz, 2H, 2-Ant-H), 7.80 (dd,  $^3J_{H,H} = 6.8$  Hz,  $^4J_{H,H} = 0.9$  Hz, 2H, 7-Ant-H), 7.70–7.66 (m, 8H, Ar-H), 7.63 (dd,  $^3J_{H,H} = 7.6$  Hz,  $^4J_{H,H} = 1.0$  Hz, 2H, 5,5''-Py-H), 7.50–7.47 (m, 2H, 3-Ant-H), 7.46–7.42 (m, 2H, 6-Ant-H), 1.10 (s, 42H,  $\text{Si}-(\text{CH}(\text{CH}_3)_2)_3$ ).

$^1\text{H-NMR}$  (500 MHz,  $\text{DMF-d}_7$ ):  $\delta$  [ppm] = 9.44 (s, 2H, 9-Ant-H), 8.86 (s, 2H, 10-Ant-H), 8.81 (dd,  $^3J_{H,H} = 8.0$  Hz,  $^4J_{H,H} = 0.9$  Hz, 2H, 3,3''-Py-H), 8.60 (d,  $^3J_{H,H} = 7.8$  Hz, 2H, 3',5'-Py-H), 8.34–8.24 (m, 5H, 4,5-Ant-H & 4'-Py), 8.20 (t, 2H,  $^3J_{H,H} = 7.8$  Hz, 4,4''-Py-H), 8.04<sup>XXIX</sup>, 7.94

<sup>XXIX</sup>The signal of 2-or-7-Ant-H overlays with the DMF reference signal

## 6. Experimental

(dd,  $^3J_{H,H} = 6.9$  Hz,  $^4J_{H,H} = 0.8$  Hz, 2H, 2-or-7-Ant-H) 7.91–7.85 (m, 10H, Ar-H & 5,5''-Py-H), 7.71–7.61 (m, 4H, 3,6-Ant-H), 1.12 (s, 42H, Si-(CH(CH<sub>3</sub>)<sub>2</sub>)<sub>3</sub>).

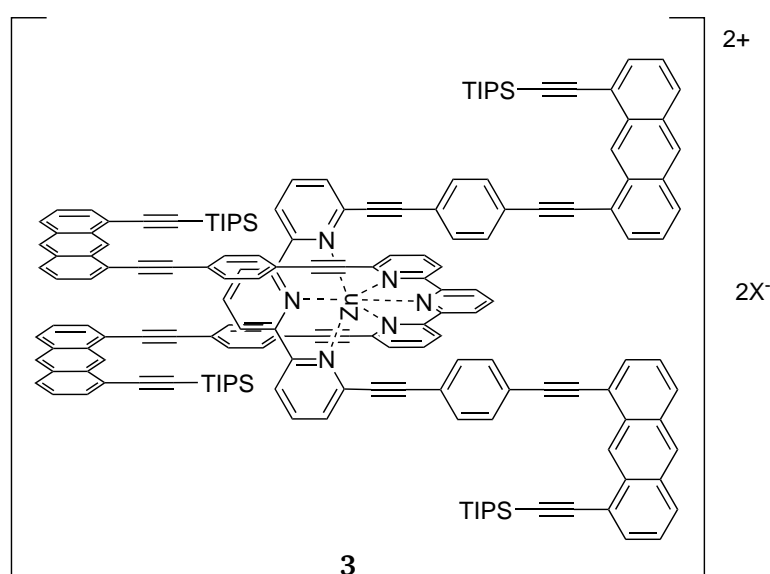
$^{13}\text{C-NMR}$  (176 MHz, CDCl<sub>3</sub>):  $\delta$  [ppm] = 156.73 (Py), 154.72 (Py), 142.74 (Py), 137.99 (4'-Py), 137.02 (4,4''-Py), 132.02 (7-Ant), 131.94 (Ar), 131.87 (Ar), 131.61, 131.55 (2-Ant), 131.51, 131.49, 131.26, 129.31 (4-or-5-Ant), 128.98 (4-or-5-Ant), 127.68 (10-Ant), 127.48 (5,5''-Py), 125.09 (6-Ant), 125.04 (3-Ant), 124.20, 123.97 (9-Ant), 122.32 (3',5'-Py), 121.86 (Py), 121.79 (Py), 121.26, 120.55 (3,3''-Py), 105.15 (C≡C), 96.73 (C≡C), 93.85 (C≡C), 90.64 (C≡C), 89.74 (C≡C), 88.69 (C≡C), 18.74 (TIPS), 11.39 (TIPS).

$^{13}\text{C-NMR}$  (126 MHz, DMF-*d*<sub>7</sub>):  $\delta$  [ppm] = 157.24 (2,2''-Py), 155.80 (2',5'-Py), 143.37, 139.81, 139.22, 133.56, 133.41, 133.34, 133.26, 133.17, 132.69, 132.64, 132.30, 132.10, 131.02, 130.86, 129.73 (10-Ant), 129.17 (5,5''-Py), 126.70 (3-or-6-Ant), 126.66 (3-or-6-Ant), 124.97, 123.76 (9-Ant), 123.42, 122.46 (3',5'-Py), 121.91, 121.85 (3,3''-Py), 121.44, 106.30 (C≡C-), 97.48 (TIPS-C≡C), 94.90 (C≡C), 91.95 (C≡C), 90.40 (C≡C), 89.15 (Py-C≡C), 19.39 (TIPS), 12.21 (TIPS).

**IR** (ATR):  $\tilde{\nu}$  [cm<sup>-1</sup>] = 2940, 2888, 2861, 2209, 2143, 1560, 1508, 1461, 1429, 1076, 987, 882, 873, 835, 794, 741, 636.

**HRMS** (ESI/MALDI-FTICR, DCTB): *m/z* calcd for C<sub>85</sub>H<sub>75</sub>N<sub>3</sub>Si<sub>2</sub> [M]<sup>+</sup> 1193.5494, found 1193.5497.

### [Zn(TpySpA-TIPS)<sub>2</sub>](X<sub>2</sub>)<sub>2</sub> **3**



A general procedure of the complexation reaction (here X = (NTf<sub>2</sub>)<sup>-</sup>):



## 6. Experimental

To a solution of **7** (120 mg, 100  $\mu\text{mol}$ ) in a  $\text{CHCl}_3/\text{MeOH}$  mixture (10.5 mL; 2 : 1),  $\text{Zn}(\text{NTf}_2)_2$  (1.90 mL, 170  $\mu\text{mol}$ ) from a stock solution (26.5 mmol/L) of  $\text{Zn}(\text{NTf}_2)_2$  in  $\text{CHCl}_3/\text{MeOH}$  (3.3 mL; 2 : 1) was added quickly in two shots (each 0.95 mL). After six days, seed crystals of a different batch were added and crystals formed within one day. These crystals were filtered with paper in the fridge and washed with hexane to give **3** (79.5 mg, 52.5 %)<sup>xxx</sup> as yellow crystals.

<sup>1</sup>H-NMR (700 MHz,  $\text{CDCl}_3$ ):  $\delta$  [ppm] = 9.34 (s, 4H, 9-Ant-H), 8.56 (d, 4H, 3,3''-Py-H), 8.45 (s, 4H, 10-Ant-H), 8.28 (t, 4H, 4,4''-Py-H), 8.12 (d, 4H, 3',5'-Py-H), 8.02 (d, 4H, 5-Ant-H), 7.99 (d, 4H, 4-Ant-H), 7.92 (d, 4H, 7-Ant-H), 7.77 (d, 4H, 2-Ant-H), 7.69 (d, 4H, 5,5''-Py-H), 7.64 (d, 8H, Ar-H), 7.55 (t, 2H, 4'-Py-H), 7.48–7.40 (m, 8H, 3,6-Ant-H), 7.00 (d, 8H, Ar-H), 1.02 (s, 84H, Si–(CH(CH<sub>3</sub>)<sub>2</sub>)<sub>3</sub>).

<sup>13</sup>C-NMR (126 MHz,  $\text{CDCl}_3$ ):  $\delta$  [ppm] = 150.05, 149.23, 143.39 (4'-Py), 142.97, 141.56 (4,4''-Py), 133.30 (5,5''-Py), 132.19 (2-or-7-Ant-or-Ar), 132.12 (2-or-7-Ant-or-Ar), 131.40 (Ar), 131.35 (Ar), 131.00, 129.67 (5-Ant), 129.08 (4-Ant), 127.79 (10-Ant), 126.22, 125.06 (3,6-Ant), 123.87 (3',5'-Py), 123.63 (9-Ant), 122.52 (3,3''-Py), 121.51, 121.30, 120.63, 119.53, 118.74, 105.30 (C≡C), 96.29 (C≡C), 95.51 (C≡C), 92.95 (C≡C), 91.57 (C≡C), 85.95 (C≡C), 18.67 (TIPS), 11.28 (TIPS). (Of the 34 expected carbon signals 32 were found, 2 signals are expected to be superimposed with other signals.)

IR (ATR):  $\tilde{\nu}$  [ $\text{cm}^{-1}$ ] =  $\text{NTf}_2^-$ : 2940, 2889, 2861, 2202, 2144, 1591, 1563, 1507, 1472, 1462, 1449, 1434, 1349, 1328, 1177, 1133, 1054, 874, 838, 788, 740, 647, 615, 598, 567.

IR (ATR):  $\tilde{\nu}$  [ $\text{cm}^{-1}$ ] =  $\text{BF}_4^-$ : 2940, 2888, 2861, 2202, 2143, 1591, 1575, 1564, 1506, 1483, 1471, 1462, 1446, 1436, 1051, 1030, 997, 882, 874, 800, 743, 650.

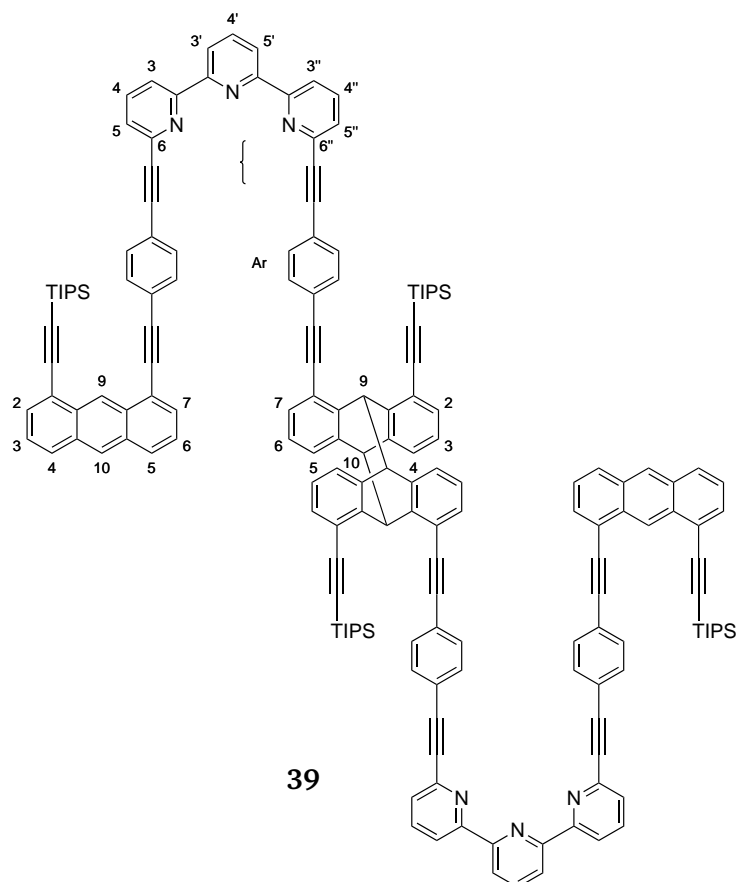
$\text{NTf}_2^-$ : **HRMS** (ESI/MALDI-FTICR, DCTB):  $m/z$  calcd for  $\text{C}_{174}\text{H}_{150}\text{F}_{12}\text{N}_8\text{O}_8\text{S}_4\text{Si}_4\text{Zn}$   $[\text{M}]^+$  3010.8631, found 3010.8595;  $\text{C}_{172}\text{H}_{151}\text{F}_6\text{N}_7\text{O}_4\text{S}_2\text{Si}_4\text{Zn}$   $[\text{M}-\text{NTf}_2+\text{H}]^+$  2731.9487, found 2731.9503;  $\text{C}_{170}\text{H}_{151}\text{N}_6\text{Si}_4\text{Zn}$   $[\text{M}-2\text{NTf}_2+\text{H}]^+$  2452.0363, found 2452.0461.

$\text{BF}_4^-$ : **HRMS** (ESI/MALDI-FTICR, DCTB):  $m/z$  calcd for  $\text{C}_{170}\text{H}_{150}\text{N}_6\text{Si}_4\text{Zn}$   $[\text{M}-2\text{BF}_4]^+$  2451.0285, found 2451.0249.

<sup>xxx</sup>This value corresponds to the isolated amount of crystals, not the effective yield.

## 6. Experimental

### Linear dimer 39



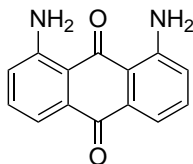
The linear dimer **39** was isolated from the crude mixture from the solution irradiation of the premonomer **7**.

$^1\text{H-NMR}$  (500 MHz,  $\text{CDCl}_3$ ):  $\delta$  [ppm] = 9.44 (s, 2H, 9-Ant-H), 8.66–8.57 (m, 8H, 3,3',5',3''-Py-H), 8.48 (s, 2H, 10-Ant-H), 8.07–7.98 (m, 6H, 4,5-Ant-H and 4'-Py-H), 7.91 (td,  $^3J_{\text{H,H}} = 7.8$  Hz,  $^4J_{\text{H,H}} = 3.2$  Hz, 4H, 4,4''-Py-H), 7.84 (dd,  $^3J_{\text{H,H}} = 6.9$  Hz,  $^4J_{\text{H,H}} = 0.7$  Hz, 2H, 2-Ant-H), 7.80 (dd,  $^3J_{\text{H,H}} = 6.9$  Hz,  $^4J_{\text{H,H}} = 0.6$  Hz, 2H, 7-Ant-H), 7.73–7.61 (m, 20H, Ar-H and 5,5''-Py-H), 7.52–7.42 (m, 4H, 3,6-Ant), 7.21–6.99 (m, 8H, 2,4,5,7-Ar-H), 6.93–6.78 (m, 4H, 3,6-Ar-H), 5.73 (d,  $^3J_{\text{H,H}} = 11.0$  Hz, 2H, 9-or-10-Ar-H), 4.71 (d,  $^3J_{\text{H,H}} = 11.1$  Hz, 2H, 9-or-10-Ar-H), 1.15–1.08 (m, 84H, Si-( $\text{CH}(\text{CH}_3)_2$ )<sub>3</sub>).

## 6. Experimental

### 6.3. Synthesis Part B

#### 1,8-Diamino-9,10-anthraquinone **46**<sup>[262]</sup>



**46**

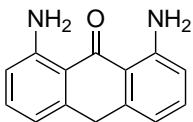
To a stirred suspension of 1,8-dinitro-9,10-anthraquinone **45** (25.3 g, 84.8 mmol) in EtOH (500 mL), a solution of Na<sub>2</sub>S · xH<sub>2</sub>O (45.3 g, 343 mmol) in water (1 L) was added, and the reaction mixture was heated to reflux °C for 17 h. After cooling to rt, the reaction mixture was poured into a stirred ice/water mixture. The precipitate was filtered through a glass filter, washed with cold water, and dried *in vacuo* to give **46** (19.8 g, 97.9 %) as a purple solid.

<sup>1</sup>H-NMR (300 MHz, DMSO-*d*<sub>6</sub>): δ [ppm] = 7.84 (*s*<sub>br</sub>, 4H, Amino-H<sub>2</sub>), 7.45 (t, <sup>3</sup>*J*<sub>H,H</sub> = 7.8 Hz, 2H, 3,6-Ar-H), 7.34 (dd, <sup>3</sup>*J*<sub>H,H</sub> = 7.2 Hz, <sup>4</sup>*J*<sub>H,H</sub> = 0.9 Hz, 2H, 4,5-Ar-H), 7.15 (dd, <sup>3</sup>*J*<sub>H,H</sub> = 8.2 Hz, <sup>4</sup>*J*<sub>H,H</sub> = 0.9 Hz, 2H, 2,7-Ar-H).

<sup>13</sup>C-NMR (76 MHz, DMSO-*d*<sub>6</sub>): δ [ppm] = 187.77 (C=O), 183.41 (C=O), 151.53, 133.67 (3,6-Ar), 133.51, 123.50 (2,7-Ar), 114.85 (4,5-Ar), 113.06.

HRMS (ESI/MALDI-FTICR, DCTB): *m/z* calcd for C<sub>14</sub>H<sub>11</sub>N<sub>2</sub>O<sub>2</sub> [M+H]<sup>+</sup> 239.0815, found 239.0814.

#### 1,8-Diamino-9-anthrone **54**<sup>[267]</sup>



**54**

A 2 L three-neck flask was charged with **46** (20.1 g, 84.4 mmol), 10 % aq. NH<sub>3</sub> solution (1 L), and iPrOH (100 mL). This reaction mixture was heated to 90 °C under a N<sub>2</sub> atmosphere. Under N<sub>2</sub>, zinc (75.0 g, 1.15 mol) was added in five equal portions within one hour and the temperature was raised to 115 °C for another 1.5 h. The reaction mixture was cooled to rt and extracted with Et<sub>2</sub>O (700 mL). The combined organic layers were dried over MgSO<sub>4</sub> before the

## 6. Experimental

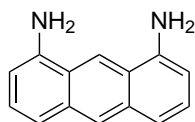
solvent was removed *in vacuo*. After recrystallization from toluene **54** (14.7 g, 77.5 %) was isolated as red crystals, sufficiently pure for the next reaction step.

$^1\text{H-NMR}$  (300 MHz, DMSO- $d_6$ ):  $\delta$  [ppm] = 7.54–7.27 (m, 4H, Amino- $\text{H}_2$ ), 7.21–7.11 (m, 2H, 3,6-Ar-H), 6.61 (d,  $^3J_{\text{H,H}} = 8.2$  Hz, 2H, 2,7-Ar-H), 6.48 (dd,  $^3J_{\text{H,H}} = 7.2$  Hz,  $^4J_{\text{H,H}} = 0.9$  Hz, 2H, 4,5-Ar-H), 4.14 (s, 2H,  $-\text{CH}_2-$ ).

$^{13}\text{C-NMR}$  (76 MHz, DMSO- $d_6$ ):  $\delta$  [ppm] = 190.05 (C=O), 151.48, 141.26, 133.03 (3,6-Ar), 114.63, 114.00 (2,7-Ar), 113.80 (4,5-Ar), 33.67 ( $-\text{CH}_2-$ ).

**HRMS** (ESI/MALDI-FTICR, DCTB):  $m/z$  calcd for  $\text{C}_{14}\text{H}_{13}\text{N}_2\text{O}$   $[\text{M}+\text{H}]^+$  225.1022, found 225.1026.

### 1,8-Diaminoanthracene **48**



**48**

Method A<sup>[262]</sup>:

To a solution of NaOH (700 mg, 17.5 mmol) in iPrOH (400 mL), a suspension of **46** (15.9 g, 66.7 mmol) in iPrOH (180 mL) was added. The reaction mixture was degassed by bubbling argon through the solution for ca. 25 minutes.  $\text{NaBH}_4$  (27.6 g, 730 mmol) was added in three equal portions under  $\text{N}_2$ , then the reaction mixture was heated at 110 °C for four days under  $\text{N}_2$  atmosphere. After cooling to rt, the reaction mixture was poured into 1.5 L of an ice/water mixture. The precipitate was filtered through a glass filter, washed with cold water, and dried under air. The crude residue was purified with silica gel column chromatography (DCM/MeOH; 9 : 1) to give **48** (7.50 g, 54.0 %) as a green solid.

Method B<sup>[267]</sup>:

A 50 mL Schlenktube was charged with **54** (10.0 g, 44.8 mmol),  $\text{NaBH}_4$  (6.77 g, 179 mmol), and dry 1,4-dioxane (10 mL) under  $\text{N}_2$  atmosphere. The suspension was heated to 130 °C for five minutes, while the solid melted upon raising the temperature to 140 °C. The reaction was heated for another 19 h, then cooled, and transferred to a beaker. The reaction mixture was quenched with MeOH and an ice/water mixture. After extraction with EtOAc (300 mL) and washing with water, the mixture was filtered over neutral aluminium oxide. The remaining

## 6. Experimental

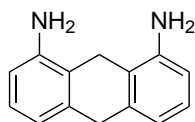
solvent was removed *in vacuo* to give a brown solid of **48** as a mixture with **40** (9.52 g, molar ratio 1.00 : 0.37 determined by  $^1\text{H-NMR}$ ). The yield of **48** was calculated as 74.5 %.

$^1\text{H-NMR}$  (300 MHz,  $\text{DMSO-}d_6$ ):  $\delta$  [ppm] = 8.79 (s, 1H, 9-Ant-H), 8.16 (s, 1H, 10-Ant-H), 7.18 (d,  $^3J_{H,H} = 4.4$  Hz, 4H, 2,4,5,7-Ant-H), 6.55 (t,  $^3J_{H,H} = 4.3, 4.0$  Hz, 2H, 3,6-Ant-H), 5.85 (s, 4H, Amino- $\text{H}_2$ ).

$^{13}\text{C-NMR}$  (76 MHz,  $\text{DMSO-}d_6$ ):  $\delta$  [ppm] = 144.62 (1,8-Ant), 132.23, 126.59 (4,5-Ant), 124.94 (10-Ant), 121.40, 115.35 (9-Ant), 114.95 (2,7-Ant), 103.88 (3,6-Ant).

**HRMS** (ESI/MALDI-FTICR, DCTB):  $m/z$  calcd for  $\text{C}_{14}\text{H}_{12}\text{N}_2$   $[\text{M}]^+$  208.0995, found 208.0995.

### 1,8-Diamino-9,10-dihydroanthracene **40**



**40**

Method A<sup>[265]</sup>:

To an argon degassed solution of NaOH (50.2 g, 1.23 mol) in water (670 mL), 1,8-Dinitro-9,10-anthraquinone **45** (12.4 g, 41.5 mmol) and zinc (168 g, 2.57 mol) were added under  $\text{N}_2$  at mechanical stirring. The reaction mixture was heated at reflux for three days and then cooled to rt. The reaction mixture was mixed with concentrated HCl (570 mL) and stirred for another two hours. Afterwards the reaction mixture was filtered, washed with water, and the filtrate was treated with aq. NaOH until pH was 6 upon which a solid precipitated. The solid was separated with a glass filter and dried *in vacuo* at 90 °C. The filter residue was then extracted with hot acetone, until the acetone was nearly colorless. The combined extracts were concentrated *in vacuo* and purified with silica gel column chromatography (DCM/MeOH; 19 : 1) to give a dark brown solid of **40** (4.00 g; 45.8 %).

Method B:

To a stirred argon degassed solution of NaOH (101 g, 2.51 mol) in water (1.35 L), **46** (19.6 g, 82.3 mmol) and zinc (323 g, 4.94 mol) were added under  $\text{N}_2$ . The reaction mixture was heated at 130 °C for three days and then cooled to rt. Afterwards the solid was filtered through a glass filter and washed with water. The filter residue was then extracted with hot acetone, until the acetone was nearly colorless. The combined extracts were evaporated *in vacuo* and the

## 6. Experimental

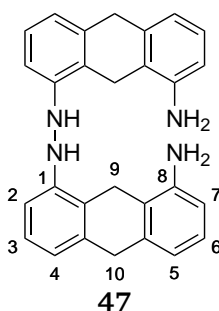
crude mixture was purified with silica gel column chromatography (DCM/MeOH; 19 : 1). The solid was dried, followed by recrystallization in abs EtOH to give green/grey crystals of **40** as a mixture with **48** (10.9 g, molar ratio 1.00 : 0.05 determined by  $^1\text{H-NMR}$ ). The yield of **40** was calculated as 56.2 %.

$^1\text{H-NMR}$  (300 MHz, DMSO- $d_6$ ):  $\delta$  [ppm] = 6.87 (t,  $^3J_{H,H} = 7.7$  Hz, 2H, 3,6-Ar-H), 6.52–6.42 (m, 4H, 2,4,5,7-Ar-H), 5.01 (s, 4H, Amino- $\text{H}_2$ ), 3.81 ( $s_{br}$ , 2H, 10- $\text{CH}_2$ -), 3.34<sup>XXXI</sup> ( $s_{br}$ , 2H, 9- $\text{CH}_2$ -).

$^{13}\text{C-NMR}$  (76 MHz, DMSO- $d_6$ ):  $\delta$  [ppm] = 145.51, 145.45, 145.40, 135.24, 126.15 (3,6-Ar), 118.28 (C- $\text{NH}_2$ ), 115.37 (3,6-Ar), 111.24 (2,7-Ar), 34.60 (10- $\text{CH}_2$ -), 24.35 (9- $\text{CH}_2$ -).

**HRMS** (ESI/MALDI-FTICR, DCTB):  $m/z$  calcd for  $\text{C}_{14}\text{H}_{15}\text{N}_2$   $[\text{M}+\text{H}]^+$  211.1230, found 211.1230.

### 8,8'-(hydrazine-1,2-diyl)bis(9,10-dihydroanthracen-1-amine) **47**



Compound **47** was isolated as a side product from the reaction of **40** via method A.

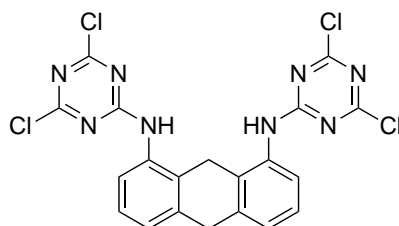
$^1\text{H-NMR}$  (300 MHz, DMSO- $d_6$ ):  $\delta$  [ppm] = 9.39 (s, 2H, Amino-H), 6.97 (t,  $^3J_{H,H} = 7.7$  Hz, 2H, 3-Ar-H), 6.87 (t,  $^3J_{H,H} = 7.6$  Hz, 2H, 6-Ar-H), 6.73–6.66 (m, 4H, 5,7-Ar-H), 6.57–6.48 (m, 4H, 2,4-Ar-H), 4.99 ( $s_{br}$ , 4H, Amino- $\text{H}_2$ ), 3.82 (s, 4H, 10- $\text{CH}_2$ -), 3.57 (s, 4H, 9- $\text{CH}_2$ -).

$^{13}\text{C-NMR}$  (76 MHz, DMSO- $d_6$ ):  $\delta$  [ppm] = 154.30 (1-Ant), 145.43 (8-Ar), 137.17, 135.79, 126.22 (3-Ar), 126.07 (6-Ar), 122.02, 119.49, 118.05 (4-or-5-Ar), 115.89 (4-or-5-Ar), 112.24 (2-Ar), 111.96 (7-Ar), 34.99 (10- $\text{CH}_2$ -), 22.88 (9- $\text{CH}_2$ -).

<sup>XXXI</sup>This signal overlaps with residual water

## 6. Experimental

### Mono-blade 41



41

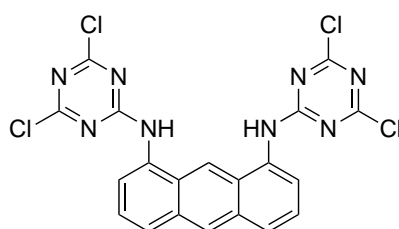
To an ice/water bath cooled solution of cyanuric chloride **43** (8.88 g, 48.2 mmol) in THF (400 mL), a solution of **40** (5.00 g, 23.8 mmol) in THF (200 mL) and DIPEA (8.40 mL, 48.6 mmol) was added dropwise within three hours. The mixture was warmed to rt and filtered. Then the solvent was evaporated and dried *in vacuo*. After dissolving the crude solid in  $\text{CHCl}_3$  and washing with cold water, the solvent was evaporated. The remaining solid was washed with  $\text{Et}_2\text{O}$  ( $\text{N}_2$  cooled) and filtered through a glass filter to gain **41** (10.8 g, 89.4 %) as a white powder. Crystals could be grown by recrystallization from acetone.

$^1\text{H-NMR}$  (300 MHz,  $\text{DMSO-}d_6$ ):  $\delta$  [ppm] = 10.89 (s, 2H, Amino-H), 7.38–7.20 (m, 6H, 2,3,4,5,6,7-Ar-H), 4.04 (s, 2H, 10- $\text{CH}_2$ -), 3.68 (s, 2H, 9- $\text{CH}_2$ -).

$^{13}\text{C-NMR}$  (76 MHz,  $\text{DMSO-}d_6$ ):  $\delta$  [ppm] = 169.82 (C-Cl), 169.03 (C-Cl), 165.08 (Triazine), 137.50, 133.24, 131.11, 126.40, 126.09, 124.26, 35.41 (10- $\text{CH}_2$ -), 26.08 (9- $\text{CH}_2$ -).

**HRMS** (ESI/MALDI-FTICR, DCTB):  $m/z$  calcd for  $\text{C}_{20}\text{H}_{12}\text{Cl}_4\text{N}_8$   $[\text{M}]^+$  503.9934, found 503.9748.

### Anthracene-mono-blade 50



50

The suspension of **41** (500 mg, 990  $\mu\text{mol}$ ) and 1,2-dichloroethane (350 mL) was dissolved at 100 °C. After degassing the reaction mixture with argon, DDQ (270 mg, 1.19 mmol) was added at once, and the reaction was stirred at 100 °C for 17 hours, then cooled to rt. The crude mixture was passed through a short silica gel column and subsequently washed with 1,2-dichloroethane,

## 6. Experimental

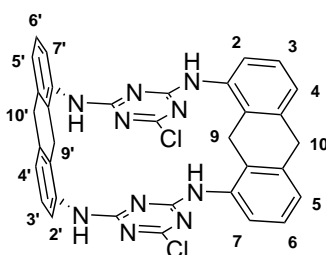
EtOAc, and hexane. A second fraction was collected by continuing the washing with more EtOAc. The solvent of the later fraction was evaporated and the crude mixture was purified by silica gel column chromatography (hexane/EtOAc; 4 : 1  $\rightarrow$  2 : 1). The product **50** (130 mg, 26.1 %) was isolated as a yellow powder. Crystals could be obtained by recrystallization from ODCB.

$^1\text{H-NMR}$  (300 MHz, DMSO- $d_6$ ):  $\delta$  [ppm] = 11.36 (s, 2H, Amino-H), 8.78 (s, 1H, 10-Ant-H), 8.61 (s, 1H, 9-Ant-H), 8.13 (d,  $^3J_{H,H}$  = 8.2 Hz, 2H, 4,5-Ant-H), 7.72–7.56 (m, 4H, 2,3,6,7-Ant-H).

$^{13}\text{C-NMR}$  (76 MHz, DMSO- $d_6$ ):  $\delta$  [ppm] = 169.86 (C-Cl), 169.17 (C-Cl), 165.94 (Triazine), 132.01, 131.82, 127.56 (4,5-Ant), 127.49 (10-Ant), 127.04, 125.53 (3,6-Ant), 123.63 (2,7-Ant), 116.71 (9-Ant).

HRMS (ESI/MALDI-FTICR, DCTB):  $m/z$  calcd for  $\text{C}_{20}\text{H}_{10}\text{Cl}_4\text{N}_8$   $[\text{M}]^+$  501.9777, found 501.9775.

### Di-blade 49



**49**

A solution of **40** (2.08 g, 9.88 mmol) in THF (3 L) was mixed with DIPEA (3.80 mL, 22.0 mmol) and THF (200 mL). After 20 minutes of stirring at rt, a solution of **41** (5.00 g, 9.88 mmol) in THF (700 mL) was added at once. The reaction mixture was stirred for 18 days in the dark at rt. The light brown precipitate was separated by centrifugation, washed twice with MeOH, MeOH/water mixture, and again with MeOH. The solid was then dried *in vacuo* to give **49** (3.81 g, 59.9 %) as a white solid. Crystallization from DMSO furnished clear cubic crystals.

$^1\text{H-NMR}$  (300 MHz, DMSO- $d_6$ ):  $\delta$  [ppm] = 9.75 (s, 4H, Amino-H), 7.36–7.00 (m, 10H, 3,3',4,4',5,5',6,6'-Ar-H & 2,7-or-2',7'-Ar-H), 6.88 (d,  $^3J_{H,H}$  = 7.7 Hz, 2H, 2,7-or-2',7'-Ar-H), 4.15–3.77 (m, 5H, 10,10'-CH<sub>2</sub>- & 9-or-9'-CH<sub>2</sub>-), 3.59–3.35 (m, 3H, 9-or-9'-CH<sub>2</sub>-).

$^1\text{H-NMR}$  (300 MHz, DMF- $d_7$ ):  $\delta$  [ppm] = 9.71 & 9.63 & 9.56 (3 x s, 4H, Amino-H), 7.42–6.99 (m, 12H, 2,2'3,3',4,4',5,5',6,6',7,7'-Ar-H), 4.19–3.87 (m, 5H, -CH<sub>2</sub>-), 3.82–3.66 (m, 3H,



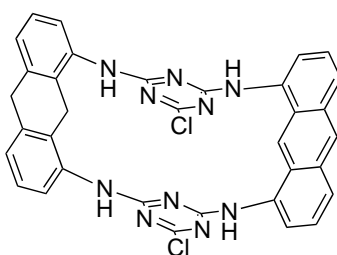
## 6. Experimental

–CH<sub>2</sub>–).

<sup>13</sup>C-NMR (76 MHz, DMSO-*d*<sub>6</sub>): δ [ppm] = 168.88 (C-Cl), 165.23 (Triazine), 165.21 (Triazine), 137.59, 137.55, 134.98, 134.68, 133.88, 133.57, 126.40, 125.95, 125.92, 125.29, 124.87, 124.01 (2,7-or-2',7'-Ar), 36.02 (10-or-10'–CH<sub>2</sub>–), 35.97 (10-or-10'–CH<sub>2</sub>–), 27.20 (9-or-9'–CH<sub>2</sub>–), 26.57 (9-or-9'–CH<sub>2</sub>–).

HRMS (ESI/MALDI-FTICR, DCTB): *m/z* calcd for C<sub>34</sub>H<sub>24</sub>Cl<sub>2</sub>N<sub>10</sub> [M]<sup>+</sup> 642.1557, found 642.1569.

### Anthracene-dihydroanthracene-di-blade 52

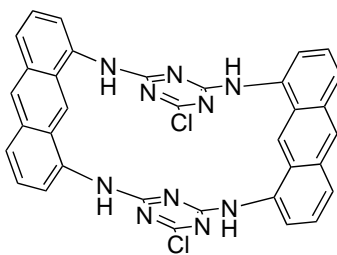


52

A solution of **48** (81.8 mg, 393 μmol) in THF (130 mL) and DIPEA (150 μL, 869 μmol) was stirred for 10 minutes, then a solution of **41** (200 mg, 395 μmol) in THF (31 mL) was added at once. The reaction mixture was stirred for 12 days at rt in the dark. The precipitate was separated via centrifugation and washed twice with THF. The filtrate was continued to stir for another 13 days at rt in the dark. More precipitate was collected by centrifuging and washing with THF. The combined white and light green solids were dried *in vacuo* and afforded **52** (112 mg, 44.3 %).

HRMS (ESI/MALDI-FTICR, DCTB): *m/z* calcd for C<sub>34</sub>H<sub>22</sub>Cl<sub>2</sub>N<sub>10</sub> [M]<sup>+</sup> 640.1400, found 640.1398.

### Anthracene-di-blade 53



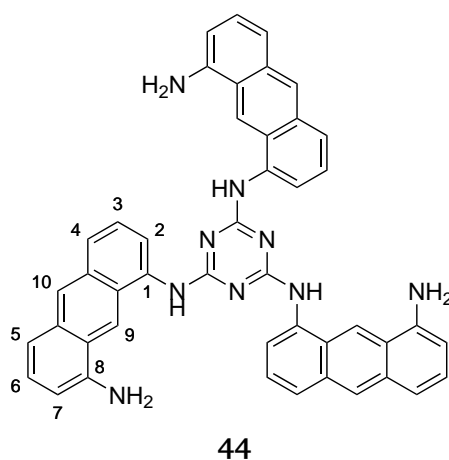
53

## 6. Experimental

A solution of **48** (26.1 mg, 126  $\mu\text{mol}$ ) in THF (40.5 mL) and DIPEA (60.0  $\mu\text{L}$ , 347  $\mu\text{mol}$ ) was stirred for five minutes, then a solution of **50** (63.3 mg, 126  $\mu\text{mol}$ ) in THF (10 mL) was added at once. The reaction mixture was stirred for 12 days at rt in the dark. The precipitate was separated with a centrifuge, washed twice with THF, a mixture of MeOH/water, and twice with MeOH. The green/light yellow solid was dried *in vacuo* to give **53** (25.0 mg, 31.1 %).

**HRMS** (ESI/MALDI-FTICR, DCTB):  $m/z$  calcd for  $\text{C}_{34}\text{H}_{20}\text{Cl}_2\text{N}_{10}$   $[\text{M}]^+$  638.1244, found: 638.1245.

### Precursor **44**<sup>[268]</sup>



A microwave vessel (80 mL) was charged with **48** (3.89 g, 18.7 mmol),  $\text{NaHCO}_3$  (3.16 g, 37.6 mmol), a mixture of 1,4-dioxane/DMF (3 : 1; 32 mL), and was cooled with an ice/water bath for 15 minutes. Within one minute cyanuric chloride **43** (690 mg, 3.74 mmol) dissolved in a 1,4-dioxane/DMF mixture (3 : 1; 8 mL) was added. The reaction was stirred at 160  $^\circ\text{C}$  under microwave irradiation for 15 minutes. After Cooling to rt, the mixture was transferred to a flask, and the solvent was evaporated *in vacuo*. Purification by silica gel column chromatography ( $\text{CHCl}_3^{\text{XXXII}}$ /MeOH/TEA; 19 : 1 : 1) afforded **44** (730 mg; 27.7 %) as a greenish solid.

**$^1\text{H-NMR}$**  (300 MHz,  $\text{DMSO-}d_6$ ):  $\delta$  [ppm] = 9.09 (s, 3H, Amino-H), 8.98 (s, 3H, 9-Ant-H), 8.35 (s, 3H, 10-Ant-H), 7.84 (d, 3H, 2-Ant-H), 7.71 (2, 3H, 4-Ant-H), 7.33–7.13 (m, 9H, 3,5,6-Ant-H), 6.64 (2, 3H, 7-Ant-H), 5.92 ( $s_{br}$ , 6H, Amino- $\text{H}_2$ ).

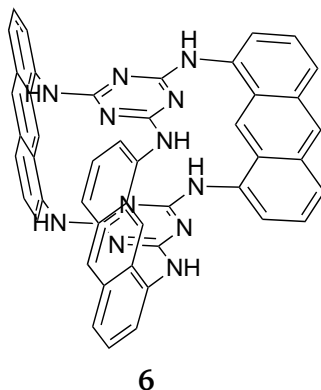
**$^{13}\text{C-NMR}$**  (76 MHz,  $\text{DMSO-}d_6$ ):  $\delta$  [ppm] = 165.89 (Triazine), 144.89, 134.87, 132.20, 131.71, 126.85 (6-Ant), 125.64 (10-Ant), 125.16, 125.01 (3-Ant), 123.53 (4-Ant), 122.70, 118.94 (2-Ant), 116.23 (9-Ant), 115.26 (5-Ant), 105.04 (7-Ant).

**HRMS** (ESI/MALDI-FTICR, DCTB):  $m/z$  calcd for  $\text{C}_{45}\text{H}_{33}\text{N}_9$   $[\text{M}]^+$  699.2853, found 699.2856.

<sup>XXXII</sup> $\text{CHCl}_3$  stabilized with Amylene.

## 6. Experimental

### Monomer 6

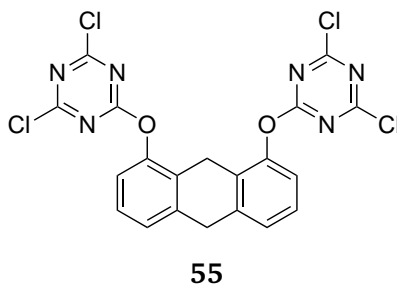


A 2 L flask was charged with **44** (690 mg, 987  $\mu\text{mol}$ ), freshly distilled THF (1.5 L), and  $\text{K}_2\text{CO}_3$  (420 mg, 3.04 mmol). The solution was cooled for 50 minutes to ca.  $-50\text{ }^\circ\text{C}$  (acetone/dry ice bath), followed by a slow dropwise addition of a solution of cyanuric chloride **43** (182 mg, 987  $\mu\text{mol}$ ) in fresh distilled THF (200 mL) within 70 minutes. The reaction flask was transferred to a  $85\text{ }^\circ\text{C}$  preheated oil bath and heated in the dark under  $\text{N}_2$  atmosphere for six days (after the 4th day the temperature was lowered to  $75\text{ }^\circ\text{C}$ ). The mixture was filtered through a glass pore filter, then the filtrate was evaporated and purified with silica gel column chromatography ( $\text{CHCl}_3^{\text{XXXIII}}$  : MeOH : TEA, 19 : 1 : 1). A brownish solid was collected, which still contained an unknown impurity that was seen in the  $^1\text{H-NMR}$  spectrum. Pure product was obtained by purifying this remaining solid with the preparative rGPC in small amounts.

$^1\text{H-NMR}$  (500 MHz,  $\text{DMSO-}d_6$ ):  $\delta$  [ppm] = 8.61 (*s<sub>br</sub>*, 9H, Amino-H & 10-Ant-H), 8.50 (s, 3H, 9-Ant-H), 8.00 (d,  $^3J_{\text{H,H}} = 8.5\text{ Hz}$ , 6H, 4,5-Ant-H), 7.54–7.47 (m, 6H, 3,6-Ant-H), 7.33 (d,  $^3J_{\text{H,H}} = 7.1\text{ Hz}$ , 6H, 2,7-Ant-H).

HRMS (ESI/MALDI-FTICR, DCTB):  $m/z$  calcd for  $\text{C}_{48}\text{H}_{30}\text{N}_{12}$   $[\text{M}]^+$  774.2711, found 774.2710.

### Mono-blade-(OH) **55**<sup>[44]</sup>



<sup>XXXIII</sup> $\text{CHCl}_3$  stabilized with Amylene.

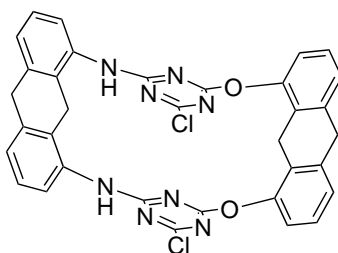
## 6. Experimental

A solution of cyanuric chloride **43** (1.09 g, 5.89 mmol) in THF (40 mL) was cooled with an ice/water bath for 25 minutes. A solution of 1,8-dihydroxy-9,10-dihydroanthracene **57** (500 mg, 5.89 mmol) in THF (20 mL) mixed with DIPEA (980  $\mu$ L, 5.65 mmol) was added dropwise within 40 minutes. The mixture was stirred for another 3.5 hours and then the solvent was evaporated *in vacuo*. The remaining solid was dissolved in  $\text{CHCl}_3$  and washed with cold water. The combined  $\text{CHCl}_3$  phase was dried with  $\text{MgSO}_4$ , passed through a filter, and washed with  $\text{CHCl}_3$ . Afterwards, the solvent was evaporated. The remaining solid was mixed with cold  $\text{Et}_2\text{O}$ , filtered through a glass filter, and washed with cold  $\text{Et}_2\text{O}$ . The white solid was dried *in vacuo* to give **55** (920 mg, 76.8 %).

$^1\text{H-NMR}$  (300 MHz,  $\text{DMSO-}d_6$ ):  $\delta$  [ppm] = 7.52–7.05 (m, 6H, 2,3,4,5,6,7-Ar-H), 4.12 (s, 2H, 9– $\text{CH}_2$ –), 3.66 (s, 2H, 10– $\text{CH}_2$ –).

**HRMS** (ESI/MALDI-FTICR, DCTB):  $m/z$  calcd for  $\text{C}_{20}\text{H}_{11}\text{Cl}_4\text{N}_6\text{O}_2$   $[\text{M}+\text{H}]^+$  506.9692, found 506.9691.

### Hybrid-di-blade-(NH-O) **56**<sup>[44]</sup>



**56**

A solution of **40** (63.5 mg, 302  $\mu$ mol) in  $\text{CHCl}_3$  (80 mL) and DIPEA (150  $\mu$ L, 869  $\mu$ mol) was stirred for 15 minutes at rt, then a solution of **55** (153 mg, 301  $\mu$ mol) in  $\text{CHCl}_3$  (10 mL) was added at once. The reaction mixture was stirred for four days at rt. The precipitate was separated with a centrifuge, washed with  $\text{CHCl}_3$  and twice with MeOH. The solid was then dried *in vacuo* to give **56** (93.6 mg, 48.1 %) as a white solid. Crystallization from DMSO furnished clear needle crystals.

$^1\text{H-NMR}$  (300 MHz,  $\text{DMSO-}d_6$ ):  $\delta$  [ppm] = 10.69–10.33 (m, 2H, Amino-H), 7.47–6.90 (m, 12H, 2,3,4,5,6,7-Ar-H), 4.30–3.95 (m, 4H, – $\text{CH}_2$ –), 3.56–3.20 (m, 4H, – $\text{CH}_2$ –).

**HRMS** (ESI/MALDI-FTICR, DCTB):  $m/z$  calcd for  $\text{C}_{34}\text{H}_{23}\text{Cl}_2\text{N}_8\text{O}_2$   $[\text{M}+\text{H}]^+$  645.1316, found 645.1317.

## 7. Appendix

## 7.1. Crystallographic data

## Mono-complex 37 – sc210711

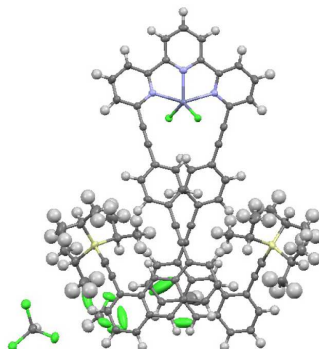


Figure 7.1: Mono-complex 37 from chloroform.

Table 2: Crystal data and structure refinement for sc210711

Identification code	sc210711	
Empirical formula	C <sub>90</sub> H <sub>80</sub> Cl <sub>17</sub> N <sub>3</sub> Si <sub>2</sub> Zn	
Formula weight	1927.77	
Temperature	100(2) K	
Crystal system	orthorhombic	
Space group	Pccn	
Unit cell dimensions	a = 14.6856(4) Å	α = 90°
	b = 18.9585(5) Å	β = 90°
	c = 32.6114(9) Å	γ = 90°
Volume	9079.6(4) Å <sup>3</sup>	
Z	4	
Density (calculated)	1.410 Mg/cm <sup>3</sup>	
Absorption coefficient	5.594 mm <sup>-1</sup>	
F(000)	3952	
Crystal size	0.020 x 0.040 x 0.100 mm <sup>3</sup>	
Radiation	MoKα (λ = 1.54178 Å)	
Theta range for data collection	2.71 to 66.07°	
Index ranges	-17 ≤ h ≤ 15, -22 ≤ k ≤ 21, -17 ≤ l ≤ 38	
Reflections collected	33023	
Independent reflections	7812 [R <sub>int</sub> = 0.0450]	
Data / restraints / parameters	7812 / 3 / 532	
Goodness-of-fit on F <sup>2</sup>	1.481	
Final R indices	I > 2σ(I)	R <sub>1</sub> = 0.0546, wR <sub>2</sub> = 0.1589
	all data	R <sub>1</sub> = 0.0688, wR <sub>2</sub> = 0.1670
Largest diff. peak and hole	0.894 and -0.982 eÅ <sup>-3</sup>	

## 7. Appendix

### Bis-complex 3 (X = BF<sub>4</sub><sup>-</sup>) – sc010312

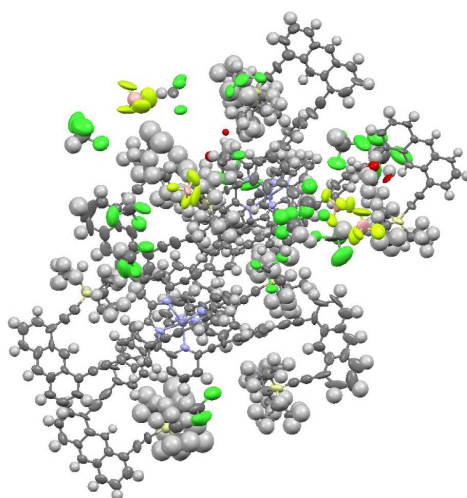


Figure 7.2: Bis-complex 3 (X = BF<sub>4</sub><sup>-</sup>) from chloroform/methanol.

Table 3: Crystal data and structure refinement for sc010312

Identification code	sc010312
Empirical formula	C <sub>176.62</sub> H <sub>159.62</sub> B <sub>2</sub> Cl <sub>16.85</sub> F <sub>8</sub> N <sub>6</sub> OSi <sub>4</sub> Zn
Formula weight	3330.70
Temperature	100(2) K
Crystal system	triclinic
Space group	P-1
Unit cell dimensions	a = 25.518(3) Å    α = 61.684(7)° b = 28.287(3) Å    β = 86.263(7)° c = 28.365(3) Å    γ = 69.319(7)°
Volume	16733.(3) Å <sup>3</sup>
Z	4
Density (calculated)	1.322 Mg/cm <sup>3</sup>
Absorption coefficient	3.459 mm <sup>-1</sup>
F(000)	6895
Crystal size	0.020 x 0.090 x 0.140 mm <sup>3</sup>
Radiation	MoKα (λ = 1.54178 Å)
Theta range for data collection	1.78 to 51.20°
Index ranges	-25 ≤ h ≤ 23, -28 ≤ k ≤ 19, -26 ≤ l ≤ 28
Reflections collected	112281
Independent reflections	33849 [R <sub>int</sub> = 0.0907]
Data / restraints / parameters	33849 / 89 / 3692
Goodness-of-fit on F <sup>2</sup>	2.302
Final R indices	I > 2σ(I)            R <sub>1</sub> = 0.1688, wR <sub>2</sub> = 0.3954 all data                R <sub>1</sub> = 0.2462, wR <sub>2</sub> = 0.4165
Largest diff. peak and hole	1.383 and -1.161 eÅ <sup>-3</sup>

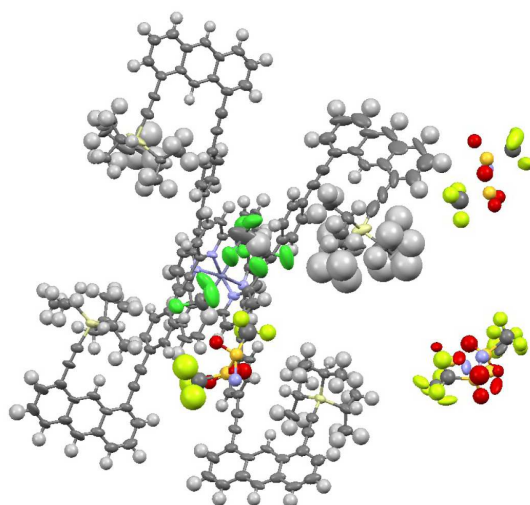
Bis-complex 3 (X = NTf<sub>2</sub><sup>-</sup>) – sc171012Figure 7.3: Bis-complex 3 (X = NTf<sub>2</sub><sup>-</sup>) from chloroform/methanol.

Table 4: Crystal data and structure refinement for sc171012

Identification code	sc171012	
Empirical formula	C <sub>177</sub> H <sub>152</sub> Cl <sub>9</sub> F <sub>12</sub> N <sub>8</sub> O <sub>8</sub> S <sub>4</sub> Si <sub>4</sub> Zn	
Formula weight	3372.09	
Temperature	100(2) K	
Crystal system	monoclinic	
Space group	P21/n	
Unit cell dimensions	23.1962(10) Å	$\alpha = 90^\circ$
	b = 22.8762(10) Å	$\beta = 108.4220(10)^\circ$
	c = 33.0394(13) Å	$\gamma = 90^\circ$
Volume	16633.6(12) Å <sup>3</sup>	
Z	4	
Density (calculated)	1.347 g/cm <sup>3</sup>	
Absorption coefficient	0.445 mm <sup>-1</sup>	
F(000)	6980	
Crystal size	0.090 x 0.240 x 0.280 mm <sup>3</sup>	
Radiation	MoK $\alpha$ ( $\lambda = 0.71073$ Å)	
Theta range for data collection	1.30 to 22.12°	
Index ranges	-24 ≤ h ≤ 24, -24 ≤ k ≤ 24, -34 ≤ l ≤ 34	
Reflections collected	182134	
Independent reflections	20601 [ $R_{int} = 0.1119$ ]	
Data / restraints / parameters	20601 / 60 / 2073	
Goodness-of-fit on F <sup>2</sup>	1.959	
Final R indices	I > 2 $\sigma$ (I)	R <sub>1</sub> = 0.1222, wR <sub>2</sub> = 0.3000
	all data	R <sub>1</sub> = 0.1958, wR <sub>2</sub> = 0.3289
Largest diff. peak and hole	1.848 and -0.969 eÅ <sup>-3</sup>	

## 7. Appendix

### Bis-complex 3 (X = NTf<sub>2</sub><sup>-</sup>) – cu\_sc071212a

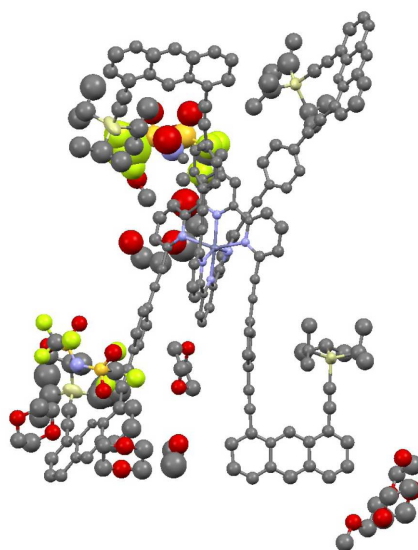


Figure 7.4: Bis-complex 3 (X = NTf<sub>2</sub><sup>-</sup>) from 1,4-dioxane/diethylene glycol monomethyl ether.

Table 5: Crystal data and structure refinement for cu\_sc071212a

Identification code	cu_sc071212a	
Empirical formula	C <sub>201</sub> F <sub>13</sub> N <sub>8</sub> O <sub>23</sub> S <sub>4</sub> Si <sub>4</sub> Zn	
Formula weight	3447.06	
Temperature	100.01 K	
Crystal system	monoclinic	
Space group	P21/n	
Unit cell dimensions	17.8999(10) Å	$\alpha = 90^\circ$
	b = 43.968(3) Å	$\beta = 103.781(3)^\circ$
	c = 25.4895(14) Å	$\gamma = 90^\circ$
Volume	19483.2(19) Å <sup>3</sup>	
Z	4	
Density (calculated)	1.175 g/cm <sup>3</sup>	
Absorption coefficient	1.457 mm <sup>-1</sup>	
F(000)	6852.0	
Crystal size	0.2 x 0.08 x 0.03 mm <sup>3</sup>	
Radiation	CuK $\alpha$ ( $\lambda = 1.54178$ Å)	
Theta range for data collection	5.466 to 101.422°	
Index ranges	-15 $\leq$ h $\leq$ 17, -44 $\leq$ k $\leq$ 38, -22 $\leq$ l $\leq$ 25	
Reflections collected	68059	
Independent reflections	19048 [ $R_{int} = 0.0751$ , $R_{sigma} = 0.0923$ ]	
Data / restraints / parameters	19048 / 44 / 1036	
Goodness-of-fit on F <sup>2</sup>	2.163	
Final R indices	I > 2 $\sigma$ (I)	$R_1 = 0.2217$ , w $R_2 = 0.5351$
	all data	$R_1 = 0.2819$ , w $R_2 = 0.5647$
Largest diff. peak and hole	1.96 and -1.14 eÅ <sup>-3</sup>	



## 7. Appendix

### Mono-blade 41 – sc051213

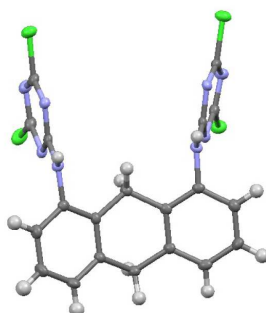


Figure 7.5: Mono-blade 41 from acetone.

Table 6: Crystal data and structure refinement for sc051213

Identification code	sc051213_Oma	
Empirical formula	C <sub>20</sub> H <sub>12</sub> N <sub>8</sub> Cl <sub>4</sub>	
Formula weight	506.18	
Temperature	100.0(2) K	
Crystal system	monoclinic	
Space group	P21/c	
Unit cell dimensions	a = 10.4062(19) Å	$\alpha = 90^\circ$
	b = 23.934(4) Å	$\beta = 90.147(5)^\circ$
	c = 8.1628(13) Å	$\gamma = 90^\circ$
Volume	2033.1(6) Å <sup>3</sup>	
Z	4	
Density (calculated)	1.654 mg/mm <sup>3</sup>	
Absorption coefficient	0.611 m/mm <sup>-1</sup>	
F(000)	1024.0	
Crystal size	0.1 x 0.05 x 0.03 mm <sup>3</sup>	
Radiation	MoK $\alpha$ ( $\lambda = 0.71073$ )	
Theta range for data collection	4.268 to 55.28°	
Index ranges	-13 ≤ h ≤ 13, -30 ≤ k ≤ 31, -10 ≤ l ≤ 10	
Reflections collected	25291	
Independent reflections	4720 [ $R_{int} = 0.0662$ , $R_{sigma} = 0.0690$ ]	
Data / restraints / parameters	4720 / 2 / 295	
Goodness-of-fit on F <sup>2</sup>	1.007	
Final R indices	I > 2 $\sigma$ (I)	$R_1 = 0.0474$ , $wR_2 = 0.0982$
	all data	$R_1 = 0.0918$ , $wR_2 = 0.1136$
Largest diff. peak and hole	0.40 and -0.39 eÅ <sup>-3</sup>	

## 7. Appendix

### Anthracene-mono-blade 50 – mo\_sc071113\_0m

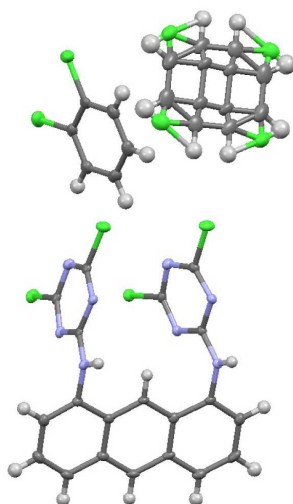


Figure 7.6: Anthracene-mono-blade 50 from ODCB.

Table 7: Crystal data and structure refinement for sc071113

<b>Identification code</b>	mo_sc071113_0m	
<b>Empirical formula</b>	$C_{29}H_{16}N_8Cl_7$	
<b>Formula weight</b>	724.65	
<b>Temperature</b>	99.97 K	
<b>Crystal system</b>	triclinic	
<b>Space group</b>	P-1	
<b>Unit cell dimensions</b>	$a = 10.941(3) \text{ \AA}$	$\alpha = 87.658(5)^\circ$
	$b = 11.836(3) \text{ \AA}$	$\beta = 71.021(5)^\circ$
	$c = 13.007(3) \text{ \AA}$	$\gamma = 71.663(5)^\circ$
<b>Volume</b>	$1508.4(6) \text{ \AA}^3$	
<b>Z</b>	2	
<b>Density (calculated)</b>	$1.595 \text{ mg/mm}^3$	
<b>Absorption coefficient</b>	$0.696 \text{ m/mm}^{-1}$	
<b>F(000)</b>	730.0	
<b>Crystal size</b>	$0.24 \times 0.05 \times 0.015 \text{ mm}^3$	
<b>Radiation</b>	MoK $\alpha$ ( $\lambda = 0.71073$ )	
<b>Theta range for data collection</b>	4.154 to $55.25^\circ$	
<b>Index ranges</b>	$-14 \leq h \leq 14, -15 \leq k \leq 15, -16 \leq l \leq 16$	
<b>Reflections collected</b>	16835	
<b>Independent reflections</b>	6982 [ $R_{int} = 0.0577$ ]	
<b>Data / restraints / parameters</b>	6982 / 56 / 439	
<b>Goodness-of-fit on <math>F^2</math></b>	0.942	
<b>Final R indices</b>	$I > 2\sigma(I)$	$R_1 = 0.0393, wR_2 = 0.0724$
	all data	$R_1 = 0.0875, wR_2 = 0.0833$
<b>Largest diff. peak and hole</b>	0.38 and $-0.39 \text{ e\AA}^{-3}$	

## 7. Appendix

### Di-blade 49 – sc011113

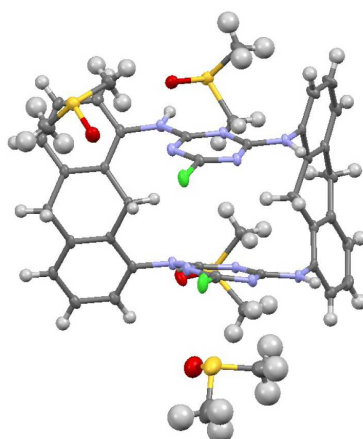


Figure 7.7: Di-blade 49 from DMSO.

Table 8: Crystal data and structure refinement for sc011113

Identification code	mo_sc011113_0m	
Empirical formula	$C_{42}H_{48}N_{10}O_4S_4Cl_2$	
Formula weight	956.04	
Temperature	99.98 K	
Crystal system	triclinic	
Space group	P-1	
Unit cell dimensions	$a = 12.778(2) \text{ \AA}$	$\alpha = 62.642(3)^\circ$
	$b = 14.281(2) \text{ \AA}$	$\beta = 66.471(3)^\circ$
	$c = 15.506(2) \text{ \AA}$	$\gamma = 70.448(3)^\circ$
Volume	$2264.2(6) \text{ \AA}^3$	
Z	2	
Density (calculated)	$1.402 \text{ mg/mm}^3$	
Absorption coefficient	$0.382 \text{ m/mm}^{-1}$	
F(000)	1000.0	
Crystal size	$0.14 \times 0.08 \times 0.035 \text{ mm}^3$	
Radiation	MoK $\alpha$ ( $\lambda = 0.71073$ )	
Theta range for data collection	$3.538$ to $55.144^\circ$	
Index ranges	$-6 \leq h \leq 16$ , $-17 \leq k \leq 18$ , $-18 \leq l \leq 20$	
Reflections collected	20009	
Independent reflections	10052 [ $R_{int} = 0.0318$ ]	
Data / restraints / parameters	10052 / 76 / 579	
Goodness-of-fit on $F^2$	1.017	
Final R indices	$I > 2\sigma(I)$	$R_1 = 0.0640$ , $wR_2 = 0.1593$
	all data	$R_1 = 0.1019$ , $wR_2 = 0.1791$
Largest diff. peak and hole	$1.67$ and $-1.64 \text{ e\AA}^{-3}$	

## 7. Appendix

### Hybrid-di-blade-(NH-O) 56 – sc160414

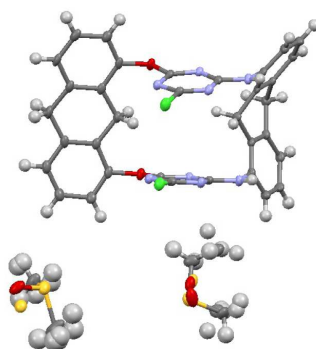


Figure 7.8: Hybrid-di-blade-(NH-O) 56 from DMSO.

Table 9: Crystal data and structure refinement for sc160414

Identification code	sc160414	
Empirical formula	$C_{38}H_{34}Cl_2N_8O_4S_2$	
Formula weight	801.75	
Temperature	100.0(2) K	
Crystal system	monoclinic	
Space group	P21/n	
Unit cell dimensions	$a = 8.7971(4) \text{ \AA}$	$\alpha = 90^\circ$
	$b = 27.8608(11) \text{ \AA}$	$\beta = 97.894(3)^\circ$
	$c = 15.0637(5) \text{ \AA}$	$\gamma = 90^\circ$
Volume	$3657.0(3) \text{ \AA}^3$	
Z	4	
Density (calculated)	$1.456 \text{ mg/mm}^3$	
Absorption coefficient	$3.113 \text{ m/mm}^{-1}$	
F(000)	1664.0	
Crystal size	$0.14 \times 0.01 \times 0.005 \text{ mm}^3$	
Radiation	CuK $\alpha$ ( $\lambda = 1.54178$ )	
Theta range for data collection	6.344 to $133.21^\circ$	
Index ranges	$-7 \leq h \leq 10, -29 \leq k \leq 32, -17 \leq l \leq 16$	
Reflections collected	24908	
Independent reflections	6366 [ $R_{int} = 0.0717, R_{sigma} = 0.0641$ ]	
Data / restraints / parameters	6366 / 628 / 544	
Goodness-of-fit on $F^2$	1.021	
Final R indices	$I > 2\sigma(I)$	$R_1 = 0.0449, wR_2 = 0.1017$
	all data	$R_1 = 0.0709, wR_2 = 0.1129$
Largest diff. peak and hole	0.30 and $-0.33 \text{ e\AA}^{-3}$	

## 8. References

- [1] H. Staudinger, *Ber. Dtsch. Chem. Ges.* **1920**, 53(6), 1073–1085.
- [2] R. Mülhaupt, *Angew. Chem. Int. Ed.* **2004**, 43(9), 1054–1063.
- [3] PlasticsEurope, <http://www.plasticseurope.org/> [Online; accessed 8-Jan-2015].
- [4] A. D. Schlüter, *CHIMIA* **2013**, 67(11), 804–810.
- [5] G. of authors, *Synthesis of Polymers: New Structures and Methods*, (Ed.: A. D. Schlüter, C. Hawker, J. Sakamoto), Wiley-VCH, Weinheim, **2012**.
- [6] H. W. Gibson, M. C. Bheda, P. T. Engen, *Prog. Polym. Sci.* **1994**, 19(5), 843–945.
- [7] S. Menzer, A. J. P. White, D. J. Williams, M. Belohradský, C. Hamers, F. M. Raymo, A. N. Shipway, J. F. Stoddart, *Macromolecules* **1998**, 31(2), 295–307.
- [8] Y. Geerts, in *Molecular Catenanes, Rotaxanes and Knots*, Wiley-VCH Verlag GmbH, Weinheim, **1999**, p. 247–276.
- [9] F. M. Raymo, J. F. Stoddart, *Chem. Rev.* **1999**, 99(7), 1643–1664.
- [10] L. Carlucci, G. Ciani, D. M. Proserpio, *Coord. Chem. Rev.* **2003**, 246(1-2), 247–289.
- [11] T. Takata, N. Kihara, Y. Furusho, in *Polymer Synthesis*, Vol. 171 of *Advances in Polymer Science*, Springer Berlin Heidelberg, **2004**, p. 1–75.
- [12] Z. Niu, H. W. Gibson, *Chem. Rev.* **2009**, 109(11), 6024–6046.
- [13] L. Fang, M. A. Olson, D. Benitez, E. Tkatchouk, W. A. Goddard III, J. F. Stoddart, *Chem. Soc. Rev.* **2010**, 39(1), 17–29.
- [14] J. Sakamoto, J. van Heijst, O. Lukin, A. D. Schlüter, *Angew. Chem. Int. Ed.* **2009**, 48(6), 1030–1069.
- [15] J. W. Colson, W. R. Dichtel, *Nat. Chem.* **2013**, 5(6), 453–465.
- [16] P. Ashton, V. Baldoni, V. Balzani, C. Claessens, A. Credi, H. D. A. Hoffmann, F. Raymo, J. F. Stoddart, M. Venturi, A. P. White, D. Williams, *Eur. J. Org. Chem.* **2000**, 2000(7), 1121–1130.
- [17] R. Mas-Balleste, C. Gomez-Navarro, J. Gomez-Herrero, F. Zamora, *Nanoscale* **2011**, 3(1), 20–30.
- [18] K. S. Novoselov, A. K. Geim, S. V. Morozov, D. Jiang, Y. Zhang, S. V. Dubonos, I. V. Grigorieva, A. A. Firsov, *Science* **2004**, 306(5696), 666–669.
- [19] The Nobel Prize in Physics 2010 was awarded jointly to Andre Geim and Konstantin Novoselov "for groundbreaking experiments regarding the two-dimensional material graphene", [http://www.nobelprize.org/nobel\\_prizes/physics/laureates/2010/](http://www.nobelprize.org/nobel_prizes/physics/laureates/2010/) [Online; accessed 8-Jan-2015].
- [20] P. Kissel, R. Erni, W. B. Schweizer, M. D. Rossell, B. T. King, T. Bauer, S. Götzinger, A. D. Schlüter, J. Sakamoto, *Nat. Chem.* **2012**, 4, 287–291.

## 8. References

---

- [21] M. D. Cohen, G. M. J. Schmidt, *J. Chem. Soc.* **1964**, 1996–2000.
- [22] G. M. J. Schmidt, *Pure Appl. Chem.* **1971**, 27(4), 647–678.
- [23] G. M. Schmidt, *Solid state photochemistry: a collection of papers; describing a symbiotic relationship between X-ray crystallography and synthetic organic photochemistry*, (Ed.: D. Ginsburg), Verlag Chemie, Weinheim, New York, **1976**.
- [24] J. W. Steed, J. L. Atwood, in *Supramolecular Chemistry*, John Wiley & Sons, Ltd, **2009**, p. 441–536.
- [25] P. Kissel, Dissertation, ETH Zurich, **2012**.
- [26] R. Bholá, P. Payamyar, D. J. Murray, B. Kumar, A. J. Teator, M. U. Schmidt, S. M. Hammer, A. Saha, J. Sakamoto, A. D. Schlüter, B. T. King, *J. Am. Chem. Soc.* **2013**, 135(38), 14134–14141.
- [27] P. Kissel, D. J. Murray, W. J. Wulftange, V. J. Catalano, B. T. King, *Nat. Chem.* **2014**, 6(6), 774–778.
- [28] M. J. Kory, M. Wörle, T. Weber, P. Payamyar, S. W. van de Poll, J. Dshemuchadse, N. Trapp, A. D. Schlüter, *Nat. Chem.* **2014**, 6, 779–784.
- [29] FROM MOLECULES TO CRYSTALS - HOW DO ORGANIC MOLECULES FORM CRYSTALS? (CRYSTALLIZE), [http://w3.cost.eu/fileadmin/domain\\_files/CMST/Action\\_CM1402/mou/CM1402-e.pdf](http://w3.cost.eu/fileadmin/domain_files/CMST/Action_CM1402/mou/CM1402-e.pdf) [Online; accessed 8-Jan-2015].
- [30] M. D. Cohen, *Angew. Chem. Int. Ed.* **1975**, 14(6), 386–393.
- [31] G. R. Desiraju, *J. Am. Chem. Soc.* **2013**, 135(27), 9952–9967.
- [32] K. Biradha, R. Santra, *Chem. Soc. Rev.* **2013**, 42(3), 950–967.
- [33] N. Watanabe, Y. Ikari, N. Kihara, T. Takata, *Macromolecules* **2004**, 37(18), 6663–6666.
- [34] R. H. Baughman, *J. Polym. Sci., Part B: Polym. Phys.* **1974**, 12(8), 1511–1535.
- [35] G. Wegner, *Pure Appl. Chem.* **1977**, 49, 443–454.
- [36] U. S. Schubert, H. Hofmeier, G. R. Newkome, *Modern Terpyridine Chemistry*, Wiley-VCH Verlag GmbH & Co. KGaA, Weinheim, **2006**.
- [37] U. S. Schubert, A. Winter, G. R. Newkome, *Terpyridine-based materials*, Wiley-VCH Verlag GmbH & Co. KGaA, Weinheim, **2011**.
- [38] A. Godt, *Eur. J. Org. Chem.* **2004**, 2004(8), 1639–1654.
- [39] P. Payamyar, K. Kaja, C. Ruiz-Vargas, A. Stemmer, D. J. Murray, C. J. Johnson, B. T. King, F. Schiffmann, J. VandeVondele, A. Renn, S. Götzinger, P. Ceroni, A. Schütz, L.-T. Lee, Z. Zheng, J. Sakamoto, A. D. Schlüter, *Adv. Mater.* **2014**, 26(13), 2052–2058.
- [40] Y. Chen, M. Li, P. Payamyar, Z. Zheng, J. Sakamoto, A. D. Schlüter, *ACS Macro Lett.* **2014**, 3(2), 153–158.
- [41] T. Bauer, Z. Zheng, A. Renn, R. Enning, A. Stemmer, J. Sakamoto, A. D. Schlüter, *Angew. Chem. Int. Ed.* **2011**, 50(34), 7879–7884.

## 8. References

---

- [42] T. Bauer, Dissertation, ETH Zurich, **2012**.
- [43] Z. Zheng, C. S. Ruiz-Vargas, T. Bauer, A. Rossi, P. Payamyar, A. Schütz, A. Stemmer, J. Sakamoto, A. D. Schlüter, *Macromol. Rapid Commun.* **2013**, *34*(21), 1670–1680.
- [44] M. J. Kory, M. Bergeler, M. Reiher, A. D. Schlüter, *Chem. Eur. J.* **2014**, *20*(23), 6934–6938.
- [45] Nobel Lecture: Concerning the Detection of X-ray Interferences, [http://www.nobelprize.org/nobel\\_prizes/physics/laureates/1914/](http://www.nobelprize.org/nobel_prizes/physics/laureates/1914/) [Online; accessed 8-Jan-2015].
- [46] W. L. Bragg, *Proc. R. Soc. London, Ser. A* **1913**, *89*(610), 248–277.
- [47] V. Enkelmann, in *Polydiacetylenes SE - 3*, Vol. 63 of *Advances in Polymer Science*, (Published by H.-J. Cantow), Springer Berlin Heidelberg, **1984**, p. 91–136.
- [48] M. D. Hollingsworth, *Science* **2002**, *295*(5564), 2410–2413.
- [49] G. R. Desiraju, *Angew. Chem. Int. Ed.* **1995**, *34*(21), 2311–2327.
- [50] G. M. J. Schmidt, *J. Chem. Soc.* **1964**, 2014–2021.
- [51] M. A. Fernandes, D. C. Levendis, C. B. de Koning, *Cryst. Eng.* **2001**, *4*(2–3), 215–231.
- [52] Y. Sonoda, *Molecules* **2011**, *16*(1), 119–148.
- [53] D.-K. Bučar, G. S. Papaefstathiou, T. D. Hamilton, Q. L. Chu, I. G. Georgiev, L. R. MacGillivray, *Eur. J. Inorg. Chem.* **2007**, *2007*(29), 4559–4568.
- [54] V. Enkelmann, in *Recent Advances in the Quantum Theory of Polymers SE - 1*, Vol. 113 of *Lecture Notes in Physics*, (Published by J. André, J.-L. Bredas, J. Delhalle, J. Ladik, G. Leroy, C. Moser), Springer Berlin Heidelberg, **1980**, p. 1–13.
- [55] Cambridge Structural Database, <http://www.ccdc.cam.ac.uk/> [Online; accessed 8-Jan-2015].
- [56] V. Ramamurthy, *Tetrahedron* **1986**, *42*(21), 5753–5839.
- [57] G. Kaupp, in *Adv. Photochem.*, John Wiley & Sons, Inc., **1994**, p. 119–177.
- [58] A. E. Keating, M. A. Garcia-Garibay, *Organic and Inorganic Photochemistry*, Marcel Dekker, New York, Vol. 2, **1998**, p. 195–248.
- [59] G. Kaupp, *Curr. Opin. Solid State Mater. Sci.* **2002**, *6*(2), 131–138.
- [60] B. Stevens, T. Dickinson, R. R. Sharpe, *Nature* **1964**, *204*(4961), 876–877.
- [61] D. P. Craig, P. Sarti-Fantoni, *Chem. Commun.* **1966**, (20), 742–743.
- [62] M. D. Cohen, Z. Ludmer, J. M. Thomas, J. O. Williams, *J. Chem. Soc. D* **1969**, (20), 1172–1173.
- [63] Z. Ludmer, *Chem. Phys.* **1977**, *26*(1), 113–121.
- [64] E.-Z. M. Ebeid, S. E. Morsi, J. O. Williams, *J. Chem. Soc., Faraday Trans. 1 F* **1979**, *75*, 1111–1119.
- [65] E.-Z. M. Ebeid, N. J. Bridge, *J. Chem. Soc., Faraday Trans. 1 F* **1984**, *80*(5), 1131–1138.

## 8. References

---

- [66] M. A. Garcia-Garibay, *Angew. Chem. Int. Ed.* **2007**, *46*(47), 8945–8947.
- [67] A. Natarajan, B. R. Bhogala, in *Supramolecular Photochemistry*, John Wiley & Sons, Inc., **2011**, p. 175–228.
- [68] P. Zhu, W. Gu, L.-Z. Zhang, X. Liu, J.-L. Tian, S.-P. Yan, *Eur. J. Inorg. Chem.* **2008**, (19), 2971–2974.
- [69] G. Kaupp, *CrystEngComm* **2003**, *5*(23), 117–133.
- [70] G. Kaupp, in *Making Crystals by Design*, Wiley-VCH Verlag GmbH & Co. KGaA, **2006**, p. 87–148.
- [71] J. Kaiser, G. Wegner, E. W. Fischer, *Isr. J. Chem.* **1972**, *10*(2), 157–171.
- [72] M. Hasegawa, Y. Suzuki, *J. Polym. Sci., Part B: Polym. Lett.* **1967**, *5*(9), 813–815.
- [73] M. Hasegawa, Academic Press, **1995**, p. 117–171.
- [74] G. Wegner, in *Polymerization Reactions and New Polymers*, Vol. 129 of *Advances in Chemistry*, American Chemical Society, **1973**, p. 255–268.
- [75] H.-G. Braun, G. Wegner, *Makromol. Chem.* **1983**, *184*(5), 1103–1119.
- [76] V. Enkelmann, G. Wegner, K. Novak, K. B. Wagener, *J. Am. Chem. Soc.* **1993**, *115*(22), 10390–10391.
- [77] W. Köhler, K. Novak, V. Enkelmann, *J. Chem. Phys.* **1994**, *101*(12), 10474–10480.
- [78] V. Enkelmann, *Mol. Cryst. Liq. Cryst.* **1998**, *313*(1), 15–23.
- [79] H.-D. Becker, *Chem. Rev.* **1993**, *93*, 145–172.
- [80] H. D. Roth, *Angew. Chem. Int. Ed.* **1989**, *28*(9), 1193–1207.
- [81] H. Bouas-Laurent, A. Castellan, J.-p. Desvergne, R. Lapouyade, *Chem. Soc. Rev.* **2000**, *29*, 43–55.
- [82] E. J. Bowen, *Adv. Photochem.* **1963**, *1*, 23–42.
- [83] A. Noyes, G. S. Hammond, J. N. Pitts, *Adv. Photochem.* **1968**, *6*, 1–122.
- [84] E. S. Michael, S. P. Zingg, R. M. Pagni, J. H. Burns **1991**, (41), 5737–5740.
- [85] R. Dabestani, K. J. Ellis, M. E. Sigman, *J. Photochem. Photobiol., A* **1995**, *86*, 231–239.
- [86] H. Bouas-Laurent, J.-P. Desvergne, A. Castellan, R. Lapouyade, *Chem. Soc. Rev.* **2001**, *30*(4), 248–263.
- [87] H. Kotani, K. Ohkubo, S. Fukuzumi, *J. Am. Chem. Soc.* **2004**, *126*(49), 15999–16006.
- [88] H. Fidder, A. Lauer, W. Freyer, B. Koeppe, K. Heyne, *J. Phys. Chem. A* **2009**, *113*(22), 6289–6296.
- [89] E. J. Bowen, The Photochemistry of Aromatic Hydrocarbon Solutions, *Advances in Photochemistry* **1963**, *1*, 23–42.



## 8. References

---

- [90] D. M. Bassani, in *Supramolecular Photochemistry*, John Wiley & Sons, Inc., **2011**, p. 53–86.
- [91] M. Kaftory, in *Supramolecular Photochemistry*, John Wiley & Sons, Inc., **2011**, p. 229–266.
- [92] H. Bouas-Laurent, A. Castellan, M. Daney, J. P. Desvergne, G. Guinand, P. Marsau, M. H. Riffaud, *J. Am. Chem. Soc.* **1986**, *108*(2), 315–317.
- [93] F. Fages, J.-P. Desvergne, I. Frisch, H. Bouas-Laurent, *J. Chem. Soc., Chem. Commun.* **1988**, (21), 1413–1415.
- [94] M. Horiguchi, Y. Ito, *J. Org. Chem.* **2006**, *71*(9), 3608–3611.
- [95] S. Tsuzuki, K. Honda, T. Uchimarū, M. Mikami, K. Tanabe, *J. Am. Chem. Soc.* **2001**, *124*(1), 104–112.
- [96] E. A. Meyer, R. K. Castellano, F. Diederich, *Angew. Chem. Int. Ed.* **2003**, *42*(11), 1210–1250.
- [97] L. M. Salonen, M. Ellermann, F. Diederich, *Angew. Chem. Int. Ed.* **2011**, *50*(21), 4808–4842.
- [98] T. Hinoue, Y. Shigenoi, M. Sugino, Y. Mizobe, I. Hisaki, M. Miyata, N. Tohnai, *Chem. Eur. J.* **2012**, *18*(15), 4634–4643.
- [99] I. Zouev, D.-K. Cao, T. V. Sreevidya, M. Telzhensky, M. Botoshansky, M. Kaftory, *CrystEngComm* **2011**, *13*(13), 4376–4381.
- [100] A. N. Sokolov, T. Frišćić, L. R. MacGillivray, *J. Am. Chem. Soc.* **2006**, *128*(9), 2806–2807.
- [101] D. M. Cho, S. R. Parkin, M. D. Watson, *Org. Lett.* **2005**, *7*(6), 1067–1068.
- [102] F. Cozzi, S. Bacchi, G. Filippini, T. Pilati, A. Gavezzotti, *Chem. Eur. J.* **2007**, *13*(25), 7177–7184.
- [103] S. T. Cerqua, diploma thesis, Johannes Gutenberg-Universität Mainz, **2011**.
- [104] S. Singh, C. Sandorfy, *Can. J. Chem.* **1969**, *47*(2), 257–263.
- [105] G. Schill, in *Catenanes, Rotaxanes, and Knots*, Vol. 22 of *Organic Chemistry: A Series of Monographs*, New York: Academic Press, **1971**.
- [106] O. Safarowsky, B. Windisch, A. Mohry, F. Vögtle, *J. Prakt. Chem.* **2000**, *342*(5), 437–444.
- [107] E. Wasserman, *J. Am. Chem. Soc.* **1960**, *82*(16), 4433–4434.
- [108] G. Schill, A. Lüttringhaus, *Angew. Chem. Int. Ed.* **1964**, *3*(8), 546–547.
- [109] G. Agam, A. Zilkha, *J. Am. Chem. Soc.* **1976**, *98*, 5214–5216.
- [110] H. L. Frisch, E. Wasserman, *J. Am. Chem. Soc.* **1961**, *83*(18), 3789–3795.
- [111] W. Vetter, G. Schill, *Tetrahedron* **1967**, *23*(7), 3079–3093.
- [112] B. Hudson, J. Vinograd, *Nature* **1967**, *216*, 647–652.
- [113] D. A. Clayton, J. Vinograd, *Nature* **1967**, *216*, 652–657.

## 8. References

---

- [114] C. O. Dietrich-Buchecker, J. P. Sauvage, J. P. Kintzinger, *Tetrahedron Lett.* **1983**, 24(46), 5095–5098.
- [115] C. O. Dietrich-Buchecker, J. P. Sauvage, J. M. Kern, *J. Am. Chem. Soc.* **1984**, 106, 3043–3045.
- [116] D. H. Busch, in *Templates in Chemistry II SE - 1*, Vol. 249 of *Topics in Current Chemistry*, (Published by C. A. Schalley, F. Vögtle, K. H. Dötz), Springer Berlin Heidelberg, **2005**, p. 1–65.
- [117] A. M. Albrecht-Gary, Z. Saad, C. O. Dietrich-Buchecker, J. P. Sauvage, *J. Am. Chem. Soc.* **1985**, 107(11), 3205–3209.
- [118] C. O. Dietrich-Buchecker, J. P. Sauvage, *Chem. Rev.* **1987**, 87, 795–810.
- [119] J.-M. Kern, J.-P. Sauvage, G. Bidan, B. Divisia-Blohorn, *J. Polym. Sci., Part A: Polym. Chem.* **2003**, 41, 3470–3477.
- [120] J.-Y. Ortholand, A. M. Z. Slawin, N. Spencer, J. F. Stoddart, D. J. Williams, *Angew. Chem. Int. Ed.* **1989**, 28, 1394–1395.
- [121] J. F. Stoddart, H.-R. Tseng, *Proc. Natl. Acad. Sci. U.S.A.* **2002**, 99(8), 4797–4800.
- [122] F. Vögtle, S. Meier, R. Hoss, *Angew. Chem. Int. Ed.* **1992**, 31(12), 1619–1622.
- [123] C. A. Hunter, *J. Am. Chem. Soc.* **1992**, 114(13), 5303–5311.
- [124] H. Adams, F. J. Carver, C. A. Hunter, *J. Chem. Soc., Chem. Commun.* **1995**, (8), 809–810.
- [125] L. C. Gilday, T. Lang, A. Caballero, P. J. Costa, V. Félix, P. D. Beer, *Angew. Chem. Int. Ed.* **2013**, 52(16), 4356–4360.
- [126] P. Ruggli, *Liebigs Ann.* **1912**, 392(1), 92–100.
- [127] K. Ziegler, H. Eberle, H. Ohlinger, *Liebigs Ann.* **1933**, 504(1), 94–130.
- [128] B. Mohr, J.-P. Sauvage, R. H. Grubbs, M. Weck, *Angew. Chem. Int. Ed.* **1997**, 36(12), 1308–1310.
- [129] D. B. Amabilino, P. R. Ashton, A. S. Reder, N. Spencer, J. F. Stoddart, *Angew. Chem. Int. Ed.* **1994**, 33(12), 1286–1290.
- [130] F. Schwanke, O. Safarowsky, C. Heim, G. Silva, F. Vögtle, *Helv. Chim. Acta* **2000**, 83(12), 3279–3290.
- [131] J.-L. Weidmann, J.-M. Kern, J.-P. Sauvage, D. Muscat, S. Mullins, W. Köhler, C. Rosenauer, H. J. Räder, K. Martin, Y. Geerts, *Chem. Eur. J.* **1999**, 5(6), 1841–1851.
- [132] C. Glaser, *Ber. Dtsch. Chem. Ges.* **1869**, 2(1), 422–424.
- [133] T. D. Shaffer, L.-M. Tsay, *J. Polym. Sci., Part A: Polym. Chem.* **1991**, 29(8), 1213–1215.
- [134] D. B. Amabilino, J. F. Stoddart, *Chem. Rev.* **1995**, 95(8), 2725–2828.
- [135] D. B. Amabilino, P. R. Ashton, V. Balzani, S. E. Boyd, A. Credi, J. Y. Lee, S. Menzer, J. F. Stoddart, M. Venturi, D. J. Williams, *J. Am. Chem. Soc.* **1998**, 120, 4295–4307.

## 8. References

---

- [136] S. R. Batten, N. R. Champness, X.-m. Chen, J. Garcia-martinez, S. Kitagawa, L. Öhrström, M. O. Keeffe, M. P. Suh, J. Reedijk, *Pure Appl. Chem.* **2013**, *85*(8), 1715–1724.
- [137] S. R. Batten, R. Robson, *Angew. Chem. Int. Ed.* **1998**, *37*(11), 1460–1494.
- [138] S. R. Batten, R. Robson, in *Molecular Catenanes, Rotaxanes and Knots*, Wiley-VCH Verlag GmbH, Weinheim, **1999**, p. 77–106.
- [139] H.-L. Jiang, T. A. Makal, H.-C. Zhou, *Coord. Chem. Rev.* **2013**, *257*(15–16), 2232–2249.
- [140] J. Heine, J. Schmedt auf der Günne, S. Dehnen, *J. Am. Chem. Soc.* **2011**, *133*(26), 10018–10021.
- [141] L. Jiang, P. Ju, X.-R. Meng, X.-J. Kuang, T.-B. Lu, *Sci. Rep.* **2012**, *2*(668), 1–5.
- [142] Q. Chen, F. Jiang, D. Yuan, G. Lyu, L. Chen, M. Hong, *Chem. Sci.* **2014**, *5*, 483–488.
- [143] G. T. Morgan, F. H. Burstall, *J. Chem. Soc.* **1932**, 20–30.
- [144] G. Morgan, F. H. Burstall, *J. Chem. Soc.* **1937**, 1649–1655.
- [145] J.-M. Lehn, in *Supramolecular Chemistry*, Wiley-VCH Verlag GmbH & Co. KGaA, **1995**.
- [146] S. Leininger, B. Olenyuk, P. J. Stang, *Chem. Rev.* **2000**, *100*(3), 853–908.
- [147] G. F. Swiegers, T. J. Malefetse, *Coord. Chem. Rev.* **2002**, *225*(1–2), 91–121.
- [148] R. H. Holyer, C. D. Hubbard, S. F. A. Kettle, R. G. Wilkins, *Inorg. Chem.* **1966**, *5*(4), 622–625.
- [149] W. Huang, H. Qian, *J. Mol. Struct.* **2007**, *832*(1-3), 108–116.
- [150] J. E. Beves, E. C. Constable, C. E. Housecroft, M. Neuburger, S. Schaffner, J. A. Zampese, *Eur. J. Org. Chem.* **2008**, (20), 3569–3581.
- [151] R. Annunziata, M. Benaglia, A. Puglisi, L. Raimondi, F. Cozzi, *Eur. J. Org. Chem.* **2008**, (23), 3976–3983.
- [152] T. N. Y. Hoang, T. Lathion, L. Guénée, E. Terazzi, C. Piguet, *Inorg. Chem.* **2012**, *51*(15), 8567–8575.
- [153] K. Lashgari, M. Kritikos, R. Norrestam, T. Norrby, *Acta Crystallogr., Sect. C: Cryst. Struct. Commun.* **1999**, *55*(1), 64–67.
- [154] G. Schwarzenbach, *Helv. Chim. Acta* **1952**, *35*(7), 2344–2359.
- [155] A. D. McNaught, A. Wilkinson, *Compendium of Chemical Terminology: IUPAC Recommendations*, IUPAC Chemical Data Series, Blackwell Science, **1997**.
- [156] E. C. Constable, in *Adv. Inorg. Chem.*, Vol. 30, (Published by H. J. Emeléus), Academic Press, **1986**, p. 69–121.
- [157] F. Blau, *Ber. Dtsch. Chem. Ges.* **1888**, *21*(1), 1077–1078.
- [158] P. R. Andres, Dissertation, Technische Universiteit Eindhoven, **2004**.
- [159] E. C. Constable, A. M. W. C. Thompson, *J. Chem. Soc., Dalton Trans.* **1992**, (24), 3467–3475.

## 8. References

---

- [160] A. M. W. Cargill Thompson, *Coord. Chem. Rev.* **1997**, *160*, 1–52.
- [161] W. Zecher, F. Kröhnke, *Chem. Ber.* **1961**, *94*(3), 690–697.
- [162] F. Kröhnke, *Synthesis* **1976**, *1976*(01), 1–24.
- [163] The Nobel Prize in Chemistry 2010 was awarded jointly to Richard F. Heck, Ei-ichi Negishi and Akira Suzuki "for palladium-catalyzed cross couplings in organic synthesis", [http://www.nobelprize.org/nobel\\_prizes/chemistry/laureates/2010/](http://www.nobelprize.org/nobel_prizes/chemistry/laureates/2010/) [Online; accessed 8-Jan-2015].
- [164] N. Miyaura, K. Yamada, A. Suzuki, *Tetrahedron Lett.* **1979**, *20*(36), 3437–3440.
- [165] N. Miyaura, A. Suzuki, *Chem. Rev.* **1995**, *95*(7), 2457–2483.
- [166] A. O. King, N. Okukado, E.-i. Negishi, *J. Chem. Soc., Chem. Commun.* **1977**, (19), 683–684.
- [167] E. Negishi, *Acc. Chem. Res.* **1982**, *15*(11), 340–348.
- [168] D. Milstein, J. K. Stille, *J. Am. Chem. Soc.* **1978**, *100*(11), 3636–3638.
- [169] J. K. Stille, *Angew. Chem. Int. Ed.* **1986**, *25*(6), 508–524.
- [170] E. C. Constable, M. D. Ward, *J. Chem. Soc., Dalton Trans.* **1990**, (4), 1405–1409.
- [171] U. S. Schubert, S. Schmatloch, A. A. Precup, *Des. Monomers Polym.* **2002**, *5*(2-3), 211–221.
- [172] S. Kelch, M. Rehahn, *Macromolecules* **1999**, *32*(18), 5818–5828.
- [173] U. S. Schubert, C. Eschbaumer, *Angew. Chem. Int. Ed.* **2002**, *41*(16), 2892–2926.
- [174] P. Andres, R. Lunkwitz, G. Pabst, K. Böhn, D. Wouters, S. Schmatloch, U. Schubert, *Eur. J. Org. Chem.* **2003**, *2003*(19), 3769–3776.
- [175] J. P. Sauvage, M. Ward, *Inorg. Chem.* **1991**, *30*(20), 3869–3874.
- [176] C. O. Dietrich-Buchecker, P. A. Marnot, J. P. Sauvage, J. P. Kintzinger, P. Maltese, *Nouv. J. Chim.* **1984**, *8*(10), 573–582.
- [177] J. R. Kirchhoff, D. R. McMillin, P. A. Marnot, J. P. Sauvage, *J. Am. Chem. Soc.* **1985**, *107*(5), 1138–1141.
- [178] J.-F. Ayme, J. Lux, J.-P. Sauvage, A. Sour, *Chem. Eur. J.* **2012**, *18*(18), 5565–5573.
- [179] S. Y. Brauchli, E. C. Constable, K. Harris, D. Haussinger, C. E. Housecroft, P. J. Rosel, J. A. Zampese, *Dalton Trans.* **2010**, *39*(44), 10739–10748.
- [180] N. W. Alcock, P. R. Barker, J. M. Haider, M. J. Hannon, C. L. Painting, Z. Pikramenou, E. A. Plummer, K. Rissanen, P. Saarenketo, *J. Chem. Soc., Dalton Trans.* **2000**, (9), 1447–1462.
- [181] B. G. G. Lohmeijer, U. S. Schubert, *J. Polym. Sci., Part A: Polym. Chem.* **2003**, *41*(10), 1413–1427.
- [182] M. L. Scudder, H. A. Goodwin, I. G. Dance, *New J. Chem.* **1999**, *23*(7), 695–705.

## 8. References

---

- [183] E. Breuning, G. S. Hanan, F. J. Romero-Salguero, A. M. Garcia, P. N. W. Baxter, J.-M. Lehn, E. Wegelius, K. Rissanen, H. Niergengarten, A. v. Dorselaer, *Chem. Eur. J.* **2002**, *2*(15), 3458–3466.
- [184] M. Barboiu, E. Petit, G. Vaughan, *Chem. Eur. J.* **2004**, *10*(9), 2263–2270.
- [185] I. Eryazici, P. Wang, C. N. Moorefield, M. Panzer, S. Durmus, C. D. Shreiner, G. R. Newkome, *Dalton Trans.* **2007**, (6), 626–628.
- [186] J. M. Ludlow Iii, M. Tominaga, Y. Chujo, A. Schultz, X. Lu, T. Xie, K. Guo, C. N. Moorefield, C. Wesdemiotis, G. R. Newkome, *Dalton Trans.* **2014**, *43*(25), 9604–9611.
- [187] S.-S. Sun, A. S. Silva, I. M. Brinn, A. J. Lees, *Inorg. Chem.* **2000**, *39*(7), 1344–1345.
- [188] S.-S. Sun, A. J. Lees, *Inorg. Chem.* **2001**, *40*(13), 3154–3160.
- [189] A. M. Garcia, D. M. Bassani, J.-M. Lehn, G. Baum, D. Fenske, *Chem. Eur. J.* **1999**, *5*(4), 1234–1238.
- [190] B. G. G. Lohmeijer, U. S. Schubert, *Angew. Chem. Int. Ed.* **2002**, *41*(20), 3825–3829.
- [191] S. Schmatloch, A. M. J. V. D. Berg, A. S. Alexeev, H. Hofmeier, U. S. Schubert, *Macromolecules* **2003**, *36*, 9943–9949.
- [192] H. Hofmeier, S. Schmatloch, D. Wouters, U. S. Schubert, *Macromol. Chem. Phys.* **2003**, *204*(18), 2197–2203.
- [193] U. S. Schubert, C. Eschbaumer, P. Andres, H. Hofmeier, C. H. Weidl, E. Herdtweck, E. Dulkeith, A. Morteani, N. E. Hecker, J. Feldmann, *Synth. Met.* **2001**, *121*(1–3), 1249–1252.
- [194] M. Heller, U. S. Schubert, *Macromol. Rapid Commun.* **2001**, *22*(16), 1358–1363.
- [195] S. Schmatloch, M. F. González, U. S. Schubert, *Macromol. Rapid Commun.* **2002**, *23*(16), 957–961.
- [196] H. Hofmeier, U. S. Schubert, *Macromol. Chem. Phys.* **2003**, *204*(11), 1391–1397.
- [197] H. Hofmeier, R. Hoogenboom, M. E. L. Wouters, U. S. Schubert, *J. Am. Chem. Soc.* **2005**, *127*(9), 2913–2921.
- [198] J.-F. Gohy, B. G. G. Lohmeijer, U. S. Schubert, *Macromol. Rapid Commun.* **2002**, *23*(9), 555–560.
- [199] Y. Ding, P. Wang, Y.-K. Tian, Y.-J. Tian, F. Wang, *Chem. Commun.* **2013**, *49*(53), 5951–5953.
- [200] H. Hofmeier, A. El-ghayoury, A. P. H. J. Schenning, U. S. Schubert, *Chem. Commun.* **2004**, (3), 318–319.
- [201] F. J. Uribe-Romo, W. R. Dichtel, *Nat. Chem.* **2012**, *4*(4), 244–245.
- [202] J. Michl, T. F. Magnera, *Proc. Natl. Acad. Sci. U.S.A.* **2002**, *99*(8), 4788–4792.
- [203] D. F. Perepichka, F. Rosei, *Science* **2009**, *323*, 216–217.
- [204] M. O’Keeffe, B. G. Hyde, *Philos. Trans. R. Soc., A* **1980**, *295*(1417), 553–618.

## 8. References

---

- [205] G. Gee, E. K. Rideal, *Proc. R. Soc. Lond. A* **1935**, *153*(878), 116–128.
- [206] G. Gee, *Proc. R. Soc. Lond. A* **1935**, *153*(878), 129–141.
- [207] G. Gee, *Trans. Faraday Soc.* **1936**, *32*, 187–195.
- [208] G. Gee, E. K. Rideal, *J. Chem. Soc.* **1937**, 772–778.
- [209] P. M. Budd, *Science* **2007**, *316*(5822), 210–211.
- [210] K. S. Novoselov, D. Jiang, F. Schedin, T. J. Booth, V. V. Khotkevich, S. V. Morozov, A. K. Geim, *Proc. Natl. Acad. Sci. U.S.A.* **2005**, *102*(30), 10451–10453.
- [211] C. Jin, F. Lin, K. Suenaga, S. Iijima, *Phys. Rev. Lett.* **2009**, *102*(19), 195505–1–195505–5.
- [212] P. Joensen, R. F. Frindt, S. Morrison, *Mater. Res. Bull.* **1986**, *21*(4), 457–461.
- [213] J. W. Colson, A. R. Woll, A. Mukherjee, M. P. Levendorf, E. L. Spitler, V. B. Shields, M. G. Spencer, J. Park, W. R. Dichtel, *Science* **2011**, *332*(6026), 228–231.
- [214] I. Berlanga, M. L. Ruiz-González, J. M. González-Calbet, J. L. G. Fierro, R. Mas-Ballesté, F. Zamora, *Small* **2011**, *7*(9), 1207–1211.
- [215] I. Berlanga, R. Mas-Balleste, F. Zamora, *Chem. Commun.* **2012**, *48*(64), 7976–7978.
- [216] D. N. Bunck, W. R. Dichtel, *J. Am. Chem. Soc.* **2013**, *135*(40), 14952–14955.
- [217] P. Amo-Ochoa, L. Welte, R. González-Prieto, P. J. Sanz Miguel, C. J. Gómez-García, E. Mateo-Martí, S. Delgado, J. Gómez-Herrero, F. Zamora, *Chem. Commun.* **2010**, *46*(19), 3262–3264.
- [218] P.-Z. Li, Y. Maeda, Q. Xu, *Chem. Commun.* **2011**, *47*(29), 8436–8438.
- [219] J.-C. Tan, P. J. Saines, E. G. Bithell, A. K. Cheetham, *ACS Nano* **2011**, *6*(1), 615–621.
- [220] M. Xu, T. Liang, M. Shi, H. Chen, *Chem. Rev.* **2013**, *113*(5), 3766–3798.
- [221] A. Gallego, C. Hermosa, O. Castillo, I. Berlanga, C. J. Gómez-García, E. Mateo-Martí, J. I. Martínez, F. Flores, C. Gómez-Navarro, J. Gómez-Herrero, S. Delgado, F. Zamora, *Adv. Mater.* **2013**, *25*(15), 2141–2146.
- [222] E. Bianco, S. Butler, S. Jiang, O. D. Restrepo, W. Windl, J. E. Goldberger, *ACS Nano* **2013**, *7*(5), 4414–4421.
- [223] T. Kambe, R. Sakamoto, K. Hoshiko, K. Takada, M. Miyachi, J.-H. Ryu, S. Sasaki, J. Kim, K. Nakazato, M. Takata, H. Nishihara, *J. Am. Chem. Soc.* **2013**, *135*(7), 2462–2465.
- [224] A. Kuhn, T. Holzmann, J. Nuss, B. V. Lotsch, *J. Mater. Chem. A* **2014**, *2*(17), 6100–6106.
- [225] C. A. Hunter, K. R. Lawson, J. Perkins, C. J. Urch, *J. Chem. Soc., Perkin Trans. 2* **2001**, (5), 651–669.
- [226] K. Baek, G. Yun, Y. Kim, D. Kim, R. Hota, I. Hwang, D. Xu, Y. H. Ko, G. H. Gu, J. H. Suh, C. G. Park, B. J. Sung, K. Kim, *J. Am. Chem. Soc.* **2013**, *135*(17), 6523–6528.
- [227] J. Sakamoto, in *Sequence-Controlled Polymers: Synthesis, Self-Assembly, and Properties*, American Chemical Society, ACS Symposium Series, **2014**, p. 369–378.

## 8. References

---

- [228] T.-y. Zhou, F. Lin, Z.-t. Li, X. Zhao, *Macromolecules* **2013**, *46*, 7745–7752.
- [229] G. R. Newkome, D. C. Hager, G. E. Kiefer, *J. Org. Chem.* **1986**, *51*(6), 850–853.
- [230] Y. Uchida, M. Okabe, H. Kobayashi, S. Oae, *Synthesis* **1995**, (8), 939–940.
- [231] Y. Uchida, N. Echikawa, S. Oae, *Heteroat. Chem.* **1994**, *5*(4), 409–413.
- [232] M. Schmittel, H. Ammon, *Synlett* **1999**, *1999*(6), 750–752.
- [233] K. Onitsuka, M. Fujimoto, H. Kitajima, N. Ohshiro, F. Takei, S. Takahashi, *Chem. Eur. J.* **2004**, *10*(24), 6433–6446.
- [234] P. Kissel, F. Weibel, L. Federer, J. Sakamoto, A. D. Schlüter, *Synlett* **2008**, (12), 1793–1796.
- [235] S. Nahm, S. M. Weinreb, *Tetrahedron Lett.* **1981**, *22*(39), 3815–3818.
- [236] Y. Uchida, Y. Takaya, S. Oae, *Heterocycles* **1990**, *30*(1), 347–351.
- [237] S. Takahashi, Y. Kuroyama, K. Sonogashira, N. Hagihara, *Synthesis* **1980**, *1980*(08), 627–630.
- [238] S. Huang, J. M. Tour, *J. Org. Chem.* **1999**, *64*(24), 8898–8906.
- [239] Y. Cakmak, E. U. Akkaya, *Org. Lett.* **2008**, *11*(1), 85–88.
- [240] M. W. Haenel, D. Jakubik, C. Krüger, P. Betz, *Chem. Ber.* **1991**, *124*(2), 333–336.
- [241] M. Pérez-Trujillo, I. Maestre, C. Jaime, A. Alvarez-Larena, J. F. Piniella, A. Virgili, *Tetrahedron: Asymmetry* **2005**, *16*(18), 3084–3093.
- [242] H. A. Dieck, F. R. Heck, *J. Organomet. Chem.* **1975**, *93*(2), 259–263.
- [243] M. S. Khan, M. R. a. Al-Mandhary, M. K. Al-Suti, A. K. Hisahm, P. R. Raithby, B. Ahrens, M. F. Mahon, L. Male, E. a. Marseglia, E. Tedesco, R. H. Friend, A. Kohler, N. Feeder, S. J. Teat, A. Köhler, *J. Chem. Soc., Dalton Trans.* **2002**, (7), 1358–1368.
- [244] A. Khatyr, R. Ziessel, *Org. Lett.* **2001**, *3*(12), 1857–1860.
- [245] S. Schmatloch, H. Hofmeier, U. S. Schubert, in *Macromolecules Containing Metal and Metal-Like Elements*, John Wiley & Sons, Inc., **2005**, p. 69–82.
- [246] B. G. G. Lohmeijer, U. S. Schubert, *Macromol. Chem. Phys.* **2003**, *204*(8), 1072–1078.
- [247] J. J. S. Lamba, C. L. Fraser, M. Road, V. Charlottes, R. V. August, *J. Am. Chem. Soc.* **1997**, *7863*, 1801–1802.
- [248] M. A. R. Meier, B. G. G. Lohmeijer, U. S. Schubert, *Macromol. Rapid Commun.* **2003**, *24*(14), 852–857.
- [249] K. Peter, M. Thelakkat, *Macromolecules* **2003**, *36*(6), 1779–1785.
- [250] M. A. R. Meier, H. Hofmeier, C. H. Abeln, C. Tziatzios, M. Rasa, D. Schubert, U. S. Schubert, *e-Polymers* **2006**, (16), 1–7.

## 8. References

---

- [251] R. Dobrawa, P. Ballester, C. R. Saha-Möller, F. Würthner, in *Metal-Containing and Metallo-supramolecular Polymers and Materials*, Vol. 928, American Chemical Society, **2006**, p. 4–43.
- [252] E. C. Constable, K. Harris, C. E. Housecroft, M. Neuburger, J. A. Zampese, *Dalton Trans.* **2011**, 40(43), 11441–11450.
- [253] M. P. Sibi, G. Petrovic, *Tetrahedron: Asymmetry* **2003**, 14(19), 2879–2882.
- [254] C. Haensch, M. Chipier, C. Ulbricht, A. Winter, S. Hoepfener, U. S. Schubert, *Langmuir* **2008**, 24(22), 12981–12985.
- [255] F. Grimm, N. Ulm, F. Gröhn, J. Düring, A. Hirsch, *Chem. Eur. J.* **2011**, 17(34), 9478–9488.
- [256] C. Hamann, J.-M. Kern, J.-P. Sauvage, *Inorg. Chem.* **2003**, 42(6), 1877–1883.
- [257] A. Wild, A. Winter, M. D. Hager, U. S. Schubert, *Analyst* **2012**, 137(10), 2333–2337.
- [258] P. Wang, C. N. Moorefield, G. R. Newkome, *Angew. Chem. Int. Ed.* **2005**, 44(11), 1679–1683.
- [259] J. Guo, P. C. Mayers, G. A. Breault, C. a. Hunter, *Nat. Chem.* **2010**, 2(3), 218–222.
- [260] J. Carney, R. Hammer, M. Hulce, C. Lomas, D. Miyashiro, *Synthesis* **2012**, 44(16), 2560–2566.
- [261] T. Dohi, N. Takenaga, A. Goto, H. Fujioka, Y. Kita, R. V. June, *J. Org. Chem.* **2008**, 73(18), 7365–7368.
- [262] A. Dahan, T. Ashkenazi, V. Kuznetsov, S. Makievski, E. Drug, L. Fadeev, M. Bramson, S. Schokoroy, E. Rozenshine-Kemelmakher, M. Gozin, *J. Org. Chem.* **2007**, 72(7), 2289–2296.
- [263] C.-Z. Zhang, H. Yang, D.-L. Wu, G.-Y. Lu, *Chin. J. Chem.* **2007**, 25(5), 653–660.
- [264] C.-Z. Zhang, C. Lu, J. Zhu, C.-y. Wang, G.-y. Lu, C.-s. Wang, D.-l. Wu, F. Liu, Y. Cui, *Chem. Mater.* **2008**, 20(14), 4628–4641.
- [265] C. Z. Zhang, J. Zhu, C. Lu, G.-Y. Lu, Y. Cui, *Mater. Chem. Phys.* **2009**, 114(2-3), 515–517.
- [266] C.-Z. Zhang, H. Cao, C. Im, G.-Y. Lu, *J. Phys. Chem. A* **2009**, 113(44), 12295–12303.
- [267] H. A. Staab, P. Kirsch, M. F. Zippies, A. Weinges, C. Krieger, *Chem. Ber.* **1994**, 127(9), 1653–1665.
- [268] Y. Sha, Y. Dong, *Synth. Commun.* **2003**, 33(15), 2599–2604.
- [269] G. Blotny, *Tetrahedron* **2006**, 62(41), 9507–9522.
- [270] T. J. Mooibroek, P. Gamez, *Inorg. Chim. Acta* **2007**, 360(1), 381–404.
- [271] H. E. Fierz-David, M. Matter, *J. Soc. Dyers Colour.* **1937**, 53, 424–436.
- [272] J. T. Thurston, J. R. Dudley, D. W. Kaiser, I. Hechenbleikner, F. C. Schaefer, D. Holm-Hansen, *J. Am. Chem. Soc.* **1951**, 73(7), 2981–2983.



## 8. References

---

- [273] K. Huthmacher, D. Most, in *Ullmann's Encyclopedia of Industrial Chemistry*, Wiley-VCH Verlag GmbH & Co. KGaA, **2000**.
- [274] M. B. Steffensen, E. Hollink, F. Kuschel, M. Bauer, E. E. Simanek, *J. Polym. Sci., Part A: Polym. Chem.* **2006**, *44*(11), 3411–3433.
- [275] M. B. Steffensen, E. E. Simanek, *Angew. Chem. Int. Ed.* **2004**, *43*(39), 5178–5180.
- [276] E. E. Simanek, H. Abdou, S. Lalwani, J. Lim, M. Mintzer, V. J. Venditto, B. Vittur, *Proc. R. Soc. A* **2010**, *466*, 1445–1468.
- [277] K. Schwetlick, *Organikum*, Wiley-VCH, Weinheim, Vol. 22, **2004**, p. 308–310.
- [278] R. Willstätter, H. Kubli, *Ber. Dtsch. Chem. Ges.* **1908**, *41*(2), 1936–1940.
- [279] H. K. Porter, in *Organic Reactions*, John Wiley & Sons, Inc., **2004**.
- [280] D. R. Coulson, L. C. Satek, S. O. Grim, John Wiley & Sons, Inc., **2007**, p. 121–124.
- [281] F.-A. Kang, N. Jain, Z. Sui, *Tetrahedron Lett.* **2006**, *47*(51), 9021–9024.
- [282] Z. Dai, G. Proni, D. Mancheno, S. Karimi, N. Berova, J. W. Canary, *J. Am. Chem. Soc.* **2004**, *126*(38), 11760–11761.
- [283] D. P. Lydon, D. Albesa-Jové, G. C. Shearman, J. M. Seddon, J. A. K. Howard, T. B. Marder, P. J. Low, *Liq. Cryst.* **2008**, *35*(2), 119–132.
- [284] D. Türp, M. Wagner, V. Enkelmann, K. Müllen, *Angew. Chem. Int. Ed.* **2011**, *50*(21), 4962–4965.
- [285] A. Andreani, M. Rambaldi, D. Bonazzi, G. Lelli, L. Greci, R. Bossa, I. Galatulas, *Arch. Pharm.* **1985**, *318*(5), 400–405.

### 9. Acknowledgments

First of all I would like to thank *Prof. A. Dieter Schlüter* for giving me the opportunity to work in his group at ETH Zurich. His support, patience, and guidance throughout my PhD was significant for the progress of the projects.

Further thanks go to my supervisor *Prof. Junji Sakamoto*. His astute ideas (especially in invigorating the research on "poly[n]catenane") as well as his guidance and suggestions were much appreciated. Also the SNF (21-129660) for their financial support.

The scientific inputs by *Prof. Benjamin T. King* and *Prof. Gerhard Wegner* are greatly acknowledged.

Furthermore, I would like to thank *Dr. Bernd Schweizer*, *Dr. Nils Trapp*, and *Michael Solar* for measuring and solving many of the XRD crystal structures.

Thanks go to the LOC at ETH Zurich for the HRMS measurements. I am very grateful for numerous measurements by *Rolf Häfliger*. The measurements by *Dr. Xiangyang Zhang*, *Louis Bertschi*, and *Oswald Greter* are also greatly acknowledged.

I am thankful to *Dr. René Verel* for the help with all NMR related issues. The support by *Doris Sutter* is also greatly appreciated.

If you need any help at measurements, at fixing broken machines, or at designing LED reactors, then *Dr. Thomas Schweizer* is the man to ask. Thank you very much, for this allround support.

The powder XRD measurements by *Dr. Julia Dshemuchadse* are greatly appreciated.

The introduction and permission to use the optical microscope by *Dr. Kirill Feldman* and *Prof. Paul Smith* is greatly appreciated.

I am also very thankful for the numerous scientific inputs by *Max J. Kory* and his suggestion to synthesize the amine-bearing monomer presented in this thesis. I also thank *Dr. Patrick Kissel* who provided the preliminary results for the poly[n]catenane approach.

I also thank *Vivian Müller* for the Langmuir through experiments, SEM, and AFM measurements.

Furthermore, I would like to thank my student *Jessica Schulz* for her help in the lab.

## 9. Acknowledgments

---

The solid-state UV/Vis spectroscopy measurements by *Dr. Andrea Grotzky* and *Dr. Florian Heiligttag*, the introduction to the fluorescence spectrometer by *Dr. Sara Fornera*, the introduction to the UV/Vis spectrometer by *Dr. Thomas Bauer*, the introduction to the IR spectrometer and to the fiber-coupled LEDs by *Payam Payamyar*, and Raman spectroscopy measurements by *Tobias Keplinger* were all gratefully acknowledged.

Thanks go to *Prof. Manfred Schmidt* for allowing me to use their analytical GPC, as well as his and *Dr. Karl Fischer's* scientific input. The remaining measurements by *Eva Wächtersbach* are greatly acknowledged.

I would also like to thank *Daniela Zehnder* for the general administrative support, *Dr. Damir Bozic* for all computer related issues.

At my stay in ETH Zurich, I have so far enjoyed the company of a number of great colleagues. My H522 lab colleagues *Dr. Samuel Jakob*, *Dr. Jingyi Rao*, *Dr. Andri Schütz*, *Wenyang Dai*, and *Vivian Müller* were great. I also enjoyed the good morning coffee sessions with the current colleague *Andreas Kuchler*. Thank you all!

I would like to set apart and thank *Dr. Julia Baettig*, *Bernd Deffner*, *Johannes Eckert*, *Chiara Gstrein*, *Dr. Tim Hungerland*, *Joëlle Kost*, *Payam Payamyar*, *Marco Servalli*, and *Jens Temmen* for any advise, proofreading, and corrections related to this thesis.

I would like to thank all the former and current members of Schlüter's group for the nice working atmosphere: *Dr. Julia Baettig*, *Dr. Thomas Bauer*, *Dr. Yougen Chen*, *Wenyang Dai*, *Dr. Swati De*, *Bernd Deffner*, *Dr. Sara Fornera*, *Dr. Ikhlas Gadwal*, *Chiara Gstrein*, *Dr. Andrea Grotzky*, *Dr. Benjamin Hohl*, *Dr. Tim Hungerland*, *Dr. Samuel Jakob*, *Dr. Katja Junker*, *Dr. Anzar Khan*, *Dr. Patrick Kissel*, *Max J. Kory*, *Andreas Kuchler*, *Dr. Anke Krebs*, *Ralph Lange*, *Sandra Luginbühl*, *Daniel Messmer*, *Dr. Li Ming*, *Vivian Müller*, *Cornelia Oprea*, *Payam Payamyar*, *Dr. Jingyi Rao*, *Dr. Dan Radu Rusu*, *Dr. Animesh Saha*, *Dr. Andri Schütz*, *Leon Šerc*, *Marco Servalli*, *Dr. Xiaoyu Sun*, *Prof. Peter Walde*, *Dr. Hao Yu*, *Dr. Baozhong Zhang*, and *Dr. Zhikun Zheng*.

As with all scientific work, the process of creating this thesis has not only depended on peers alone. Special thanks go to my closest friend "the native speaker" *Jens Temmen* and my girlfriend *Joëlle Kost*.

The greatest support has of course come from my parents, *Irmgard E. Cerqua* and *Henry J. Cerqua*, who were committed to giving me all the opportunities and were a true support in times of need. Without them all this would have not been possible.

### 10. Curriculum Vitae

#### Personal data

Name	Simon Timothy Cerqua
Date of birth	August 1st, 1984
Place of birth	Stuttgart - Bad Cannstatt, Germany
Nationality	German, US-American
Marital status	Unmarried

#### Education

04/2011–01/2015	PhD candidate Swiss Federal Institute of Technology in Zurich (ETHZ), Zurich, Switzerland Department of Materials, Institute of Polymers, Polymer Chemistry
02/2011	Diploma thesis in Chemistry Johannes Gutenberg-University (JGU) Mainz, Germany Faculty of chemistry, pharmaceutical sciences, and geosciences
05/2010–02/2011	External Diploma thesis in Chemistry Swiss Federal Institute of Technology in Zurich (ETHZ), Zurich, Switzerland Department of Materials, Institute of Polymers, Polymer Chemistry
08/2008–02/2009	DAAD exchange student University of Massachusetts (UMASS) Amherst, USA Polymer Science and Engineering
08/2005–02/2011	Study of Chemistry Johannes Gutenberg-University (JGU) Mainz, Germany Faculty of chemistry, pharmaceutical sciences, and geosciences

## 10. Curriculum Vitae

---

08/2004–08/2005 Study of Biomedical Chemistry  
Johannes Gutenberg-University (JGU) Mainz, Germany  
Faculty of chemistry, pharmaceutical sciences, and geosciences

1995–2004 Grammar school (Abitur)  
Graf-Stauffenberg-Gymnasium, Flörsheim am Main, Germany

### Academic and professional development

2005–2010 Student at Casino Wiesbaden

2002–2008 Fire and disaster protection

### Other qualifications

Languages German (mother tongue)  
English (fluent)  
French (basics)

Voluntary basis Junior firefighter, then firefighter at the voluntary fire department of Main-Taunus-Kreis, Germany  
(1994–2010)

### 11. Publications

#### 11.1. Poster Presentations

"Towards Facile Exfoliation and Functionalization of 2D-Polymers by a Photoreactive Rotor-shaped Monomer", International Symposium on Synthetic Two-Dimensional Polymers, June 2nd - 3rd 2014, Zurich, Switzerland.

"Towards Facile Exfoliation and Functionalization of 2D-Polymers by a Photoreactive Rotor-shaped Monomer", PolyColl 2014, June 20th 2014, Dübendorf, Switzerland.

"Towards 2D-Polymers: Synthesis of an Amine-bearing Rotor-shaped Monomer", 5th EuCheMS Chemistry Congress, August 31st - September 4th 2014, Istanbul, Turkey.

"Towards 2D-Polymers: Synthesis of an Amine-bearing Rotor-shaped Monomer", SCS Fall Meeting 2014, September 11th 2014, Zurich, Switzerland.